Alternative mechanisms in skin allergy processes : contribution of radical reactions from the molecule to the tissue

Salen Kuresepi

UNIVERSITÉ DE STRASBOURG

ÉCOLE DOCTORALE DES SCIENCES CHIMIQUES

Institut de chimie

THÈSE présentée par :

Salen KURESEPI

soutenue le : **11 mai 2018**

pour obtenir le grade de : **Docteur de l'Université de Strasbourg**

Discipline/ Spécialité : Chimie organique

Alternative mechanisms in skin allergy processes: contribution of radical reactions from the molecule to the tissue

THÈSE dirigée par :

Dr. E. GIMÉNEZ-ARNAU Directeur de thèse, Université de Strasbourg

RAPPORTEURS :

Pr. L. GROSSI Rapporteur externe, Université de Bologne

Pr. B. BLÖMEKE Rapporteur externe, Université de Trier

AUTRES MEMBRES DU JURY :

Dr. A. SPECHT Examinateur, Université de Strasbourg

Salen KURESEPI

Alternative mechanisms in skin allergy processes: contribution of radical reactions from the molecule to the tissue

L'allergie de contact est une pathologie touchant de 15 à 20 % de la population occidentale. A l'heure actuelle il n'existe aucun traitement, la seule façon efficace de prévention étant l'éviction totale des allergènes. Les tests de sensibilisation de nouvelles molécules avant leur mise sur le marché ont été réalisés sur l'animal jusqu'à l'interdiction dans le 7ème amendement à la directive Européenne concernant l'industrie cosmétique. Dans ce contexte il est primordial de développer des méthodes alternatives.

Ce travail de thèse propose d'analyser la problématique de l'allergie de contact en allant de la molécule au tissu pour les allergènes réagissant par voie radicalaire :

In chemico : étude de la réactivité des hydroperoxydes allyliques vis-à-vis des acides aminés par la RMN

In situ : études de radicaux issus de ces composés sur des épidermes humains reconstitués par RPE

In cellulo : étude du stress oxydant sur les cellules dendritiques et la voie de signalisation Keap1/Nrf2/ARE

Mots clés : allergie de contact, allergène, interaction haptène-protéine, radicaux, épiderme humain reconstitué, RPE, piégeage de spin

Allergic contact dermatitis is a pathology affecting 15 to 20% of the Western population. Until now no treatment exists, the prevention is the eviction of allergens. In the past, tests concerning new molecules for the market were tested on animals until the prohibition in the 7th amendment of the European directive concerning the cosmetics industry. In this context it is essential to develop alternative methods to assess the allergenic potential of chemicals.

This manuscript proposes to analyze the problem of the allergic contact dermatitis from the molecule to the tissue for allergens reacting through radical mechanisms:

In chemico: study of the reactivity profile of allylic hydroperoxides toward amino acids by NMR

In situ: radical intermediates formation on reconstructed human epidermis from allylic hydroperoxides by EPR

In cellulo: study of the oxidative stress from allylic hydroperoxides on dendritic cells trough the Keap1/Nrf2/ARE sensor pathway

Key words: allergic contact dermatitis, allergen, hapten-protein interaction, radical intermediates, reconstructed human epidermis, electronic paramagnetic resonance, spin trapping

« Vous n'y pouvez rien, messieurs, la Science est et demeure internationale. »

Albert Einstein

Comment je vois le monde

A mes parents, mon frère, mon neveu, mes grands-parents disparues, ma famille, mes amis et à ma femme.

Ce travail de thèse a été réalisé au sein du laboratoire de Dermatochimie de l'université de Strasbourg sous la direction du Dr. Elena Gimenez-Arnau.

Rédiger une thèse de doctorat n'est pas chose aisée et peut être que cela a été un peu plus le cas pour moi ou pas ! Il s'agit ici d'un exercice qui a ses propres règles, qui ne laisse aucune place au coté humain du scientifique, or c'est ce que l'on est, en fin de compte. Ce travail de plus de trois ans, m'a fait grandir aussi bien sur le plan professionnel que privé. Ce temps, ponctué de petits succès et échecs m'a appris en plus de la formation scientifique qu'avant tout on travaille avec l'être humain et que l'on dépend des autres pour exister et s'accomplir. Etant issu de l'immigration suite à la guerre du Kosovo en 1999, j'aimerais remercier la France de m'avoir donné les opportunités d'apprendre et montrer ce dont je suis capable.

Ma chère Elena, j'aimerais te remercier pour tout ce que tu as fait pour moi. Merci de m'avoir donné la chance de travailler sur un sujet que j'adore, merci de m'avoir écouté, conseillé et dirigé durant ces quelques années. Merci d'avoir été là pour moi aussi bien sur le plan technique que privé. La thèse a tes coté m'a fait grandir sur tous les plans et je t'en suis très reconnaissant.

Dr Bertrand Vileno, un scientifique passionné par son travail dont la passion transparait et est même contagieuse, un être humain extraordinaire, merci pour tout ce que tu as fait pour moi, merci pour ces soirées passées aux cotés de Lucie avec moi.

J'aimerais plus particulièrement remercier le jury qui a jugé ce travail de manière objective :

Pr Loris Grossi, Pr Brunhilde Blömeke ainsi que le Dr Alexandre Specht.

Egalement je voudrais remercier la Fondation pour la Recherche en Chimie pour le financement de cette thèse.

Je tiens à remercier l'ensemble des services de la RMN et du magasin et plus particulièrement Maurice Cope, Bruno Vincent, Lydia Tortroteau pour leur aide précieuse tout au long de ces années.

J'aimerais remercier le Pr Lepoittevin pour son coté pédagogue ainsi que pour m'avoir accepté au sein de son équipe de Dermatochimie, mais également le Dr Valérie Berl-Bauder pour m'avoir donné ma chance pour le master Chimie-Biologie.

A tous mes collègues dermatochimistes passés et présents un grand merci pour tout : Marie Betou, Marion Greco, Hassan Srour, Fatma Salhi, François-Marie Moussallieh, Eric Moss, Amélie Godard, Elodie Beroux, Maxime Schlienger, etc.

J'adresse également mes plus sincères remerciements à tous les gens qui ont une contribution dans ce travail de thèse : le Pr Saadia Kerdine-Romer, le Pr Marc Pallardy, la Dr Chloé Raffali ainsi que le Pr. Philipe Turek.

Je tiens à remercier mes amis Hervé Dekkiche, Sebastien Jenni, Régis Boehringer, Ryan Djemili, Ervin Suljevic, Endi Huduti, Amer Alijevic, Elvis Huduti et Endi Ajradini pour leur indéfectible soutien, merci pour toutes ses soirées et ces lendemains difficiles vivement que ça continue.

Pour finir je remercie ma famille, mes parents Jasmin et Jasminka Kuresepi pour m'avoir soutenu durant toutes mes études, mon frère Mehid, sa femme Ermelina ainsi que mon très cher neveu Dino Kuresepi. Je tiens plus particulièrement à remercier ma grand-mère d'adoption Hanifa Kuresepi qui est mon exemple de vie. Egalement je tiens à remercier mes grand-pères et grand-mères disparus Redzep Kuresepi, Rukija Kuresepi, Mehmed Ajradini et Sefka Ajradini, j'espère vous avoir rendu fière de moi.

La dernière personne que je voudrais remercier est ma femme qui a partagé avec moi mes bons et mauvais jours, qui me soutient inlassablement et sans conditions, merci à toi Sabina Hodza-Kuresepi.

KS

List of Abbreviations

°C	degree Celsius
°K	degree Kelvin
µM	micromole
ACD	allergic contact dermatitis
$a_{H\beta}$	electron to proton hyperfine coupling constant
AM	assay medium
a_N	electron to azote hyperfine coupling constant
Anis.	anisaldehyde solution
AOP	adverse outcome pathway
a_P	electron to phosphor hyperfine coupling constant
APM/Ce	phosphomolybdic acid solution
ARE	antioxidant response element
Cat.	catalytic
CH_3CN	acetonitrile
Cum-OOH	cumene hydroperoxide
cw-EPR	continuous wave electron paramagnetic resonance
d	doublet
Da	Dalton
DCs	dendritic cells
dd	doublet of doublets
DEPMPO	5-diethoxyphosphoryl-5-methyl-1-pyrroline-*N*-oxide
DEREK	deduction and estimation of risk from existing knowledge
DIBAL-H	di-isobutyl aluminum hydride
DMAPP	dimethylallyl pyrophosphate
DMPO	5,5-dimethyl-1-pyrroline-*N*-oxide, 2,2-dimethyl-3,4-dihydro-2*H*-pyrrole 1-oxide

DMSO	dimethyl sulfoxide
DNCB	2,4-dinitrochlorobenzene
DPRA	direct peptide reactivity assay
DTT	dithiothreitol
ECVAM	European center for validation of alternative methods
eq.	equivalent
Et	ethyl
et al.	et alii
Fe (II)	iron (II)
G	gauss
g	gram
g factor	Landé's factor
GHz	gigahertz
GPMT	guinea pig maximization test
h-CLAT	human cell line activation test
hfccs	hyperfine coupling constants
HMBC	heteronuclear multiple bond correlation
ho-1	heme oxygenase-1
HOMO	highest occupied molecular orbital
HPLC	high-performance liquid chromatography
HSQC	heteronuclear single quantum correlation
Hz	hertz
IL12	interleukine 12
IL18	interleukine 18
il-8	pro-inflammatory cytokines
INF-γ	interferon γ
IPP	isopentenyl pyrophosphate
*i*PrMgCl	isopropyl magnesium chloride

J	NMR coupling constant
KCN	potassium cyanide
Keap1	Kelch-like ECH-associated protein 1
KJ	kilojoule
$KMnO_4$	potassium permanganate
Limo	limonene
Limo-OOH	limonene hydroperoxyde
Lina	linalool
Lina-6-OOH	6-hydroperoxy-3,7-dimethyl octa-1,7-dien-3-ol
Lina-7-OOH	(5E) -7-hydroperoxy-3,7-dimethyl octa-1,5-dien-3-ol
Lina-OOHs	linalool hydroperoxyde
LLNA	mouse local lymph node assay
M	molar
m	multiplet
m/z	ratio mass on charge
Maf	musculoaponeurotic fibrosarcoma
MC	cell culture media
Me_2AlCl	dimethyl aluminum chloride
Me_3Al	trimethylaluminum
MEST	mouse ear swelling test
MHC II	major histocompatibility complex of class II
min	minute
mL	milliliter
mM	millimolar
mM	millimole
Mod-OOH	monocycle hydroperoxide
mol	mole
ms	millisecond

MUSST	Myeloid U937 Skin Sensitization Test
mW	milliwatt
NMR	nuclear magnetic resonance
nqo1	NADPH quinone oxidoreductase 1
Nrf2	Nuclear Factor Erythroid 2-Related Factor 2
Nu	nucleophilic function
PB	phosphate buffer
PBN	N-*tert*-butyl-α-phenylnitrone
p-EPR	pulsed Electron Paramagnetic Resonance
Ph	phenyl
ppm	parts per million
PPRA	peroxidase peptide reactivity assay
QSARs	quantitative structure-activity relationships
RAI	relative alkylation index
REACH	registration, evaluation, authorization, and restriction of chemical substances
RHE	reconstructed human epidermis
RNS	reactive nitrogen
ROAT	repeated open application test study
R-OOHs	hydroperoxides
ROS	reactive oxygen species
rt	room temperature
s	singlet
S/N	signal to noise ratio
sl	singlet large
S_N1	nucleophilic substitution
S_N2	nucleophilic substitution
t	triplet
*t*BHP	*tert*-butyl hydroperoxide

THF	tetrahydrofuran
TLC	thin layer chromatography
TOPKAT	toxicity Prediction by Computer Assisted Technology
TPP	5,10,15,20-tetraphenyl-21*H*,23*H*-porphyrine
δ	chemical shift
ν	frequency

Implication des mécanismes de type radicalaire dans les processus de sensibilisation cutanée : compréhension en allant de la molécule au tissu

La peau étant en contact permanent avec l'environnement, elle constitue la première interface de l'organisme vis-à-vis du monde extérieur. C'est par son intermédiaire que se font des échanges avec des xénobiotiques, dont certains sont capables de franchir la couche cornée se retrouvant ainsi dans l'épiderme. L'allergie de contact (ADC) est une réaction d'immunotoxicité cutanée induite par le contact répété de l'individu avec certains de ces xénobiotiques.

Une fois entrés dans l'épiderme et trop petits pour activer le système immunitaire (poids moléculaire inférieur à 1000 Da), ces xénobiotiques allergisants, ou haptènes, doivent réagir avec les protéines de la peau, formant ainsi une entité antigénique qui déclenchera tout le processus immunologique caractérisant l'ADC. Le mécanisme le plus souvent rencontré pour l'interaction haptène-protéine est celui de type nucléophile-électrophile (mécanisme à 2 électrons), mais des mécanismes de type radicalaire (mécanisme à 1 électron) sont également suspectés.

Le sujet de ce travail de thèse a été d'étudier la contribution des réactions radicalaires dans la sensibilisation cutanée aux hydroperoxydes allyliques dérivés de l'autoxydation de terpènes d'origine naturelle, largement utilisés dans la composition de parfums, produits cosmétiques ainsi que dans des produits d'entretien ménagers.

Le travail a été organisé autour de trois axes, comprenant des études de la molécule au tissu :

• ***in chemico***, en étudiant le profil de réactivité chimique d'un hydroperoxyde allylique sensibilisant

• ***in situ***, en étudiant par résonance paramagnétique électronique (RPE) le comportement des espèces radicalaires formées à partir de ces hydroperoxydes sur un modèle 3D d'épiderme humain reconstitué

• ***in cellulo***, en mesurant le stress oxydant induit par les hydroperoxydes allergènes sur l'activation des cellules dendritiques.

Profil de réactivité *in chemico* au travers de mécanismes radicalaires

Le (5E)-7-hydroperoxy-3,7-diméthylocta-1,5-dièn-3-ol **2,** l'un des principaux produits issus de l'autoxydation du linalol **1**, est un sensibilisant fort. Il est admis que cet hydroperoxyde réagit avec les protéines cutanées par des mécanismes de type radicalaire.

Une technique utilisée au laboratoire permettant le suivi de la formation d'adduits haptène-protéine est basée sur l'utilisation de l'haptène contenant un carbone 13 (^{13}C) dans les positions réactives afin de suivre la réactivité vis-à-vis des acides aminés par RMN du ^{13}C. Plusieurs positions radicalaires potentiellement réactives peuvent se former à partir de **2** (**Figure 1**). La liaison O-O de la fonction hydroperoxyde a une faible énergie de dissociation (175 $kJ.mol^{-1}$), elle peut être facilement clivée par un mécanisme de transition électronique et conduire à la formation de radicaux oxygénés tels le radical allyloxyle. En raison de la présence de doubles liaisons allyliques, des réarrangements intramoléculaires ou de l'abstraction d'hydrogène allylique peuvent avoir lieux et ainsi former des radicaux carbonés dans les positions 2, 4 et 5, par exemple.

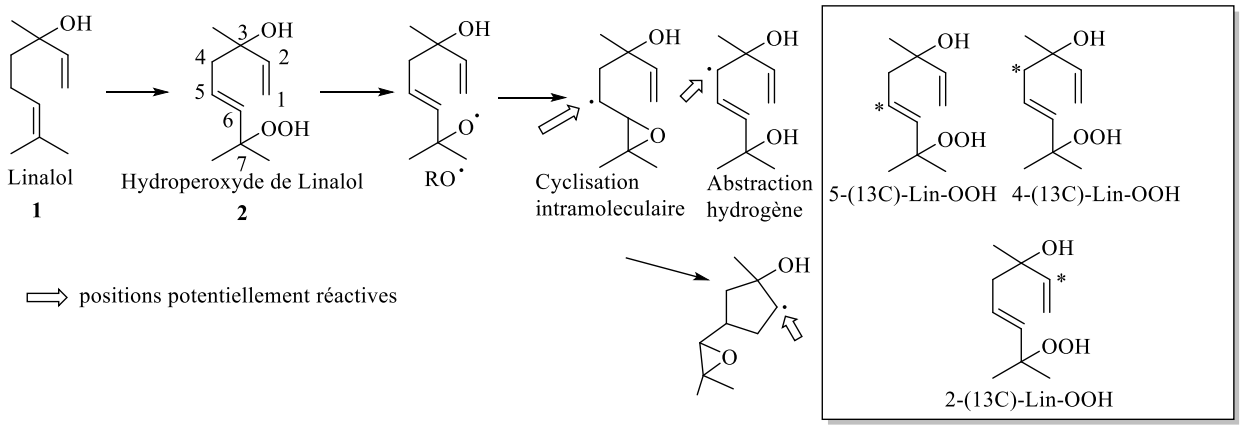

Figure 1 : Structure du linalol **1** et du (5E)-7-hydroperoxy-3,7-diméthylocta-1,5-dièn-3-ol **2** et réarrangements radicalaires

L'objectif était de synthétiser l'hydroperoxyde allylique **2** isotopiquement substitué au ^{13}C dans les positions 2, 4 ou 5, où un radical carboné peut se former par décomposition de l'hydroperoxyde, et d'étudier la réactivité de chacun de ces composés vis-à-vis des acides aminés protéiques. L'objectif principal était d'étudier, de cette façon, s'il existe une spécificité de réaction d'un certain radical carboné vis-à-vis d'un acide aminé précis.

Les synthèses de l'hydroperoxyde allylique isotopiquement substitué au ^{13}C dans les positions 4 et 5 ont été réalisées (exemple en **Figure 2**). Cependant, la synthèse est bloquée en position

2 et n'a pas pu être menée à terme. Ces synthèses ont été initialement optimisées sans isotope ^{13}C, puis réalisées avec l'introduction de ^{13}C dans les meilleures conditions expérimentales.

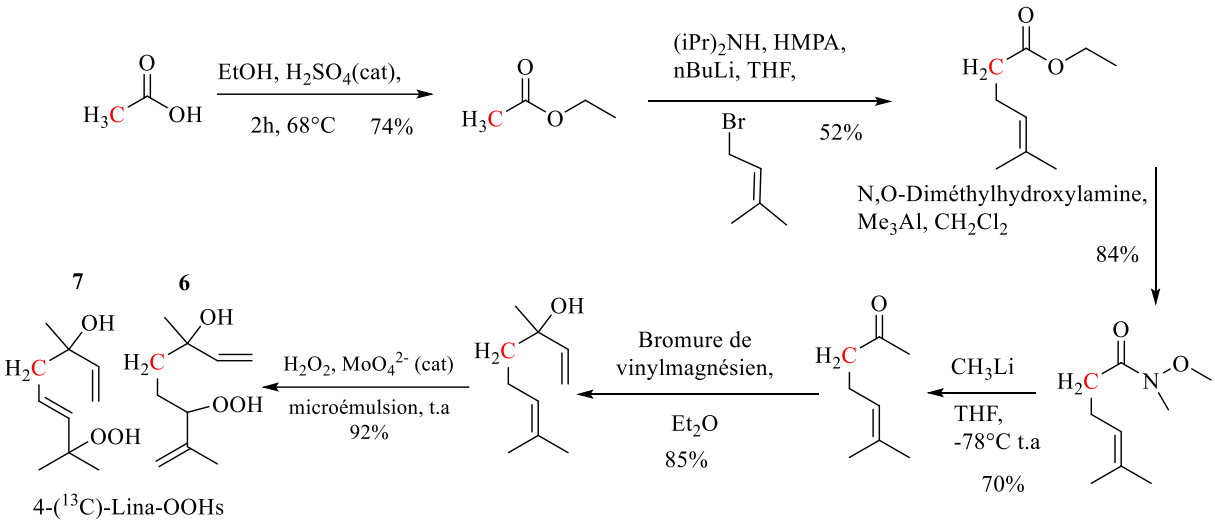

Figure 2 : Synthèse de l'hydroperoxyde allylique substitué au ^{13}C en position 4

Une deuxième partie de ce volet de recherche a consisté en l'étude de la réactivité vis-à-vis des acides aminés par RMN du ^{13}C.

Les composés synthétisés 4-(^{13}C)-LinaOOHs et 5-(^{13}C)-LinaOOHs (**Figure 3**) ont été mis en présence de différents acides aminés et la réactivité suivie par RMN du ^{13}C 1D , puis on a utilisé le RMN 2D pour essayer de résoudre la structure de l'adduit formé.

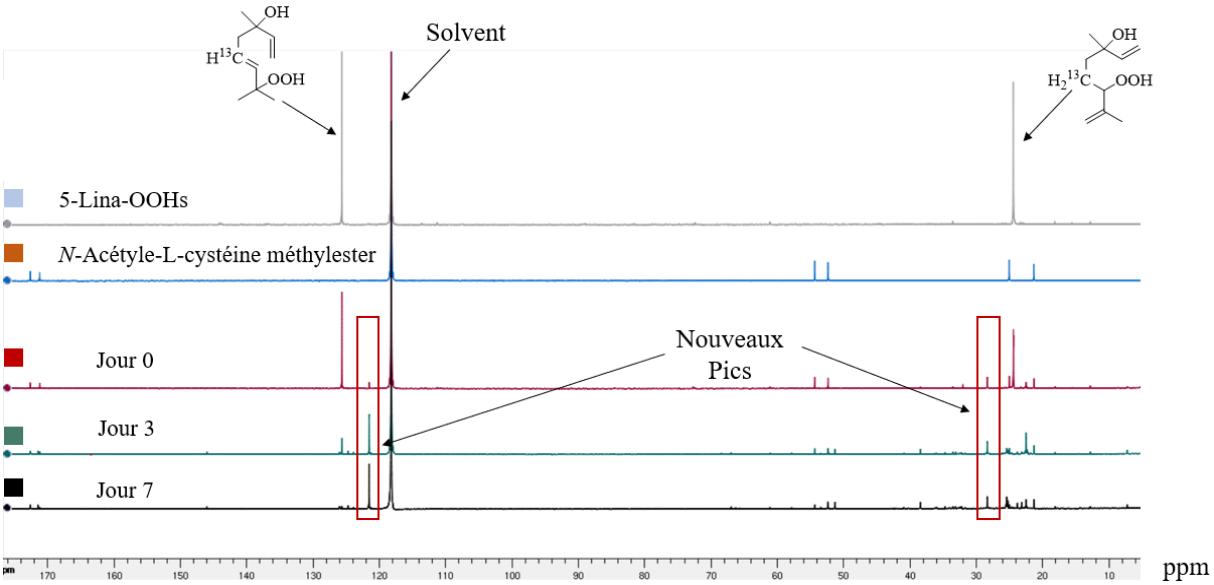

Figure 3 : 5-^{13}C-Lina-OOHs (1 éq., 5.37 µM), *N*-Acétyle-L-cystéine méthylester (2éq., 10.74 µM) et une quantité catalytique de fer (II) (0.1 éq.) dans un milieu CD_3CN/H_2O 1/1 durant une semaine de réactivité

Les spectres de RMN du ^{13}C ont illustré la réactivité entre 5-(^{13}C)-LinaOOHs ainsi que 4-(^{13}C)-LinaOOHs et uniquement avec l'acide aminé ester méthylique de la *N*-acétyle-L-cystéine avec ou sans initiateur fer (II). Nous avons observé que les pics correspondant au composé substitué au ^{13}C diminuent avec le temps (sur sept jours) ainsi que la formation de plusieurs nouveaux pics correspondant à des modifications de la cystéine par les hydroperoxydes. Ces modifications correspondent entre autres, à la formation d'adduits dont la structure moléculaire a été estimé grâce aux simulations par ordinateur des déplacements chimiques (**Figure 4**).

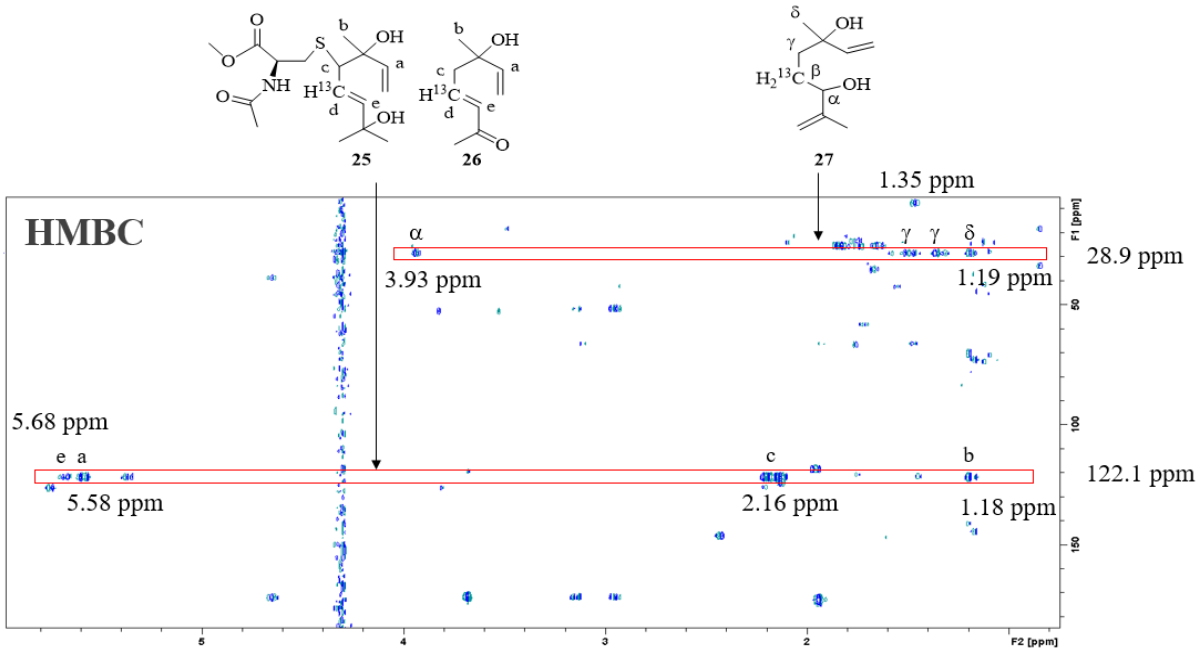

Figure 4 : Structures hypothétiques des composes **25**, **26** et **27** basées sur l'interprétation du spectre HMBC

Le composé 4-(^{13}C)-LinaOOHs a aussi montré une réactivité vis-à-vis du même acide aminé cystéine. Les composés **25** et **26** ont été confirmés et un nouveau composé **28** est apparu (**Figure 5**).

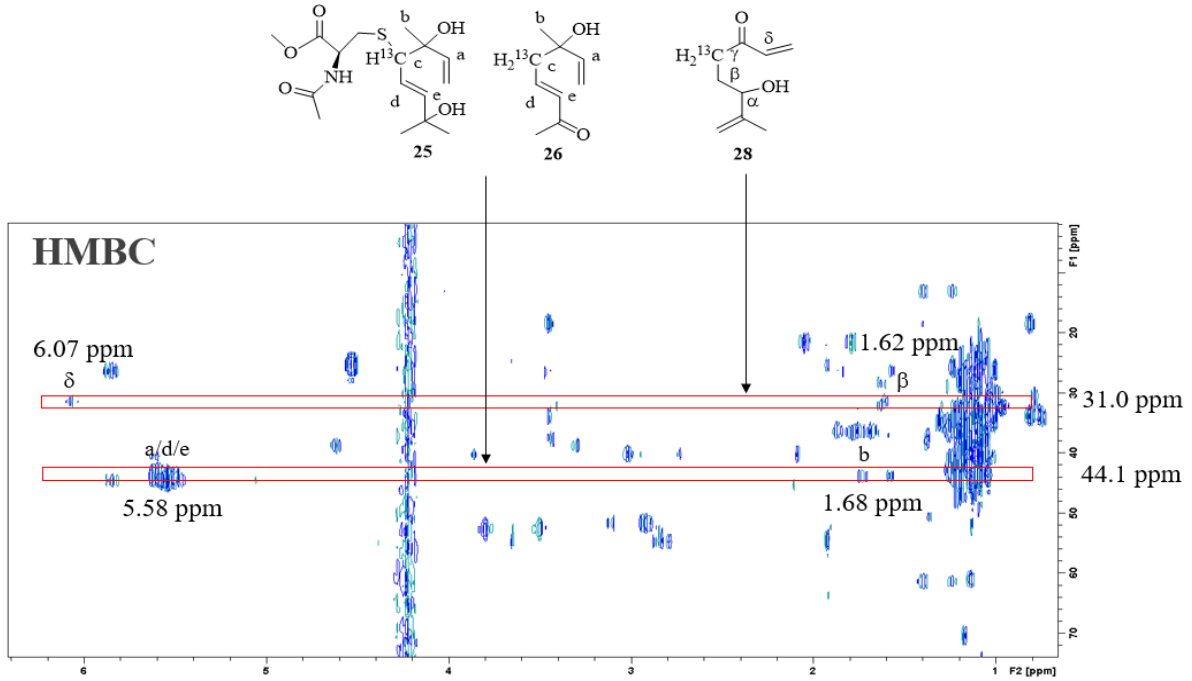

Figure 5 : Structures hypothétiques des composés **25**, **26** et **28** basées sur l'interprétation du spectre HMBC

Les composés **25** et **26** présentent des déplacements chimiques très similaires en RMN étant donc impossible de les discerner.

Pour conclure, il a été possible de réaliser deux synthèses sur trois de manière reproductible. Il a été aussi observée une réactivité uniquement en présence de l'acide aminé cystéine. Pour finir concernant les études de réactivité, il a été à chaque fois observé que l'isomère de position **6** disparait plus rapidement que le **7**, donc est-il plus réactif ou tout simplement moins stable ?

La partie moléculaire *in chemico* de cette étude étant fini nous allons maintenant voir la partie *in situ* concernant l'étude dans les épidermes humains reconstitués.

Investigation *in situ* par RPE sur un épiderme humain reconstitué

En collaboration avec le laboratoire POMAM, Propriétés Optiques et Magnétiques des Architectures Moléculaires, Université de Strasbourg, CNRS-UMR 7177

Nous avons développé dans le deuxième chapitre de ce manuscrit, l'utilisation de la RPE combinée aux techniques de piégeage de spin afin d'étudier la formation et le comportement des radicaux provenant des hydroperoxydes allyliques sensibilisants (Lina-OOHs et Limo-OOH) dans un modèle 3D d'épiderme humain reconstitué (RHE). Nous avons choisi de travailler avec le modèle Episkin^{TM} (Lyon, France). Il se compose d'une culture de kératinocytes humains à couches multiples normales et est similaire histologiquement à l'épiderme humain. L'objectif était d'évaluer le comportement de ces espèces radicalaires dans un modèle plus proche de ce qui peut arriver *in vivo*.

La méthodologie a été développée à l'aide de l'hydroperoxyde de cumène commercial (Cum-OOH) comme composé modèle, référence connue utilisée souvent dans des études de RPE, et des piégeurs de spin tels que le 5-diméthyl-1-pyrroline *N*-oxyde (DMPO) et le 5-diéthoxyphosphoryl-5-méthyl-1-pyrroline *N*-oxyde (DEPMPO) afin d'avoir une vue large de tous les radicaux générés, oxygénés et aussi carbonés (**Figure 6**).

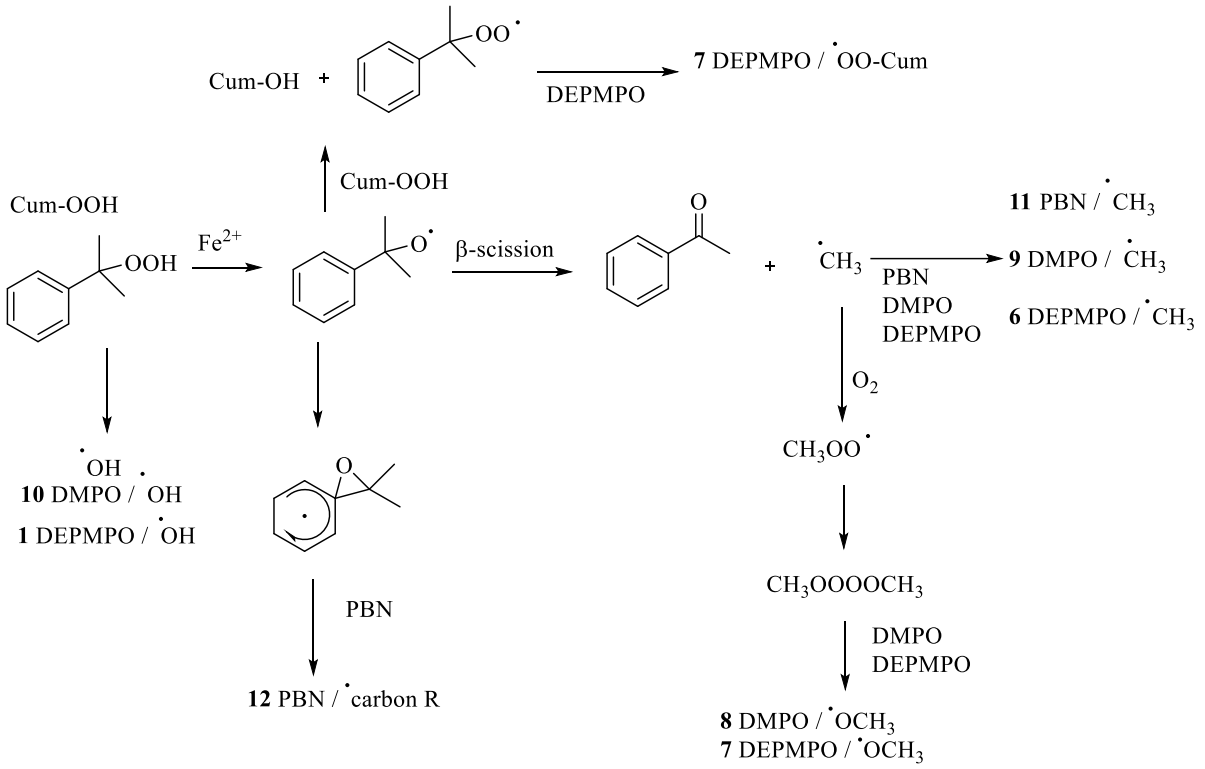

Figure 6 : Formation de spin adduit du système Cum-OOH/spin trap/fer (II)

Au départ, nous avons réalisé les études en solution dans le but de définir les conditions expérimentales optimales de solvant (mélange acétonitrile / eau, tampon phosphate, tampon HEPES) et la concentration des composés chimiques afin d'être aussi proche que possible des conditions physiologiquement compatibles. Une réactivité similaire est observée pour le mélange Lina-OOHs que pour le Cum-OOH, ainsi qu'une réactivité moindre pour le Limo-OOH (**Figure 7**).

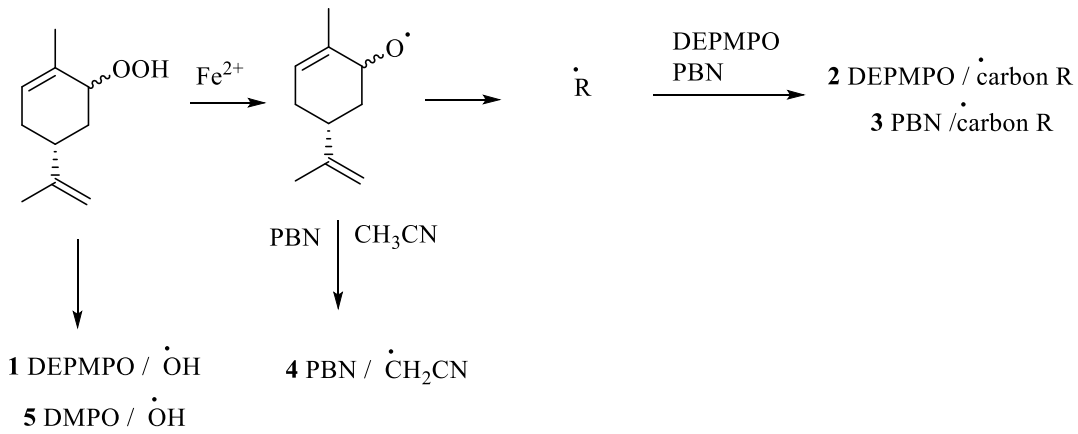

Figure 7 : Formation de spin adduit du système Limo-OOH/spin trap/fer (II)

Les études de RPE sur les RHE incubées ont été menées en surmontant les défis techniques et analytiques que cela pose, étant donné qu'il s'agit d'une matrice beaucoup plus complexe que les études en solution, ainsi que cela n'a jamais été fait auparavant. Des radicaux centrés sur le carbone ont été détectés dans les RHE après incubation avec le Cum-OOH (**Figure 8**). Un radical méthyle issu de la décomposition de Cum-OOH a pu être mis en évidence dans les RHE.

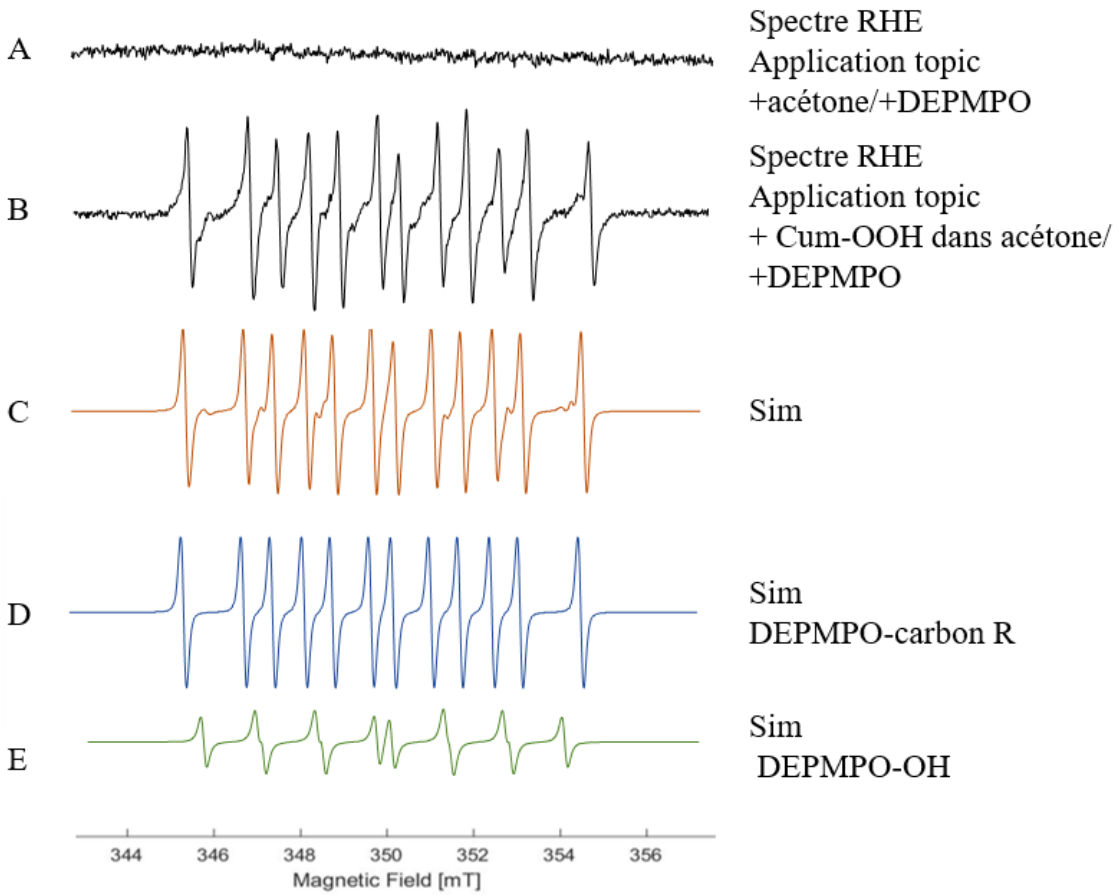

Figure 8 : Spectre RPE obtenu dans les RHE par application topic : expérience utilisant du Cum-OOH (1 mM dans l'acétone), DEPMPO (50mM dans l'HEPES): (A) expérience control avec uniquement du DEPMPO et le véhicule; (B) Spectre RHE avec application du CumOOH et incubation (5 min, 37 °C, 5% CO_2) suivie par l' addition du DEPMPO; (C) simulation des spectres par ordinateur (B); (D–E) déconvolution de DEPMPO-carbone R et DEPMPO-OH.

Une fois la méthode mise en place, les hydroperoxydes dérivés de l'autoxydation du linalol et du limonène ont également été testés. Selon l'environnement, nous avons montré qu'ils génèrent également des radicaux oxygénés et carbonés, cependant il a été montré qu'il faut travailler avec une quantité dix fois supérieure à celle de l'hydroperoxyde de cumène afin d'obtenir un signal. Compte tenu de ce fait et du fait que dans les études en solution aucune différence de

réactivité n'avait été observée, on peut émettre l'hypothèse que les hydroperoxydes dérivés du linalol et limonène pénètrent plus en profondeur dans le RHE que le Cum-OOH.
La partie *in situ* de cette étude étant finie nous allons maintenant voir la partie *in cellulo* concernant l'étude du stress oxydant.

Mesure du stress oxydant *in cellulo*

En collaboration avec le laboratoire de Signalisation en Immunotoxicologie et en Immunopharmacologie, Université de Paris Sud, INSERM-UMR 996

Le but ici a été d'évaluer le stress oxydant produit par des hydroperoxydes allyliques allergisants comparés à leur molécule d'origine non sensibilisante sur la lignée cellulaire THP-1, modèle reconnu des cellules dendritiques présentatrices d'antigène jouant un rôle clé dans l'ADC. La voie de signalisation Keap1-Nrf2, impliquée dans la réponse cellulaire antioxydante, a été utilisée afin de détecter le stress oxydant induit par ces composés. Quatre hydroperoxydes allyliques de structure chimique différente ont été testés : un modèle cyclique, le Cum-OOH, et les hydroperoxydes de linalol et de limonène (**Figure 9**).

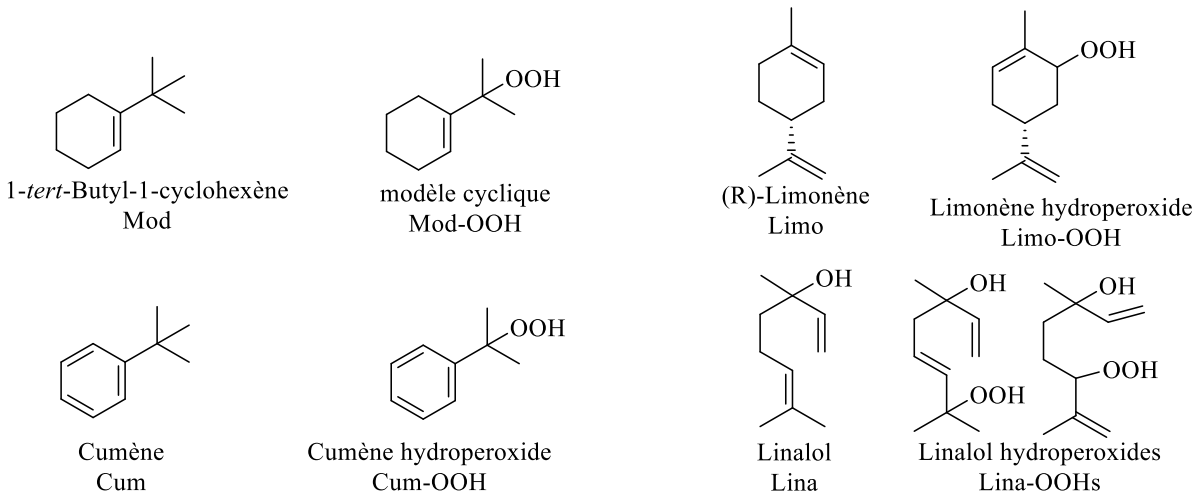

Figure 9 : Hydroperoxydes allyliques pour l'étude d'activation de la voie Keap1-Nrf2

L'expression des gènes antioxydants (*ho-1*, *il8* et *nqo1*) par réaction en chaîne de la polymérase (PCR) et l'accumulation de la protéine Nrf2 par Western Blot ont été mesurées (**Figures 10 et 11**). Au cours des deux semaines et demi que j'ai passées dans le laboratoire de Signalisation en Immunotoxicologie et en Immunopharmacologie, nous avons travaillé sur le développement des conditions expérimentales du modèle et sur la cytotoxicité des hydroperoxydes sur la culture de cellules THP-1.

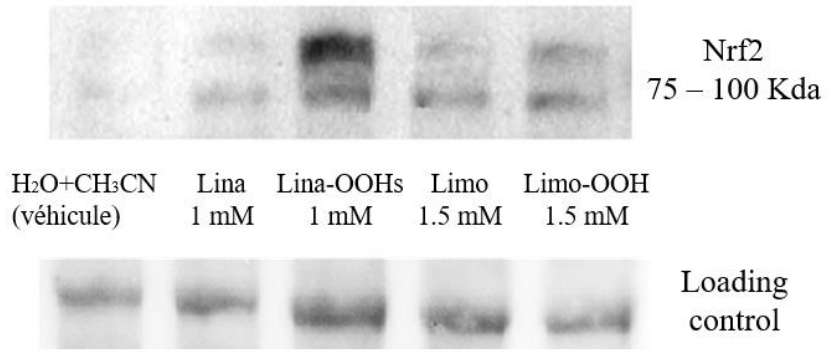

Figure 10 : Accumulation cytoplasmique de Nrf2 suivant l'exposition aux Lina, Limo, Lina-OOHs et Limo-OOH en comparaison avec le véhicule (acétonitrile/eau) comme contrôle négatif et aussi au « loading » control

Après exposition de la lignée cellulaire THP-1 au Lina-OOHs une forte accumulation de la proteine Nrf2 cytoplasmique a été observée en comparaison avec la molécule parent Lina et aussi au véhicule. Cette forte accumulation a aussi été relevée pour le Cum-OOH en comparaison avec la molécule parent et les contrôles négatifs. Curieusement une forte accumulation a été observée pour la molécule Mod-OOH mais aussi pour sa molécule parent alors que les contrôles négatifs sont bons. Ce qui a été encore plus curieux est que le Limo-OOH engendre une très faible accumulation de la protéine cytoplasmique Nrf2 en comparaison avec les contrôles négatifs.

Nous avons observé une surexpression des gènes *ho-1*, *nqo-1* et *il-8* (**Figure 11**) après exposition aux LinaOOHs, CumOOH et Mod-OOH alors que le Limo-OOH n'avait pas donné de réponse une fois de plus.

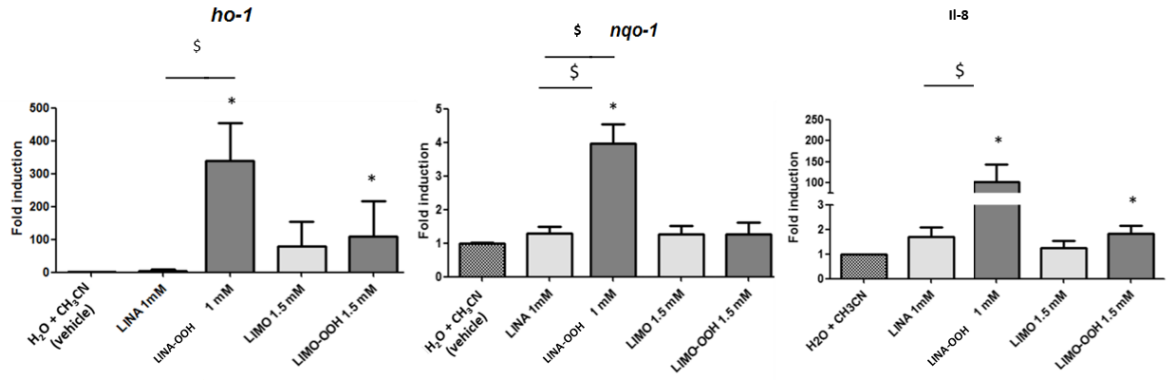

Figure 11 : Surexpression des gènes *ho-1*, *nqo-1* et *il-8* après exposition aux LinaOOHs et Limo-OOH comparé à leurs molécules parentes et aux véhicules

Même si une concentration plus élevée de Limo-OOH (1,5 mM) en comparaison aux autres hydroperoxydes (1 mM) a été appliquée aux cellules THP-1, ici aussi la même réponse est observée. Le Limo-OOH n'induit pas vraiment une surexpression génétique des gènes antioxydants alors qu'il fait partie des allergènes connus. Cependant, les autres hydroperoxydes testés induisent une surexpression des gènes *ho-1*, *nqo-1* et *il-8*. Il est important ici de souligner le fait que la molécule Mod induit aussi la surexpression génétique.

Pour conclure, les hydroperoxydes allyliques ne semblent pas êtres égaux dans l'activation des cellules dendritiques par la voie de l'accumulation cytoplasmique de la protéine Nrf2. De plus, uniquement les hydroperoxydes allyliques peuvent engendrer une surexpression génétique à l'exception de la molécule Mod.

Conclusion générale

Lors de ce travail de thèse, nous avons tout d'abord mis au point la synthèse du 4-(^{13}C)-Lina-OOHs et du 5-(^{13}C)-Lina-OOHs.

Les premières études de réactivité par RMN du ^{13}C ont montré que ces composés peuvent modifier les acides aminés et plus spécialement la *N*-Acétyle cystéine. On a émis plusieurs hypothèses quant à la nature des composés obtenus dans ces conditions. Il serait intéressant dans l'avenir de refaire ces tests dans un milieu plus proche du milieu biologique tel un tampon phosphate ou HEPES à 37 °C.

Dans une deuxième partie de ce travail, nous avons développé une méthodologie nouvelle basée sur la RPE et le piégeage de spin qui permet de mettre en évidence, pour la première fois, la formation de radicaux carbonés issus d'allergènes dans un modèle 3D de RHE et en utilisant les hydroperoxydes allyliques sensibilisants. Ces radicaux se formant donc i*n situ* seraient capables de réagir avec les acides aminés par des mécanismes de type radicalaire afin de former le complexe antigénique qui sera reconnu par le système immunitaire. Le modèle développé dans cette étude est aujourd'hui utilisé au laboratoire pour tester d'autres allergènes réagissant au travers de mécanismes radicalaires.

Enfin dans la dernière partie, le potentiel oxydant de ces molécules a été confirmé par l'étude de l'activation de la voie Keap1-Nrf2 à l'aide de cellules de la lignée THP-1.

Pour le moment et en conclusion, l'ensemble de nos études montre que les hydroperoxydes dérivés de l'autoxydation du linalol sont plus réactifs, du point de vue de réactivité chimique et du point de vue d'activation biologique, que ceux dérivés du limonène. Un lien pourrait être donc fait avec la plus grande capacité de ce composé à former plusieurs espèces radicalaires carbonées.

Ces travaux ont ouvert une nouvelle perspective de travail au laboratoire ayant comme objectif principal de faire un lien entre les données de réactivité *in chemico* et les études de formation de radicaux *in situ* avec une réponse biologique *in cellulo* associée à la sensibilisation cutanée, afin de pouvoir mieux évaluer le potentiel sensibilisant de composés réagissant par voie radicalaire.

Références

Saint-Mezard P., Bernard F., Dubois B., Kaiserlian D. and Nicolas J.F. *Eur J Dermatol* (2004) 14, 131-138

Rober L.R. and Flower J.F. *Contact Dermatitis* (1998) 81-111

Christensson J.B., Hellsén S., Börje A. and Karlberg A.T. *Contact Dermatitis* (2014) 70, 291-299

Basketter D.A., Blaikie L., Dearman R.J., Kimber I., Ruan C.A., Gerberick G.F., Harvey P., Evans P., White I.R. and Rycroft R.J. *Contact Dermatitis* (2000) 42, 344-348

Karlberg A.T., Börje A., Johansen J.D., Liden C., Carola R.S., Suresh R., David U.W. and White I.R. *Contact Dermatitis* (2013) 69, 323-334

Urbisch D.,Mehling A., Guth K., Ramirez T., Hanarvar N., Kolle S., Landseidel R., Jaworska J., Kern P.S., Gerberick F., Natsch A., Emter R., Ashikaga T., Miyazawa M. and Sakaguchi H. *Regul Toxicol Pharmacol* (2015) 71, 337-351

Kao D., Chaintreau A., Lepoittevin J-P. and Giménez-Arnau E. *J Org Chem* (2011), 76, 6188-6200

Aubry J.M., Adam W., Alster P.L., Borde C., Queste S., Marko J. and Nardello V. *Tetrahedron* (2006) 62, 10753-10761

Bjorkman Y.A., Hagvall L., Siwmark C., Niklasson B., Karlberg A.T. and Christensson J.B. *Contact Dermatitis* (2014) 70, 129-138

Foote C.S., Valentine J., Greenberg A. and Liebman J.F. *Active Oxygen in Chemistry* (1995) 2, 147-148

Raffalli C., Clouet E,. Kuresepi S., Damiens M.-H., Lepoittevin J.-P., Pallardy M., Ferret, P.-J., Giménez-Arnau E., Kerdine-Römer S. *Toxicol. Sci.* (2018), *161* (1), 139–148

Kuresepi S., Vileno B., Turek P., Lepoittevin J.-P., Giménez-Arnau E. *Free Radic. Res.* (2018), 52, 171–179

Introduction

Allergic contact dermatitis (ACD) is today a common occupational and environmental issue. Prevalence is rising worldwide, being more important in developed countries. In Europe, 15 to 20 % of the general population is suffering from ACD to at least one chemical allergen.[1] More than one hundred natural or synthetic compounds are today recognized playing a role in ACD as confirmed skin-sensitizers.[2–6] These compounds are found almost everywhere in everyday life, cosmetics, perfumes, textiles, householding products, plants and also in many industrial products, among others.[7,8]

Up to now, medical treatments have not been able to heal skin allergy or ACD. Once the person is sensitized, it is for life. Only symptomatic treatments are available to relieve patient's pain. The best way to treat ACD is thus prevention and the eviction of sensitizing compounds.

As an example for prevention, the 7th Amendment to the European Cosmetics Directive obliges the cosmetics industry to label 26 compounds present in fragrances that are important skin sensitizers.[9]

Gell and Coombs classified ACD as a delayed-type hypersensitivity reaction or type IV hypersensitivity.[10] It is a cell-mediated immune reaction that is dependent on the presence of antigen-specific T-cells, where chemistry plays a key role.

1 ALLERGIC CONTACT DERMATITIS

ACD is the clinical manifestation of an immunotoxicity reaction resulting from skin sensitization to a chemical. It usually manifests with symptoms such as eczema, edema (swelling), erythema (redness), or pruritus (itching). It is induced by skin contact of the individual with a sensitizing substance. After penetration into the epidermis and too small to activate the immune system (molecular weight below 1000 Da), these allergenic substances, also called haptens, must react with skin proteins to form the antigenic immunogenic entity.[11]

1.1 The skin

The skin is in constant contact with the environment and is the first interface of the human body with the outside. It covers the entire human body and is, by its surface (circa 2 m^2), one of the largest organs. It protects us from ultraviolet radiations and shocks while keeping constant the body temperature by retention or elimination of water. It's permeability, constant renewal and elasticity make of it a great natural physical barrier between the organism and external aggressions and

xenobiotics. However, the skin is not hermetic and some compounds are able to penetrate into the epidermis and be at the origin of skin sensitization and ACD.

Mammalian skin is composed of three primary layers: the epidermis, the dermis and the hypodermis.

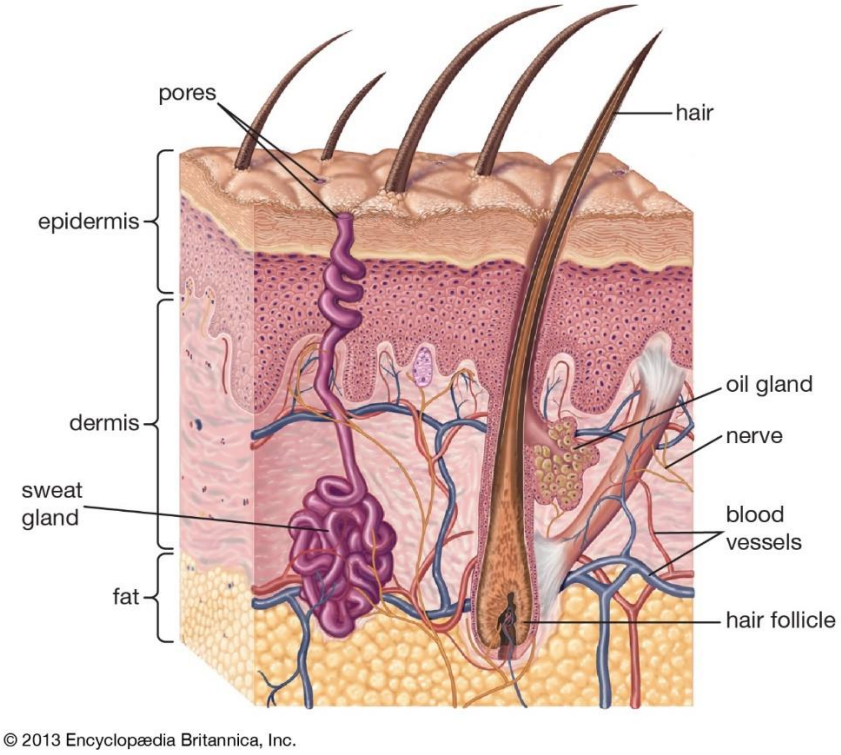

Figure I.1: Anatomy of the skin[12]

The epidermis is composing the external layer of the skin. It is a circa 200 micrometers thick non-vascularized tissue.[13] The epidermis is a multistratified keratinized epithelium subdivided into five successively superimposed layers from the surface towards the depth: the *stratum corneum*, the *stratum lucidum*, the *stratum granulosum*, the *stratum spinosum* and the *stratum basal*.

Major cells in the epidermis are keratinocytes (approximately 90 % of all cells). Keratinocytes are produced in the stratum basal, then they differentiate through migration from the stratum basal to the stratum corneum.

The *stratum corneum*, the most superficial layer, consists of a stack of keratinized dead cells, which are eliminated by desquamation, the skin thus renewing itself in a perpetual manner. Other cells

composing the epidermis are melanocytes (8 % in the deepest layers), Langerhans cells (3 to 5 % in the deepest layers) and Merkel cells (also in the deepest layers), whose main functions are skin pigmentation, immunity and perception, respectively.[14–16]

The epidermis and the dermis are separated by the basal lamina, controlling the traffic of cells and molecules between both. It is responsible for the nourishment and waste removal from the dermis and the epidermis. The dermis plays a key role in the thermoregulation of the body and nutrition of the epidermis through the blood vessels. It contains blood and lymph vessels, fibroblasts and an extracellular matrix composed of collagen and elastin fibers that give the skin its strength and elasticity.[13] It is 10 to 40 times thicker than the epidermis.

The hypodermis is the deeper localized part of the skin and also the thicker. Collagen fibers are connecting the hypodermis to the dermis. It is composed of adipocytes, fibroblasts, blood vessels and nerve fibers in a conjunctive tissue. The role of the hypodermis is to stock energy and keep constant the temperature of the body. It stock and release energy trough degradation of fatty acids (lipids), allows cells to obtain energy through b-oxidation of lipids in mitochondria.

1.2 ACD mechanism: sensitization and elicitation phases

Figure I.2 resumes the mechanism inducing ACD to a chemical after skin penetration. It is based on two distinct phases: sensitization and elicitation.

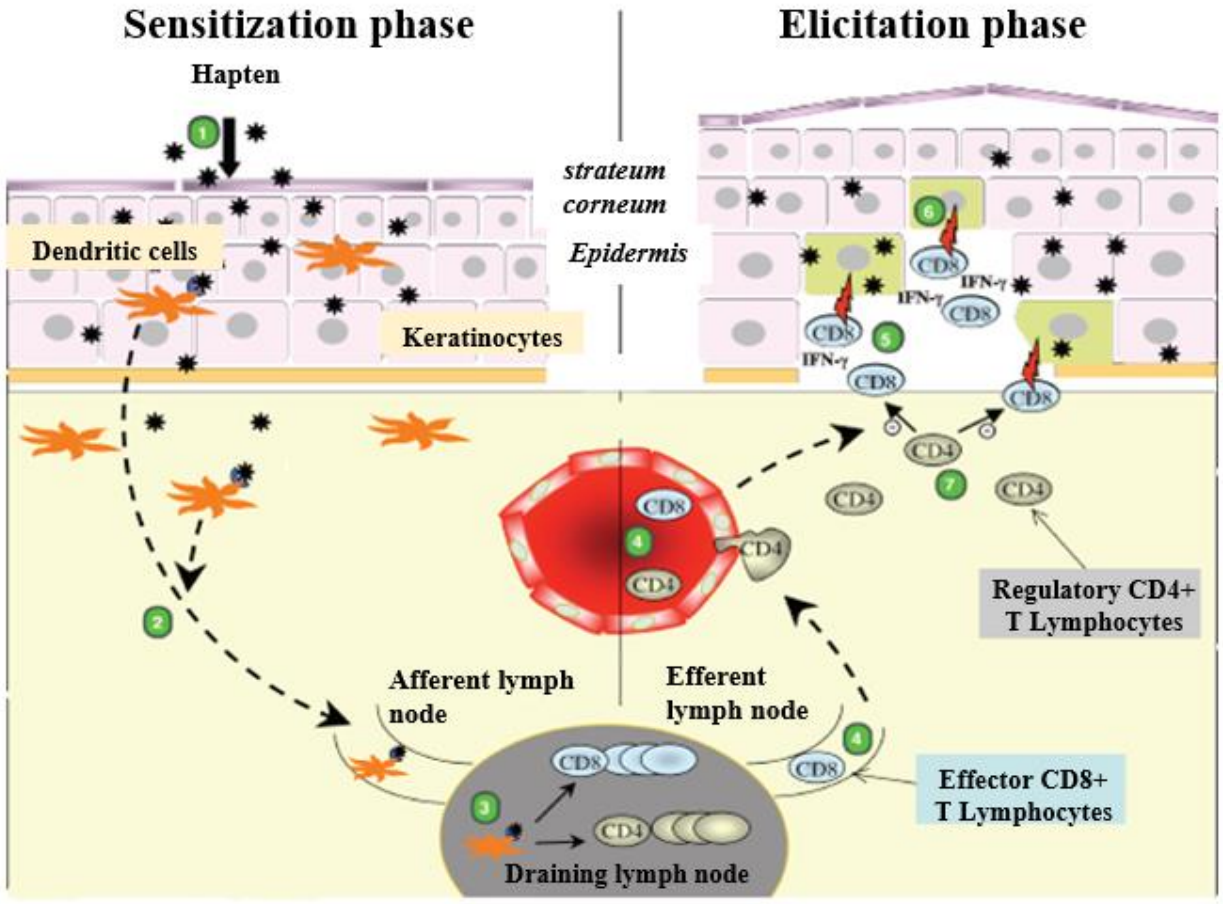

Figure I.2: ACD mechanism based on the sensitization and elicitation phases

(1) Hapten penetration into the epidermis, antigenic complex formation and take up by dendritic cells; (2) Maturation of dendritic cells containing the antigenic complex and migration to the local lymph nodes; (3) Dendritic cells presenting on their surface the antigenic complex to naïve T lymphocytes. Clonal expansion of effector and memory T lymphocytes; (4) Recirculation in the blood of antigen-specific T lymphocytes; (5) New exposition to the same hapten; (6) Cytokine and chemokine production leading to the affluence of T specific lymphocytes; (7) The inflammatory reaction is stopped by anti-inflammatory cytokines released by regulatory T lymphocytes.[17,18]

1.2.1 *The sensitization phase*

The sensitization phase is the result of a first contact between the allergenic compound and the immune system. At this stage, the immune system is alerted but there are no clinical symptoms.

After penetration of the allergen or hapten into the epidermis, an antigenic complex is formed by its reaction with skin proteins through the formation of stable covalent bonds.

Once the antigenic hapten-protein complex is formed, the immune surveillance system present in the epidermis is able to recognize it as foreign to the organism. At this moment, the antigenic complex is captured by dendritic cells (DCs) playing the role of antigen-presenting cells. They are organized in a cellular network, in a way that any substance penetrating into the epidermis is detected. DCs are the only cells in the epidermis presenting on their surface the major histocompatibility complex of class II (MHC II). The DCs will then indicate the presence of the antigenic complex to the immune system and this way induce proliferation of antigen-specific T lymphocytes. During this phase, there will be production of memory T lymphocytes that will recognize the allergen in question during subsequent exposures.

Two cases are possible for the hapten-protein interaction process. Haptens can either react with extracellular proteins and then DCs take up the antigenic complex by endocytosis, either react with DCs intracellular proteins.

The antigenic complex will then undergo an enzymatic degradation in the cytoplasm. During this process, DCs will maturate and migrate to the local lymph nodes. In the lymph nodes, the peptides containing the chemical modification induced by the hapten will be presented to T cells receptors at the surface of DCs via the MHC II.

Maturation of DCs leads to the production of co-stimulative molecules on their surface such as CD54, CD86 and CD40, playing a key role in the activation of naïve T lymphocytes.[19]

As said, once the DCs are in the local lymph nodes they will present to naïve T lymphocytes the haptenized-peptide or antigenic peptide through the MHC II on their surface. Naïve T lymphocytes will then be differentiated in Th1 lymphocytes in the presence of cytokines such as interleukins IL12 and IL18 and also INF-γ.[20] A clonal expansion of the Th1 lymphocytes occurs, and the newly differentiated cells migrate to the dermis. At this moment, the organism is sensitized to the allergen but is clinically asymptomatic.

The sensitization phase takes 10 to 15 days in humans, leading to the activation and proliferation of antigenic-specific T lymphocytes.

1.2.2 The elicitation phase

The elicitation phase occurs 24 to 48 hours after a second exposure to the same allergen. Initial steps are the same as those happening in the sensitization phase but here Th1 lymphocytes directly recognize the haptenized peptide. Allergen-specific Th1 cells release then cytokines and chemokines as a response to the antigenic complex. This causes an inflammatory reaction and further eczema. It also results in a massive influx of other non-specific T lymphocytes and other inflammatory cells amplifying the reaction even more. The eczematous reaction develops at the site of contact with the allergen.

Figure I.3: Photography of an ACD patient (courtesy Pr Ann Goossens)

1.3 The allergen

Every day we are exposed to a multitude of chemicals, synthetic or natural. Many of these compounds are able to react with human cells and induce mutagen, carcinogen, toxic and immune system reactions.[21] Allergens such as metallic ions (nickel Ni^{2+}, cobalt Co^{2+}) or fragrances are responsible for circa 20 % of ACD developed by the general European population.[1] European regulations are thus controlling exposure to skin allergens for consumers prevention. For example, a European directive from 1994 regulates nickel concentration in jewelry and as a result a decrease of nickel sensitization has been observed in Europe.[22] The risk to develop ACD is also depending on the exposition to skin sensitizers and the way of living. The most concerned occupational sectors are health-care workers, dental workers, hairdressers, construction workers, employees in the food industry, cleaners and painters.[23,24]

1.3.1 Chemicals directly reactive with skin proteins: haptens

Haptens are small molecules (molecular weight < 1000 Da) unable to activate themselves the immune system. They need to react with a carrier protein to form an antigenic hapten-protein complex that will then be recognized by the immune system. Landsteiner and Jacobs were the first authors to introduce the hapten concept.[25]

Metals react with proteins via the formation of coordinate bonds (Figure I.4).

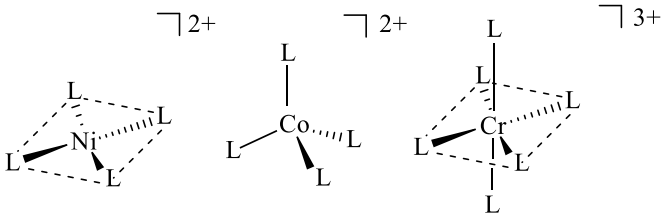

Figure I.4: Coordinate bond examples for nickel, cobalt and chromium

However, all other haptens react with skin proteins through the formation of stable covalent bonds. The majority of sensitizing molecules contain an electrophilic chemical function in their molecular structure that is able to react with nucleophilic groups in proteins via two electrons covalent bond formation.[26] In the literature, several electrophilic chemical groups reacting with nucleophilic functions of proteins are described (Table I.1).[11]

Table I.1 Classification of the main families of allergenic compounds referred as to the electrophilic chemical function encountered in the molecular structure and the mechanism by which they bind covalently to nucleophilic sites (Nu) of amino acids in proteins (⟶ = electrophilic chemical function, Nu = nucleophile).

Electrophilic site and hapten type	Molecular mechanism	Adduct	Hapten example
 alkyl halide X = Cl, Br, I	nucleophilic susbtitution on a saturated center	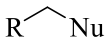	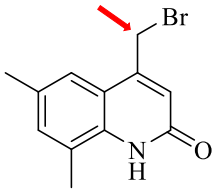 4-bromomethyl-6,8-dimethylquinolin-2(1H)-one
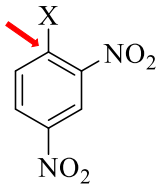 aryl halide X = F, Cl, Br, I	aromatic nucleophilic substitution on a non-saturated center	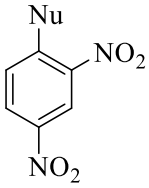	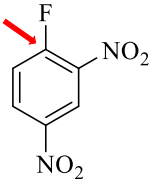 2,4-dinitrofluorobenzene
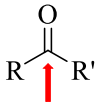 aldehyde : R' = H ketone : R' = alkyl or aryl	nucleophilic addition	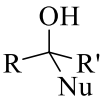	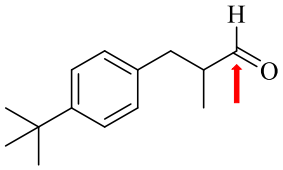 Lilial®
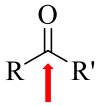 ester : R' = OR" amide : R' = NHR"	nucleophilic substitution on a non-saturated center	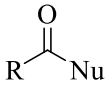	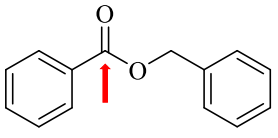 benzyl benzoate

Electrophilic site and hapten type	Molecular mechanism	Adduct	Hapten example
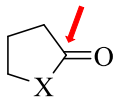 lactone : X = O lactame : X = NH	nucleophilic substitution on a non-saturated center	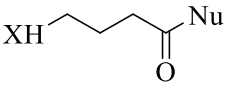	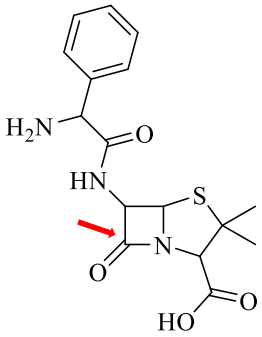 ampicilline
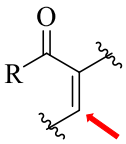 aldehyde, ketone or ester α,β-unsaturated R = H, R' or OR'	nucleophilic addition: 1,4-Michael addition	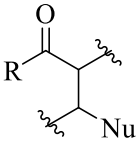	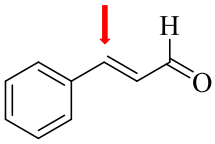 cinnamaldehyde

Amino acids cysteine and lysine are the most described in the literature but also other amino acids having electron-rich heteroatoms, such as histidine, can form covalent bonds with electrophilic haptens.[27]

1.3.2 Chemicals needing an activation to become reactive: pre- and pro-haptens

The terms pre- and pro-hapten (Figure I.5) describe a category of molecules initially non-reactive, that become sensitizing after a chemical transformation.

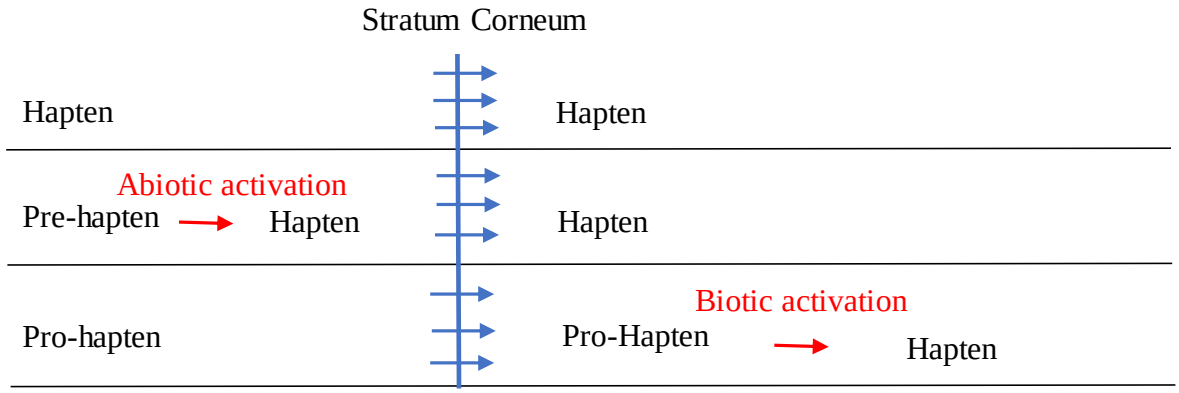

Figure I.5: Activation of different types of haptens[28]

Pre-haptens were described by Lepoittevin as intrinsically non-reactive molecules, which are abiotically transformed to reactive compounds by air oxidation (autoxidation) or photoactivation, for example.[29] Several studies have shown that allylic positions of many terpenes are oxidized during air exposition to form skin sensitizing hydroperoxides (Figure I.6).[30]

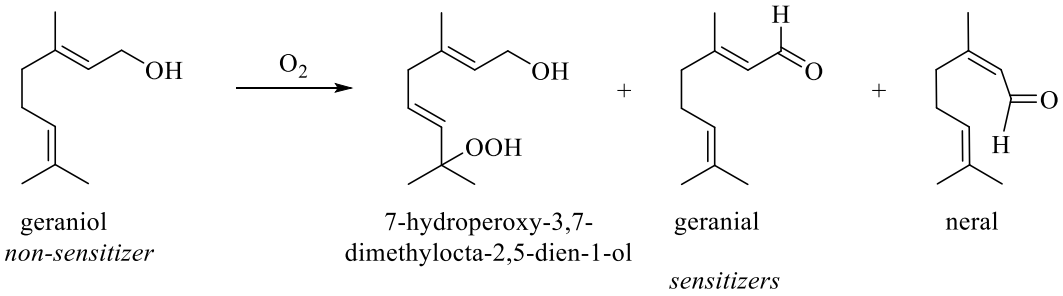

Figure I.6: Example of geraniol autoxidation: generation of an allylic skin sensitizing hydroperoxide among other sensitizers

Pro-haptens are intrinsically non-reactive molecules that need a biotic transformation to become reactive, mainly via enzymatic activation in the skin (Figure I.7). Two types of enzymes exist in the skin. Phase I enzymes are responsible for the oxidation of xenobiotics (alcohol dehydrogenases, monooxygenases, monoamine oxidases, etc.) and phase II enzymes are responsible for the

conversion of products generated by phase I enzymes in order to be eliminated (sulfotransferases, acetyltransferases, glutathione-S-transferases, etc.).[28] During these detoxication processes, reactive species can be formed and induce skin sensitization (Figure I.7).

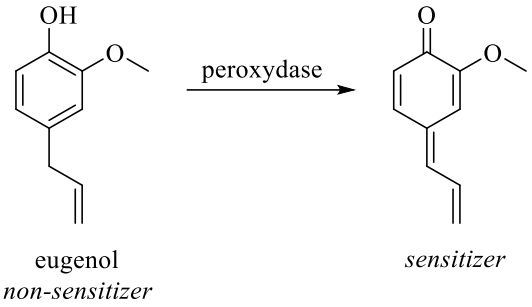

Figure I.7: Eugenol biotic activation

This Ph.D. thesis will focus on pre-haptens and more specifically in terpenes that easily autoxidize to form sensitizing allylic hydroperoxides. Terpenes are natural products used by plants as odorants to communicate with their environment but also as growth regulators. Terpenes are widespread in plants and largely used in perfumery because of their great smell.

The general chemical formula of terpenes is $(C_5H_8)n$ as they derive from units of isoprene. Dimethylallyl pyrophosphate (DMAPP) and isopentenyl pyrophosphate (IPP) are the components in the biosynthesis pathway of terpenes. When n (number of linked isoprene units) is equal to 2 the molecule is called monoterpene (i.e. geraniol, limonene, linalool), when n = 3 sesquiterpene (i.e. farnesol), when n = 4 diterpene (i.e. cafestol), etc.

2 PREDICTION OF THE SENSITIZING POTENTIAL

Historically, the sensitizing and allergenic potential of chemicals were evaluated by testing on animals. In 1959 Russell and Burch enunciated the deontological concept of the 3 R (replace, reduce, refine).[31] The idea was to "replace" animal testing by *in vitro* assays, maximally "reduce" the number of animals used and "refine" the techniques used in order to reduce animal suffering. However, the social pressure and several European directives have ended these practices especially in the cosmetics and fragrances context.

European directives and legislation are today asking the industry to do risk assessment concerning chemicals in order to protect human health and the environment. The REACH legislation

(Registration, Evaluation, Authorization, and Restriction of Chemical Substances) of the European Parliament and of the council from the 1st of June 2007 should allow collecting information on more than 30 000 compounds over eleven years. Moreover, REACH encourages the industry to use animal alternative assays to do toxicity assessment.[32] In 2013, animal testing for the evaluation of the toxicity of cosmetic ingredients was forbidden, as indicated in the 7th amendment to the European Directive on cosmetic products.[9]

Today and as consequence, several animal testing alternative methods have been developed for the evaluation of the sensitizing potential of chemicals and have been approved by the European Center for Validation of Alternative Methods (ECVAM), together with the establishment of OECD guidelines. These methods are based on different physiological steps leading to skin sensitization.

2.1 In vivo methods

First tests on allergens were done on human volunteers in 1936 by Landsteiner and Jacobs, they were followed by animal tests such as the guinea pig maximization test (GPMT), the mouse ear swelling test (MEST) and the mouse local lymph node assay (LLNA) developed by Kimber and Basketter in the 1990's.[33–35]

The LLNA, based on the sensitization phase of ACD, is today forbidden in the field of cosmetics even if it uses a decreased number of animals. As specified in the OECD guideline, this assay measures the lymphocytes proliferation after exposition to the chemical.[36] The chemical to test is dispensed on to the dorsum of the mouse ear once a day for five days. On the fifth-day, tritiated thymidine is injected into the animal. The animal is then sacrificed, and proximal lymph nodes of the mouse ear are excised. The proliferation is based on the measure of the radioactivity level. If the rate is three times higher compared to that of a not exposed control mouse, the molecule is considered as being a sensitizer. The concentration used to have a threefold factor proliferation of lymphocytes (EC_3) allows quantifying the sensitizing potential of the chemical tested and classify it as low, moderate or strong sensitizer.[37]

2.2 In silico methods

Different chemical and physical properties of compounds linked to a specific biological answer are the basis of computer models. *In silico* methods in skin allergy are essentially databases, expert softwares and studies on quantitative structure-activity relationships (QSARs). Databases compile information on observations of allergy cases in different hospitals, but a low number of cases are reported. Benezra *et al*. developed a complete general observation issued in *The Journal of Investigative Dermatology* from 1975 to 1982.[38] The resulting program was called PROPHET and allowed to search compounds by chemical structures. However, PROPHET collects just atypical ACD cases and it does not reflect the most relevant allergens in the general population.

Expert softwares search is based on molecular structures supposed to be protein reactive.[39,40] Among them, DEREK (Deduction and Estimation of Risk from Existing Knowledge) and TOPKAT (Toxicity Prediction by Computer Assisted Technology). DEREK was developed on the basis of 294 molecules assigned as allergenic by the GPMT. Heterocycle or aromatic cycles, ionizable functions and reactive chemical functions are considered. TOPKAT is also based on GPMT studies. It is able to predict if a poly-aromatic molecule is a skin sensitizer and for aliphatic structures it can distinguish the degree of the allergen potency from low to moderate and strong. That two softwares continue to be updated by new data.

One of the oldest QSARs is the RAI assay (Relative Alkylation Index), developed in the 1990's. The RAI is essentially based on electrophilic chemicals, their hydrophobic properties and the concentrations of the molecules tested.[41] As a QSAR method, it is based on chemical structures being linked to a biological response, in this case skin sensitization. It is assumed that the chemical structure of a molecule (chemical functions, geometric and electronic properties, etc.) is responsible for its chemical, physical and biological properties. QSARs give information on the toxicity and also on the intensity of the biological response and are based on a mathematical model activity being function of physicochemical properties. Most of them are recommended by the OECD and even a toolbox has been developed as software providing an approach to predict skin sensitization. All these softwares, based on the reaction mechanisms for the hapten-protein interaction, are very valuable but may be limited by contradictory results coming from *in vivo* methods such as the LLNA.[42]

2.3 In chemico methods

As described previously, the first key step in the sensitization process to a chemical is its ability to covalently bind to skin proteins in order to form the antigenic complex. Based on this, it might be supposed that more a molecule is able to react with amino acids in proteins the more this molecule has a sensitizing potential. This was the basis for Gerberick *et al*. to develop the Direct Peptide Reactivity Assay (DPRA) in 2004, an hapten-peptide based reactivity assay.[43] The test compound is incubated for 24 hours with a peptide, then the depletion of the peptide is measured using high-performance liquid chromatography (HPLC) coupled to a UV detection. At the beginning and to develop the assay, glutathione and three synthetic peptides were used. The main sequence is *N*-Ac-Arg-Phe-Ala-Ala-X-Ala-Ala, X being cysteine, histidine or lysine. The final assay was developed with cysteine and lysine peptides as they gave the more accurate and reproducible results. A decisional tree was then built allowing the classification of allergens according to their reactivity (Figure I.8).[44]

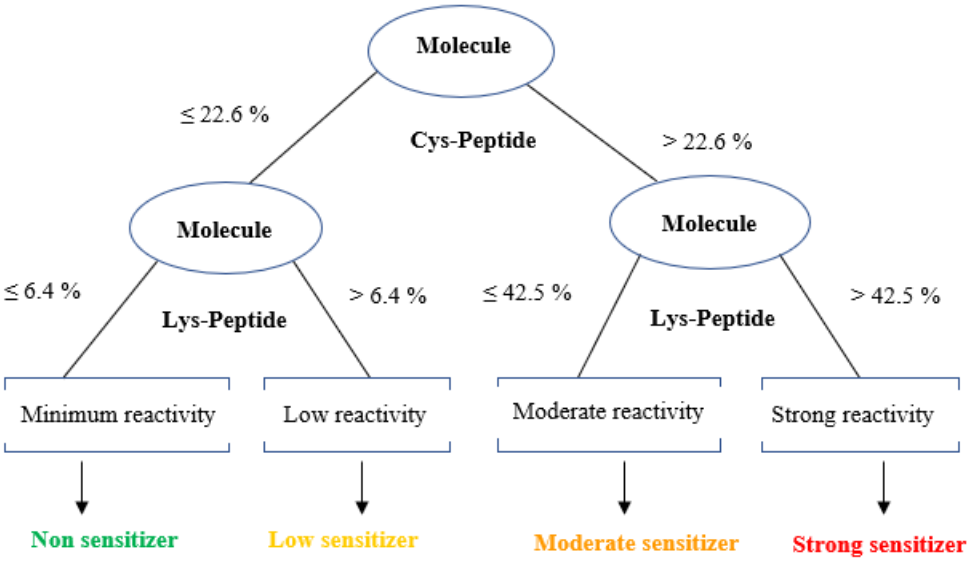

Figure I.8: Decisional tree from DPRA classifying sensitizers according to their reactivity toward Cys-Pep and Lys-Pep

The study of 82 molecules led to the identification of 89 % of them as allergens with a good correlation between their sensitizing potential and their reactivity against peptides Cys-Pep and Lys-Pep. The DPRA was validated by ECVAM in 2012 and has an OECD guideline.[45] A major

drawback of DPRA was that it only could be applied to directly reactive chemicals or haptens, not considering the case of pre- and pro-haptens. To solve this issue, Gerberick *et al.* developed a second-generation test, the Peroxidase Peptide Reactivity Assay (PPRA) in which an oxidation step was added to the system by using the tandem horseradish peroxidase/hydrogen peroxide.[46]

Other *in chemico* methods exist based on mass spectroscopy or the use of glutathione, but DPRA is today the only validated method representing the first key step of the Adverse Outcome Pathway (AOP) defined for skin sensitization, to say the hapten covalent modification of epidermal proteins.[47]

2.4 In vitro methods

In vitro validated methods are based on the key steps in the AOP described for skin sensitization considering activation of epidermal keratinocytes and DCs.

The KeratinoSens® assay is based on genetically modified human cells.[48] Keratinocytes are able to synthesize the enzyme luciferase in presence of sensitizers, as described in its OECD guideline.[49] This enzyme is fluorescent when the substrate luciferin is present. It is based on the human keratinocytes cell line HaCaT, transfected in a stable manner by a gene coding for luciferase. After 48 hours of incubation with the test compound, luciferase substrate is added and luminescence is measured after 20 minutes. Luciferase induction is then correlated to the concentration needed to induce 1.5 induction. An induction rate (EC 1.5) higher to the threshold of 1.5 of luciferase activity (corresponding to a 50 % increase of the gene activity) is considered as predicting a significant positive answer.

The MUSST (Myeloid U937 Skin Sensitization Test) and the h-CLAT (human Cell Line Activation Test) are two methods based on here activation of DCs.[50] In these assays, the cell surface protein expression is measured when exposed to a sensitizer. Indeed, the cell surface proteins CD54 and CD86 are overexpressed when cells are exposed to an allergen. In both tests, after 24 hours in h-CLAT and 48 hours in MUSST, of exposition of cells to the allergen, CD54 and CD86 are overexpressed and measured by flow cytometry. The difference for both tests is the cell type used. h-CLAT uses the THP-1 cell line, a human monocytic cell-line, and MUSST uses myeloid cells

type 937.[51,52] The results show a correlation between the sensitization potential and the overexpression of cell surface proteins.

3 PRESENTATION OF THE SUBJECT

3.1 Hapten-protein interaction: radical mechanisms

As already discussed above, ACD is an adverse reaction of the immune system towards low-molecular-weight chemicals also called haptens. It is a delayed type hypersensitivity reaction dealing with T-cells.[17] Chemical allergen molecules, too small to be recognized by the immune system, first react with skin proteins through the formation of stable covalent bonds. The so formed antigenic complex will then be recognized by the immune system which will lead to the delayed type hypersensitivity process. Most of the time the hapten-protein interaction occurs via the reaction of an electrophilic chemical function present in the allergen and nucleophilic chemical functions present in the lateral chain of some amino acids via a two-electrons mechanism (Figure I.9). However, some allergenic substances do not fit in this reaction pattern. For these, one electron radical mechanisms are suspected.

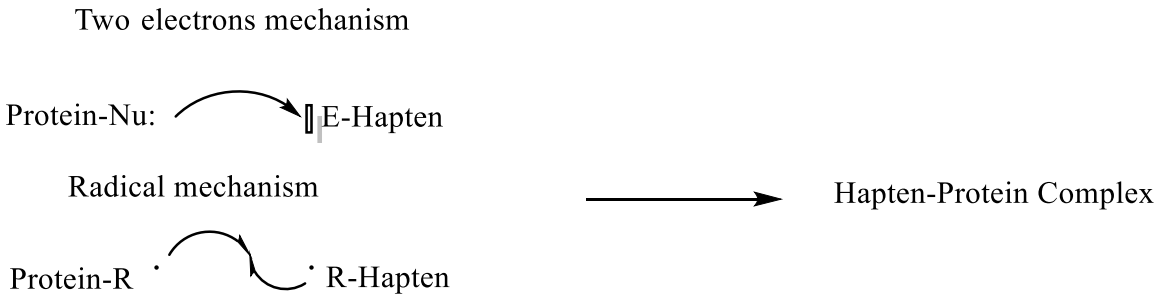

Figure I.9: Hapten-protein reaction mechanisms via two-electrons and radical pathways

This is the case for sensitizing allylic hydroperoxides derived from autoxidation of natural terpenes widely used in fragrance compositions.

Terpenes such as limonene and linalool form, after air exposure, limonene hydroperoxides and linalool hydroperoxides as primary oxidation products (Figure I.10).[53,54] These autoxidation products have been described as strong sensitizing compounds.[55]

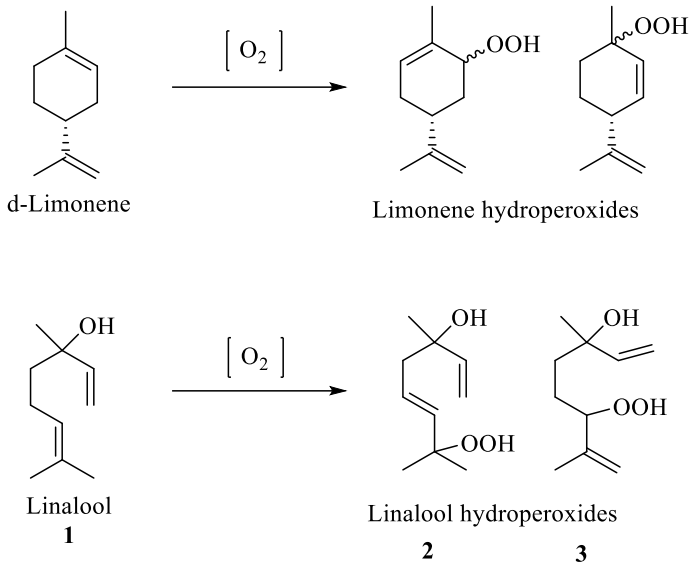

Figure I.10: Limonene and linalool autoxidation primary products

Allylic hydroperoxides derived from autoxidation of limonene and linalool are not electrophilic compounds. However, they can easily form radical intermediates by cleavage of the O-O-bond of the hydroperoxide chemical function, through electronic transition mechanism leading to alkoxy radical and hydroxyl ions.

In the laboratory Kao *et al*. showed that linalool hydroperoxide **2** may form antigenic complexes most probably via radical mechanisms starting with the cleavage of O-O bond of weak dissociation energy (175 kJ/mol^{-1}).[56] Cleavage of the O-O bonds, is thus an easy process affording unstable alkoxyl radicals RO•, which rapidly can lead via intramolecular cyclization, β-scission or hydrogen abstraction to the formation of longer half-life carbon-centered radicals R• (Figure I.11).

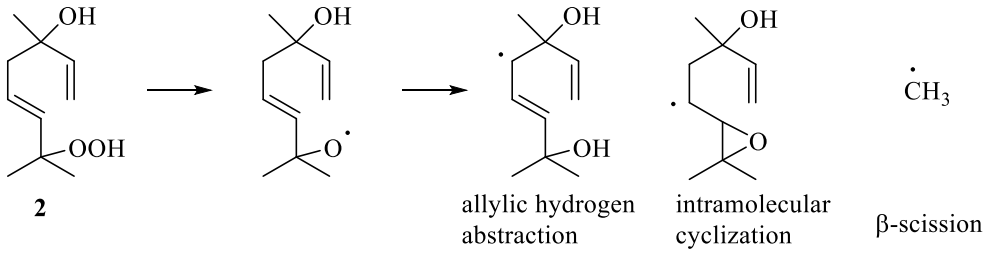

Figure I.11: Radical intermediates derived from linalool hydroperoxide **2**

For risk assessment commitments, studies helping to understand all mechanisms leading to allergic reactions by chemical sensitizers are essential in order to cover all categories of molecules.

This Ph.D. work focuses on the identification of free radicals derived from skin sensitizing substances and in the study of their involvement in ACD, from the molecule to the tissue.

3.2 Target compounds: allylic hydroperoxides derived from autoxidation of limonene and linalool

Many natural terpenes are used in fine perfumes, cosmetics, household and industrial products due to their odorant properties. Among them, limonene (Limo) and linalool (Lina) are probably the most used. Both belong to the pre-haptens category of skin sensitizers as they need to autoxidize to form reactive and sensitizing derived products. The general mechanism for autoxidation processes is described in Figure I.12. The first step or initiation, probably induced by daylight, heat or a catalytic amount of metal, generates radicals R• from organic compounds.

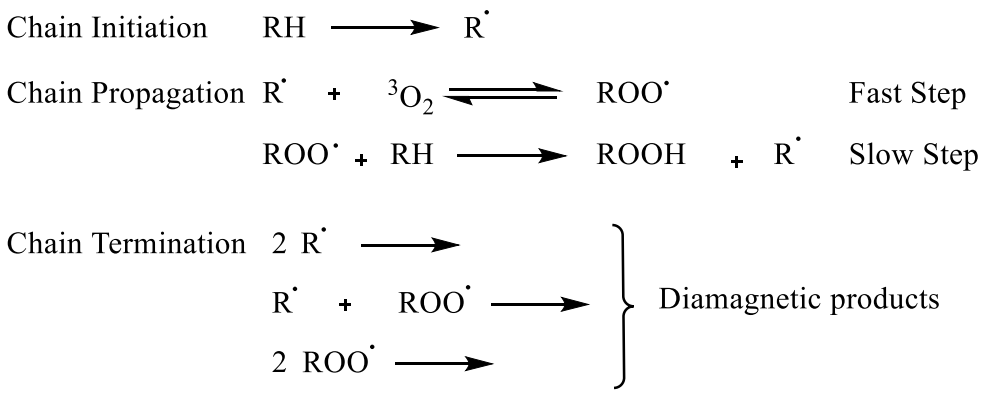

Figure I.12: Autoxidation general mechanism

Then, in a second step called propagation, radicals R• can react with triplet state oxygen $^3O_2$ to form peroxyl radicals ROO•, which are able to abstract a hydrogen from an organic compound to form a hydroperoxide and a new radical R•. Hydrogen abstraction is a slower step favorized by the presence of labile hydrogens such as allylic hydrogens in terpenes. The final step or termination concerns two radical interactions such as R• and ROO• forming a non-radical substance or diamagnetic products.

As it was shown in Figure I.10 primary autoxidation derivatives of Limo and Lina, are allylic hydroperoxides. Secondary autoxidation products are epoxides, ketones and diols (Figure I.13).

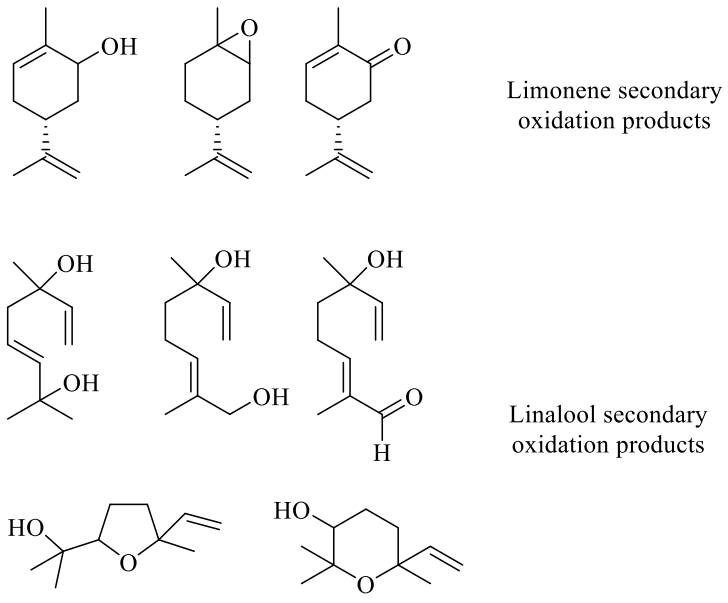

Figure I.13: Limonene and linalool secondary autoxidation products

Limo and Lina allylic hydroperoxides have been classified as moderate to strong sensitizers in the mouse local lymph node assay (LLNA), with LLNA EC_3 values between 0.3 and 1.6 % (Table I.2), whereas Limo and Lina are classified as non-sensitizers.[28,57,58]

Table I.2: LLNA EC_3 values for Limo, Lina and derived autoxidation allylic hydroperoxide

Terpene	EC_3	EC_3 Oxidation mixture	Target compounds	EC_3 [a)]
Limonene	30	3.0	Lim-1-OOH	0.33
			Lim-2-OOH	0.83
Linalool	46.2	9.4	Lin-OOH (mix two OOH)	1.6

a) The EC_3 value is the estimated concentration of chemical necessary to cause a 3-fold increase in its proliferating activity. Skin sensitization classification up to EC_3 values: < 0.1 % extreme, 0.1-< 1 % strong, 1-< 10 % moderate and 10-< 100 % non-sensitizer.

Clinical data have also shown frequent allergic reactions to Lina and Limo hydroperoxides. In an European multicenter study, patch tests on 2900 consecutive patients resulted in 5.2 % positive reactions to oxidized limonene 3 % in petrolatum (Limo-OOHs 0.33 %) and 6.9 % positive reactions to oxidized linalool 6 % in petrolatum (Lina-OOHs 1 %). Also, a repeated open application test study (ROAT) showed that repeated exposure to low concentrations of oxidized linalool elicited ACD in sensitized patients.[59–62]

Target compounds for this study were Limo and Lina hydroperoxides (Figure I.14). Commercial cumene hydroperoxide (Cum-OOH) and a synthetic monocycle hydroperoxide (Mod-OOH) have been used as reference compounds for some of the studies developed here. Cum-OOH is a reference molecule widely used in Electron Paramagnetic Resonance studies and Mod-OOH is a model molecule for the study of allergenic 15-hydroperoxiabietic acid.[63,64]

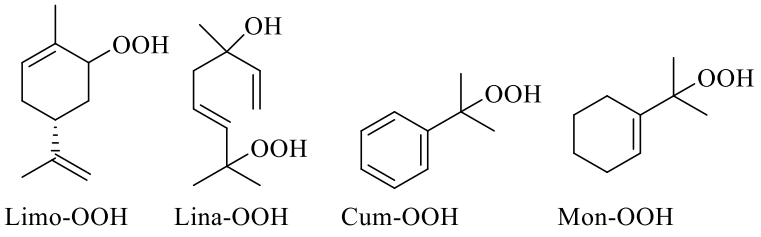

Figure I.14: Target compounds: limonene hydroperoxide, linalool hydroperoxides, cumene hydroperoxide and monocycle hydroperoxide

It is believed that allergenic antigens are formed from carbon-centered radicals issued from the cleavage of the hydroperoxide O-O bond (Figure I.15).

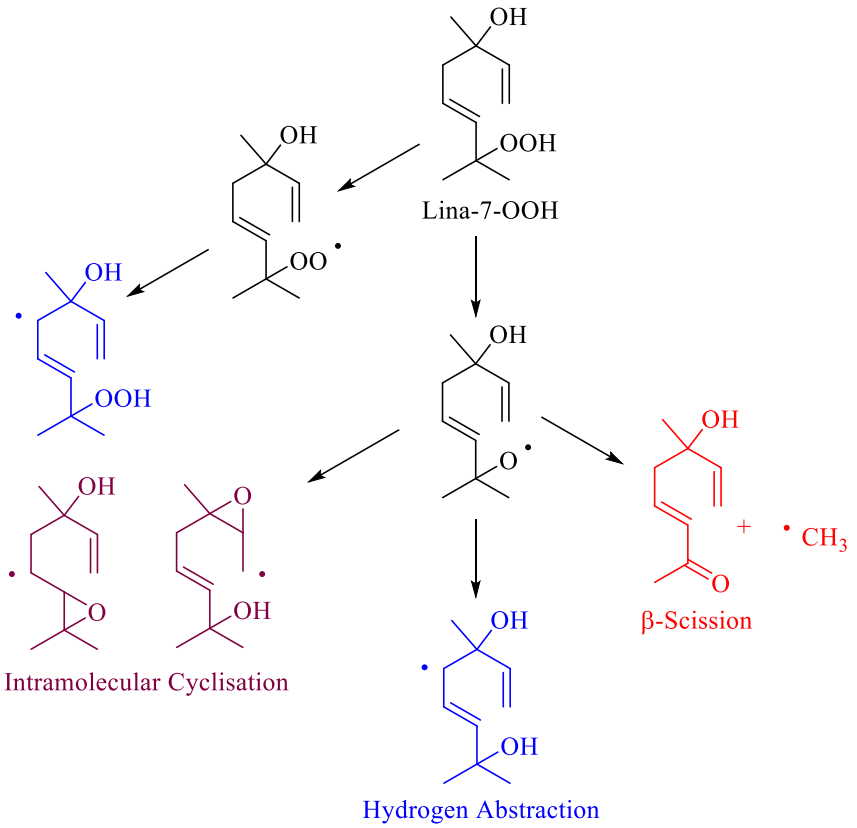

Figure I.15: Different types of radical intermediate issued from Lina-7-OOH based on Kao *et al.*[56]

3.3 Project structure

Radical mechanisms have been poorly considered in the skin allergy field, and therefore little studied to be firmly demonstrated. This project aimed at understanding alternative haptenation processes in skin sensitization involving radical mechanisms. In parallel, skin sensitizers derived from oxidation processes, enzymatic or not, are often potent oxidants able to interfere with the cellular redox balance. There is a real belief that oxidative stress induced by these compounds on epithelial cells may produce a new danger signal for the immune system, synergistic with reactivity, and thus would greatly help to explain the strong allergenic activity. This PhD work was thus based on studies helping to understand radical mechanisms leading to epidermal protein modifications by allylic hydroperoxides and cellular redox homeostasis perturbation because of the inherent oxidative potential related to the chemical structure.

The work has been built on the basis of three complementary approaches: *in chemico* by conducting reactivity studies, *in situ* by studying the behavior in reconstructed human epidermis tissue model, and *in cellulo* by evaluating the response from DCs to the danger signals produced.

Objectives and deliverables of the project were:

1) to understand, from a chemical reactivity profile level, the contribution of radical mechanisms on the formation of antigenic complexes;

2) to examine the *in situ* production of these danger signals (radical modifications of amino acids, stress induction) on a reconstructed human epidermis (RHE) model;

3) to investigate *in cellulo* the influence of oxidative stress on the allergenic potential of the chemicals.

For fulfilling the objectives, the work has been built around three major chapters.

3.3.1 Chemical reactivity profile through radical mechanisms

For many years it has been demonstrated in the laboratory the formation of oxygen alkoxyl RO• / peroxyl ROO• and carbon-centered R• free radicals derived from several allylic hydroperoxides, by using chemical trapping and electron paramagnetic resonance spectroscopy (EPR) associated to spin-trapping techniques.[56,65–67] The generation of these radicals could be thus possible *in vivo*, in the epidermis, once molecules have penetrated into the skin. This is substantial information indicating that if a certain number of reactive radical intermediates can issue from these compounds, different potentially immunogenic chemical modifications are possible on proteins leading to sensitization. Preliminary studies carried out on their reactivity toward amino acids, followed by NMR and LC-MS, corroborated the formation of adducts originating from radical reactions, together with redox processes producing chemical modifications of the amino acids.[68] However, elucidation of the exact chemical structure of reaction products was difficult, isolation complex, NMR identification not sensitive enough and MS did not discriminate adducts with the same *m/z* value formed at different radical positions. The use in the laboratory of NMR techniques with ^{13}C-substituted molecules has been shown to be a very effective tool for the investigation of

hapten-protein interaction mechanisms.[69] In here, it was decided to use ^{13}C-substituted compounds to elucidate the exact molecular structure of hapten-amino acid adducts involving radical mechanisms. Lina-7-OOH, one of the culprits for the allergenic potential of autoxidized linalool was chosen as target compound. Indeed Kao *et al*. showed previously that Lina-7-OOH decomposes in the presence of ferrous salts affording carbon R• free radicals at different positions (Figure I.16).[56] It was thus decided to synthesize Lina-7-OOH ^{13}C-substituted at carbon positions that are precursors of these potentially reactive radicals.

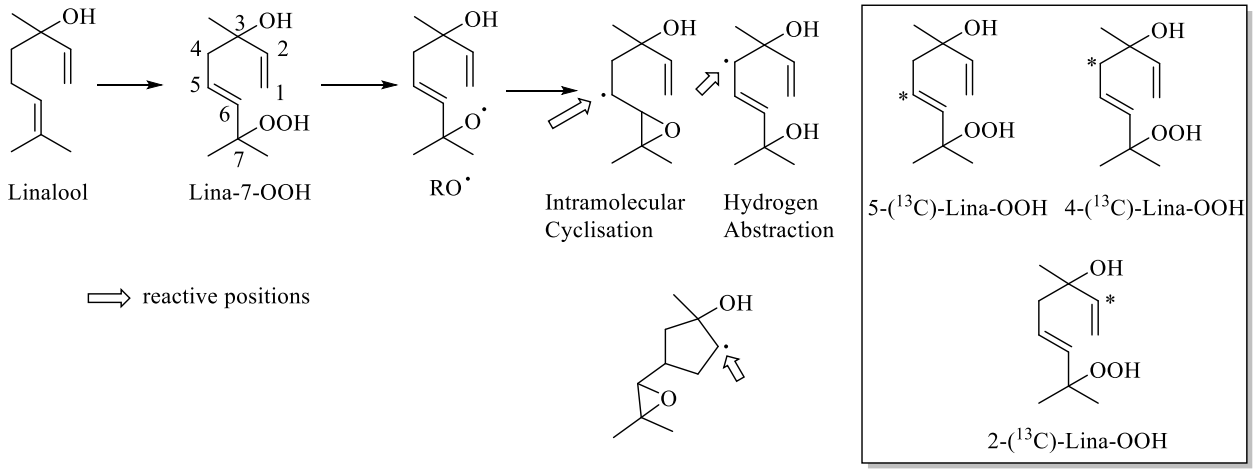

Figure I.16: ^{13}C-target compounds: 5-(^{13}C)-Lina-OOH, 4-(^{13}C)-Lina-OOH and 2-(^{13}C)-Lina-OOH

Further, the reactivity profile toward several amino acids prompt to radical reactions was studied by qualitative mechanistic studies based on one-dimensional ^{13}C-NMR and two-dimensional ^{1}H-^{13}C correlation NMR experiments (HSQC, HMBC). The main objective was to provide a data set of spectroscopic data and likely reaction mechanisms and to enlight if there is any specificity related to the fixation of a specific carbon radical with a certain amino acid.

3.3.2 In situ investigation of danger signals production in reconstructed human epidermis (RHE)

In collaboration with Dr. Bertrand Vileno, POMAM Laboratory, Magnetic and Optical Properties of Molecular Architectures, University of Strasbourg-CNRS UMR 7177

Electron paramagnetic resonance (EPR) is one of the major investigative tools for the study of radical species. EPR has been successfully used in biology to understand many physiological processes ranging from *in vivo* detection/characterization of reactive nitrogen/oxygen species and tumors oximetry, to the assessment of redox state in biological tissues.[70] EPR has also been successfully used for dermatological purposes and skin research, such as detection of free radicals in UV-irradiated skin, melanoma investigation and *in vivo* EPR imaging, a non-invasive method able to measure the distribution and decay of free radicals in the skin of human volunteers. Besides, EPR spectroscopy has been applied to probe free radical processes in skin cells in culture or skin biopsies.[71]

Keratinocytes represent the major cell type in the epidermis and play a key role in skin inflammatory reactions.[72] The Episkin™ reconstructed human epidermis (RHE) model (Lyon, France) consists of a normal human multi-layered keratinocytes culture that is histologically similar to human epidermis. In here we developed the use of EPR spin-trapping techniques to follow, in this RHE model, the behavior of radicals issued from allylic hydroperoxides and the production of danger signals (radical reactivity, oxidative stress) for the immune system. To do so, allylic hydroperoxides derived from autoxidation of linalool (Lina), and limonene (Limo) and commercial Cum-OOH were employed (Figure I.17). The methodology was firstly optimized in solution and further transferred to the use of Episkin™ RHE.

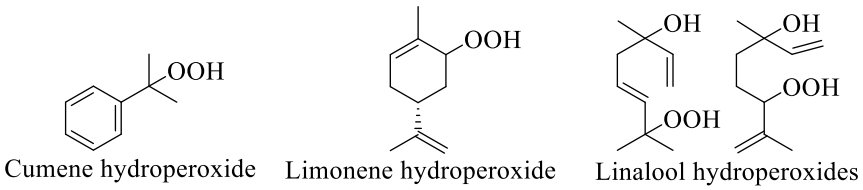

Figure I.17: Allylic hydroperoxide models for EPR study

The major aim was the detection and characterization of free radical spin adducts testimony of radicals derived from R-OOHs in a human skin model, and to probe their behavior and decay.

3.3.3 Measure of oxidative stress in cellulo

In collaboration with Pr. Saadia Kerdine-Römer, Allergy, Immunotoxicology and Immunopharmacology, University Paris Sud-INSERM UMR 996

The Keap1-Nrf2 cellular sensor pathway, implicated in the antioxidant response of cells, can detect chemical and oxidative stresses. Under normal conditions, the Kelch-like ECH-associated protein 1 (Keap1) sequesters the transcriptional regulator nuclear factor-erythroid 2-related factor (Nrf2) in the cytoplasm provoking its proteasomal degradation. In the presence of chemicals or oxidants, cysteine residues of Keap1 are chemically modified leading to its dissociation from Nrf2. Nrf2 translocate then to the nucleus and forms heterodimers with MAF proteins inducing the transcription of antioxidant genes such as heme oxygenase-1 (*ho-1*) and NADPH quinone oxidoreductase 1 (*nqo1*). Keap1-Nrf2 is thus one of the cellular sensor mechanisms that recognize intrinsic chemical reactivity of molecules. A collaboration conducted with the Allergy Immunotoxicology and Immunopharmacology Unit at INSERM UMR 996 shows that allergens, depending on their chemical structure, may also activate the Nrf2 pathway in DCs.[73] The aim herein was to evaluate how the inherent oxidative properties of allylic hydroperoxides, together with their reactivity through radical mechanisms, behave as danger signals and translate into a biological response using the activation of the Nrf2 pathway, assessed by the induction of Nrf2-target genes (*ho-1, nqo1* and *il8*) involved in detoxification and anti-oxidant effects. Four allylic hydroperoxides of different chemical structures were used the monocyclic model (Mod-OOH), cumene hydroperoxide (Cum-OOH) and the allergenic hydroperoxides derived from autoxidation of linalool (Lina) and limonene (Limo)) and tested in a model of human dendritic cells, measuring target antioxidant genes production by real-time PCR (Figure I.18). The DCs phenotype status and Nrf2 cytoplasm accumulation were studied by Western Blot.

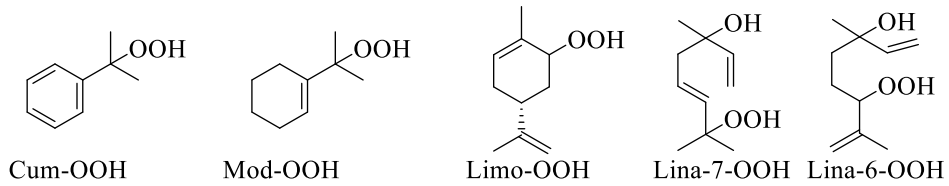

Figure I.18: Allylic hydroperoxide models for Keap1-Nrf2 activation study

Literature

(1) Peiser, M.; Tralau, T.; Heidler, J.; Api, A. M.; Arts, J. H. E.; Basketter, D. A.; English, J.; Diepgen, T. L.; Fuhlbrigge, R. C.; Gaspari, A. A.; et al. Allergic Contact Dermatitis: Epidemiology, Molecular Mechanisms, in Vitro Methods and Regulatory Aspects: Current Knowledge Assembled at an International Workshop at BfR, Germany. *Cell. Mol. Life Sci.* **2012**, *69* (5), 763–781.

(2) Lepoittevin, J.-P.; Benezra, C. Allergic Contact Dermatitis Caused by Naturally Occurring Quinones. *Pharm. Weekbl. Sci.* **1991**, *13* (3), 119–122.

(3) Mitchell, J. C. Allergy to Lichens: Allergic Contact Dermatitis From Usnic Acid Produced by Lichenized Fungi. *Arch. Dermatol.* **1965**, *92* (2), 142.

(4) Heydorn, S.; Menné, T.; Andersen, K. E.; Bruze, M.; Svedman, C.; White, I. R.; Basketter, D. A. Citral a Fragrance Allergen and Irritant. *Contact Dermatitis* **2003**, *49* (1), 32–36.

(5) Connolly, M.; Buckley, D. A. Contact Dermatitis from Propylene Glycol in ECG Electrodes, Complicated by Medicament Allergy. *Contact Dermatitis* **2004**, *50* (1), 42.

(6) Johnson, R. C.; Elston, D. M. Wrist Dermatitis: Contact Allergy to Neoprene in a Keyboard Wrist Rest. *Am. J. Contact Dermat.* **1997**, *8* (3), 172–174.

(7) Bercovitch, L.; Luo, J. Cellphone Contact Dermatitis with Nickel Allergy. *Can. Med. Assoc. J.* **2008**, *178* (1), 23–24.

(8) Ryberg, K.; Isaksson, M.; Gruvberger, B.; Hindsen, M.; Zimerson, E.; Bruze, M. Contact Allergy to Textile Dyes in Southern Sweden. *Contact Dermatitis* **2006**, *54* (6), 313–321.

(9) Directive 2003/15/EC of the European Parliament and of the Council of 27 February 2003 Amending Council Directive 76/768/EEC on the Approximation of the Laws of the Member States Relating to Cosmetic Products. 7th Amendment to the European Cosmetics Directive. Off. J. Eur. Union. **2003**, L66, 26-35.

(10) Gell, P. G. H.; Coombs, R. R. A. Classification of Allergic Reaction Responsible for Clinical Hypersensitivity and Disease. In: Clinical Aspects of Immunology. Blackwell Scientific Publication, Oxford, United Kingdom, **1975**, 761-781.

(11) Karlberg, A.-T.; Bergström, M. A.; Börje, A.; Luthman, K.; Nilsson, J. L. G. Allergic Contact Dermatitis—Formation, Structural Requirements, and Reactivity of Skin Sensitizers. *Chem. Res. Toxicol.* **2008**, *21* (1), 53–69.

(12) *Encyclopædia Britannica 2013.*; Focus Multimedia Ltd.: Rugeley, **2012**.

(13) Tortora, G. J. *Principles of Anatomy and Physiology*; J. Wiley: Hoboken, USA, 2007.

(14) Proksch, E.; Brandner, J. M.; Jensen, J.-M. The Skin: An Indispensable Barrier. *Exp. Dermatol.* **2008**, *17* (12), 1063–1072.

(15) McLafferty, E.; Hendry, C.; Farley, A. The Integumentary System: Anatomy, Physiology and Function of Skin. *Nurs. Stand.* **2012**, *27* (3), 35–42.

(16) Merad, M.; Sathe, P.; Helft, J.; Miller, J.; Mortha, A. The Dendritic Cell Lineage: Ontogeny and Function of Dendritic Cells and Their Subsets in the Steady State and the Inflamed Setting. *Annu. Rev. Immunol.* **2013**, *31* (1), 563–604.

(17) Martin, S. F. Immunological Mechanisms in Allergic Contact Dermatitis. *Curr. Opin. Allergy Clin. Immunol.* **2015**, *15* (2), 124–130.

(18) Saint-Mezard, P.; Berard, F.; Dubois, B.; Kaiserlian, D.; Nicolas, J.-F. The Role of CD4+ and CD8+ T Cells in Contact Hypersensitivity and Allergic Contact Dermatitis. *Eur. J. Dermatol. EJD* **2004**, *14* (3), 131–138.

(19) Santin, A. D.; Hermonat, P. L.; Ravaggi, A.; Chiriva-Internati, M.; Cannon, M. J.; Hiserodt, J. C.; Pecorelli, S.; Parham, G. P. Expression of Surface Antigens during the Differentiation of Human Dendritic Cells vs Macrophages from Blood Monocytes in Vitro. *Immunobiology* **1999**, *200* (2), 187–204.

(20) Hsieh, C.-S.; Macatonia, S. E.; Tripp, C. S.; Wolf, S. F.; O'Garra, A.; Murphy, K. M. Development of TH1 CD4+ T Cells through IL-12 Produced by Listeria-Induced Macrophages. 1993. *J. Immunol. Baltim. Md 1950* **2008**, *181* (7), 4437–4439.

(21) Martin, S. F.; Esser, P. R.; Weber, F. C.; Jakob, T.; Freudenberg, M. A.; Schmidt, M.; Goebeler, M. Mechanisms of Chemical-Induced Innate Immunity in Allergic Contact Dermatitis: Contact Allergen-Induced Innate Immunity. *Allergy* **2011**, *66* (9), 1152–1163.

(22) Thyssen, J. P.; Ross-Hansen, K.; Menné, T.; Johansen, J. D. Patch Test Reactivity to Metal Allergens Following Regulatory Interventions: A 33-Year Retrospective Study. *Contact Dermatitis* **2010**, *63* (2), 102–106.

(23) Qin, R.; Lampel, H. P. Review of Occupational Contact Dermatitis—Top Allergens, Best Avoidance Measures. *Curr. Treat. Options Allergy* **2015**, *2* (4), 349–364.

(24) Martin, S. F. New Concepts in Cutaneous Allergy. *Contact Dermatitis* **2015**, *72* (1), 2–10.

(25) Landsteiner, K.; Jacobs, J. Studies on the sensitization of animals with simple chemical compounds. *J. Exp. Med.* **1935**, *61* (5), 643–656.

(26) Divkovic, M.; Pease, C. K.; Gerberick, G. F.; Basketter, D. A. Hapten-Protein Binding: From Theory to Practical Application in the in Vitro Prediction of Skin Sensitization. *Contact Dermatitis* **2005**, *53* (4), 189–200.

(27) Lepoittevin, J.-P.; Benezra, C. 13C-Enriched Methyl Alkanesulfonates: New Lipophilic Methylating Agents for the Identification of Nucleophilic Amino Acids of Proteins by NMR. *Tetrahedron Lett.* **1992**, *33* (27), 3875–3878.

(28) Karlberg, A.-T.; Börje, A.; Duus Johansen, J.; Lidén, C.; Rastogi, S.; Roberts, D.; Uter, W.; White, I. R. Activation of Non-Sensitizing or Low-Sensitizing Fragrance Substances into Potent Sensitizers - Prehaptens and Prohaptens. *Contact Dermatitis* **2013**, *69* (6), 323–334.

(29) Lepoittevin, J.-P. Metabolism versus Chemical Transformation or Pro- versus Prehaptens? *Contact Dermatitis* **2006**, *54* (2), 73–74.

(30) Bråred Christensson, J.; Matura, M.; Bäcktorp, C.; Börje, A.; Nilsson, J. L. G.; Karlberg, A.-T. Hydroperoxides Form Specific Antigens in Contact Allergy. *Contact Dermatitis* **2006**, *55* (4), 230–237.

(31) Russell, W. M. S.; Burch, R. L. *The Principles of Humane Experimental Technique*, Methuen.; London, **1959**.

(32) Regulation (EC) No 1907/2006 of the European Parliament and of the Council of 18 December 2006 Concerning the Registration, Evaluation, Authorisation and Restriction of Chemicals (REACH), Establishing a European Chemicals Agency, Amending Directive 1999/45/EC and Repealing Council Regulation (EEC) No 793/93 and Commission Regulation (EC) No 1488/94 as Well as Council Directive 76/769/EEC and Commission Directives 91/155/EEC, 93/67/EEC, 93/105/EC and 2000/21/EC. *Off. J. Eur. Union* **2006** L 396, 1 - 849.

(33) Landsteiner, K. Jacobs, J. Studies on the sensitization of animals with simple chemical compounds. II. *J. Exp. Med.* **1936**, *64* (4), 625–639.

(34) Gad, S. C.; Dunn, B. J.; Dobbs, D. W.; Reilly, C.; Walsh, R. D. Development and Validation of an Alternative Dermal Sensitization Test: The Mouse Ear Swelling Test (MEST). *Toxicol. Appl. Pharmacol.* **1986**, *84* (1), 93–114.

(35) Kimber, I.; Basketter, D. A. The Murine Local Lymph Node Assay: A Commentary on Collaborative Studies and New Directions. *Food Chem. Toxicol.* **1992**, *30* (2), 165–169.

(36) OECD. *Test No. 429: Skin Sensitisation*; OECD Guidelines for the Testing of Chemicals, Section 4; OECD Publishing, **2010**.

(37) Gerberick, G. F.; Ryan, C. A.; Kern, P. S.; Dearman, R. J.; Kimber, I.; Patlewicz, G. Y.; Basketter, D. A. A Chemical Dataset for Evaluation of Alternative Approaches to Skin-Sensitization Testing. *Contact Dermatitis* **2004**, *50* (5), 274–288.

(38) Benezra, C.; Sigman, C. C.; Perry, L. R.; Helmes, C. T.; Maibach, H. I. A Systematic Search for Structure-Activity Relationships of Skin Contact Sensitizers: Methodology. *J. Invest. Dermatol.* **1985**, *85* (4), 351–356.

(39) Barratt, M. D.; Basketter, D. A.; Chamberlain, M.; Admans, G. D.; Langowski, J. J. An Expert System Rulebase for Identifying Contact Allergens. *Toxic. In Vitro* **1994**, *8* (5), 1053–1060.

(40) Fedorowicz, A.; Singh, H.; Soderholm, S.; Demchuk, E. Structure−Activity Models for Contact Sensitization. *Chem. Res. Toxicol.* **2005**, *18* (6), 954–969.

(41) Roberts, D. W.; Fraginals, R.; Lepoittevin, J. P.; Benezra, C. Refinement of the Relative Alkylation Index (RAI) Model for Skin Sensitization and Application to Mouse and Guinea-Pig Test Data for Alkyl Alkanesulphonates. *Arch. Dermatol. Res.* **1991**, *283* (6), 387–394.

(42) Roberts, D. W.; Patlewicz, G.; Dimitrov, S. D.; Low, L. K.; Aptula, A. O.; Kern, P. S.; Dimitrova, G. D.; Comber, M. I. H.; Phillips, R. D.; Niemelä, J.; et al. A Mechanistic Evaluation of an External Validation Study Using Reaction Chemistry Principles. *Chem. Res. Toxicol.* **2007**, *20* (9), 1321–1330.

(43) Gerberick, G. F. Vassallo, J. D. Bailey, R. E. Chaney, J. G. Morrall, S. W. Lepoittevin, J. P. Development of a Peptide Reactivity Assay for Screening Contact Allergens. *Toxicol. Sci.* **2004**, *81* (2), 332–343.

(44) Gerberick, G. F.; Vassallo, J. D.; Foertsch, L. M.; Price, B. B.; Chaney, J. G.; Lepoittevin, J.-P. Quantification of Chemical Peptide Reactivity for Screening Contact Allergens: A Classification Tree Model Approach. *Toxicol. Sci.* **2007**, *97* (2), 417–427.

(45) OECD Guideline for the testing of chemicals. Skin sensitization: Local lymphnode assay. OECD testing guidelines 429 (**2010**).

(46) Gerberick, G. F.; Troutman, J. A.; Foertsch, L. M.; Vassallo, J. D.; Quijano, M.; Dobson, R. L. M.; Goebel, C.; Lepoittevin, J.-P. Investigation of Peptide Reactivity of Pro-Hapten Skin Sensitizers Using a Peroxidase-Peroxide Oxidation System. *Toxicol. Sci.* **2009**, *112* (1), 164–174.

(47) Reisinger, K.; Hoffmann, S.; Alépée, N.; Ashikaga, T.; Barroso, J.; Elcombe, C.; Gellatly, N.; Galbiati, V.; Gibbs, S.; Groux, H.; et al. Systematic Evaluation of Non-Animal Test Methods for Skin Sensitisation Safety Assessment. *Toxicol. In Vitro* **2015**, *29* (1), 259–270.

(48) Andreas, N.; Caroline, B.; Leslie, F.; Frank, G.; Kimberly, N.; Allison, H.; Heather, I.; Robert, L.; Stefan, O.; Hendrik, R.; et al. The Intra- and Inter-Laboratory Reproducibility and Predictivity of the KeratinoSens Assay to Predict Skin Sensitizers in Vitro: Results of a Ring-Study in Five Laboratories. *Toxicol. In Vitro* **2011**, *25* (3), 733–744.

(49) OECD Guideline for the testing of chemicals: In Chemico skin sensitization: Direct Peptide Reactivity Assay (DPRA)OECD Testing Guidelines 442c (2015).

(50) OECD Guideline for the testing of chemicals: In vitro skin sensitization: ARE-Nrf2 luciferase Test method. OECD testing guideline 442d (2015).

(51) Nukada, Y.; Ashikaga, T.; Miyazawa, M.; Hirota, M.; Sakaguchi, H.; Sasa, H.; Nishiyama, N. Prediction of Skin Sensitization Potency of Chemicals by Human Cell Line Activation Test (h-CLAT) and an Attempt at Classifying Skin Sensitization Potency. *Toxicol. In Vitro* **2012**, *26* (7), 1150–1160.

(52) Python, F.; Goebel, C.; Aeby, P. Assessment of the U937 Cell Line for the Detection of Contact Allergens. *Toxicol. Appl. Pharmacol.* **2007**, *220* (2), 113–124.

(53) Karlberg, A.-T.; Dooms-Goossens, A. Contact Allergy to Oxidized *d* -Limonene among Dermatitis Patients. *Contact Dermatitis* **1997**, *36* (4), 201–206.

(54) Matura, M.; Skold, M.; Borje, A.; Andersen, K. E.; Bruze, M.; Frosch, P.; Goossens, A.; Johansen, J. D.; Svedman, C.; White, I. R.; et al. Selected Oxidized Fragrance Terpenes Are Common Contact Allergens. *Contact Dermatitis* **2005**, *52* (6), 320–328.

(55) Sköld, M.; Börje, A.; Harambasic, E.; Karlberg, A.-T. Contact Allergens Formed on Air Exposure of Linalool. Identification and Quantification of Primary and Secondary Oxidation Products and the Effect on Skin Sensitization. *Chem. Res. Toxicol.* **2004**, *17* (12), 1697–1705.

(56) Kao, D.; Chaintreau, A.; Lepoittevin, J.-P.; Giménez-Arnau, E. Synthesis of Allylic Hydroperoxides and EPR Spin-Trapping Studies on the Formation of Radicals in Iron Systems as Potential Initiators of the Sensitizing Pathway. *J. Org. Chem.* **2011**, *76* (15), 6188–6200.

(57) Basketter, D. A.; Blaikie, L.; Dearman, R. J.; Kimber, I.; Ryan, C. A.; Gerberick, G. F.; Harvey, P.; Evans, P.; White, I. R.; Rycroft, R. J. G. Use of the Local Lymph Node Assay for the Estimation of Relative Contact Allergenic Potency. *Contact Dermatitis* **2000**, *42* (6), 344–348.

(58) Urbisch, D.; Mehling, A.; Guth, K.; Ramirez, T.; Honarvar, N.; Kolle, S.; Landsiedel, R.; Jaworska, J.; Kern, P. S.; Gerberick, F.; et al. Assessing Skin Sensitization Hazard in Mice and Men Using Non-Animal Test Methods. *Regul. Toxicol. Pharmacol.* **2015**, *71* (2), 337–351.

(59) Andersch Björkman, Y.; Hagvall, L.; Siwmark, C.; Niklasson, B.; Karlberg, A.-T.; Bråred Christensson, J. Air-Oxidized Linalool Elicits Eczema in Allergic Patients - a Repeated Open Application Test Study: Roat of Oxydized Linalool. *Contact Dermatitis* **2014**, *70* (3), 129–138.

(60) Bråred Christensson, J.; Andersen, K. E.; Bruze, M.; Johansen, J. D.; Garcia-Bravo, B.; Gimenez Arnau, A.; Goh, C.-L.; Nixon, R.; White, I. R. Air-Oxidized Linalool-a Frequent Cause of Fragrance Contact Allergy. *Contact Dermatitis* **2012**, *67* (5), 247–259.

(61) Bråred Christensson, J.; Andersen, K. E.; Bruze, M.; Johansen, J. D.; Garcia-Bravo, B.; Giménez-Arnau, A.; Goh, C.-L.; Nixon, R.; White, I. R. An International Multicentre Study on the Allergenic Activity of Air-Oxidized *R* -Limonene. *Contact Dermatitis* **2013**, *68* (4), 214–223.

(62) Bråred Christensson, J.; Andersen, K. E.; Bruze, M.; Johansen, J. D.; Garcia-Bravo, B.; Gimenez Arnau, A.; Goh, C.-L.; Nixon, R.; White, I. R. Positive Patch Test Reactions to Oxidized Limonene: Exposure and Relevance: Exposure and allergy to oxidized limonene. *Contact Dermatitis* **2014**, *71* (5), 264–272.

(63) Mutterer, V.; Gimenez-Arnau, E.; Karlberg, A.-T.; Lepoittevin, J.-P. Synthesis and Allergenic Potential of a 15-Hydroperoxyabietic Acid-like Model: Trapping of Radical Intermediates. *Chem. Res. Toxicol.* **2000**, *13* (10), 1028–1036.

(64) Pazos, M.; Andersen, M. L.; Skibsted, L. H. Amino Acid and Protein Scavenging of Radicals Generated by Iron/Hydroperoxide System: An Electron Spin Resonance Spin Trapping Study. *J. Agric. Food Chem.* **2006**, *54* (26), 10215–10221.

(65) Giménez-Arnau, E.; Haberkorn, L.; Grossi, L.; Lepoittevin, J.-P. Identification of Radical Species Derived from Allergenic 15-Hydroperoxyabietic Acid and Insights into the Behaviour of Cyclic Tertiary Allylic Hydroperoxides in Fe(II)/Fe(III) Systems. *Tetrahedron* **2008**, *64* (24), 5680–5691.

(66) Giménez Arnau, E.; Haberkorn, L.; Grossi, L.; Lepoittevin, J.-P. Identification of Alkyl Radicals Derived from an Allergenic Cyclic Tertiary Allylic Hydroperoxide by Combined Use of Radical Trapping and ESR Studies. *Tetrahedron* **2002**, *58* (27), 5535–5545.

(67) Johansson, S.; Giménez-Arnau, E.; Grøtli, M.; Karlberg, A.-T.; Börje, A. Carbon- and Oxygen-Centered Radicals Are Equally Important Haptens of Allylic Hydroperoxides in Allergic Contact Dermatitis. *Chem. Res. Toxicol.* **2008**, *21* (8), 1536–1547.

(68) Kao, D.; Chaintreau, A.; Lepoittevin, J.-P.; Giménez-Arnau, E. Mechanistic Studies on the Reactivity of Sensitizing Allylic Hydroperoxides: Investigation of the Covalent Modification of Amino Acids by Carbon-Radical Intermediates. *Toxicol. Res.* **2014**, *3* (4), 278–289.

(69) Eilstein, J.; Giménez-Arnau, E.; Duché, D.; Rousset, F.; Lepoittevin, J.-P. Synthesis and Reactivity Toward Nucleophilic Amino Acids of 2,5-[13 C]-Dimethyl- p -Benzoquinonediimine. *Chem. Res. Toxicol.* **2006**, *19* (9), 1248–1256.

(70) *Biomedical EPR*. Eaton, S. S., Eaton, G. R., Berliner, L. J., Eds.; Biological magnetic resonance; Kluwer Academic/Plenum Publishers: New York, 2004.

(71) Jurkiewicz, B. A.; Buettnerf, G. R. EPR Detection of Free Radicals in UV-Irradiated Skin: Mouse Versus Human. *Photochem. Photobiol.* **1996**, *64* (6), 918–922.

(72) Netzlaff, F.; Lehr, C.-M.; Wertz, P. W.; Schaefer, U. F. The Human Epidermis Models EpiSkin®, SkinEthic® and EpiDerm®: An Evaluation of Morphology and Their Suitability for Testing Phototoxicity, Irritancy, Corrosivity, and Substance Transport. *Eur. J. Pharm. Biopharm.* **2005**, *60* (2), 167–178.

(73) Migdal, C.; Botton, J.; El Ali, Z.; Azoury, M.-E.; Guldemann, J.; Giménez-Arnau, E.; Lepoittevin, J.-P.; Kerdine-Römer, S.; Pallardy, M. Reactivity of Chemical Sensitizers Toward Amino Acids In Cellulo Plays a Role in the Activation of the Nrf2-ARE Pathway in Human Monocyte Dendritic Cells and the THP-1 Cell Line. *Toxicol. Sci.* **2013**, *133* (2), 259–274.

Chapter 1

Chemical reactivity profile through radical mechanisms: Synthesis of target compounds and reactivity studies

In this chapter the synthetic pathways developed for the obtention of target compounds 5-(^{13}C)-Lina-OOHs, 4-(^{13}C)-Lina-OOHs and 2-(^{13}C)-Lina-OOHs will firstly be exposed. In the second part of this chapter results on the follow up of their reactivity with different amino acids by ^{13}C-NMR will be described.

1 SYNTHESIS OF ALLYLIC HYDROPEROXIDES IN THE LITERATURE

Due to the instability and intrinsic reactivity of the O-O bond hydroperoxides can decompose through highly exothermic processes.[1] Those of low molecular weight can even be explosive. In fact, the percentage of the total mass formed by the peroxidic oxygen atoms present in the skeleton of hydroperoxides is an indicator of the lability degree of these molecules. Thus, with 33% active oxygen methyl hydroperoxide is known to be a detonating substance, while with 11% active oxygen octyl hydroperoxide is easily purified on a small scale. The high propensity of hydroperoxides to decompose has resulted in the collective opinion that they are far too unstable to be of interest as synthetic intermediates. Hydroperoxides are mostly used as oxidizing reagents. In the case of allylic hydroperoxides, they are used as precursors for the formation of allylic alcohols, which are key intermediates that can be subjected to a wide variety of synthetic transformations.

In the sections below, the processes traditionally used for the synthesis of allylic hydroperoxides will briefly be described. A special focus will be given to the autoxidation of olefins and to their reactions with singlet oxygen.

1.1 Basic concepts: autoxidation, triplet and singlet oxygen

Atmospheric oxygen is an oxidizing agent easily reacting with a lot of organic molecules at room temperature. This process is called autoxidation. It has a crucial importance in fatty acid oxidation in the food industry.

The main autoxidation mechanism is a radical chain reaction leading to hydroperoxides as primary oxidation products. It is divided into three different steps: initiation, propagation and termination (Figure 1.1).

The initiation reaction occurs because of heat, light or a catalytic amount of metal, and organic compound radicals R$^{\bullet}$ are generated by abstraction of an atom of hydrogen of the substrate RH. Then propagation reactions occur, R$^{\bullet}$ can react with atmospheric oxygen to form peroxyl radicals ROO$^{\bullet}$, that can then abstract a hydrogen atom from RH to form a hydroperoxide ROOH

and also a new R$^{\bullet}$. The termination reaction occurs when two radicals react together to form a non-radical species.

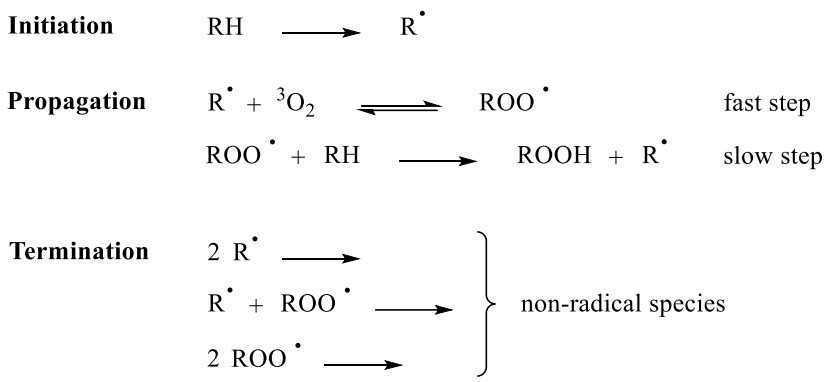

Figure 1.1: General mechanism for autoxidation processes based on three steps: initiation, propagation and termination

The dioxygen molecule at its ground state is paramagnetic and is a triplet ($^3O_2$). Molecules of triplet oxygen $^3O_2$ contain two unpaired electrons in two different molecular orbitals. It is a biradical molecule, each electron occupying a high occupied molecular orbital π_{2p}* (HOMO). Autoxidation processes in nature occur in the presence of triplet oxygen $^3O_2$. In the excited state, $^3O_2$ becomes singlet oxygen $^1O_2$, that is diamagnetic and contains the two electrons antiparallel in the same molecular orbital. Singlet oxygen $^1O_2$ is far more reactive toward organic compounds than triplet ground state oxygen $^3O_2$ (Figure 1.2).

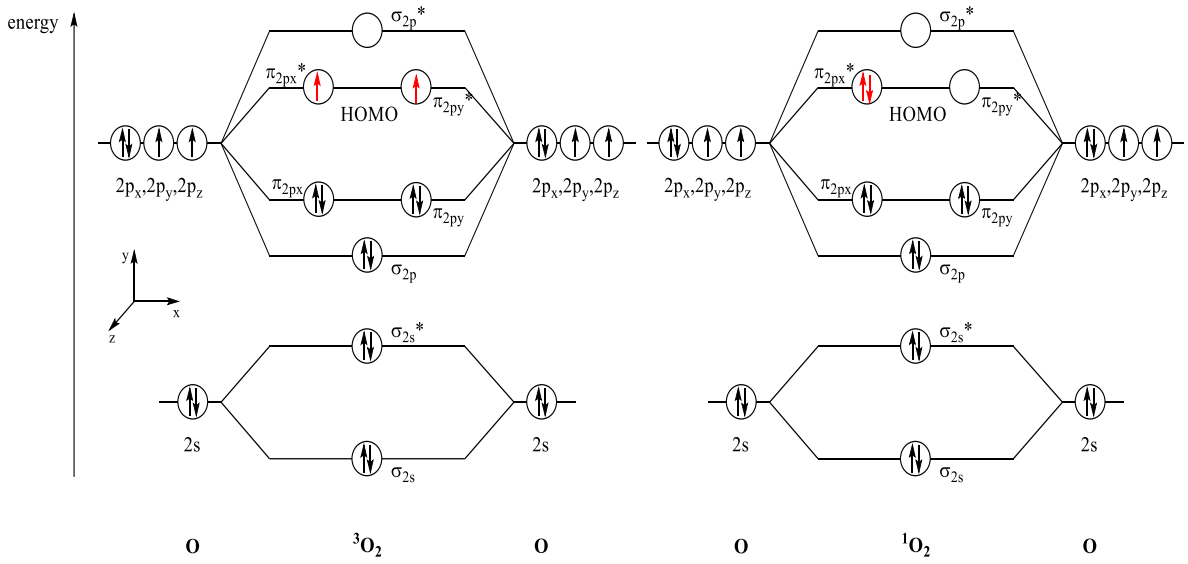

Figure 1.2: Molecular orbitals diagram of the triplet oxygen state $^3O_2$, the two-red spins are in two orbitals π_{2px}* and π_{2py}* and in the singlet oxygen state $^1O_2$, the two-red spins are in the same orbital π_{2px}*

The most commonly used method to generate singlet oxygen $^1O_2$ is by photosensitization of $^3O_2$ in the presence of photosensitizers such as porphyrinic, phthalocyanine pigments, methylene blue or Bengal rose (Figure 1.3), also used in phototherapy in oncology. Initially, the sensitizer absorbs a photon and at the excited state transfers energy to $^3O_2$ that becomes $^1O_2$, the sensitizer recovering its initial electronic configuration.[2]

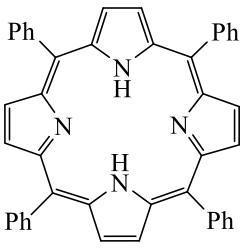

5,10,15,20-Tetraphenyl-
21*H*,23*H*-porphyrine

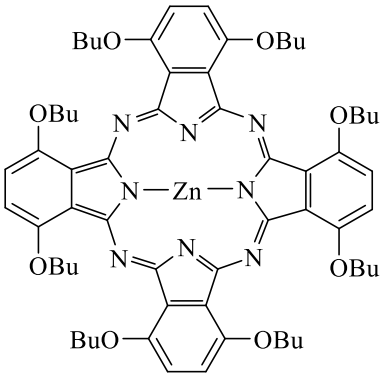

1,4,8,11,15,18,22,25-Octabutoxy-
29*H*,31*H*-phtalocyanine of zinc (II)

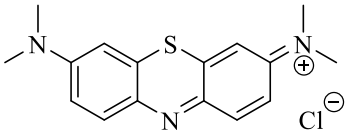

Methylene blue

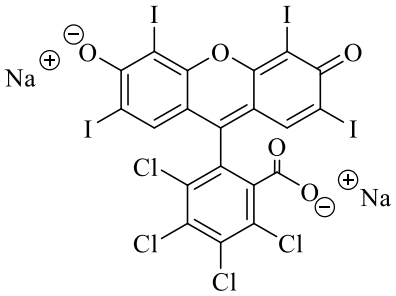

Bengale rose

Figure 1.3: Examples of photosensitizers used to produce $^1O_2$ from $^3O_2$

There are several methods to generate singlet oxygen $^1O_2$ chemically without the use of a light source. Chemically it is possible to generate $^1O_2$ by using trioxaphosphetane decomposition or sodium hypochlorite and hydrogen peroxide, but also sodium molybdate (Figure 1.4).[2]

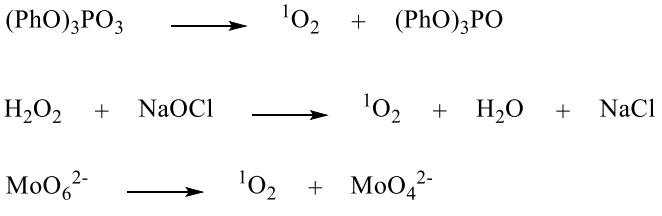

Figure 1.4: Different ways to generate $^1O_2$ by non-photochemical chemical procedures

1.2 Autoxidation on unsaturated molecules

The autoxidation of unsaturated compounds to obtain allylic hydroperoxides is considered of low value as a synthetic tool. It leads very often to the formation of a multitude of oxidized products. In a study on the oxidative degradation of linalool in contact with air for example, in addition to various allylic alcohols, furan and pyran derivatives, several allylic hydroperoxides could be identified.[3]

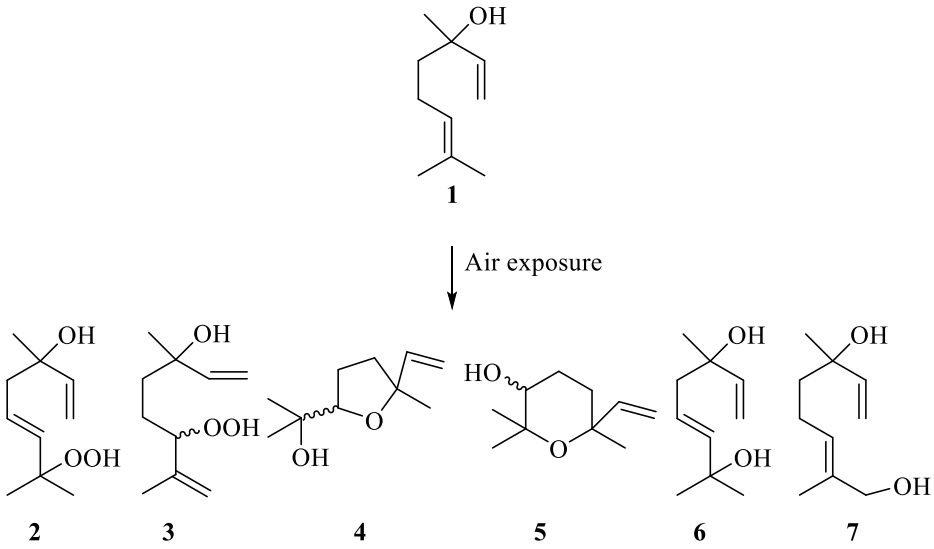

Figure 1.5: Autoxidation of linalool: 45 weeks of oxygen exposure gave the best yield 15 % of compounds **2** and **3**; after 50 weeks of oxygen exposure was obtained the best yield 20% of compound **4**; after 79 weeks of oxygen exposure was obtained the best yield 4 % of compound **5**; **6** and **7** compounds are secondary oxidation products

1.3 Schenck reaction: ene-reaction with singlet oxygen

In previous studies in the laboratory a way was found to synthesize a proper mixture of hydroperoxides **2** and **3** by employing the so-called Schenck or ene-reaction with singlet oxygen.[4]

This reaction, happening between compounds containing hydrogen atoms on allylic positions and singlet oxygen was discovered by Schenck in 1940 and revised by Foot in the 60's.[5,6]

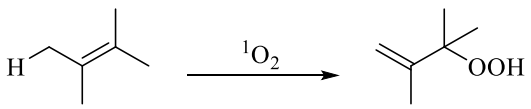

Figure 1.6: Schenck reaction: general representation

This reaction triggered the curiosity of chemists because of its particular stereo and regio-selectivity. The reaction mechanism is still controversial, a concerted mechanism being opposed to a sequential mechanism. Several intermediates have been reported to be involved in these mechanisms such as a zwitterionic intermediate, a biradical, an exciplex and a perepoxide (Figure 1.7). For some authors, the most probable intermediate is a perepoxide even if this one looks like to be formed from an exciplex intermediate. The perepoxide intermediate allows explaining the regioselectivity and stereoselectivity observed depending on the oxidized substrate.[5,7]

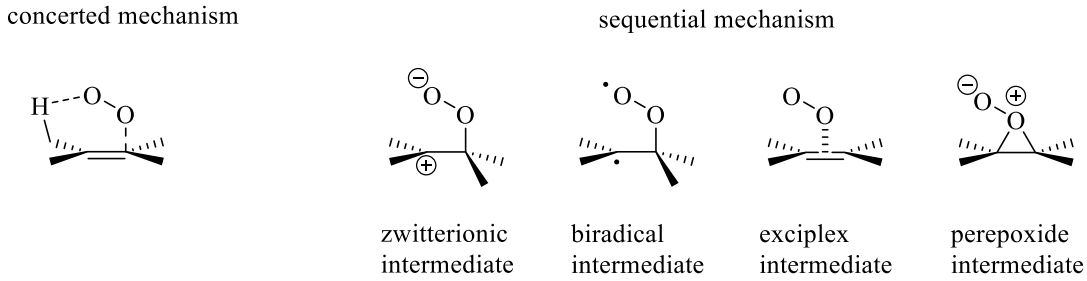

Figure 1.7: Possible intermediates described for the Schenck reaction

Several factors govern the mechanism of this reaction involving steric hindrance, electronic effects and also hydrogen bonds. We will concentrate here on the example of linalool **1** where the trisubstituted alkene chemical function has a hydrogen atom on the allylic position. In theory, the Schenck reaction would lead to the product having the hydroperoxide chemical function on the most substituted carbon atom due to the difference of energy between the transition states from the resulting hydrogen abstraction. The transition state where the created C-O bond is placed in a tertiary carbon atom has a lower energy than the one where the C-O bond is a secondary carbon atom. In consequence, the steric hindrance plays a key role.[7] The more the R substituent is a bulky group (Figure 1.8), higher is the percentage of the major product.

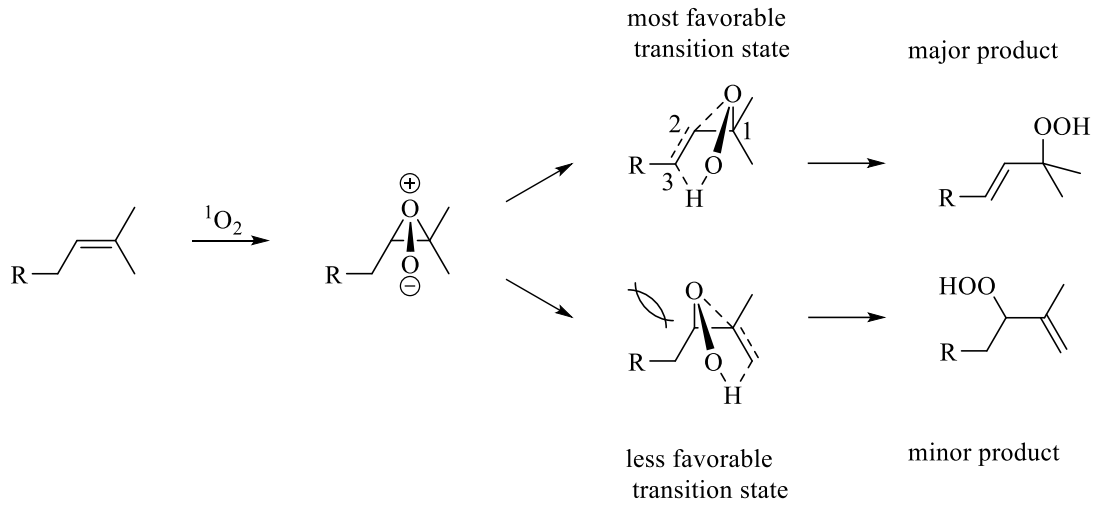

Figure 1.8: Steric hindrance influence on the transition states in the Schenck ene-reaction with $^1O_2$

The Schenck ene-reaction was applied to linalool **1** by reaction with singlet oxygen $^1O_2$ obtained from hydrogen peroxide in the presence of sodium molybdate (H_2O_2/MoO_4^{2-}) in a microemulsion medium. This method to generate quantitatively $^1O_2$ was developed by Aubry and is based on the disproportionation of hydrogen peroxide in basic media catalyzed by sodium molybdate (Figure 1.9).[8]

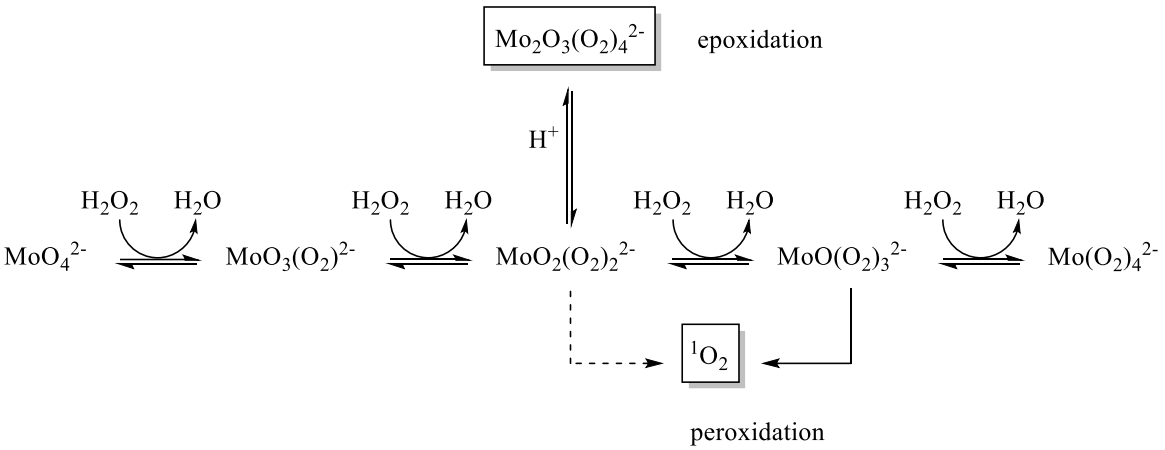

Figure 1.9: Hydrogen peroxide disproportionation in the presence of sodium molybdate

In addition to the ability to peroxidise allylic compounds using $^1O_2$ generated from triperoxymolybdate $MoO(O_2)_3^{2-}$ intermediate, the H_2O_2/MoO_4^{2-} system also shows in neutral or acidic medium epoxidation properties to which allylic alcohols are very sensitive trough the tetraperoxodimolybdate $Mo_2O_3(O_2)_4^{2-}$ (Figure 1.9).[9] Epoxidation is avoided favoring peroxidation in a microemulsion system. A microemulsion water in oil with dichloromethane, stabilized by a monolayer of surfactant sulfate dodecyl sodium and a co-surfactant butanol was

employed. By using this microemulsion singlet oxygen generated in the aqueous phase joins the hydrophobic media where linalool is and hydroperoxides are generated thanks to the peroxidation species $MoO(O_2)_3^{2-}$. Basic pH is maintained by successive and controlled amounts of H_2O_2 addition, keeping the triperoxymolybdate $MoO(O_2)_3^{2-}$ intermediate as major compound, avoiding the epoxydation.

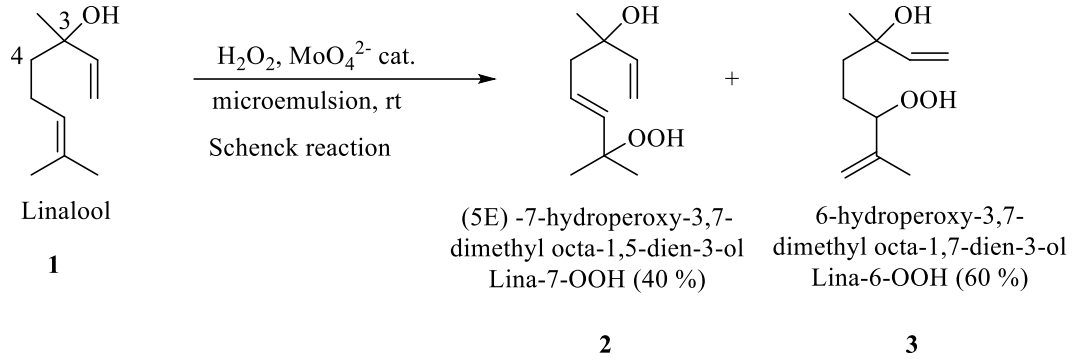

Figure 1.10: Schenck reaction on linalool **1** and obtention of Lina-7-OOH **2** / Lina-6-OOH **3**

It is important to stress that the Schenck reaction on linalool **1** produces a different distribution of oxidation products as the one expected. According to the theory above described, the ene-reaction on linalool **1** using singlet oxygen $^1O_2$ should afford Lina-7-OOH **2** as the major product. The steric hindrance of the R substituent at position 4 should promote formation of Lina-7-OOH **2**. However, it appears that steric hindrance is minimized in this position due to the free rotation around the C_3-C_4 bond (Figure 1.10). Thus, the isomer Lina-6-OOH **3** was formed as the major product with a ratio 2:3 for compounds **2** and **3**.

On thin layer chromatography these two isomers have the same retention factor, as well as on gel column chromatography on silica or on alumina. Therefore, it is very difficult to isolate **2** and **3** from the obtained Schenck reaction mixture.

1.4 Nucleophilic substitution on allylic alcohols

Two different synthetic pathways can in general be used to afford allylic hydroperoxides from primary, secondary or tertiary alcohols.

In the first one, the hydroxyl function is transformed into a good leaving group followed by a nucleophilic substitution with hydrogen peroxide (Figure 1.11). Primary and secondary hydroperoxides are thus mostly prepared via an S_N2 nucleophilic substitution.

In the second one, tertiary hydroperoxides are prepared via a S_N1 nucleophilic substitution using hydrogen peroxide in acidic media, favoring a stable carbocation formation.

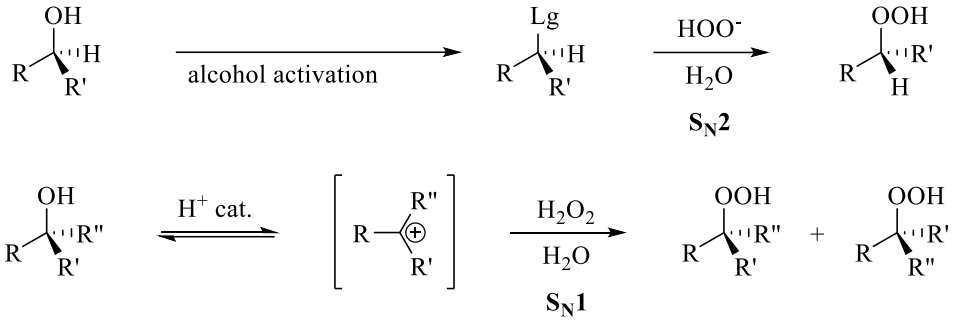

Figure 1.11: Synthesis of hydroperoxides from tertiary, secondary and primary alcohols (R = allylic chain; R' = H, alkyl; R'' = alkyl; Lg = leaving group)

2 SYNTHESIS OF TARGET COMPOUNDS

2.1 Introduction of a ^{13}C-substitution on linalool

The enthalpy of dissociation of the O-O bond of the hydroperoxide chemical function is of a relatively weak order of 175.8 kJ/mol compared to the one of the C-C bond that is around 347-356 kJ/mol. It is therefore generally accepted that the cleavage of O-O bonds is an easy process leading to the formation of alkoxyl radicals. In the case of linalool **1** and due to the presence of double bonds, these radical intermediates are able to further evolve towards the formation of carbon-centered radicals, for example by abstraction of allylic hydrogen atoms, by intramolecular cyclization processes or by β-scission (Figure 1.12). Each of these oxygen- and carbon-centered radical intermediates could be reactive towards the side chains of amino acids having a propensity to participate in radical mechanisms.

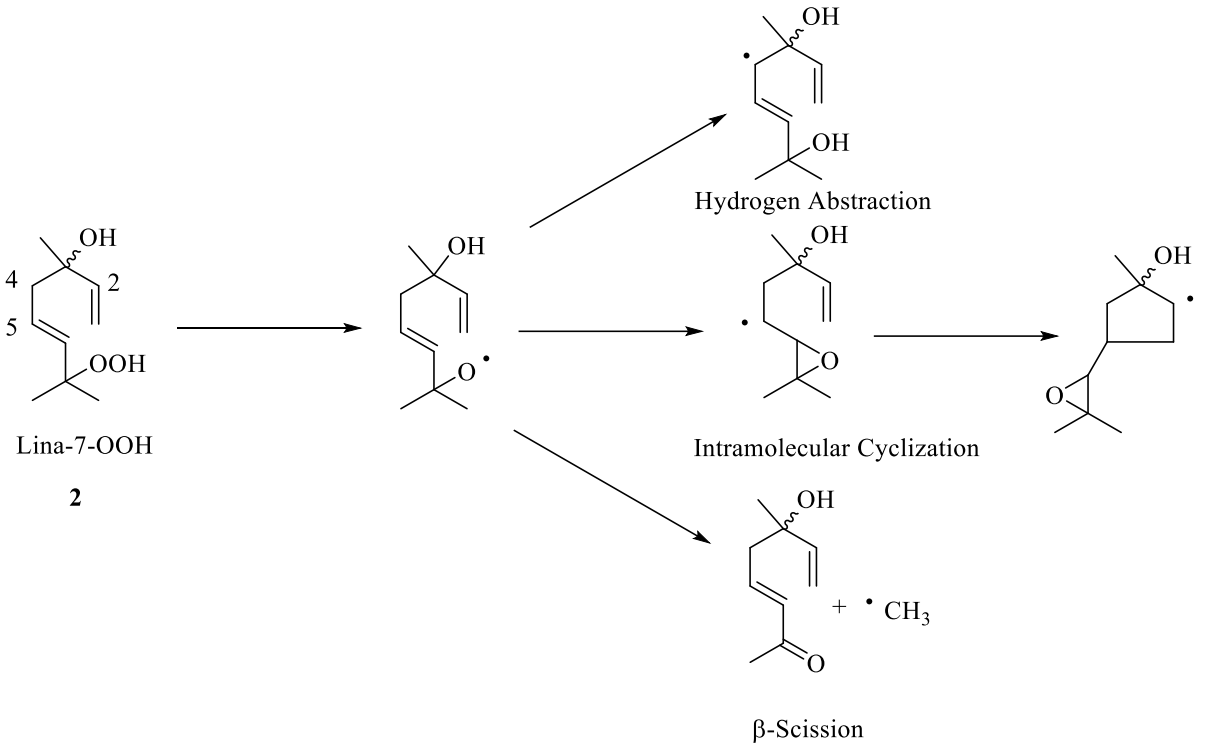

Figure 1.12: Lina-7-OOH oxygen and carbon-centered radical intermediates

From these radical rearrangement processes, it can be seen that positions 2, 4 and 5 of Lina-7-OOH are precursors of carbon-centered radicals.

Preliminary reactivity studies in the laboratory between Lina-7-OOH **2** and several amino acids, followed by liquid chromatography combined to mass spectroscopy, corroborated the formation of stable covalent bonds between carbon-centered radicals derived from Lina-7-OOH **2** and the side chain of cysteine, for example.[10]

However, it was not possible to exactly elucidate which was the carbon radical position reacting as different hypothetical adducts would have the same observed *m/z* (Figure 1.13).

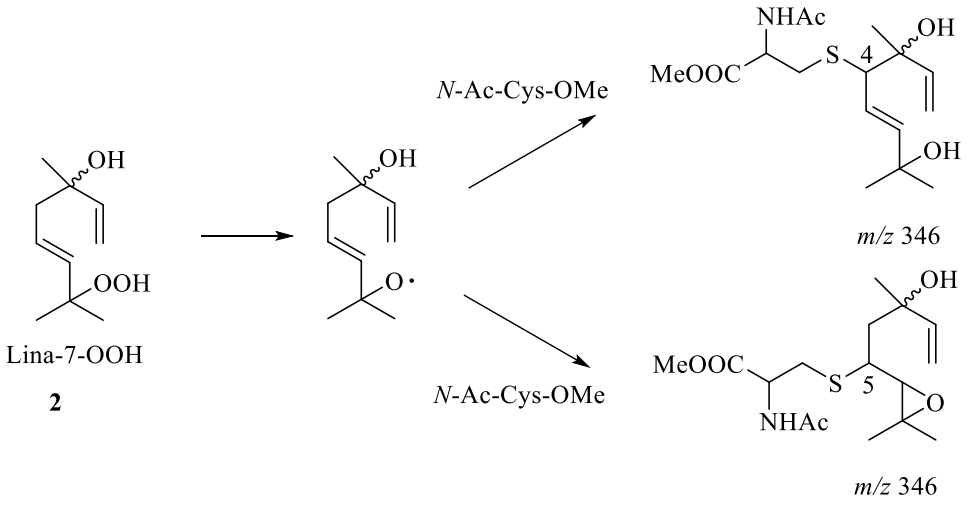

Figure 1.13: Example of adducts with same *m/z* value

In order to elucidate which is exactly the carbon-centered radical position that could react with amino acids prompt to radical reactions, it was decided to synthesize linalool hydroperoxides containing a ^{13}C-substitution at position 2, 4 or 5. The aim was to further follow the reactivity of 5-(^{13}C)-Lina-OOHs, 4-(^{13}C)-Lina-OOHs and 2-(^{13}C)-Lina-OOHs towards amino acids by mono- and bi-dimensional ^{13}C-NMR. Indeed, this methodology has been developed successfully in the laboratory in order to study the reactivity of electrophilic sensitizers towards amino acids and proteins. By introducing a ^{13}C-substitution in a reactive position of the allergen it is possible to follow its reactivity by mono-dimensional ^{13}C-NMR and bidimensional ^{1}H-^{13}C heteronuclear NMR.

In this chapter, we will first present the synthetic routes that have been designed to obtain linalool **1** ^{13}C-substituted at position 2, 4 and 5 (Figure 1.14). The Schenck reaction will then be applied to each of them to obtain the mixture of hydroperoxides Lina-7-OOH and Lina-6-OOH (^{13}C)-substituted. In a second part, the reactivity of these compounds towards some tested amino acids will be described.

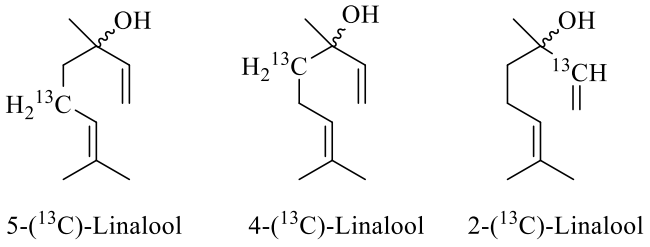

Figure 1.14: Chemical structures of (^{13}C)-substituted linalool target compounds

2.2 Synthetic strategies proposed

Syntheses of target compounds are based on the use of three different reagents to introduce the ^{13}C-substitution at the desired positions (Figure: 1.15).

For position 5, the synthetic pathway starts with the use of 1-(^{13}C)-acetic acid that can be converted into 1-(^{13}C)-ethyl 2-(diethoxyphosphoryl)acetate, which leads to a 1-(^{13}C)-butenyl alcohol. Synthesis then of the key intermediate 4-(^{13}C)-6-methyl-5-hepten-2-one allows the final obtention of 5-(^{13}C)-linalool.

4-(^{13}C)-Linalool can be formed starting from 2-(^{13}C)-acetic acid, converted through a 2-(^{13}C)-Weinreb amide into 3-(^{13}C)-6-methyl-5-hepten-2-one, same, above key intermediate allowing the obtention of 4-(^{13}C)-linalool.

Finally, for position 2 potassium-1-(^{13}C)-cyanide can be used as starting synthon to form first of all 1-(^{13}C)-trimethylsilyl cyanide, that can be added on 6-methyl-5-hepten-2-one to form a 1-(^{13}C)-nitrile intermediate. This one can be reduced to a 1-(^{13}C)-aldehyde function leading to 2-(^{13}C)-linalool.

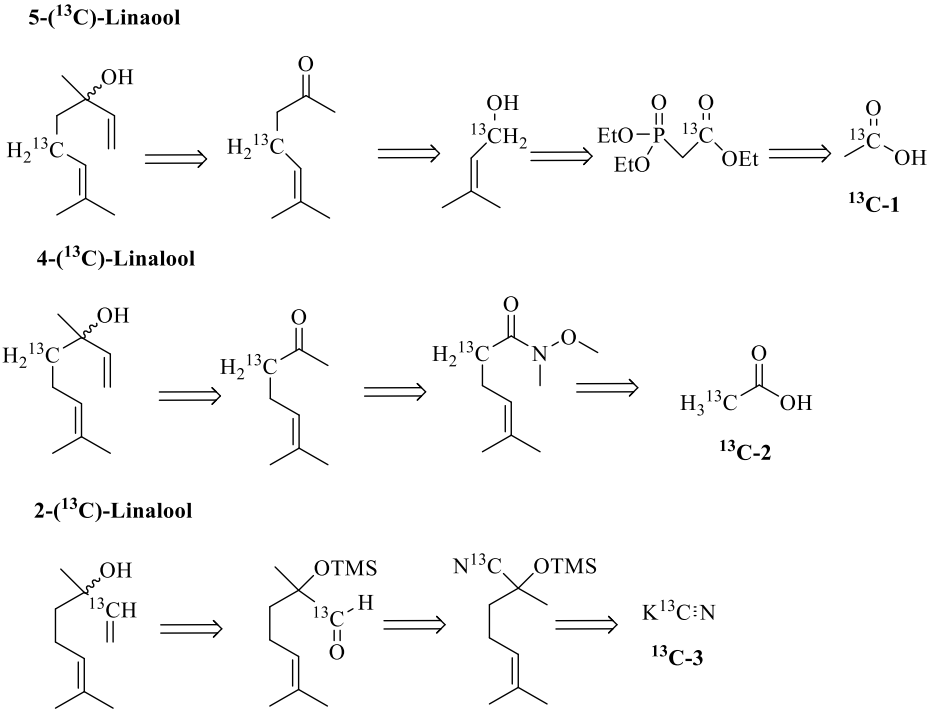

Figure 1.15: Proposed retrosynthesis for the obtention of linalool (^{13}C)-substituted in positions 5, 4 and 2

All synthetic pathways were initially developed to set the optimal experimental conditions without ^{13}C-substitution. Finally, obtained linalool needed to be converted, for all positions, into the hydroperoxides responsible for skin sensitization and at the origin of radical reactions.

2.3 Synthesis of 5-(^{13}C)-Lina-OOHs

Initially, **^{13}C-4** was synthesized from 1-(^{13}C)-acetic acid, itself used for the introduction of the (^{13}C)-substitution in the synthesis. The first step occurred in a two-steps mechanism. 1-(^{13}C)-Acetic acid was submitted to a Hell-Vollhardt-Zellinsky reaction, allowing bromination of the α-carbon to the carbonyl chemical function, in presence of bromine and phosphorous tribromide. Then, the obtained intermediate was esterified using ethanol (Figure 1.16).

The reaction gave 2-bromo-1-(^{13}C)-ethylacetate **^{13}C-4** that was used without further purification for the next step based on Klei *et al*. studies.[11]

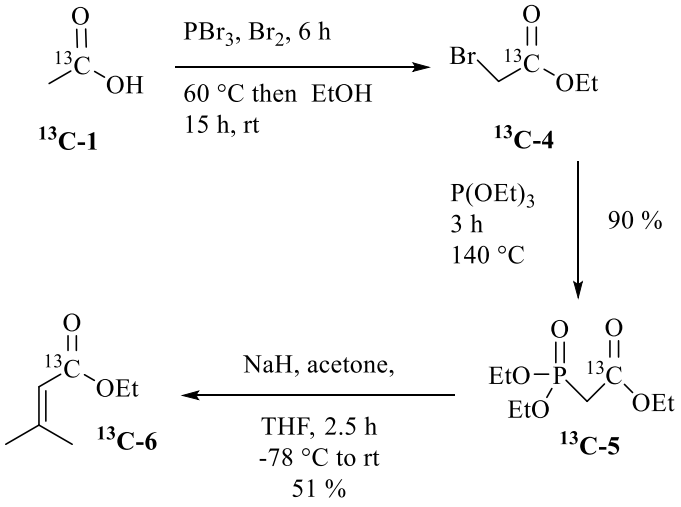

Figure 1.16: Synthesis of **^{13}C-6**

A nucleophilic substitution of bromine by triethyl phosphite afforded 2-(diethoxyphosphoryl)-1-(^{13}C)- ethylacetate **^{13}C-5** through a Michaelis-Arbuzov reaction with a yield of 90 % (Figure 1.16).

Based on Sharma *et al.* studies describing azinomycin epoxide molecular origin, the stabilized phosphonate carbanion of **^{13}C-5** was then obtained by treatment with a strong base and further a Horner-Wadsworth-Emmons reaction with acetone produced the alkene **^{13}C-6** with a yield of 51 % (Figure 1.16).[12] Further reduction of the ester to the allylic alcohol **^{13}C-7** was carried out by using di-isobutyl aluminum hydride (DIBAL-H) (Figure 1.17).

The product **^{13}C-7** was used without further purification for the next step, which was a

nucleophilic substitution of the alcohol by bromine in the presence of hydrobromic acid leading to 1-(^{13}C)-1-bromo-3-methyl but-2-ene **^{13}C-8**, with a yield of 52 %.

Further, deprotonation at the α position of the carbonyl group of ethyl acetoacetate by sodium ethoxide in ethanol and the addition of the anion formed on **^{13}C-8** afforded ethyl-3-(^{13}C)-2-acetyl-5-methylhex-4-enoate **^{13}C-9**, with a yield of 67 %. This last reaction needed to be carried out protected from daylight in order to avoid addition of hydrobromic acid on the double bond of **^{13}C-8**.

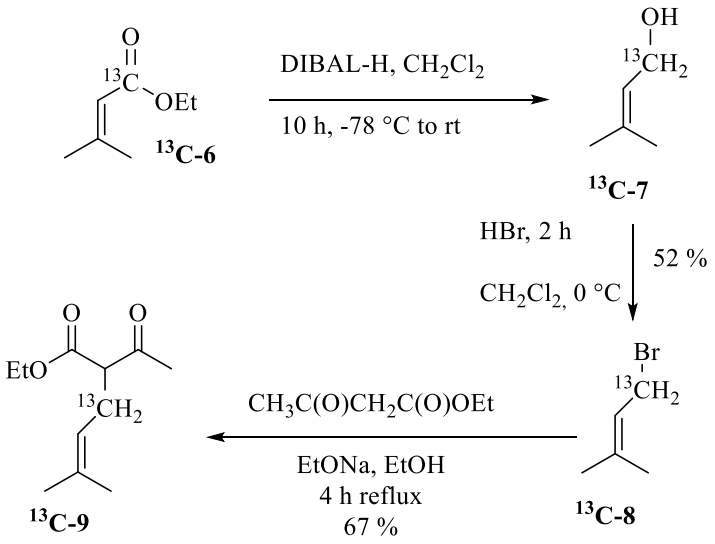

Figure 1.17: Synthesis of **^{13}C-9**

In order to obtain the ketone intermediate **^{13}C-10**, β-keto ester **^{13}C-9** was saponified by reaction with sodium hydroxide in order to obtain the corresponding carboxylic acid, that was further decarboxylated in presence of hydrochloric acid. The obtained product was used without further purification for the synthesis of 5- (^{13}C)-linalool.

The reaction of non-purified **^{13}C-10** with vinyl magnesium bromide afforded linalool ^{13}C-substituted at position 5 with a yield of 63% (Figure 1.18).

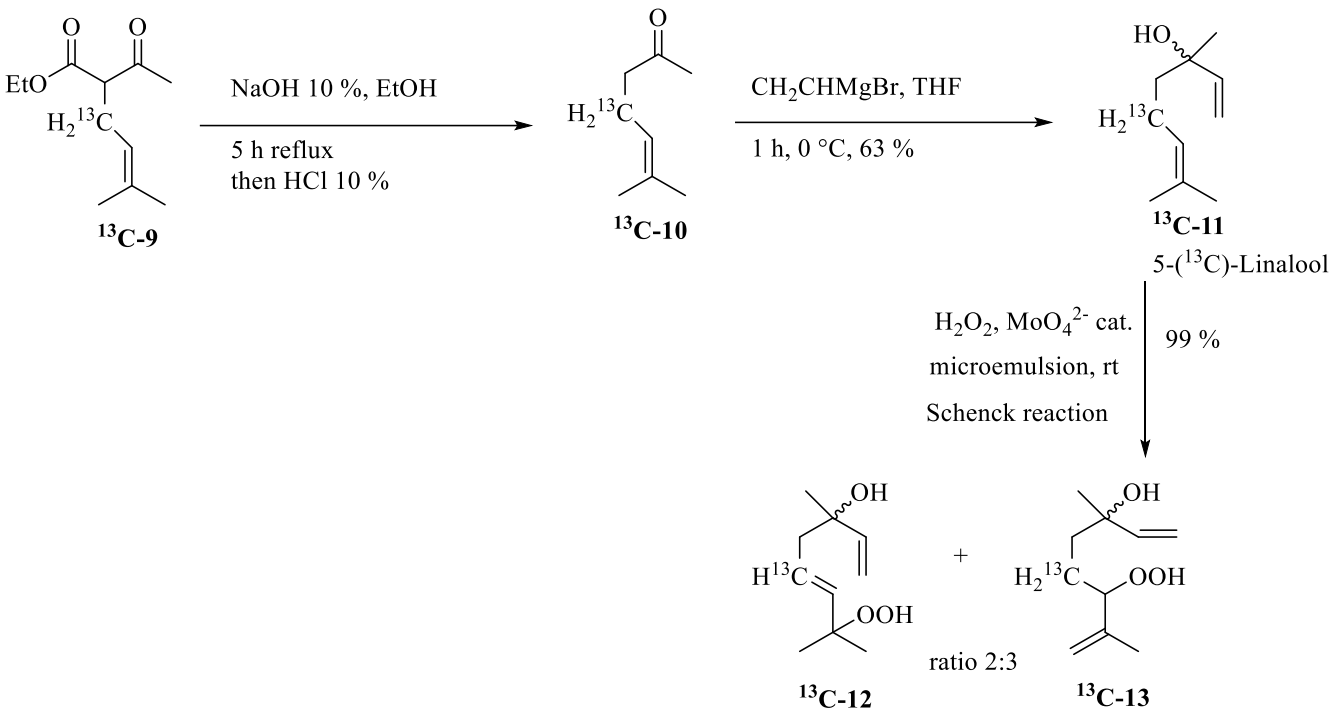

Figure 1.18: Synthesis of **^{13}C-12** and **^{13}C-13**

Finally, the mixture of isomers **^{13}C-12** and **^{13}C-13** was obtained with a yield of 99 % when applying the Schenck ene-reaction to 5-(^{13}C)-linalool in which singlet oxygen $^1O_2$ was chemically produced by disproportionation of hydrogen peroxide, catalyzed by a sodium molybdate system in a microemulsion.

In summary the final synthetic pathway developed to obtain 5-(^{13}C)-Lina-OOHs **^{13}C-12** and **^{13}C-13**, is a nine-steps synthesis with a global yield of 3.8 %.

2.4 Synthesis of 4-(^{13}C)-Lina-OOHs

The first step was a classical esterification of 2-(^{13}C)-acetic acid in acidic medium to obtain 2-(^{13}C)-ethyl acetate with a yield of 58 % (Figure 1.19).

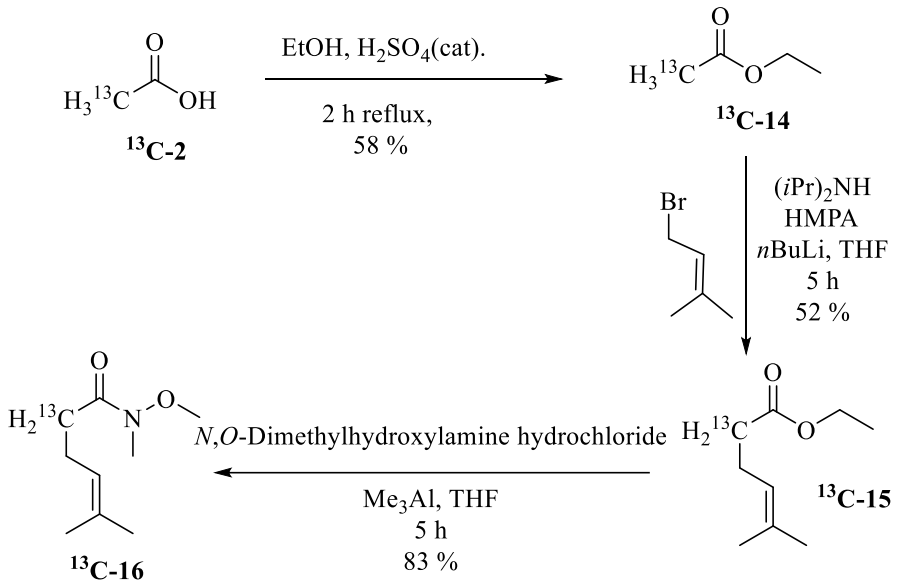

Figure 1.19: Synthesis of (**^{13}C-16**)

Initially, the synthesis of the next intermediate was tried using MacPhee and Dubois experimental conditions using isopropyl magnesium chloride without success.[13] We then used the experimental conditions described by Debeuckelaere *et al.*[14]

For the synthesis of 2-(^{13}C)-ethyl-5-methyl-4-hexenoate **^{13}C-15**, the lithium enolate of **^{13}C-14** was initially prepared in the presence of diisopropylamine and *n*-butyllithium and then reacted on 1-bromo-3-methyl-but-2-ene (Figure 1.19). The non-nucleophilic lithium diisopropylamide formed behaves in solution as a strong base (pKa = 36) and was ideal to deprotonate on the α-carbon atom of the carbonyl chemical function. The role of hexamethylphosphoramide was to render the lithium enolate more nucleophilic by complexing the lithium ions. This step was carried out with a yield of 52 %.

To continue the synthesis, it was necessary to obtain the ketone 3-(^{13}C)-6-methyl-5-hepten-2-one from **^{13}C-15**. For this reason, it was decided to revert the electrophilicity of the carbonyl chemical function of **^{13}C-15** by converting it into a Weinreb amide (Figure 1.19). The method described by Nahm and Weinreb using *N*-methoxy-*N*-methyl amide as an acylating agent was here used.[15] This method is described as being very useful for the formation of ketones or aldehydes and increasingly used in total synthesis processes on an industrial scale. We first used the methodology described by Liu *et al.* using isopropyl magnesium chloride as an activating agent before adding ester **^{13}C-15**, but yields were very low.[16] In a second time, we used conditions described by Guanti and Riva using trimethylaluminum as a coupling agent.[17] Also,

the conditions using dimethyl aluminum chloride reported by Shimizu *et al*. were tested (Table 1.1).[18]

Table 1.1: Experimental conditions tested for the conversion of **^{13}C-15** into the Weinreb amide **^{13}C-16** using *N*,*O*-dimethylhydroxylamine hydrochloride

Experimental conditions: time, temperature, agent	**Yield (%)**
1 hour, -20 °C, *i*PrMgCl	10
1 hour, -78 °C, *i*PrMgCl	38 %
30 minutes, -20 °C, *i*PrMgCl	40 %
30 minutes, 0 °C then room temperature, Me_2AlCl	70 %
3 hours, 0 °C then room temperature, Me_2AlCl	63 %
5 hours, 0 °C, Me_3Al	83 %

Using isopropyl magnesium chloride as activating agent yields were never higher than 40 %, even when varying the temperature and reaction times. Using dimethyl aluminum chloride a better yield of 70 % was obtained by varying the time of the reaction from 30 minutes to three hours. The best yield of the Weinreb amide **^{13}C-16** 83% was however obtained when using trimethylaluminum as activating agent for 5 hours at 0 °C.

The following addition of methyllithium to this particular amide made possible to synthesize the desired ketone **^{13}C-17** with a yield of 70 % (Figure 1.20). The conditions described by Reetz *et al*. using organometallic reagents to realize this step were employed.[19]

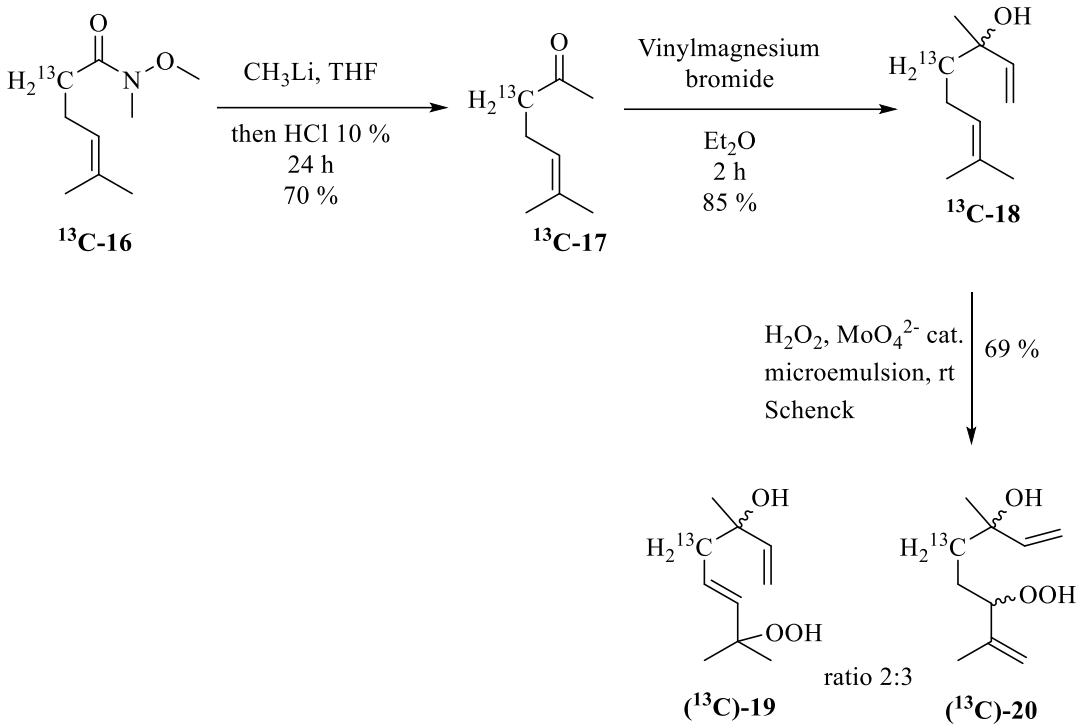

^{13}C-16 **^{13}C-17** **^{13}C-18** **(^{13}C)-19** **(^{13}C)-20**

Figure 1.20: Synthesis of **^{13}C-19** and **^{13}C-20**

Finally, 4-(^{13}C)-linalool **^{13}C-18** was obtained by nucleophilic addition of vinyl magnesium bromide on the carbonyl chemical function of **^{13}C-17** (Figure 1.20). Stereochemistry here was not controlled because there has been no reported any distinction in the literature of the sensitizing potential of hydroperoxides derived from autoxidation of both **(^{13}C)-18** enantiomers.

In order to obtain 4-(^{13}C)-Lina-OOHs **^{13}C-19** and **^{13}C-20** from linalool **^{13}C-18**, a Schenck ene-reaction was used with the same experimental conditions as previously described for the synthesis of 5-(^{13}C)-Lina-OOHs.

2.5 Synthesis of 2-(^{13}C)-Lina-OOHs

This synthesis was initially based on the use of potassium (^{13}C)-cyanide as reagent introducing the ^{13}C-substitution. The key step consisted in the synthesis of trimethylsilyl (^{13}C)-cyanide **^{13}C-21** starting from potassium-(^{13}C)-cyanide **^{13}C-3**. In order to carry out the synthesis of trimethylsilyl (^{13}C)-cyanide **^{13}C-21**, better experimental conditions were set up without ^{13}C-substituted reagents.

A method based on Cao *et al*. work suggested the use of potassium cyanide or sodium cyanide, with zinc iodide and polyethylene glycol 400 (PEG 400), either in acetonitrile or in

dichloromethane (Figure 1.21).[20] Iodide ions have an excellent catalytic effect for S_N2 reactions, zinc iodide being a Lewis acid which facilitates the cleavage of the Si-Cl bond.

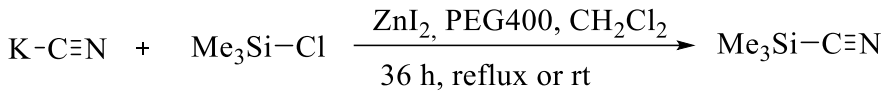

Figure 1.21: Me_3SiCN synthesis using zinc iodide and PEG400 and the experimental conditions described by Cao *et al*.[20]

The silane bound to the iodide will be more positively polarized becoming more electrophilic and the nucleophilic cyanide ions reaction will, therefore, be favored. In addition, PEG400 increases the solubility of salts such as potassium cyanide in a consistent manner promoting the reaction. Cao's work suggested to carry out the reaction in acetonitrile to improve its kinetics, in comparison with the reaction rates when carried out in dichloromethane. Based on these studies we have tested the reaction in both solvents, at room temperature for 3 hours, and using either potassium cyanide or sodium cyanide. Unfortunately, we have not been able to reproduce this reaction to obtain trimethylsilyl cyanide. We thought to compare the influence of the purity of the two different potassium cyanides used (97% and 98%) in the experiments on the one hand and to play on the kinetics and reaction temperature on the other hand. Only dichloromethane was used as solvent. The use of acetonitrile was indeed compromised as during the distillation procedure to isolate trimethylsilyl cyanide there was a high risk of formation of an azeotrope between acetonitrile (bp = 82 ° C) and the desired trimethylsilyl cyanide (bp = 112 ° C), thereby compromising purification. But again, assays were still unsuccessful.

Another attempt was then carried out by using trimethylsilyl chloride, potassium cyanide, potassium iodide and *N*-methyl pyrrolidone, upon the methodology reported in the literature by Reetz and Chatzhosifidis and Rasmussen and Heilmann.[21-22] Potassium iodide acts now as the catalyst, the iodine ions being good nucleophiles and also good leaving groups. Due to the high boiling point of *N*-methyl pyrrolidone, it was possible this time to easily isolate the desired trimethylsilyl cyanide by simple distillation at atmospheric pressure.

Initially, potassium cyanide known as “European Pharmacopoeia” (Ph. Eur.) 97% purity was used, without success (Table 1.2). In a second time, with potassium cyanide labeled "BioUltra"

98% purity we were able to obtain the expected product with a yield of 38 %. It turned out that comparing both potassium cyanides, it was noted that traces of metals (Fe, Na, Pb) and other elements (Cl, SO_4, S) present in potassium cyanide 97% were 100-fold higher than those found in potassium cyanide 98%. These could be the cause of side reactions and therefore disrupt the effectiveness of the reaction. Indeed, carrying out other assays in such a way to compare the reactivity of the two reagents, it was concluded that pure potassium cyanide 98% was most effective. Table 1.2 resumes the different conditions tested. The best experimental conditions were found to be 24 hours at room temperature, with a yield of obtained trimethylsilyl cyanide of 82 %.

Table 1.2: Experimental conditions tested for the synthesis of Me_3SiCN from different KCN

Experimental conditions: time, temperature and KCN	**Yield in % (± 5)**
3 hours, reflux 110 °C, KCN (97 %)	-
3 hours, reflux 110 °C, KCN (98 %)	38 %
24 hours, room temperature, KCN (97 %)	-
24 hours, room temperature, KCN (98 %)	82 %

Reagents: TMSCl (1eq), KCN (1eq), KI (0.1 eq) and NMP

We have also tested an alternative approach replacing potassium cyanide and potassium iodide by sodium cyanide and sodium iodide. However, very low yields of trimethylsilyl cyanide were obtained. It was observed that the solution passed from light yellow to brown-black. It could be assumed that iodine ions had oxidized to iodide instead of catalyzing the reaction since only 23 % of product was obtained after 24 hours reflux. However, at room temperature after 3 days of reaction, a better yield of trimethylsilyl cyanide of 64% was obtained.

In conclusion, the reaction at room temperature for 24 hours of potassium cyanide (98 %) on trimethylsilyl chloride in *N*-methyl pyrrolidone and in the presence of potassium iodide were the best conditions for the synthesis of trimethylsilyl cyanide with a yield of 82%. With the use of the ^{13}C-substituted reagent trimethylsilyl (^{13}C)-cyanide **^{13}C-21** was also obtained with a yield of 82 %.

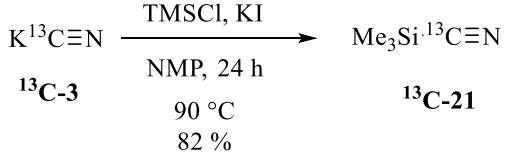

Figure 1.22: Trimethylsilyl cyanide synthesis containing a ^{13}CN group

The second step consisted in a cyanosilylation on 6-methyl-5-hept-2-one using trimethylsilyl (^{13}C)-cyanide **^{13}C-21** (Figure 1.23). Kündig and Enriquez-Garcia proposed to carry out the cyanosilylation using iodine in dichloromethane.[23]

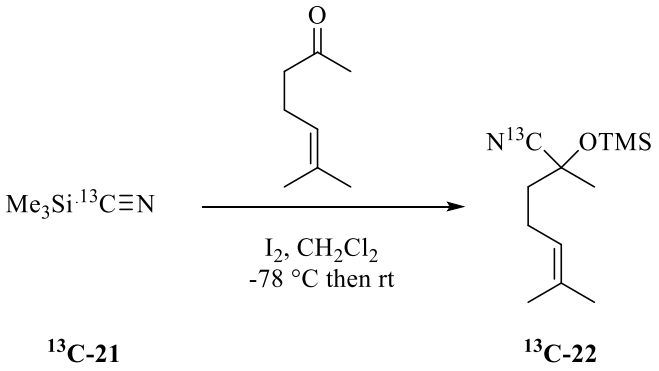

Figure 1.23: Synthesis of **^{13}C-22** using trimethylsilyl (^{13}C)-cyanide **^{13}C-21**

On the other hand, Evans *et al*. reported the same type of reaction by refraining from using solvent.[24] The presence of simple iodine allowed the cyano group of trimethylsilyl cyanide to be detached from the silane and to attack the carbonyl chemical function of the ketone. The oxygen anion formed could then capture the trimethylsilyl and thus became protected in the form of a trimethyl silane ether. We also found ourselves that the use of a solvent was not in favor of cyanosilylation, perhaps because of too much dilution of the reagents, even if the yields with solvent remain acceptable. In table 1.3 all experimental conditions tested are resumed.

Table 1.3: Synthesis of **^{13}C-22** using **^{13}C-21** as a synthon

Experimental conditions: temperature, time, solvent	**Yield % (± 5)**
-78 °C then r.t., 30 min, CH_2Cl_2	84
-78 °C then r.t., 30 min, Ø solvent	98
-78 °C then r.t., 3 h, CH_2Cl_2	89
-78 °C then r.t., 3 h, Ø solvent	94
-78 °C then r.t., 15 h, CH_2Cl_2	79
-78 °C then r.t., 15 h, Ø solvent	98

Regents: Ketone (1 eq), Me_3SiCN (1.2 eq) and I_2 (cat)

Finally, by following the reaction by thin layer chromatography, the reaction was observed to be very rapid and practically quantitative after only 30 minutes and without solvent.

The nitrile chemical function of **^{13}C-22** was then reduced to afford aldehyde **^{13}C-23** by using di-isobutyl aluminum hydride (Figure 1.24).

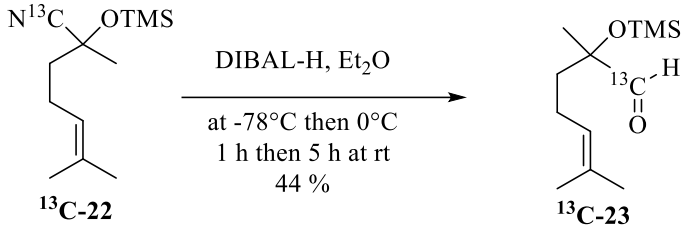

Figure 1.24: Reduction of **^{13}C-22** nitrile to aldehyde **^{13}C-23**

In the literature Ma *et al*. proposed a reduction of nitrile groups in diethyl ether, while Vinson *et al*. and more recently also Wisse *et al*. achieved the reduction in tetrahydrofuran, with yields of the order of 90%.[25–27]

We have therefore tried this reduction step in the two solvents, following the described experimental conditions described in Table 1.4.

Table 1.4: Experimental conditions tested for the reduction of **^{13}C-22** to obtain aldehyde **^{13}C-23**

Experimental conditions: DIBAL-H, temperature, time, solvent	**Yield % (± 5)**
1.2 eq. DIBAL-H, -78 °C then 0 °C, 3 h, diethyl ether	20 %
1.2 eq. DIBAL-H, -78 °C then 0 °C, 15 h, tetrahydrofuran	39 %
2.5 eq. DIBAL-H, -78 °C then 0 °C, 24 h, diethyl ether	31 %
3 eq. DIBAL-H, -78 °C then 0 °C, 3 h, tetrahydrofuran	-
5.0 eq. DIBAL-H, -78 °C then 0 °C, 3 h, tetrahydrofuran	20 %
5.0 eq. DIBAL-H, -78 °C then 0 °C, 48 h, diethyl ether	35 %

It appeared that the reaction was as difficult in tetrahydrofuran as in diethyl ether. Indeed, after 3 hours at 0°C and regardless of the solvent used the yields were very low. The reactions were nevertheless stopped in order to attempt a purification of the product on silica gel column chromatography, but the difficulties encountered to find a suitable eluent to separate **^{13}C-23** from the crude made the purification much more complicated than expected. We next increased the amount of DIBAL-H to 3 equivalents. After 3 hours of reaction, the analysis revealed the absence of **^{13}C-22** in the reaction medium. Unfortunately, after purification on silica gel column chromatography, very low yields were obtained of the aldehyde. Another solution could be to increase the reaction time ensuring complete conversion of the nitrile to the aldehyde. But even after 24 hours with 2.5 equivalents of DIBAL-H, did not totally reduce **^{13}C-22**. The synthetic pathway containing the ^{13}C-substitution for the synthesis of 2-(^{13}C)-Lina-OOHs seemed to reach in here an impasse. Next steps were therefore only conducted without ^{13}C-substitution.

Binns *et al*. reported Wittig reaction conditions using methylentriphenylphosphorane to convert an aldehyde chemical function into an alkene.[28] These experimental conditions were initially employed to prepare linalool **24** from non ^{13}C-substituted aldehyde **23**.

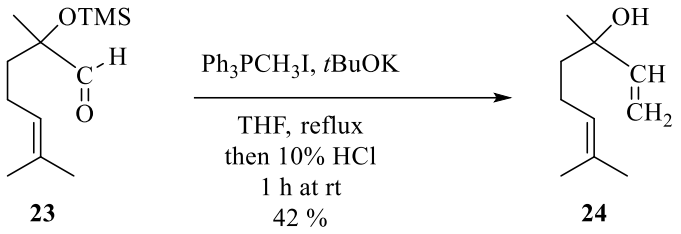

Figure 1.25: Synthesis of linalool **24** from aldehyde **23** using methylentriphenylphosphorane, parent member of phosphorous ylides

Methylene triphenylphosphorane was obtained from methyltriphenylphosphonium iodide salt deprotonated by potassium *tert*-butanolate. The carbonyl chemical group of the aldehyde was then attacked by the nucleophilic carbon of methylentriphenylphosphorane to form linalool, after removal of the silylated protecting group by the addition of hydrochloric acid. Linalool **24** was obtained with a yield of only 42%. The presence of a by-product was observed by thin layer chromatography, but it could not be identified.

Thus, for the envisaged synthesis for the obtention of linalool ^{13}C-substituted in position 2, the three first steps have been successfully realized with a ^{13}C-substitution, whereas the last two steps are still under optimization.

2.6 Conclusion and perspectives

The synthesis of 5-(^{13}C)-Lina-OOHs, **^{13}C-12** and **^{13}C-13**, was carried out with an overall reproducible yield of 3.8 %. This was a relatively long synthetic pathway consisting of nine steps. Moreover, the synthon used for the introduction of the ^{13}C isotopic substitution was used from the first step which is a drawback. However, the obtained amount of the mixture **^{13}C-12** - **^{13}C-13** was enough in order to study the reactivity with amino acids by ^{13}C-NMR.

The synthesis of 4-(^{13}C)-Lina-OOHs, **^{13}C-19** and **^{13}C-20**, was carried out with an overall reproducible yield of 9.5 %. This was an advantageous synthetic route as it was shorter with six steps even if the ^{13}C isotopic substitution was also introduced in the first step.

The synthesis of 2-(^{13}C)-Lina-OOHs could not be accomplished. The problem of the reduction of nitrile **^{13}C-22** to aldehyde **^{13}C-23** could not be resolved.

Further reactivity studies were thus only conducted with 5-(^{13}C)-Lina-OOHs and 4-(^{13}C)-Lina-OOHs.

3 REACTIVITY STUDIES TOWARDS AMINO ACIDS

In order to study radical-type processes involved in the haptenization of cutaneous proteins by allergenic allylic hydroperoxides, we were interested in the reactivity of ^{13}C-substituted Lina-OOHs towards various amino acids. Reactions were followed by one dimensional ^{13}C-NMR. The analysis of chemical structures of products resulting from the reactivity studies was carried out by two-dimensional ^{1}H-^{13}C heteronuclear NMR experiments HSQC and HMBC.

Several amino acids susceptible to conjugate with radical intermediates were selected. Amino acids having a sulfur atom have been demonstrated to be particularly labile and to be involved in radical reactions. Thus, cysteine was used as a potential spin trap for radicals derived from linalool hydroperoxides. Gardner *et al*. reported in the literature the formation of an adduct between *N*-acetyl-cysteine and 13-hydroperoxylinoleic acid (Figure 1.26).[29]

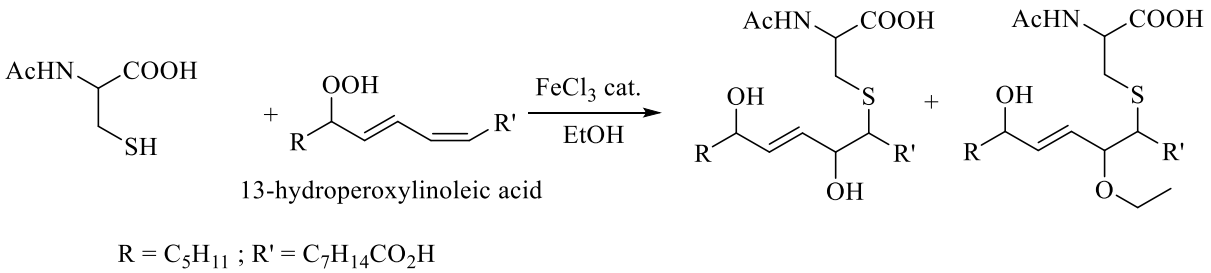

Figure 1.26: Adduct formation between 13-hydroperoxylinoleic acid and *N*-acetyl-cysteine in presence of a catalytic amount of iron chloride (III)[29]

Also, aromatic amino acids are involved in mono electron reaction mechanisms as shown by Grossi using peroxynitrite $ONOO^-$ on tyrosine in a DEPMPO spin trap environment (Figure 1.27).[30] We also used tryptophan and lysine as they contain lateral chains prompt to radical reactions.[31]

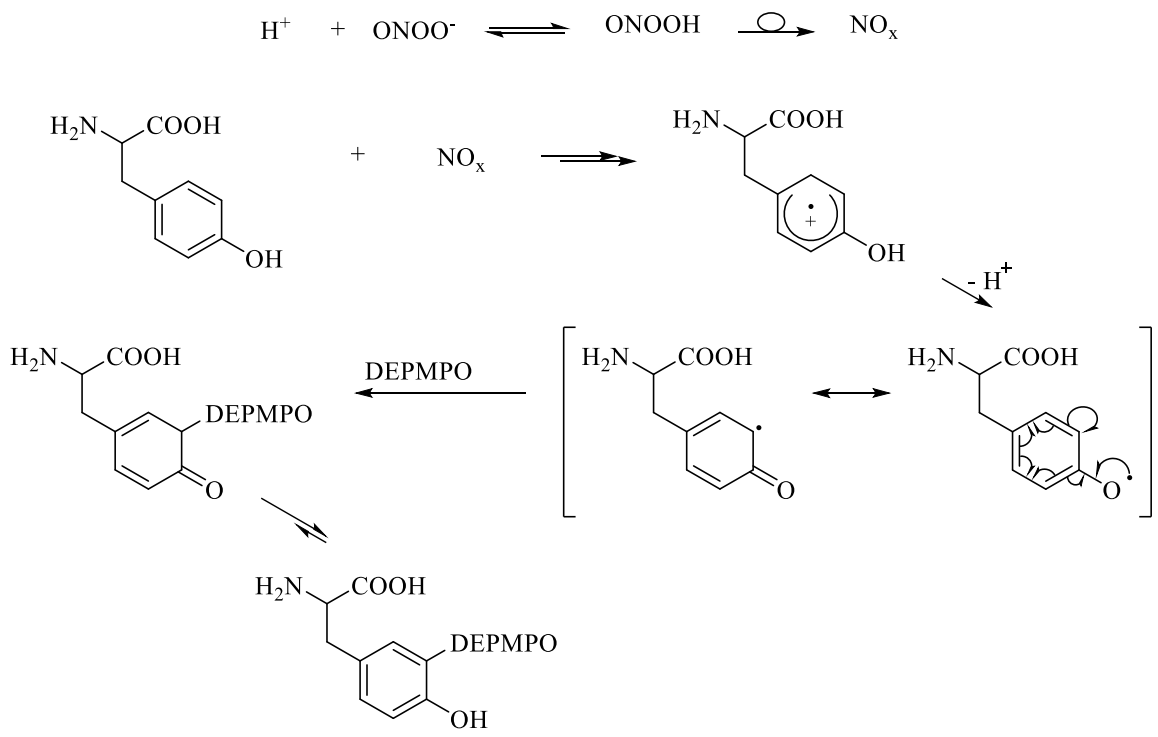

Figure 1.27: Spin trapping of a tyrosine carbon-centered radical by 5-diethoxyphosphoryl-5-methyl-1-pyrroline-*N*-oxide (DEPMPO)[30]

3.1 Experimental conditions

All experiments were performed using *N*-acetylated and esterified amino acids to mimic their chemical structure in a peptide sequence and to let free the potentially reactive side chain. In addition, the protection of the amino group represents a way of preventing the formation of Schiff bases with the carbonyl group of any allylic hydroperoxide degradation product.

^{13}C-Substituted Lina-OOHs (1 mg, 5.37 µM) in the presence of an excess of a methylic ester of the *N*-acetyl amino acids cysteine, tryptophan, tyrosine or lysine (2 to 10 eq. for each one), in a degassed mixture of deuterated acetonitrile and water (1/1, v/v) were treated with a catalytic amount of iron (II) sulfate at room temperature. The progress of the reaction was monitored by ^{13}C-NMR (on a Brucker Avance 500 MHz spectrometer) until complete disappearance of Lina-OOHs or no more evolution of the reaction.

3.2 Results and discussion

3.2.1 Reactivity profile using N-acetyl-L-cysteine methyl ester

The reaction of 5-(^{13}C)-Lina-OOHs (mixture **^{13}C-12**/**^{13}C-13**, 2/3), (1 eq., 5.37 µM) in CD_3CN/H_2O 1/1 with *N*-acetyl-L-cysteine methyl ester (2 and 10 eq., 10.74 and 53.70 µM) was followed by one dimensional ^{13}C-NMR at room temperature during one week. The catalytic amount of iron (II) sulfate heptahydrate (0.1 eq., 0.5 µM) was sufficient to induce radical initiation (Figure 1.28). Control experiments were realized without the presence of iron (II) as initiator.

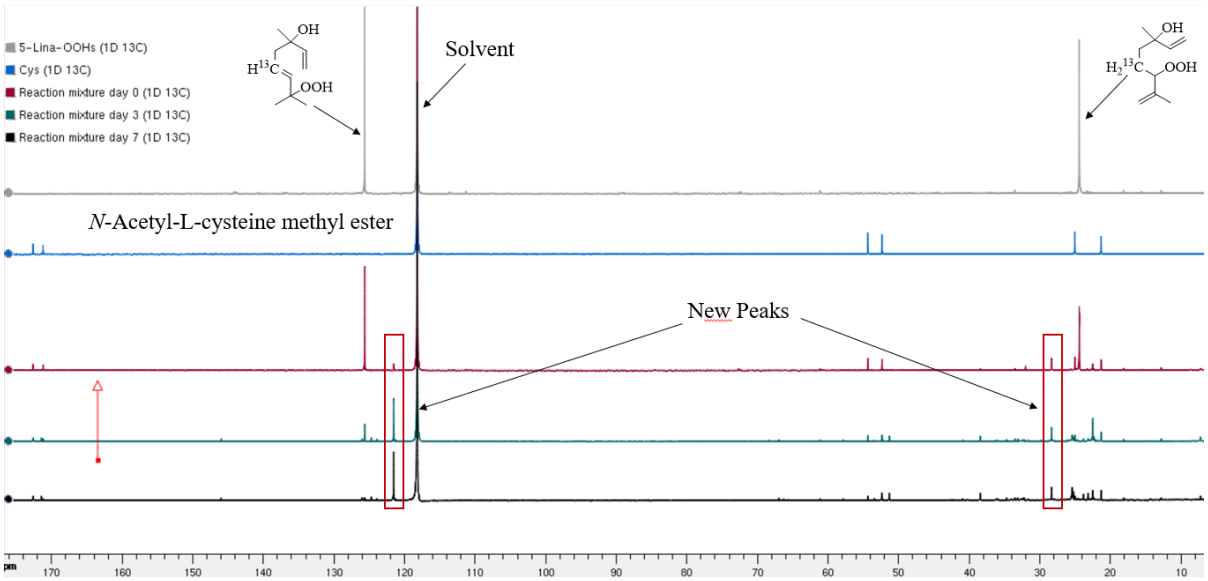

Figure 1.28: 5-^{13}C-Lina-OOHs (1 eq., 5.37 µM), *N*-Acetyl-L-cysteine methyl ester (2eq., 10.74 µM) and a catalytic amount of iron (II) (0.1 eq.) in CD_3CN/H_2O 1/1 medium during one week reaction time

In the spectra, it can be seen that ^{13}C peaks of 5-(^{13}C)-Lina-6-OOH **^{13}C-13** at 24.30 ppm and of 5-(^{13}C)-Lina-7-OOHs **^{13}C-12** at 125.70 ppm disappeared with time, and that new peaks appeared at 28.85 ppm and 122.06 ppm. Prediction of ^{13}C-NMR shifts by computer simulation suggested that the ^{13}C peak at 28.42 ppm could correspond to compound **27** and the ^{13}C peak at 122.06 ppm to compounds **25** or **26** (Figure 1.29).

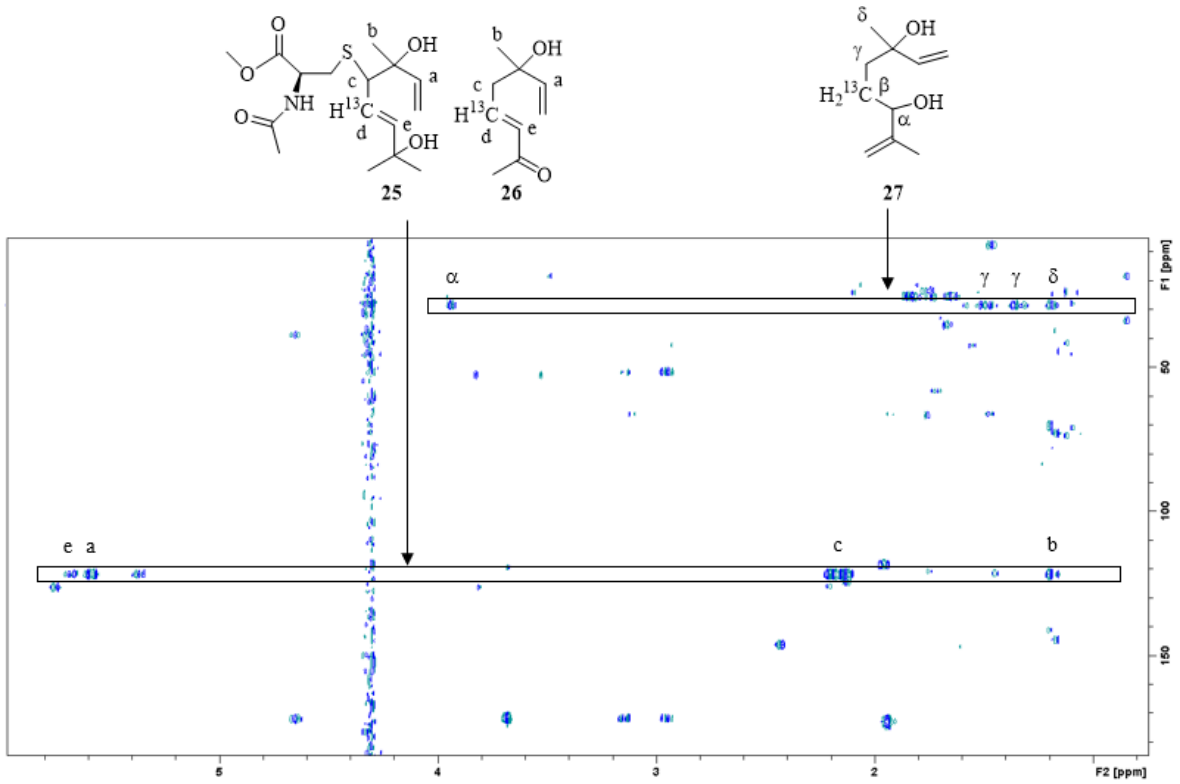

Figure 1.29: Hypothetical chemical structures of compounds **25**, **26** and **27** based on HMBC interpretation

Compound **25** and **26** have theoretically similar shifts for the terpene unit. We have seen on the HSQC the coupling carbon-proton shift **d** at 5.54/122.1 ppm. Furthermore, the HMBC shows coupling with protons at 1.18 ppm (**b**), 2.16 ppm (**c**), 5.58 ppm (**a**) and 5.68 ppm (**e**). This results indicated the presence of the **d-e** double bond in the chemical structure. However, carbon at 122.1 ppm coupled on HMBC with a protein at 5.58 ppm (**c**) corresponding more to compound **27** and not to a CH containing a cysteine linked.

On an other hand, carbon at 28.8 ppm (β) was coupled to protons at 1.45 ppm characteristic of a mehylene CH_2 carbon atom for compound **27**. Also, carbon β saw by HMBC protons at 1.19 ppm (δ), 1.35 ppm (γ) and 3.93 ppm (α).

Surprisingly, the same reactivity was observed without iron (II) acting as initiator of the radical reaction. This result suggested that radical initiation could happen spontaneously such as with daylight (Figure 1.30).

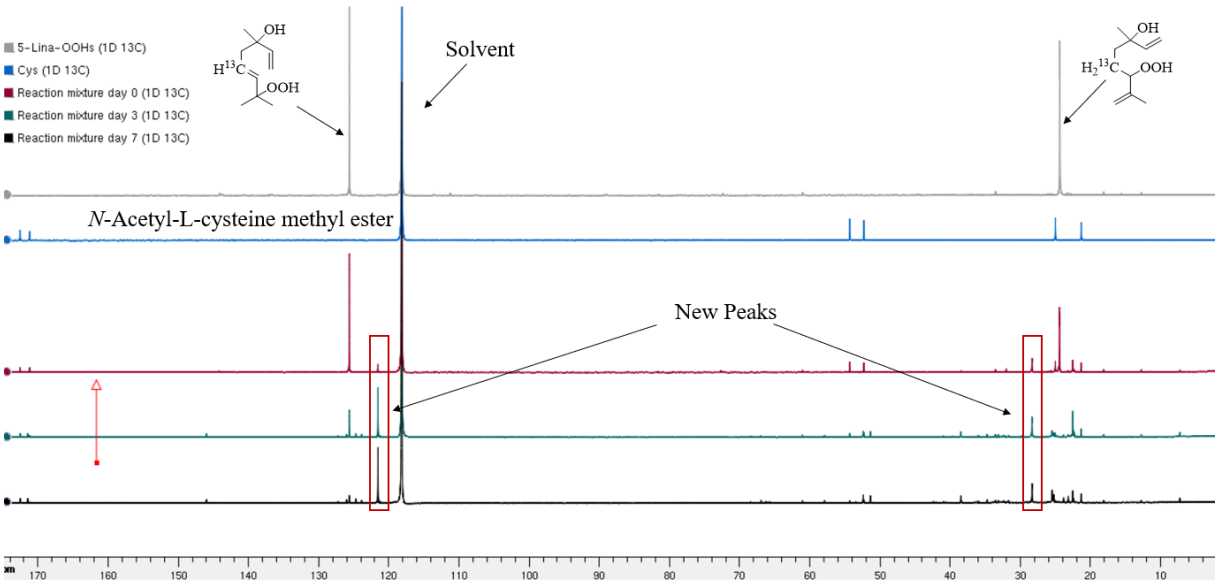

Figure 1.30: 5-^{13}C-Lina-OOHs (1 eq., 5.37 µM), *N*-Acetyl-L-cysteine methyl ester (2eq., 10.74 µM) without iron (II) in CD_3CN/H_2O 1/1 medium during one week reaction time

When a large excess of 10 equivalents of *N*-acetyl-L-cysteine methyl ester was used without iron (II) the reaction time was much shorter and almost all 5-^{13}C-Lina-OOHs reacted in just one day, instead of seven days for 2 equivalents. In the presence of iron (II) the reaction was even faster, about five hours. However, it was shown to be much more difficult to follow the reaction because carbon signals corresponding to cysteine were much more important. For this reason, it was decided to continue the studies using 2 equivalents of amino acid.

The reaction of 4-(^{13}C)-Lina-OOHs (1 eq. 5.37 µM) in CD_3CN/H_2O 1/1 with *N*-acetyl-L-cysteine methyl ester (2 eq. 10.74 µM) was followed by one dimensional ^{13}C-NMR at room temperature during one week. The catalytic amount of iron (II) sulfate heptahydrate (0.1 eq. 0.5 µM) was sufficient to induce radical initiation (Figure 1.31). Control experiments were realized without the presence of iron (II) as initiator.

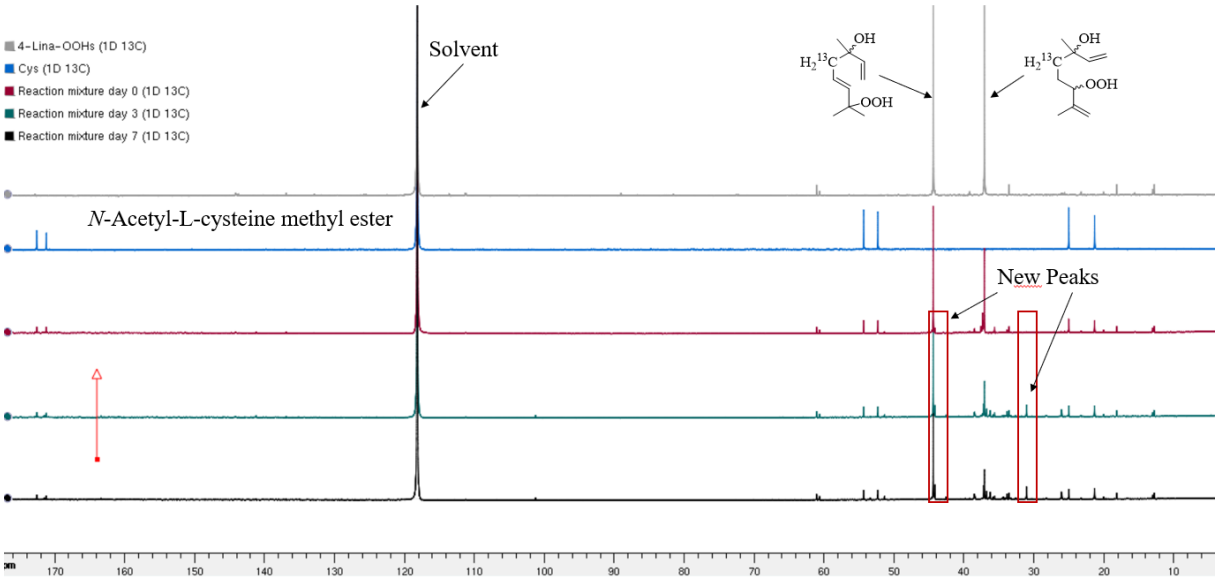

Figure 1.31: 4-^{13}C-Lina-OOHs (1 eq., 5.37 µM), *N*-Acetyl-L-cysteine methyl ester (2eq., 10.74 µM) and a catalytic amount of iron (II) (0.1 eq.) in CD_3CN/H_2O 1/1 medium during one week reaction time

In the spectra, it can be seen that especially the ^{13}C peak of 4-(^{13}C)-Lina-6-OOH **^{13}C-20** at 36.9 ppm disappeared with time and of 4-(^{13}C)-Lina-7-OOH **^{13}C-19** at 44.3 ppm. New peaks appeared at 31.04 ppm and 44.14 ppm. By meanings of computer simulation the ^{13}C peak at 31.04 ppm could correspond to compound **27** and at 44.14 ppm to adduct **25** or **26** (Figure 1.32). Here even a week after, 4-(^{13}C)-Lina-7-OOH **^{13}C-19** was not at all completely consumed. But it seems that 4-(^{13}C)-Lina-6-OOH **^{13}C-20** was consumed much more. Without iron (II) the same kind of reactivity was observed.

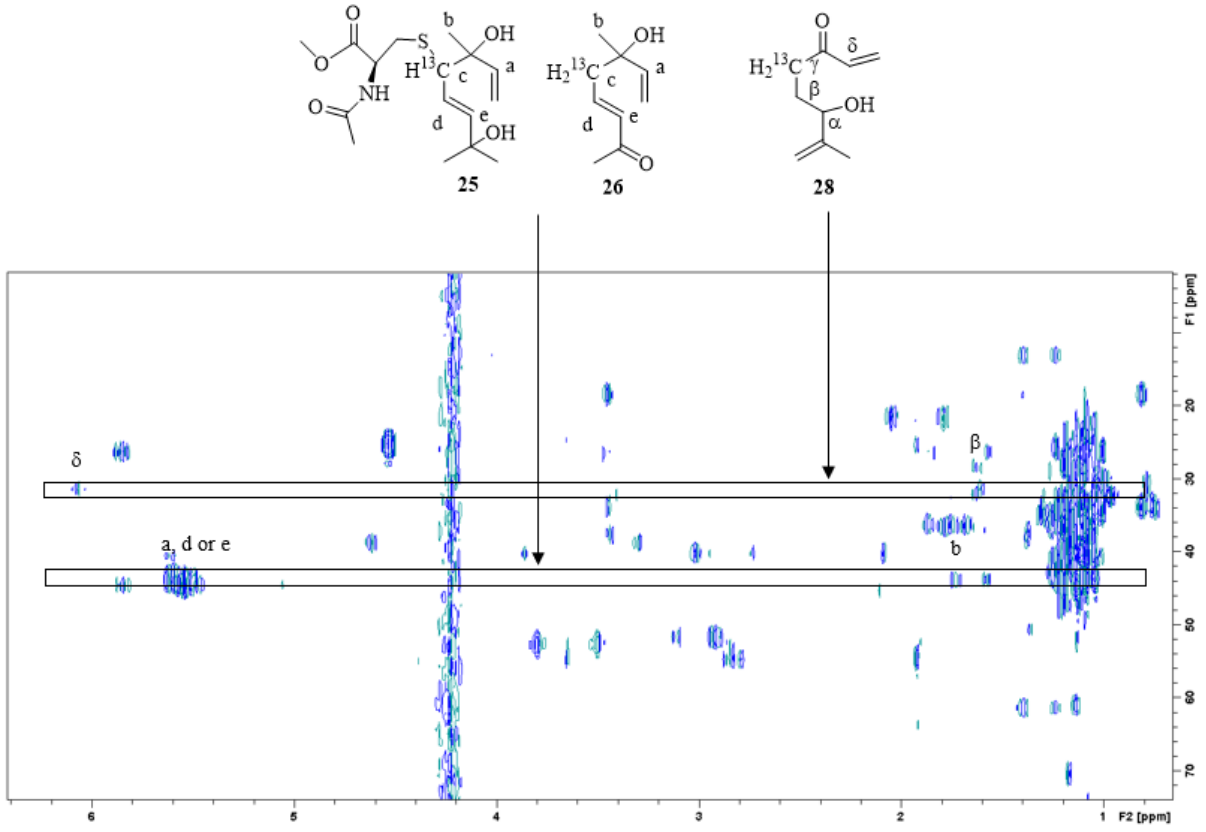

Figure 1.32: Hypothetical chemical structures of compounds **25**, **26** and **28** based on HMBC/HSQC interpretation

Compound **25** and **26** have theoretically similar shifts for the terpene unit. We have seen on the HSQC the coupling carbon-proton shift **c** 2.7/44.14 ppm, **γ** at 2.06/31.04 ppm. However, the HMBC shows coupling with protons at 1.68 ppm (**b**), 5.58 ppm (**a, d or e**). This results indicated the presence of the **d-e** double bond in the chemical structure. However, carbon at 44.14 ppm coupled on HMBC with a proton at 5.58 ppm (**d**) was not observed.

On an other hand, carbon at 31.04 ppm (γ) was coupled to protons at 2.06 ppm characteristic of a mehylene CH_2 carbon atom for compound **28**. Also, carbon **γ** saw by HMBC protons at 1.62 ppm (β) and 6.07 ppm (δ). The α shift was probably hidden by the pressaturation of the water sift, the band from 4.15 to 4.30 ppm. As seen in the part using 5-(^{13}C)-Lina-OOH two compounds can correspond, here by using 4-(^{13}C)-Lina-OOH it wasn't possible to gave more precision in. The difficulty here is that the 4-(^{13}C)-Lina-7-OOH didn't completely react and also the new compound appearing with pracitacly the same shift as the starting material (Figure 1.31). Unfortunately, this second step using 4-(^{13}C)-Lina-6-OOH doesn't entirely confirm the results obtained using 5-(^{13}C)-Lina-6-OOH.

3.2.2 Reactivity profile using N-acetyl-L-tyrosine methyl ester

The reaction of 5-(^{13}C)-Lina-OOHs (mixture **^{13}C-12/^{13}C-13,** 2/3), (1 eq., 5.37 µM) in CD_3CN/H_2O 1/1 with *N*-acetyl-L-tyrosine methyl ester (2 eq., 10.74 µM) was followed by one dimensional ^{13}C-NMR at room temperature during one week. The catalytic amount of iron (II) sulfate heptahydrate (0.1 eq., 0.5 µM) was sufficient to induce radical initiation (Figure 1.33). Control experiments were realized without the presence of iron (II) as initiator.

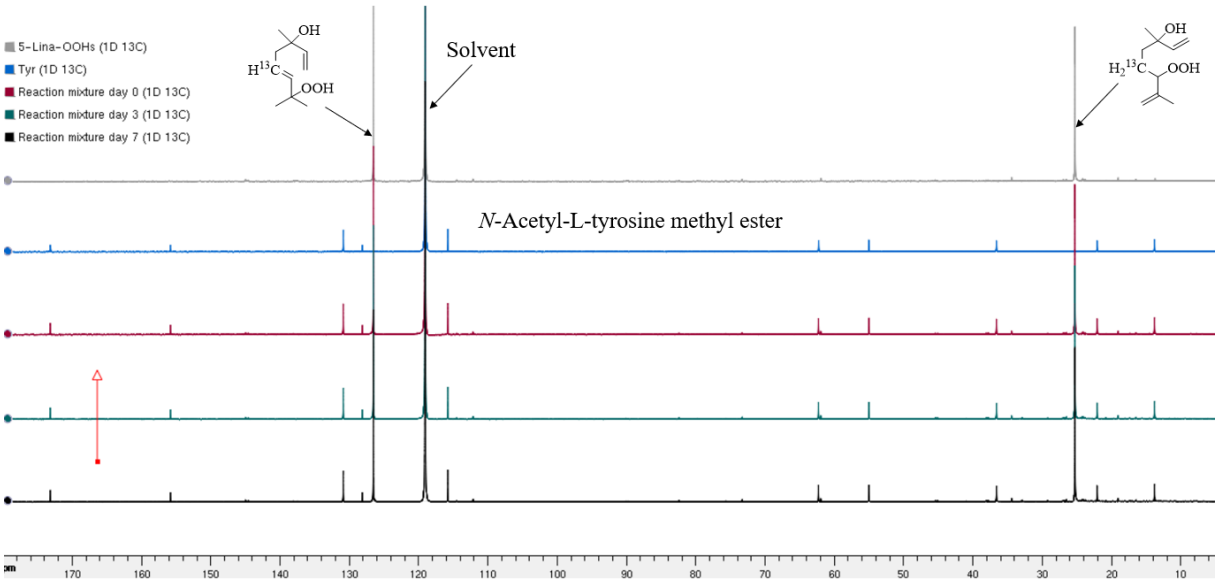

Figure 1.33: 5-^{13}C-Lina-OOHs (1 eq., 5.37 µM), *N*-acetyl-L-tyrosine methyl ester (2eq., 10.74 µM) and a catalytic amount of iron (II) (0.1 eq.) in CD_3CN/H_2O 1/1 medium during one week reaction time

No reaction was observed with unchanged ^{13}C peaks of 5-(^{13}C)-Lina-6-OOH at 24.3 ppm and of 5-(^{13}C)-Lina-7-OOH at 125.7 ppm, with and without iron (II).

The reaction of 4-(^{13}C)-Lina-OOHs (mixture **^{13}C-12/^{13}C-13**, 2/3), (1 eq., 5.37 µM) in CD_3CN/H_2O 1/1 with *N*-acetyl-L-tyrosine methyl ester (2 eq., 10.74 µM) was followed by one dimensional ^{13}C-NMR at room temperature during a week. The catalytic amount of iron (II) sulfate heptahydrate (0.1 eq., 0.5 µM) was sufficient to induce radical initiation (Figure 1.34). Control experiments were realized without the presence of iron (II) as initiator.

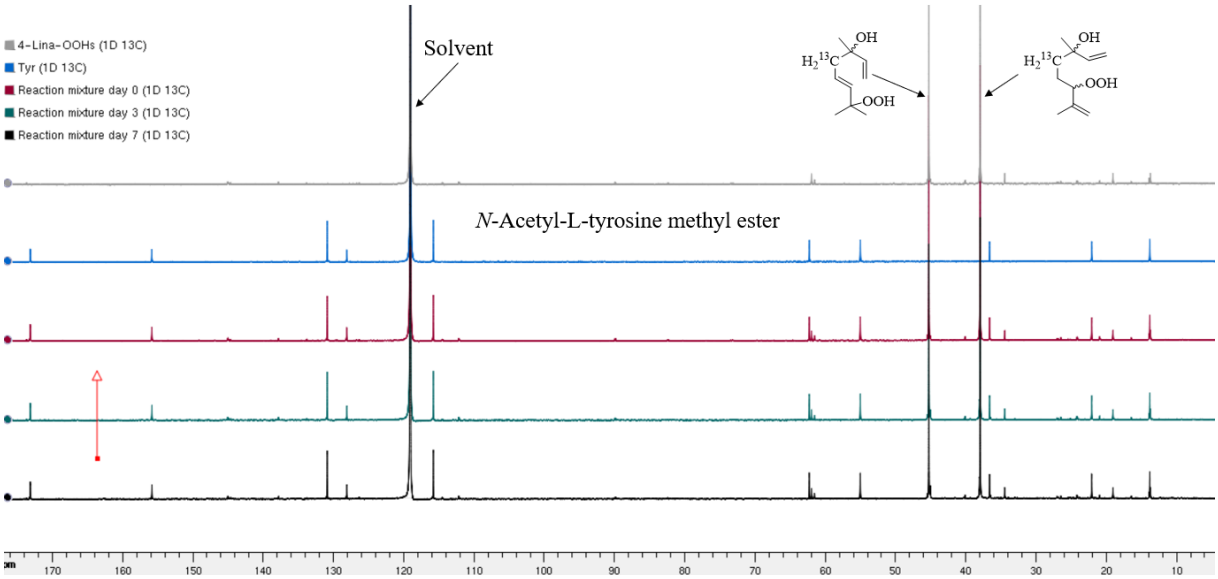

Figure 1.34: 4-^{13}C-Lina-OOHs (1 eq., 5.37 µM), *N*-acetyl-L-tyrosine methyl ester (2eq., 10.74 µM) and a catalytic amount of iron (II) (0.1 eq.) in CD_3CN/H_2O 1/1 medium during one week reaction time

Non-reaction was observed neither.

3.2.3 Reactivity profile using N-acetyl-L-tryptophan methyl ester

The reaction of 5-^{13}C-Lina-OOHs (mixture **^{13}C-12/^{13}C-13,** 2/3), (1 eq., 5.37 µM) in CD_3CN/H_2O 1/1 with *N*-acetyl-L-tryptophan methyl ester (2 eq., 10.74 µM) was followed by one dimensional ^{13}C-NMR at room temperature during a week. The catalytic amount of iron (II) sulfate heptahydrate (0.1 eq., 0.5 µM) was sufficient to induce radical initiation (Figure 1.35). Control experiments were realized without the presence of iron (II) as initiator.

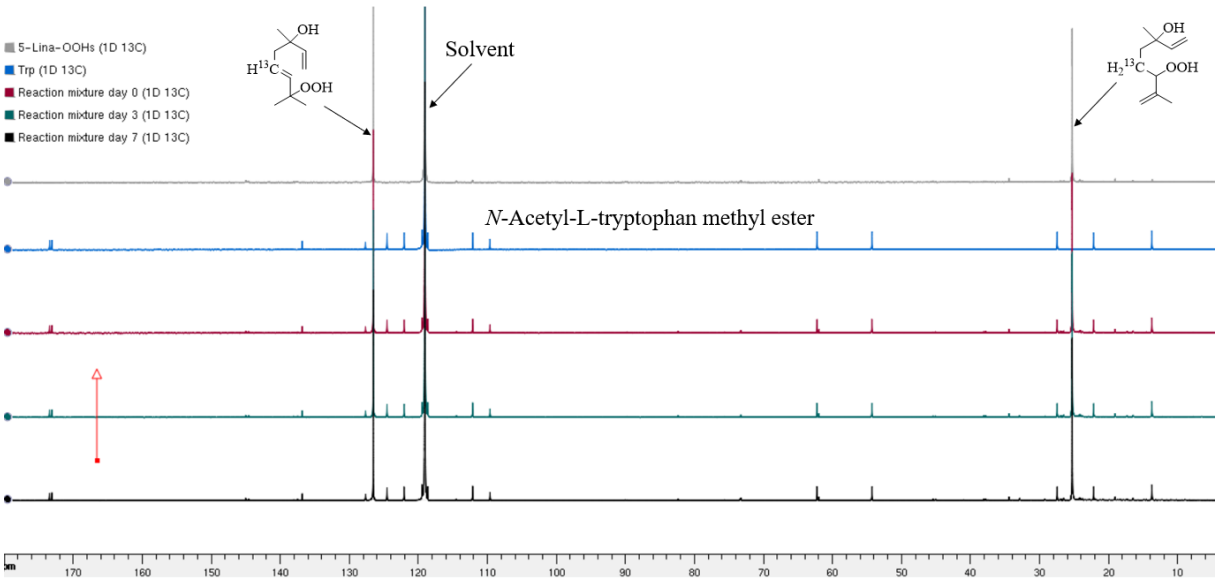

Figure 1.35: 5-^{13}C-Lina-OOHs (1 eq., 5.37 µM), *N*-Acetyl-L-tryptophan methyl ester (2eq., 10.74 µM) and a catalytic amount of iron (II) (0.1 eq.) in CD_3CN/H_2O 1/1 medium during one week reaction time

No-reaction was observed with unchanged ^{13}C peaks of 5-(^{13}C)-Lina-6-OOH at 24.3 ppm and of 5-(^{13}C)-Lina-7-OOH at 125.7 ppm, with and without iron (II).

The reaction of 4-(^{13}C)-Lina-OOHs (mixture **^{13}C-12/^{13}C-13**, 2/3), (1 eq., 5.37 µM) in CD_3CN/H_2O 1/1 with *N*-acetyl-L-tryptophan methyl ester (2 eq., 10.74 µM) was followed by one dimensional ^{13}C-NMR at room temperature during a week. The catalytic amount of iron (II) sulfate heptahydrate (0.1 eq., 0.5 µM) was sufficient to induce radical initiation (Figure 1.36). Control experiments were realized without the presence of iron (II) as initiator.

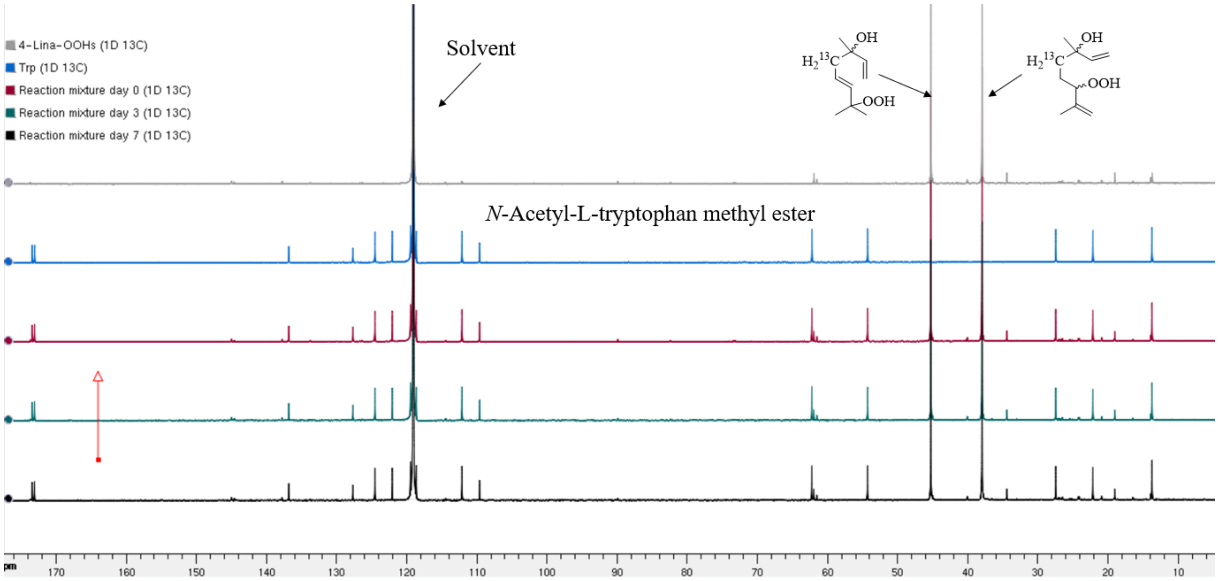

Figure 1.36: 4-^{13}C-Lina-OOHs (1 eq., 5.37 µM), *N*-Acetyl-L-tyrosine methyl ester (2eq., 10.74 µM) and a catalytic amount of iron (II) (0.1 eq.) in CD_3CN/H_2O 1/1 medium during one week reaction time

Non-reaction was observed neither.

3.2.4 Reactivity profile using N-acetyl-L-lysine methyl ester

The reaction of 5-^{13}C-Lina-OOHs (mixture **^{13}C-12/^{13}C-13,** 2/3), (1 eq., 5.37 µM) in CD_3CN/H_2O 1/1 with *N*-acetyl-L-lysine methyl ester (2 eq., 10.74 µM) was followed by one dimensional ^{13}C-NMR at room temperature during a week. The catalytic amount of iron (II) sulfate heptahydrate (0.1 eq., 0.5 µM) was sufficient to induce radical initiation (Figure 1.37). Control experiments were realized without the presence of iron (II) as initiator.

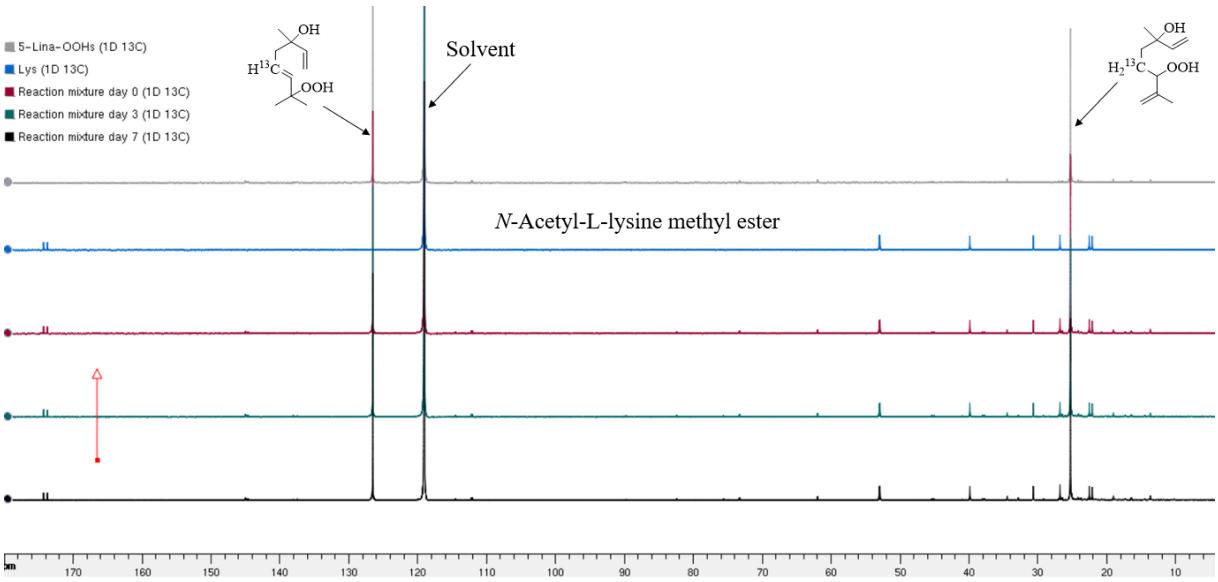

Figure 1.37: 5-(^{13}C)-Lina-OOHs (1 eq., 5.37 µM), *N*-acetyl-L-lysine methyl ester (2eq., 10.74 µM) and a catalytic amount of iron (II) (0.1 eq.) in CD_3CN/H_2O 1/1 medium during one week reaction time

No-reaction was observed with unchanged, ^{13}C peaks of 5-(^{13}C)-Lina-6-OOH at 24.3 ppm and of 5-(^{13}C)-Lina-7-OOH at 125.7 ppm, with and without iron (II).

The reaction of 4-(^{13}C)-Lina-OOHs (mixture **^{13}C-12/^{13}C-13**, 2/3), (1 eq., 5.37 µM) in CD_3CN/H_2O 1/1 with *N*-acetyl-L-lysine methyl ester (2 eq., 10.74 µM) was followed by one dimensional ^{13}C-NMR at room temperature during a week. The catalytic amount of iron (II) sulfate heptahydrate (0.1 eq. 0.5 µM) was sufficient to induce radical initiation (Figure 1.38). Control experiments were realized without the presence of iron (II) as initiator.

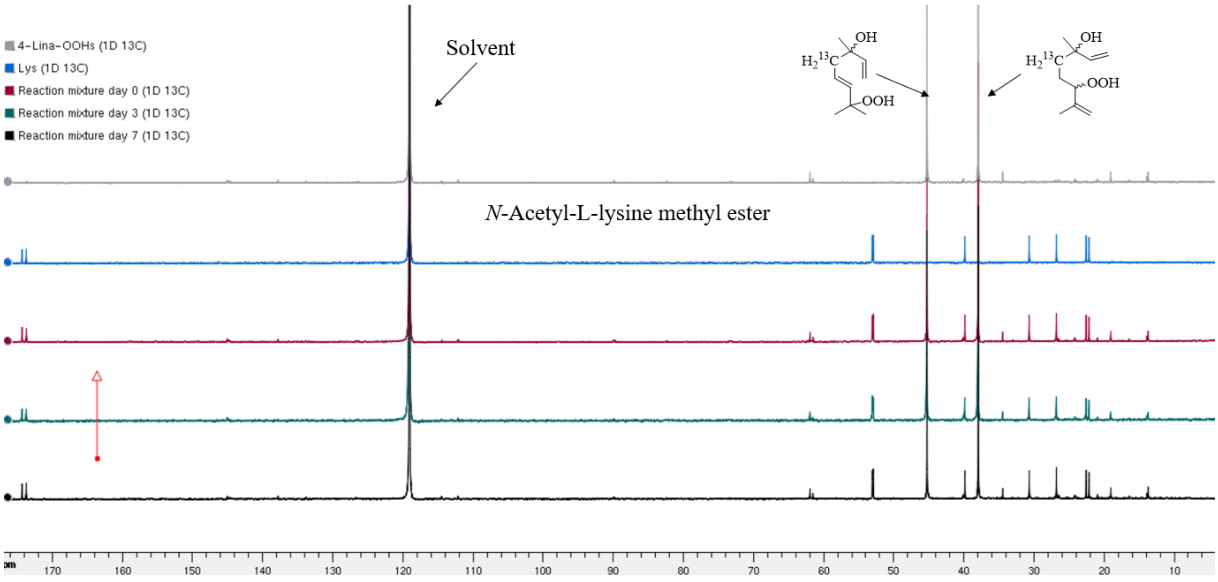

Figure 1.38: 4-^{13}C-Lina-OOHs (1 eq., 5.37 µM), *N*-acetyl-L-tyrosine methyl ester (2eq., 10.74 µM) and a catalytic amount of iron (II) (0.1 eq.) in CD_3CN/H_2O 1/1 medium during one week reaction time

Non-reaction was observed neither.

3.3 Conclusion:

The reactivity of 5-(^{13}C)-Lina-OOHs, **^{13}C-12** and **^{13}C**-13, and of 4-(^{13}C)-Lina-OOHs, **^{13}C-19** and **^{13}C-20**, was carried out with four different protected amino acids. This study showed transformation of 5-(^{13}C)-Lina-OOHs (**^{13}C-12** and **^{13}C-13**) and 4-(^{13}C)-Lina-OOHs (**^{13}C-19** and **^{13}C-20**) only in presence of *N*-acetyl-L-cysteine methyl ester. The 5-(^{13}C)-Lina-OOHs (**^{13}C-12** and **^{13}C-13**) ^{13}C peaks disappeared completely in a week reaction time whereas 4-(^{13}C)-Lina-OOHs (**^{13}C-19** and **^{13}C-20**) didn't completely disappear after a week reaction time. Furthermore, 5-(^{13}C)-Lina-6-OOHs **^{13}C-13** disappeared faster than **^{13}C-12**, also 4-(^{13}C)-Lina-6-OOHs **^{13}C-20** disappeared faster than 4-(^{13}C)-Lina-7-OOHs **^{13}C-19**, so is Lina-6-OOH hypothetically more reactive then Lina-7-OOH.

In this study only some hypothetical new compounds formed could be proposed.

Experimental section: Chapter 1

4 MATERIALS AND METHODS

4.1 Chemicals and reagents

Anhydrous solvents were obtained by distillation under an inert atmosphere of argon and kept on molecular sieves (4 Å):

- Dimethylformamide was dried on phosphorous pentoxide then distilled under reduced pressure
- Ethanol and diisopropylamine were distilled on sodium hydroxide
- Triethylamine was distilled with potassium hydroxide
- Tetrahydrofuran, diethyl ether, toluene, methanol, dichloromethane and acetonitrile were dried through activated alumina columns

All reactions needing anhydrous conditions were carried out under argon atmosphere in flame-dried glassware.

Limonene, linalool, and (-)-carveol were purchased from Sigma-Aldrich (Saint Quentin Fallavier, France) as a mixture of isomers and were used without further purification.

1-(^{13}C)-Acetic acid, 2-(^{13}C)-acetic acid and potassium-1-(^{13}C)-cyanide were purchased from Euriso-top (Saint-Aubin, France).

All other reagents and solvents were purchased from Sigma-Aldrich or Fisher Scientific (Illkirch-Graffenstaden, France) and were used as received.

n-Butyllithium was purchased as a 1.6 M solution in hexane and the solution was titrated using the method described by Suffert[32]

Follow-up of the reactions

Reactions were followed by thin layer chromatography (TLC) using silica gel plates 60 F_{254} (Merck 60 F_{254}; thickness 0.25 mm). After elution, the plates were revealed under short-wave UV radiation (254 nm), then immersed in phosphomolybdic acid, anisaldehyde or potassium permanganate solutions followed by heating.

Phosphomolybdic acid solution (APM/Ce):

- phosphomolybdic acid (5 g) and cerium sulfate tetrahydrate (2 g) in a mixture of sulfuric acid (12 mL) and distilled water (188 mL)

Anisaldehyde solution (Anis.):

- *para*-anisaldehyde (0.5 mL) and *ortho*-anisaldehyde (0.5 mL) in a mixture of sulfuric acid (5 mL), acetic acid (100 mL) and ethanol (8 mL)

Potassium permanganate solution:

- Dissolve 1.5 g $KMnO_4$, 1.25 mL NaOH 10% and 10 g K_2CO_3 in 200 mL water

Chemical purifications

Column chromatography purifications were performed using silica 60 (Merck; Geduran, 40-63 µm) or previously neutralized silica gel.

Neutralized silica was prepared by adding to a homogeneous water solution of silica 60 a saturated solution of sodium hydrogen carbonate up to pH of about 8. After decantation, the silica precipitate was washed with water to reach a pH around 7, filtered and dried in an oven at least for 24 hours.

NMR characterization

^1H and ^{13}C-NMR spectra were recorded on a Bruker Avance 300 (300 MHz for ^1H and 75 MHz for ^{13}C) and a Bruker Avance 500 (500 MHz for ^1H and 125 MHz for ^{13}C) spectrometers. The chemical shifts (δ) are reported in ppm and coupling constants (J) are reported in Hz. The chemical shifts (δ) are indirectly referenced to TMS via the solvent signal $CHCl_3$ ($CDCl_3$ δ^1H = 7.26 ppm; $\delta^{13}C$ = 77.2 ppm). Multiplicity was denoted as s (singlet), sl (singlet large), d (doublet), dd (doublet of doublets), t (triplet) and m (multiplet).

4.2 Synthesis of 5-(^{13}C)Lina-OOHs

2-Bromo-1-(^{13}C)-ethyl acetate (^{13}C-4)

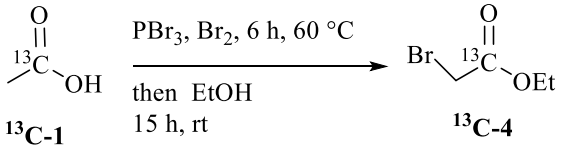

^{13}C-1 **^{13}C-4**

In a flame-dried double-necked flask under argon, to a solution of 1-(^{13}C)-acetic acid **^{13}C-1** (2.0 g; 33.3 mmol; 1 eq.) and phosphorus tribromide (1.60 mL; 16.66 mmol; 0.5 eq.) was slowly added bromine (6.0 mL; 116.56 mmol; 3.5 eq.). The mixture was stirred during 30 minutes at room temperature, then heated at 60 °C for 6 hours. After that time the mixture was cooled to room temperature before anhydrous ethanol (3.6 mL; 63.28 mmol; 1.9 eq.) was added. After one night at room temperature, the reaction mixture was hydrolyzed with ethanol (10 mL) and

distilled water (30 mL). The mixture was extracted with diethyl ether (3 × 30 mL). Collected organic phases were neutralized using a saturated solution of sodium bicarbonate (2 × 30 mL) and washed with a saturated solution of sodium thiosulfate (30 mL then 20 mL). Organic phases were dried over magnesium sulfate, filtered and concentrated under reduced pressure. 2-Bromo-1-(^{13}C)-ethyl acetate **^{13}C-4** (3.67 g) was obtained as an orange oil and was used without further purification.

Formula: $C_3{}^{13}C\ H_7BrO_2$

Molar mass: 167.99 g.mol^{-1}

CAS (non ^{13}C-substituted): 105-36-2

NMR ^{1}H (CDCl$_3$, δ, ppm): 1.28 (t, 3H, OCH$_2$C**H$_3$**, $^3J_{HH}$ = 7.5 Hz), 3.81 (d, 2H, C**H$_2$**, $^2J_{HC}$ = 5.0 Hz), 4.22 (qd, 2H, OC**H$_2$**CH$_3$, $^3J_{HH}$ = 7.0 Hz, $^3J_{HC}$ = 3.0 Hz).
NMR ^{13}C (CDCl$_3$, δ, ppm): 14.1 (**C**H$_3$), 26.3 (d, **C**H$_2$Br, $^1J_{CC}$ = 64.6 Hz), 62.4 (O**C**H$_2$CH$_3$), 167.4 (^{13}**C**=O).

2-(Diethoxyphosphoryl)-1-(^{13}C)-ethyl acetate (^{13}C-5)

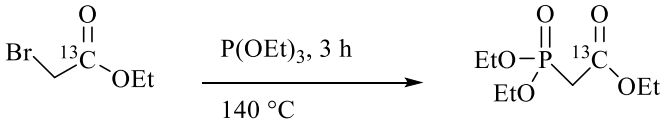

^{13}C-4 **^{13}C-5**

In a flame-dried round bottom flask under argon triethyl phosphite (4.7 mL; 26.21 mmol; 1.2 eq.) was added to 2-bromo-1-(^{13}C)-ethyl acetate (**^{13}C-4**) (3.67 g; 21.84 mmol; 1eq.). The mixture was heated at 140°C for 3 hours and then cooled to room temperature. The product was purified by silica gel chromatography (AcOEt/pentane 8/2). 2-(Diethoxyphosphoryl)-1-(^{13}C)-ethyl acetate (**^{13}C-5**) was obtained as a yellow oil (4.95 g; 90 %).

Formula: $C_7{}^{13}CH_{17}O_5P$

Molar mass: 225.19 g.mol^{-1}

CAS (non ^{13}C-substituted): 864-13-0

TLC: Rf = 0.24 (AcOEt/pentane 8/2): APM/Ce

NMR ^{1}H ($CDCl_3$, δ, ppm) : 1.26 (t, 3H, $OCH_2C\mathbf{H_3}$, $^{3}J_{HH}$ = 7.0 Hz), 1.32 (t, 6H, 2 × $OCH_2C\mathbf{H_3}$, $^{3}J_{HH}$ = 7.5 Hz), 2.94 (dd, 2H, $C\mathbf{H_2}$, $^{2}J_{HP}$ = 22.0 Hz, $^{2}J_{HC}$ = 7.5 Hz), 4.06-4.20 (m, 6H, 3 × $OC\mathbf{H_2}CH_3$).

NMR ^{13}C ($CDCl_3$, δ, ppm) : 14.1 ($OCH_2\mathbf{C}H_3$), 16.4 (d, 2 × $OCH_2\mathbf{C}H_3$, $^{3}J_{CP}$ = 6.5 Hz), 34.5 (dd, $\mathbf{C}H_2$, $^{1}J_{CC}$ = 59.0 Hz, $^{1}J_{CP}$ = 134.0 Hz), 61.6 ($O\mathbf{C}H_2CH_3$), 62.7 (d, 2 × $O\mathbf{C}H_2CH_3$, $^{2}J_{CP}$ = 6.5 Hz), 166.0 (d, $^{13}\mathbf{C}$=O, $^{2}J_{CP}$ = 6.1 Hz).

Ethyl-1-(^{13}C)-3-methyl but-2-enoate (^{13}C-6)

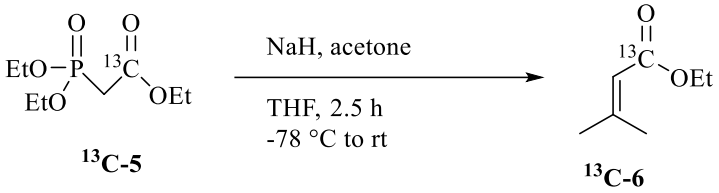

^{13}C-5 **^{13}C-6**

Sodium hydride (60 % in mineral oil, 0.87 g; 22.10 mmol; 1 eq.) was introduced in a flamed dried flask under argon. 2-(Diethoxyphosphoryl)-1-(^{13}C)-ethyl acetate (**^{13}C-5**) (4.95 g; 22.10 mmol; 1eq.) dissolved in anhydrous tetrahydrofuran (50 mL) was added at 0 °C. The mixture was stirred for 15 minutes. Anhydrous acetone (1.57 mL; 20.1 mmol; 0.95 eq.) was added to the reaction and the mixture was stirred during 30 minutes at 0°C then allowed to warm to room temperature overnight. The reaction was quenched using a saturated solution of ammonium chloride (25 mL). The aqueous phase was extracted with diethyl ether (3 × 80mL), organic fractions collected, dried over magnesium sulfate, filtered then concentrated under reduced pressure. The product was purified by silica gel column chromatography (pentane/diethyl ether 97/3), to obtain **^{13}C-6** as a yellow oil (1.46 g; 51 %).

Formula: $C_6{}^{13}CH_{12}O_2$

Molar mass: 129.16 g.mol^{-1}

CAS (non ^{13}C-substituted): 638-10-8

TLC: Rf = 0.3 (pentane/diethylether 97/3): $KMnO_4$

NMR ^{1}H ($CDCl_3$, δ, ppm): 1.25 (t, 3H, $OCH_2C\mathbf{H_3}$, $^{3}J_{HH}$ = 7.1 Hz), 1.88 (s, 3H, $C\mathbf{H_3}$ *cis*), 2.14 (s, 3H, $C\mathbf{H_3}$ *trans*), 4.15 (dd, 2H, $C\mathbf{H_2}$, $^{3}J_{HH}$ = 7.1 Hz, $^{3}J_{HC}$ = 3.1 Hz), 5.67 (m, 1H, =C**H**).

NMR ^{13}C ($CDCl_3$, δ, ppm): 13.9 ($OCH_2\mathbf{C}H_3$), 19.9 ($\mathbf{C}H_3$ *cis*), 27.7 ($\mathbf{C}H_3$ *trans*), 59.2 ($O\mathbf{C}H_2CH_3$), 116.0 (d, =**C**H, $^{1}J_{CC}$ = 75.4 Hz), 156.5 (($CH_3)_2\mathbf{C}$=), 166.7 ($^{13}\mathbf{C}$=O).

1-(^{13}C)-3-Methylbut-2-en-1-ol (^{13}C-7)

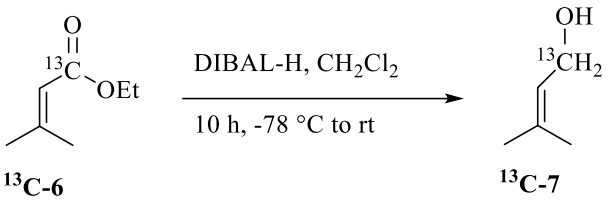

^{13}C-6 **^{13}C-7**

A diisobutylaluminum hydride solution in dichloromethane (27.50 mL; 27.50 mmol; 2.4 eq.) was introduced into a flame-dried round bottom flask equipped with an addition funnel and cooled at -78°C. **^{13}C-6** (1.46 g; 11.43 mmol; 1 eq.) dissolved in anhydrous dichloromethane (20 mL) was slowly added. The reaction mixture was allowed to warm to room temperature overnight. The reaction was stopped by adding ethyl acetate (10 mL) and water (10 mL). The solution was filtered on celite and the organic phase was separated. The aqueous phase was extracted with diethyl ether (2 × 10 mL). The combined organic phases were dried over magnesium sulfate, filtered and concentrated under reduced pressure. 1-(^{13}C)-3-Methyl but-2-en-1-ol (**^{13}C-7**) (1.65 g) was obtained as a transparent oil and used without further purification.

Formula: $C_4{}^{13}CH_{10}O$

Molar mass: 87.13 g.mol^{-1}

CAS (non ^{13}C-substituted): 556-82-1

NMR ^{1}H (CDCl$_3$, δ, ppm): 1.69 (s, 3H, C**H$_3$** *cis*), 1.75 (s, 3H, C**H$_3$** *trans*), 4.10 (dd, 2H, ^{13}C**H$_2$**, $^{3}J_{HH}$ = 7.1 Hz, $^{1}J_{HC}$ = 142.1 Hz), 5.41 (m, 1H, =C**H**).
NMR ^{13}C (CDCl$_3$, δ, ppm): 17.8 (**C**H$_3$ *cis*), 25.7 (**C**H$_3$ *trans*), 59.3 (HO^{13}**C**H$_2$), 123.6 (d, =**C**H, $^{1}J_{CC}$ = 47.0 Hz), 136.3 ((CH$_3$)$_2$**C**=).

1-(^{13}C)-1-Bromo-3-methyl but-2-ene (^{13}C-8)

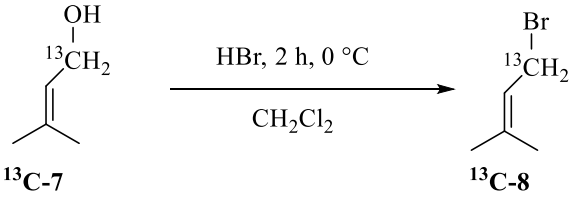

^{13}C-7 **^{13}C-8**

To a solution of 1-(^{13}C)-3-methylbut-2-en-1-ol (**^{13}C-7**) (1.65 g; 19.17 mmol; 1 eq.) in dichloromethane (7 mL) cooled at 0°C was added hydrobromic acid (48%; 24.3 mL; 214.2

mmol; 11.2 eq.). The mixture, protected from daylight, was vigorously stirred for 2 hours. Magnesium sulfate (6.69 g; 55.72 mmol; 2.9 eq.) and dichloromethane (30 mL) were then added and the solution was allowed to warm to room temperature. The organic phase was separated, and the aqueous phase was extracted using dichloromethane (2 × 20 mL). The combined organics layers were assembled and dried over magnesium sulfate. The solvent was evaporated under reduced pressure. 1-(^{13}C)-1-Bromo-3-methyl but-2-ene (**^{13}C-8**) (1.44 g) was obtained as a brown oil, used without further purification.

Formula: $C_4{}^{13}CH_9Br$

Molar mass: 150.02 g.mol^{-1}

CAS (non ^{13}C-substituted): 870-63-3

NMR ^{1}H ($CDCl_3$, δ, ppm): 1.73 (s, 3H, C**H$_3$** *cis*), 1.78 (s, 3H, C**H$_3$** *trans*), 4.15 (dd, 2H, C**H$_2$**, $^3J_{HH}$ = 8.5 Hz, $^1J_{HC}$ = 153.0 Hz), 5.48-5.56 (m, 1H, =C**H**).
NMR ^{13}C ($CDCl_3$, δ, ppm): 17.5 (**C**H$_3$ *cis*), 25.8 (**C**H$_3$ *trans*), 29.7 (^{13}**C**H$_2$), 121.6 (d, =**C**H, $^1J_{CC}$ = 47.0 Hz), 137.9 ((CH$_3$)$_2$**C**=).

Ethyl-3-(^{13}C)-2-acetyl-5-methylhex-4-enoate (^{13}C-9)

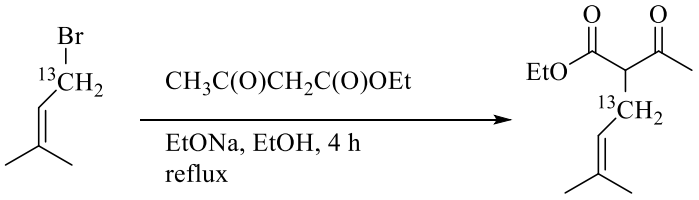

^{13}C-8 **^{13}C-9**

In a flame-dried round bottom flask, sodium ethoxide (4.34 mL; 11.62 mmol; 1.2 eq.) was added to a solution of ethyl acetoacetate (2.47 mL; 19.37 mmol; 2 eq.) in anhydrous ethanol (20 mL). The mixture was cooled to 0°C and a solution of 1-(^{13}C)-1-bromo-3-methylbut-2-ene (**^{13}C-8**) (1.44 g; 9.6 mmol; 1 eq.) in ethanol (10 mL) was added to the mixture. After stirring 1 hour at 0 °C, the solution was refluxed for 4 hours. The solvent was evaporated under reduced pressure, then water (5 mL) was added and the aqueous phase was extracted with ethyl acetate (3 × 15 mL). The combined organic phases were dried over magnesium sulfate and evaporated under reduced pressure. The crude product was purified using silica gel chromatography (pentane/Et_2O 9/1) and ethyl-3-(^{13}C)-2-acetyl-5-methylhex-4-enoate (**^{13}C-9)** was obtained as a

colorless oil (1.289 g; 67%).

Formula: $C_{10}{}^{13}CH_{18}O_3$

Molar mass: 199.25 g.mol^{-1}

CAS (non ^{13}C-substituted): 1845-52-9

TLC : Rf = 0.33 (Pentane/Et_2O 9/1) : APM/Ce

NMR ^{1}H ($CDCl_3$, δ, ppm): 1.25 (t, 3H, $OCH_2C\mathbf{H_3}$, $^3J_{HH}$ = 7.1 Hz), 1.63 (s, 3H, C**H$_3$** *cis*), 1.67 (s, 3H, C**H$_3$** *trans*), 2.22 (s, 3H, $COC\mathbf{H_3}$), 2.53 (m, 2H, $^{13}C\mathbf{H_2}$), 3.40 (m, 1H, C**H**), 4.19 (q, 2H, $OC\mathbf{H_2}$ CH_3, $^3J_{HH}$ = 7.1 Hz), 4.98-5.06 (m, 1H, =C**H**).

NMR ^{13}C ($CDCl_3$, δ, ppm): 14.0 (OCH_2 **C**H_3), 17.6 (**C**H_3 *cis*), 25.8 (**C**H_3 *trans*), 27.1 (^{13}**C**H_2), 59.8 (d, **C**H, $^1J_{CC}$ = 34.2 Hz), 60.4 (CO**C**H_3), 61.4 (O**C**H_2CH_3), 120.1 (d, =**C**H, $^1J_{CC}$ = 44.1 Hz), 134.9 (($CH_3)_2$**C**=), 169.6 ((O)**C**=O), 203.0 (**C**=O).

4-(^{13}C)-6-Methylhept-5-en-2-one (^{13}C-10)

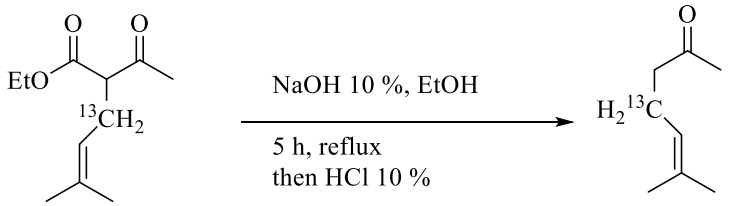

^{13}C-9 **^{13}C-10**

An aqueous solution of sodium hydroxide (10%, 18 mL) was added to a solution of ethyl-3-(^{13}C)-2-acetyl-5-methylhex-4-enoate (**^{13}C-9**) (1.29 g; 6.50 mmol; 1 eq.) in ethanol (20 mL) at 0°C. The mixture was refluxed during 5 hours before allowing to warm to room temperature. Then it was acidified using a solution of hydrochloric acid 10% down to pH 4-5. The aqueous phase was extracted with diethyl ether (3 × 50 mL). The combined organic phases were dried over magnesium sulfate and evaporated under reduced pressure. 4-(^{13}C)-6-Methylhept-5-en-2-one (**^{13}C-10**) (0.26 g) was obtained as colorless oil and was used without further purification.

Formula: $C_7{}^{13}CH_{14}O$

Molar mass: 127.19 g.mol^{-1}

CAS (non ^{13}C-substituted): 110-93-0

TLC: Rf = 0.3 (petroleum ether/Et_2O 9/1): APM/Ce

NMR ^{1}H ($CDCl_3$, δ, ppm): 1.61 (s, 3H, C**H$_3$** *cis*), 1.67 (s, 3H, C**H$_3$** *trans*), 2.13 (s, 3H, COC**H$_3$**), 2.36 (m, 2H, C**H$_2$**CO), 2.53 (m, 2H, ^{13}C**H$_2$**CH), 5.01-5.08 (m, 1H, =C**H**).
NMR ^{13}C ($CDCl_3$, δ, ppm): 17.6 (**C**H$_3$ *cis*), 22.5 (^{13}**C**H$_2$CH), 25.7 (**C**H$_3$ *trans*), 29.9 (CO**C**H$_3$), 44.3 (d, **C**H$_2$ CO, $^1J_{CC}$ = 34.5 Hz), 122.6 (d, =C**H**, $^1J_{CC}$ = 44.2 Hz), 132.7 ((CH$_3$)$_2$**C**=), 208.9 (**C**=O).

5-(^{13}C)-3,7-Dimethylocta-1,6-dien-3-ol; 5-(^{13}C)-Linalool (^{13}C-11)

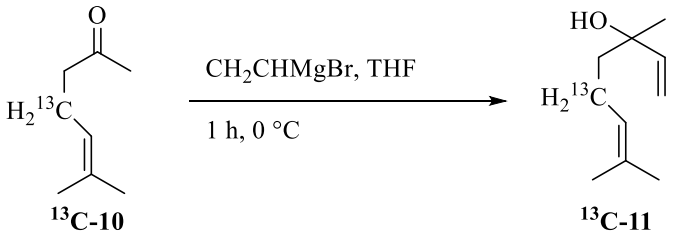

^{13}C-10 **^{13}C-11**

In a flame-dried round bottom flask, vinyl magnesium bromide (4.12 mL; 4.12 mmol; 2 eq.) was added to a solution of 4-(^{13}C)-6-methylhept-5-en-2-one (**^{13}C-10**) (0.26 g; 2.06 mmol; 1 eq.) in anhydrous tetrahydrofuran (10 mL) previously cooled to 0 °C. After stirring 1 hour at 0 °C, the reaction was stopped using a saturated solution of ammonium chloride (10 mL). The aqueous phase was extracted with diethyl ether (3 × 30 mL). The combined organic phases were dried over magnesium sulfate and evaporated under reduced pressure. The crude product was purified by silica gel column chromatography (pentane/Et_2O 8/2) and 5-(^{13}C)-linalool (**^{13}C-11**) was obtained as a yellow oil (0.198 g; 63 %).

Formula: $C_9{}^{13}CH_{18}O$

Molar mass: 155.25 g.mol^{-1}

CAS (non ^{13}C-substituted): 78-70-6

TLC: Rf = 0.30 (pentane/Et_2O 8/2) : APM/Ce

NMR ^{1}H ($CDCl_3$, δ, ppm): 1.27 (s, 3H, C**H$_3$**), 1.52-1.57 (m, 2H, =CHCH$_2$C**H$_2$**), 1.60 (s, 3H, C**H$_3$** *cis*), 1.67 (s, 3H, C**H$_3$** *trans*), 1.92-2.09 (m, 2H, =CH^{13}C**H$_2$**CH$_2$), 5.05 (dd, 1H, CH=C**H$_2$**

trans, $^3J_{HH}$ = 1.1 Hz, $^2J_{HH}$ = 10.8 Hz), 5.11 (m, 1H, =C**H**), 5.20 (dd, 1H, CH=C**H₂** *cis*, $^3J_{HH}$ = 1.1 Hz, $^2J_{HH}$ = 17.3 Hz), 5,90 (dd, 1H, C**H**^{13}CH$_2$, $^3J_{HH}$ = 10.8 Hz, $^2J_{HC}$ = 17.3 Hz).

NMR ^{13}C (CDCl$_3$, δ, ppm): 17.7 (**C**H$_3$ *cis*), 22.8 (^{13}**C**H$_2$CH), 25.7 (**C**H$_3$ *trans*), 27.9 (**C**H$_3$), 42.0 (d, **C**H$_2$COH, $^1J_{CC}$ = 34.4 Hz), 73.5 (**C**OH), 111.7 (=**C**H$_2$), 124.3 (d, =**C**H, $^1J_{CC}$ = 43.6 Hz) 131.9 ((CH$_3$)$_2$**C**=), 145.0 (CH$_2$=**C**H).

5-(^{13}C)-(5*E*)-7-Hydroperoxy-3,7-dimethylocta-1,5-dien-3-ol (^{13}C-12) et 5-(^{13}C)-6-hydroperoxy-3,7-dimethylocta-1,7-dien-3-ol (^{13}C-13)

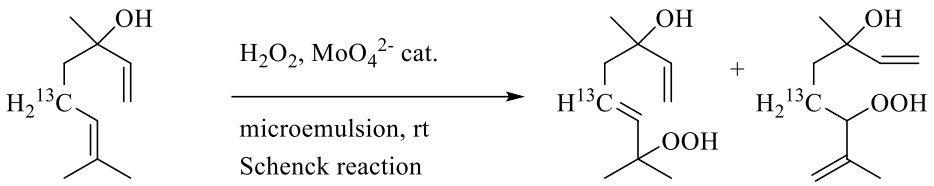

^{13}C-11 **^{13}C-12** **^{13}C-13**

A microemulsion was prepared by slowly adding a sodium molybdate solution (0.239 g in 1.27 mL distilled water) to a suspension of sodium dodecyl sulfate (1.975 g) in butanol (2.41 mL) and dichloromethane (11.76 mL). At the end of the addition, the microemulsion became clear after 5 minutes stirring.

5-(^{13}C)-Linalool **^{13}C-11** (0.198 g; 1.26 mmol; 1 eq.) was introduced in the microemulsion at room temperature. Hydrogen peroxide (aqueous solution 35%; 71 µL one fraction) was then added. The solution was instantly red colored. After 20 minutes stirring the solution became yellow. Fourteen other fractions of hydrogen peroxide (aqueous solution 35%; 71 µL EACH) were added successively by an interval of 10 minutes each. The resulting yellow solution was stirred overnight at room temperature. When the reaction was thoroughly translucent, 5-(^{13}C)-Linalool (**^{13}C-11**) was completely oxidized. The solvent was removed under reduced pressure at 40 °C. The semi-solid white product obtained was suspended in dichloromethane (65 mL) and vigorously stirred for 48 hours. The suspension was filtered to recover sodium molybdate and sodium dodecyl sulfate. The filtrate, partially evaporated under reduced pressure, was washed using distilled water (3 × 50 mL) and the aqueous phase was extracted with dichloromethane (50 mL). Combined organic phases were dried over magnesium sulfate, filtered and concentrated under reduced pressure to give a crude yellow oil. A mixture of hydroperoxides (**^{13}C-12**) and (**^{13}C-13**) (ratio 2/3) was obtained using silica gel column

chromatography (petroleum ether/AcOEt 8/2, then 6/4) as a yellow oil (0.238 g; 1.25 mmol; 99%).

Formula: $C_9{}^{13}CH_{18}O_3$

Molar mass: 187.24 g.mol^{-1}

CAS (non ^{13}C-substituted): Isomer (**^{13}C-12**): 51276-32-5 - Isomer (**^{13}C-13**): 51276-31-4

TLC = 0,24 (petroleum ether/AcOEt 7/3): APM/Ce

NMR ^{1}H (CDCl$_3$, δ, ppm)

Isomer (**^{13}C-12**) (mixture of two enantiomers): 1.27 (s, 3H, C**H$_3$**C(OH)), 1.31 (s, 6H, (C**H$_3$**)$_2$C(OOH)), 2.28 (m, 2H, C**H$_2$**C(OH)), 5.05 (dd, 1H, C**H**$_2$(CH)C(OH), $^{3}J_{HH}$ = 1.1 Hz, $^{2}J_{HH}$ = 10.8 Hz), 5.21 (dd, 1H, C**H**$_2$(CH)C(OH), $^{3}J_{HH}$ = 1.1 Hz, $^{2}J_{HH}$ = 17.4 Hz), 5.50-5.64 (m, 2H, ^{13}C**H**C**H**), 5.92 (dd, 1H, C**H**C(OH), $^{3}J_{HH}$ = 10.7 Hz, $^{2}J_{HH}$ = 17.3 Hz).

Isomer (**^{13}C-13**) (mixture of four diastereoisomers) : 1.29 (s, 6H, 2 × C**H$_3$**C(OH)), 1.51-1.66 (m, 4H, 2 × ^{13}C**H$_2$**CH$_2$), 1.73 (s, 6H, 2 × C**H$_3$**(C)CH(OOH)), 4.29 (m, 2H, 2 × C**H**(OOH)), 5.00 (m, 4H, 2 × C**H$_2$**(C)CH(OOH)), 5.07 (dd, 2H, 2 × C**H**$_2$(CH)C(OH), $^{3}J_{HH}$ = 1.1 Hz, $^{2}J_{HH}$ = 10.8 Hz), 5.17 (dd, 1H, C**H**$_2$(CH)C(OH), $^{3}J_{HH}$ = 1.1 Hz, $^{2}J_{HH}$ = 17.4 Hz), 5.20 (dd, 1H, C**H**$_2$(CH)C(OH), $^{3}J_{HH}$ =1.6 Hz, $^{3}J_{HH}$ = 17.4 Hz), 5.86 (dd, 1H, C**H**C(OH), $^{3}J_{HH}$ = 10.8 Hz, $^{2}J_{HH}$ = 17.4 Hz), 5.88 (dd, 1H, C**H**C(OH), $^{3}J_{HH}$ =10.8 Hz, $^{2}J_{HH}$ = 17.4 Hz).

NMR ^{13}C (CDCl$_3$, δ, ppm):

Isomer **^{13}C-12** (mixture of two enantiomers): 24.4 (2 × (**C**H$_3$)$_2$C(OOH)), 27.8 (**C**H$_3$C(OH)), 45.1 (d, **C**H$_2$C(OH), $^{1}J_{CC}$ = 43.5 Hz), 72.8 (**C**(OH)), 82.1 (**C**(OOH)), 112.3 (**C**H$_2$(CH)C(OH)), 126.7 (CH$_2$(**^{13}C**H)CH), 138.0 (d, **C**HC(OOH), $^{1}J_{CC}$ = 70.9 Hz), 144.8 (**C**HC(OH))

Isomer **^{13}C-13** (mixture of four diastereoisomers) : 17.1 (2 × **C**H$_3$(C)CH(OOH)), 25.1 (d, 2 × **^{13}C**H$_2$(CH)OOH, $^{1}J_{CC}$ = 3.5 Hz), 28.2 and 28.4 (2 × **C**H$_3$C(OH)), 37.7 and 37.8 (d, 2 × **C**H$_2$C(OH), $^{1}J_{CC}$ = 23.8 Hz), 73.1 (2 × **C**(OH)), 89.2 and 89.7 (d, 2 × **C**H(OOH), $^{1}J_{CC}$ = 20.5 Hz), 112.3 (2 × **C**H$_2$(CH)C(OH)), 114.2 and 114.3 (2 × **C**H$_2$(C)CH(OOH)), 143.6 (2 × **C**(CH)OOH), 144.7 and 144.8 (2 × **C**HC(OH)).

4.3 Synthesis of 4-(^{13}C)-Lina-OOHs

2-(^{13}C)-Ethyl acetate (^{13}C-14)

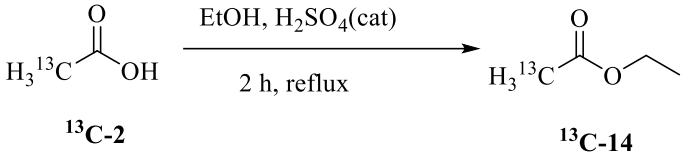

^{13}C-2 **^{13}C-14**

In a round bottom flask combined to a distillation column, to a mixture of 2-(^{13}C)-acetic acid (**^{13}C-2**) (1.92 mL; 33.33 mmol; 1 eq) and ethanol (1.95 mL; 33.33 mmol; 1 eq) was slowly added sulfuric acid (0.4 mL; 7.50 mmol; 0.2 eq). The reaction mixture was refluxed for 2 hours and the designed product was obtained by distillation and recovered as a colorless oil (1.68 g; 19.07 mmol; 58 %).

Formula: $C_3{}^{13}CH_8O_2$

Molar mass: 89.10 g.mol^{-1}

CAS (non ^{13}C-substituted): 141-78-6

NMR ^{1}H (CDCl$_3$, δ, ppm): 1.27 (t, 3H, C**H$_3$**, $^{3}J_{HH}$ = 7,5 Hz), 2.06 (d, ^{13}C**H$_3$**, 3H, $^{1}J_{HC}$ = 130.1 Hz), 4.15-4.21 (q, C**H$_2$**, 2H, $^{3}J_{HH}$ = 7.1 Hz).

NMR ^{13}C (CDCl$_3$, δ, ppm): 14.1 (**C**H$_3$), 20.7 (^{13}**C**H$_3$-C=O), 60.5 (CH$_3$-**C**H$_2$-O), 170.2 (d, ^{13}CH$_3$-**C**=O, $^{1}J_{CC}$ = 60 Hz).

2-(^{13}C)-Ethyl 5-methyl-4-hexenoate (^{13}C-15)

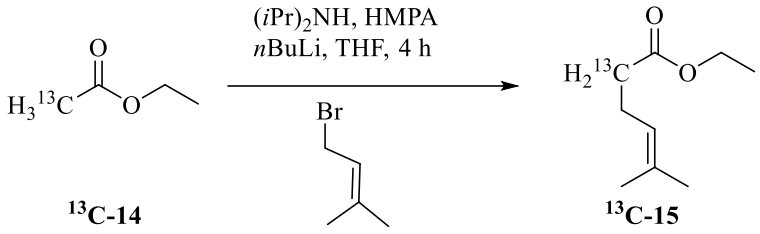

^{13}C-14 **^{13}C-15**

To a solution of diisopropylamine (4.0 mL; 28.60 mmol; 1.5 eq.) in dry tetrahydrofuran (20 mL) at 0 °C, a solution of *n*-butyllithium (1.6 M in pentane; 17.9 mL; 28.60 mmol; 1.5 eq.) was added very slowly. After 10 minutes stirring at 0 °C 2-(^{13}C)-ethyl acetate (**^{13}C-14**) (1.68 g; 19.07 mmol; 1 eq.) in tetrahydrofuran (20 mL) was very slowly added and the reaction mixture was stirred for 30 minutes at 0 °C. After this time, the reaction mixture was cooled to -78°C

and a solution of 3,3-dimethylallyl bromide (3.30 mL; 28.60 mmol; 1.5 eq.) in tetrahydrofuran (17.5 mL) containing hexamethylphosphoramide (5.0 mL; 28.60 mmol; 1.5 eq.) was added to the reaction mixture. After 4 hours at - 78 °C, the reaction mixture was allowed to warm to 0 °C. A solution of hydrochloric acid 10% (60 mL) was added and the mixture extracted with diethyl ether (3 × 30 mL). The combined organic phases were dried over magnesium sulfate and evaporated under reduced pressure. The crude product was purified using silica gel column chromatography (petroleum ether/AcOEt 95/5) to give 2-(^{13}C)-ethyl-5-methyl-4-hexenoate (**^{13}C-15**) as an orange oil (1.788 g; 11.45 mmol; 60%).

Formula: $C_8{}^{13}CH_{16}O_2$

Molar mass: 157.22 g.mol^{-1}

CAS (non ^{13}C-substituted): 42272-93-5

TLC: Rf = 0.24 (pethroleum ether/AcOEt 95/5): APM/Ce

NMR ^{1}H ($CDCl_3$, δ, ppm): 1.23 (t, 3H, $OCH_2C\mathbf{H_3}$, $^{3}J_{HH}$ = 7.1 Hz), 1.60 (s, 3H, C**H$_3$** *cis*), 1.66 (s, 3H, C**H$_3$** *trans*), 2.15 (m, 2H, C**H$_2$**), 2.42 (m, 2H, ^{13}C**H$_2$**), 4.10 (q, 2H, OC**H$_2$** CH_3, $^{3}J_{HH}$ = 7.1 Hz), 5.07 (m, 1H, =C**H**).

NMR ^{13}C ($CDCl_3$, δ, ppm): 14.7 (OCH_2 **C**H_3), 17.9 (**C**H_3 *cis*), 23.9 (d, **C**H_2CH, $^{1}J_{CC}$ = 35.9 Hz), 25.7 (**C**H_3 *trans*), 34.5 (^{13}**C**H_2), 60.4 (O**C**H_2CH_3), 122.7 (=**C**H), 133.2 ($(CH_3)_2$**C**=), 173.6 ((O)**C**=O).

2-(^{13}C)-*N*-Methoxy-*N*,5-dimethylhex-4-enamide (^{13}C-16)

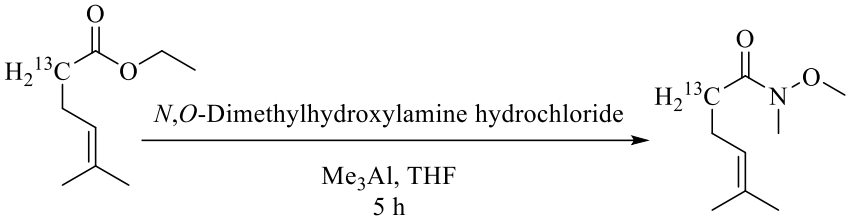

^{13}C-15 **^{13}C-16**

To a solution of *N*,*O*-dimethyl hydroxylamine hydrochloride (3.346 g; 34.35 mmol; 3 eq.) in dry tetrahydrofuran (15 mL) at 0 °C, was added a solution of trimethyl aluminum (17.8 mL; 34.35 mmol; 3 eq.) in tetrahydrofuran (10 mL) over 5 minutes. The mixture was allowed to warm up to room temperature and became pink. The solution was then cooled again to 0 °C and 2-(^{13}C)-ethyl 5-methyl-4-hexenoate (**^{13}C-15**) in dichloromethane (5 mL) was very slowly

added. The mixture was allowed to warm up to room temperature and was stirred for 5 hours. After this time a hydrochloric acid solution 10 % was carefully added. The aqueous phase was extracted with dichloromethane (4 × 50 mL), washed with sodium bicarbonate (150 mL) then water (150 mL). The combined organic phases were dried over magnesium sulfate and evaporated under reduced pressure. The crude product was obtained as a yellow oil (1.645 g).

Formula: $C_8{}^{13}CH_{17}NO_2$

Molar mass: 172.23 g.mol^{-1}

CAS (non ^{13}C-substituted): 1110631-07-6

TLC: Rf = 0.24 (pethroleum ether/AcOEt 95/5): APM/Ce

NMR ^{1}H ($CDCl_3$, δ, ppm): 1.70 (s, 3H, C**H**$_3$ *cis*), 1.82 (s, 3H, C**H**$_3$ *trans*), 2.26 (m, 2H, C**H**$_2$), 2.28 (m, 2H, ^{13}C**H**$_2$), 3.16 (s, 3H, C**H**$_3$), 3.66 (s, 3H, OC**H**$_3$), 5.11 (m, 1H, =C**H**).
NMR ^{13}C ($CDCl_3$, δ, ppm): 17.9 (**C**H$_3$ *trans),* 23.3 (**C**H$_3$ *cis*), 26.9 (d, **C**H$_2$, $^1J_{CC}$ = 11.4 Hz), 32.1 (^{13}**C**H$_2$), 34.6 (N**C**H$_3$), 61.2 (O**C**H$_3$), 123.1 (=C**H**), 132.7 ((CH$_3$)$_2$**C**=), 171.2 ((O)**C**-N).

3-(^{13}C)-6-Methyl-5-heptene-2-one (^{13}C-17)

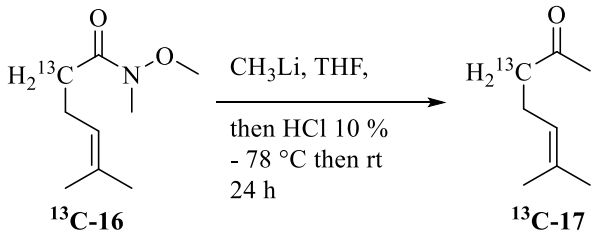

^{13}C-16 **^{13}C-17**

In a flame-dried flask, to a solution of 2-(^{13}C)-*N*-methoxy-*N*,5-dimethylhex-4-enamide (**^{13}C-16**) (1.645 g; 9.55 mmol; 1 eq.) in tetrahydrofuran (25 mL) previously cooled to -78 °C was added very slowly a solution of methyllithium (1.6 M in diethyl ether; 7.8 mL; 12.49 mmol; 1.3 eq.). The mixture was stirred for 1 hour 30 minutes at -78 °C and 24 hours at room temperature. The reaction was quenched using a solution of hydrochloric acid 10 % (20 mL). Diethyl ether (40 mL) and water (40 mL) were then added and the organic phases were recovered. The aqueous phase was extracted with diethyl ether (4 × 80 mL). The combined organic phases were dried over magnesium sulfate and evaporated under reduced pressure. The crude product was purified by silica gel chromatography (petroleum ether/diethyl ether 9/1), to afford 3-(^{13}C)-6-methyl-5-heptene-2-one (**^{13}C-17**) as a yellow oil (0.733 g; 70 %)

Formula: $C_7{}^{13}CH_{14}O$

Molar mass: 127.19 g.mol^{-1}

CAS (non ^{13}C-substituted): 110-93-0

TLC: Rf = 0.30 (petroleum ether/diethylether 9/1): APM/Ce

NMR ^{1}H ($CDCl_3$, δ, ppm): 1.63 (s, 3H, C**H$_3$** *cis*), 1.69 (s, 3H, C**H$_3$** *trans*), 2.14 (s, 3H, COC**H$_3$**), 2.26 (m, 2H, C**H$_2$**CH), 2.46 (m, 2H, ^{13}C**H$_2$**CO), 5.08 (m, 1H, =C**H**).
NMR ^{13}C ($CDCl_3$, δ, ppm): 17.6 (**C**H$_3$ *cis*), 22.5 (d, **C**H$_2$CH, $^1J_{CC}$ = 34.5 Hz), 25.6 (**C**H$_3$ *trans*), 29.9 (CO**C**H$_3$), 43.7 (^{13}**C**H$_2$ C=O), 122.6 (=C**H**), 132.8 ((CH$_3$)$_2$**C**=), 209.0 (d, **C**=O, $^1J_{CC}$ = 41.5 Hz).

4-(^{13}C)-3,7-Dimethylocta-1,6-dien-3-ol or 4-(^{13}C)-Linalool (^{13}C-18)

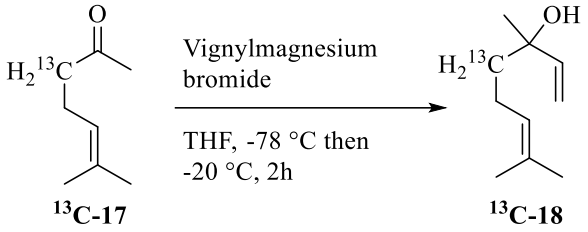

^{13}C-17 **^{13}C-18**

In a flame-dried flask, to a solution of 3-(^{13}C)-6-methyl-5-heptene-2-one (**^{13}C-17**) (0.733 g; 5.81 mmol; 1 eq.) in tetrahydrofuran (20 mL) previously cooled to -78 °C was added a solution of vinyl magnesium bromide (1.6 M in THF; 7.26 mL; 11.62 mmol; 2 eq.) in tetrahydrofuran. After 2 hours stirring at -20 °C, the reaction was quenched using a saturated ammonium chloride solution (20 mL). The aqueous phase was extracted with diethyl ether (3 × 60 mL), the combined organic phases were dried over magnesium sulfate and evaporated under reduced pressure. The crude product was purified by silica gel column chromatography (petroleum ether/diethyl ether 8/2) to give 4-(^{13}C)-3,7-dimethylocta-1,6-dien-3-ol (**^{13}C-18**) as a yellow oil (0.712 g; 85 %).

Formula: $C_9{}^{13}CH_{18}O$

Molar mass: 155.25 g.mol^{-1}

CAS (non ^{13}C-substituted): 78-70-6

TLC: Rf = 0.9 (pethroleum ether/Et_2O 8/2): APM/Ce

NMR ^{1}H ($CDCl_3$, δ, ppm) : 1.26 (d, 3H C**H**$_3$, $^{3}J_{HC}$ = 4.0 Hz), 1.50-1.55 (m, 2H, =CHC**H**$_2$^{13}CH$_2$), 1.58 (s, 3H, C**H**$_3$ *cis*), 1.66 (s, 3H, C**H**$_3$ *trans*), 1.92-2.09 (m, 2H, =CHCH$_2$^{13}C**H**$_2$), 5.05 (d, 1H, CH=C**H**$_2$ *trans*, $^{3}J_{HH}$ = 10.8 Hz), 5.11 (m, 1H, =C**H**), 5.20 (d, 1H, CH=C**H**$_2$ *cis*, $^{3}J_{HH}$ = 17.4 Hz), 5.90 (dd, 1H, C**H**=CH$_2$ *cis*, $^{3}J_{HH}$ = 10.8 Hz, $^{3}J_{HH}$ = 17.3 Hz).
NMR ^{13}C ($CDCl_3$, δ, ppm): 17.5 (**C**H$_3$ *cis*), 22.8 (d, **C**H$_2$CH, $^{1}J_{CC}$ = 4.1 Hz), 25.7 (**C**H$_3$ *trans*), 27.9 (**C**H$_3$), 41.7 (^{13}**C**H$_2$ COH), 73.5 (d, **C**OH, $^{1}J_{CC}$ = 38.1 Hz), 111.7 (=**C**H$_2$), 124.3 (=**C**H), 131.9 ((CH$_3$)$_2$**C**=), 145.0 (CH$_2$=**C**H).

4-(^{13}C)-(5*E*)-7-Hydroperoxy-3,7-dimethylocta-1,5-dien-3-ol (^{13}C-19) and 4-(^{13}C)-6-hydroperoxy-3,7-dimethylocta-1,7-dien-3-ol (^{13}C-20)

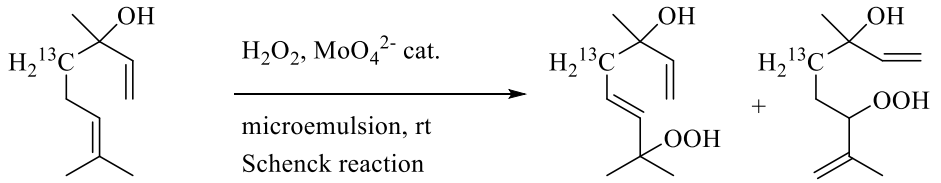

^{13}C-18 **^{13}C-19** **^{13}C-20**

A microemulsion was prepared by slowly adding a sodium molybdate solution (0.876 g in 5 mL distilled water) to a suspension of sodium dodecyl sulfate (7.47g) in butanol (8.8 mL) and dichloromethane (45 mL). At the end of the addition, the microemulsion became clear after 5 minutes stirring.

4-(^{13}C)-Linalool **^{13}C-18** (0.712 g; 4.62 mmol; 1 eq) was introduced in the microemulsion at room temperature. Hydrogen peroxide (aqueous solution 35%; 260 µL one fraction) was then added. The solution was instantly red colored. After 20 minutes stirring, it became yellow. Fourteen other fractions of hydrogen peroxide (aqueous solution 35%; 260 µL each) were added successively by an interval of 10 minutes each. The yellow solution was stirred overnight at room temperature. When the reaction was thoroughly translucent, it meant that 4-(^{13}C)-linalool **^{13}C-18** was completely oxidized. The solvent was removed under reduced pressure at 40 °C. The semi-solid white product obtained was suspended in dichloromethane (233 mL) and vigorously stirred for 48 hours. The suspension was filtered to recover sodium molybdate and sodium dodecyl sulfate. The filtrate, partially evaporated under reduced pressure, was washed using distilled water (3 × 100 mL) and the aqueous phase was extracted with dichloromethane (100 mL). Combined organic phases were dried over magnesium sulfate, filtered and concentrated under reduced pressure to give a crude yellow oil. A mixture of hydroperoxides

4-(^{13}C)-(5*E*)-7-Hydroperoxy-3,7-dimethylocta-1,5-dien-3-ol (**^{13}C-19**) and 4-(^{13}C)-6-hydroperoxy-3,7-dimethylocta-1,7-dien-3-ol (**^{13}C-20**) (ratio 2/3) was purified using silica gel column chromatography (petroleum ether/ethyl acetate 4/1, then 3/2) as a yellow oil (0.588 g; 3.14 mmol; 69%).

Formula: $C_9{}^{13}CH_{18}O_3$

Molar mass: 187.24 g.mol^{-1}

CAS (non ^{13}C-substituted): Isomer (**^{13}C-19**): 51276-32-5 - Isomer (**^{13}C-20**): 51276-31-4

TLC = 0.24 (petroleum ether/ethyl acetate 7/3): APM/Ce

NMR ^{1}H (CDCl$_3$, δ, ppm)

Isomer (**^{13}C-19**) (mixture of two enantiomers): 1.28 (s, 3H, C**H$_3$**C(OH)), 1.32 (s, 6H, (C**H$_3$**)$_2$C(OOH)), 2.29 (m, 2H, ^{13}C**H$_2$**C(OH)), 5.07 (dd, 1H, C**H$_2$**(CH)C(OH), $^{3}J_{HH}$ = 1.1 Hz, $^{2}J_{HH}$ = 10.8 Hz), 5.21 (dd, 1H, C**H$_2$**(CH)C(OH), $^{3}J_{HH}$ = 1.1 Hz, $^{2}J_{HH}$ = 17.4 Hz,), 5.50-5.64 (m, 2H, C**H**C**H**), 5.91 (dd, 1H, C**H**C(OH), $^{3}J_{HH}$ 10.7 Hz, $^{2}J_{HH}$ = 17.3 Hz).

Isomer (**^{13}C-20**) (mixture of four diastereoisomers) : 1.29 (s, 6H, 2 × C**H$_3$**C(OH)), 1.51-1.66 (m, 4H, 2 × C**H$_2$**^{13}CH$_2$), 1.73 (s, 6H, 2 × C**H$_3$**(C)CH(OOH)), 4.29 (m, 2H, 2 × C**H**(OOH)), 5.00 (m, 4H, 2 × C**H$_2$**(C)CH(OOH)), 5.07 (dd, 2H, 2 × C**H$_2$**(CH)C(OH), $^{3}J_{HH}$ = 1.1 Hz, $^{2}J_{HH}$ = 10.8 Hz), 5.20 (dd, 1H, C**H$_2$**(CH)C(OH), $^{3}J_{HH}$ = 1.1 Hz, $^{2}J_{HH}$ = 17.4 Hz), 5.21 (dd, 1H, C**H$_2$**(CH)C(OH), $^{3}J_{HH}$ =1.6 Hz, $^{2}J_{HH}$ = 17.4 Hz), 5.87 (dd, 1H, C**H**C(OH), $^{3}J_{HH}$ = 10.8 Hz, $^{2}J_{HH}$ = 17.4 Hz), 5.88 (dd, 1H, C**H**C(OH), $^{3}J_{HH}$ =10.8 Hz, $^{2}J_{HH}$ = 17.4 Hz,).

NMR ^{13}C (CDCl$_3$, δ, ppm):

Isomer (**^{13}C-19**) (mixture of two enantiomers): 24.4 (2 × (**C**H$_3$)$_2$C(OOH)), 27.8 (**C**H$_3$C(OH)), 45.4 (s, **^{13}C**H$_2$C(OH)), 72.7 (**C**(OH)), 82.2 (**C**(OOH)), 112.3 (**C**H$_2$(CH)C(OH)), 126.8 (d, CH$_2$(**C**H)CH, $^{1}J_{CC}$ = 43.4 Hz), 138.0 (s, **C**HC(OOH)), 144.8 (**C**HC(OH))

Isomer (**^{13}C-20**) (mixture of four diastereoisomers) : 17.6 (2 × **C**H$_3$(C)CH(OOH)), 25.1 (s, 2 × **C**H$_2$(CH)OOH), 28.2 and 28.3 (2 × **C**H$_3$C(OH)), 37.7 (d, 2 × **^{13}C**H$_2$C(OH), $^{1}J_{CC}$ = 23.8 Hz), 73.1 (2 × **C**(OH)), 89.7 (d, 2 × **C**H(OOH), $^{1}J_{CC}$ = 20.5 Hz), 112.3 (2 × **C**H$_2$(CH)C(OH)), 114.2 and 114.3 (2 × **C**H$_2$(C)CH(OOH)), 143.7 (2 × **C**(CH)OOH), 144.7 et 144.8 (2 × **C**HC(OH))

4.4 Synthesis of 2-(^{13}C)-Lina-OOHs

Trimethylsilyl (^{13}C)-cyanide (^{13}C-21)

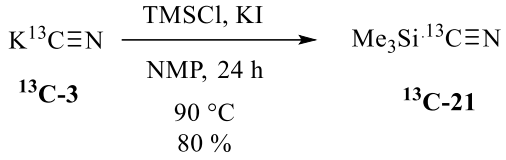

In a flame-dried round bottom flask under argon 1-(^{13}C)-potassium cyanide (**^{13}C-3**) (98 %; 2.0 g; 31 mmol; 1 eq) and potassium iodide (0.55 g; 3.3 mmol; 0.11 eq) were dried at 120 °C under a vacuum pump for 24 hours. Anhydrous *N*-methyl-2-pyrrolidone (2.0 mL) and anhydrous trimethylsilyl chloride (3.8 mL; 30 mmol; 0.97 eq.) were added very slowly. The solution color changed from white to yellow. The mixture was stirred for 24 hours at room temperature. 1 Trimethylsilyl (^{13}C)-cyanide **^{13}C-21** was obtained by distillation (bp = 112 °C) as a colorless oil (2.4 g; 82 %).

Formula: $C_3{}^{13}CH_9NSi$

Molar mass: 100.20 g.mol^{-1}

CAS (non ^{13}C-substituted): 7677-24-9

NMR ^{1}H ($CDCl_3$, *δ*, ppm): 0.35 (s, 9H, -Si(C**H**$_3$)$_3$).

NMR ^{13}C ($CDCl_3$, *δ*, ppm): 0.1 (Si(**C**H$_3$)$_3$), 124.9 (-^{13}**C**≡N).

1-(^{13}C)-2,6-Dimethyl-2-((trimethylsilyl)oxy)hept-5-enenitrile (^{13}C-22)

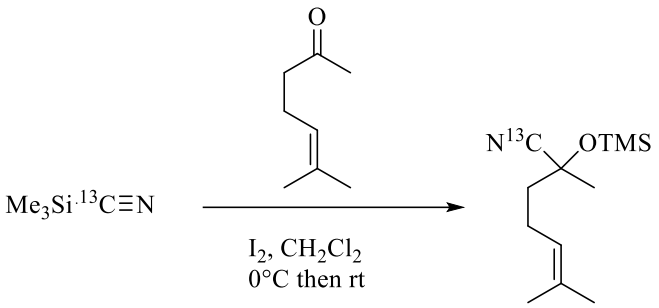

^{13}C-21 **^{13}C-22**

In a flame-dried round bottom flask under argon 6-methyl-5-hepten-2-one (3.62 mL; 24.25 mmol; 1 eq) and anhydrous iodine (0.492 g; 1.94 mmol; 0.08 eq) were introduced in dichloromethane (10 mL) and cooled to -78 °C. Trimethylsilyl (^{13}C)-cyanide (**^{13}C-21**) (2.4 g; 24.25 mmol; 1 eq) was then added very slowly. The mixture was stirred for 30 minutes at room temperature. Water (100 mL) was added and the solution color changed from brown to red. The aqueous phase was extracted with dichloromethane (2 × 100 mL). The combined organic phases were washed with a saturated solution of sodium thiosulfate (100 mL), dried over magnesium sulfate, filtered, and evaporated under reduced pressure. The crude product was purified by silica gel column chromatography (pentane/AcOEt 9/1) to give 1-(^{13}C)-2,6-dimethyl-2-((trimethylsilyl)oxy)hept-5-enenitrile **^{13}C-22** as a light-yellow oil (4.378 g; 80 %).

Formula: $C_{11}{}^{13}CH_{23}NOSi$

Molar mass: 226.40 g.mol^{-1}

CAS (non ^{13}C-substituted): 58422-84-7

CCM : Rf = 0.90 (pentane/AcOEt 9/1) : APM/Ce

NMR ^{1}H ($CDCl_3$, δ, ppm): 0.21 (s, 9H, -Si(C**H**$_3$)$_3$), 1.55 (s, 3H, -C(CN)(OTMS)-C**H**$_3$), 1.61 (d, 3H, -CH=C-C**H**$_3$ *cis*, $^4J_{HH}$ = 1.1 Hz,), 1.67 (d, 3H, -CH=C-C**H**$_3$ *trans*, $^4J_{HH}$ = 1.3 Hz), 1.70 (m, 2H, -C**H**$_2$-CH$_2$-CH=C(CH$_3$)$_2$), 2.15 (m, 2H, -C**H**$_2$-CH=C(CH$_3$)$_2$), 5.08 (m, 1H, -C**H**=C(CH$_3$)$_2$)

NMR ^{13}C ($CDCl_3$, δ, ppm): 0.1 (-Si(**C**H$_3$)$_3$), 16.4 (-CH=C-**C**H$_3$ *cis*), 21.8 (-CH=C-**C**H$_3$ *trans*), 24.4 (-**C**H$_2$-CH=C(CH$_3$)$_2$), 27.7 (-C(^{13}CN)(OTMS)-**C**H$_3$), 42.0 (-**C**H$_2$-CH$_2$-CH=C(CH$_3$)$_2$), 68.1 (d, -**C**(^{13}CN)(OTMS)-CH$_3$, $^1J_{CC}$ = 57.5 Hz), 120.8 (-^{13}**C**≡N), 121.2 (-**C**H=C(CH$_3$)$_2$), 131.5 (-CH=**C**(CH$_3$)$_2$)

1-(^{13}C)-2,6-Dimethyl-2-((trimethylsilyl)oxy)hept-5-enal (^{13}C-23)

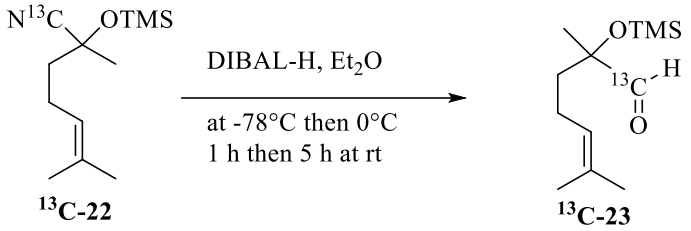

^{13}C-22 **^{13}C-23**

In a flame-dried round bottom flask under argon 1-(^{13}C)-2,6-dimethyl-2-((trimethylsilyl)oxy)hept-5-enenitrile **^{13}C-22** (0.57 mL; 2.2 mmol; 1.0 eq.) was dissolved in anhydrous diethyl ether (13 mL), cooled to -78 °C and a solution of diisobutylaluminium hydride (1 M in THF; 5.6 mL; 5.6 mmol; 2.5 eq.) was added very slowly. The mixture was stirred 1 hour at 0 °C than at room temperature for 5 hours. Di-isobutyl aluminum hydride excess was neutralized by adding ethyl acetate (10 mL). The reaction mixture was diluted with diethyl ether (13 mL), then silica (10 g) was added. The slurry was stirred at -78 °C overnight. Silica was removed by filtration and the solvent of the filtrate was evaporated under reduced pressure. The crude product was purified by silica gel column chromatography (pentane/diethyl ether 95/5).

Formula: $C_{11}{}^{13}CH_{24}O_2Si$

Molar mass: 228.41 g.mol^{-1}

CAS (non ^{13}C-substituted): 78-70-6

CCM: Rf = 0.80 (pentane/diethyl ether 95/5): APM/Ce

NMR ^{1}H ($CDCl_3$, δ, ppm): 0.14 (s, 9H, -Si(C**H**$_3$)$_3$), 1.26 (s, 3H, -C(CO)(OTMS)-C**H**$_3$), 1.56 (s, 3H, -CH=C-C**H**$_3$ *cis*), 1.64 (s, 3H, -CH=C-C**H**$_3$ *trans*), 1.51-1.68 (m, 2H, -C**H**$_2$-CH$_2$-CH=C(CH$_3$)$_2$), 1.97 (m, 2H, -C**H**$_2$-CH=C(CH$_3$)$_2$), 5,01 (m, 1H, -C**H**=C(CH$_3$)$_2$), 9.51 (s, 1H, -C**H**=O).

NMR ^{13}C ($CDCl_3$, δ, ppm): 0.1 (-Si(**C**H$_3$)$_3$), 15.4 (-CH=C-**C**H$_3$ *cis*), 19.8 (-**C**H$_2$-CH=C(CH$_3$)$_2$), 20.8 (-CH=C-**C**H$_3$ *trans*), 23.4 (-C(CO)(OTMS)-**C**H$_3$), 37.0 (-**C**H$_2$-CH$_2$-CH=C(CH$_3$)$_2$), 78.5 (-**C**(CO)(OTMS)-CH$_3$), 121.6 (-**C**H=C(CH$_3$)$_2$), 130.0 (-CH=**C**(CH$_3$)$_2$), 202.9 (-**C**H=O).

Linalool (24)

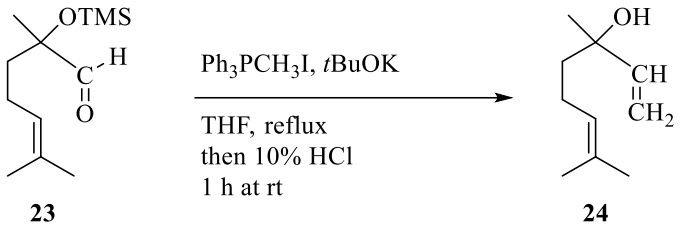

23 **24**

In a flame-dried round bottom flask under argon methyltriphenylphosphonium iodide (0.18 g; 0.44 mmol; 2.0 eq.) previously dried for 24 hours was dissolved in anhydrous tetrahydrofuran (3.8 mL). Potassium *tert*-butoxide (59 mg; 0.53 mmol; 2.4 eq.) was added and the mixture was refluxed. After 1 hour the mixture was cooled to 0 °C and, 2,6-dimethyl-2-((trimethylsilyl)oxy)hept-5-en-al **23** (60 µL; 0.22 mmol; 1.0 eq.) was added very slowly. Reflux was carried on for 1 hour. After cooling to room temperature, a solution of hydrochloric acid 10 % (7.0 mL; 23 mmol) was added. After 1 hour at room temperature, the reaction mixture was extracted with diethyl ether (3 × 25 mL). The combined organic phases were dried over magnesium sulfate, filtered, and evaporated under reduced pressure. The product was purified by silica gel column chromatography (pentane/ethyl acetate 80/20) to obtain linalool **24** as a colorless oil (14 mg; 42 %).

Formula: $C_{10}H_{18}O$

Molar mass: 155.25 $g.mol^{-1}$

CAS (non ^{13}C-substituted): 78-70-6

TLC: Rf = 0.9 (pethroleum ether/diethyl ether 8/2): APM/Ce

NMR ^{1}H ($CDCl_3$, δ, ppm): 1.23 (s, 3H, -C(C**H**$_3$)(OH)-CH=CH_2), 1.47-1.65 (m, 8H, -CH=C(C**H**$_3$)$_2$ and -C**H**$_2$-CH_2-CH=C(CH_3)$_2$), 2.01 (m, 2H, -C**H**$_2$-CH=C(CH_3)$_2$), 4.81 (s, 1H, -O**H**), 5.02-5.20 (m, 3H, -CH=C**H**$_2$ et -C**H**=C(CH_3)$_2$), 5.88 (m, 1H, -C**H**=CH_2).
NMR ^{13}C ($CDCl_3$, δ, ppm): 17.8 (-CH=C-**C**H_3 *cis*), 22.9 (-**C**H_2-CH=C(CH_3)$_2$), 25.9 (-CH=C-**C**H_3 *trans*), 27.9 (-C(**C**H_3)(OH)-CH=CH_2), 42.2 (-**C**H_2-CH_2-CH=C(CH_3)$_2$), 73.7 (-**C**(CH_3)(OH)-CH=CH_2), 111.8 (-CH=**C**H_2), 124.4 (-**C**H=C(CH_3)$_2$), 132.1 (-CH=**C**(CH_3)$_2$), 145.1 (-**C**H=CH_2).

Literature

(1) Luo, Y.-R.; Luo, Y.-R. *Comprehensive Handbook of Chemical Bond Energies*; CRC Press: Boca Raton, 2007, 255-368.
(2) *Active Oxygen in Chemistry*; Foote, C. S., Valentine, J. S., Greenberg, A., Liebman, J. F., Eds.; Springer Netherlands: Dordrecht, 1996.
(3) Sköld, M.; Börje, A.; Harambasic, E.; Karlberg, A.-T. Contact Allergens Formed on Air Exposure of Linalool. Identification and Quantification of Primary and Secondary Oxidation Products and the Effect on Skin Sensitization. *Chem. Res. Toxicol.* **2004**, *17* (12), 1697–1705.
(4) Kao, D.; Chaintreau, A.; Lepoittevin, J.-P.; Giménez-Arnau, E. Synthesis of Allylic Hydroperoxides and EPR Spin-Trapping Studies on the Formation of Radicals in Iron Systems as Potential Initiators of the Sensitizing Pathway. *J. Org. Chem.* **2011**, *76* (15), 6188–6200.
(5) Alberti, M. N.; Orfanopoulos, M. Stereoelectronic and Solvent Effects on the Allylic Oxyfunctionalization of Alkenes with Singlet Oxygen. *Tetrahedron* **2006**, *62* (46), 10660–10675.
(6) Foote, C.; Selverstone Valentine, J.; Greenberg, A.; Liebman, J. F. *Properties and Reactions of Singlet Dioxygen. Active Oxygen in Chemistry.*, Chapman & Hall.; New York, États-Unis, 1995.
(7) Stratakis, M.; Orfanopoulos, M. Regioselectivity in the Ene Reaction of Singlet Oxygen with Alkenes. *Tetrahedron* **2000**, *56* (12), 1595–1615.
(8) Aubry, J-M. Search for Singlet Oxygen in the Decomposition of Hydrogen Peroxide by Mineral Compounds in Aqueous Solutions. *J. Am. Chem. Soc.* **1985**, *107* (21), 5844–5849.
(9) Nardello, V.; Bouttemy, S.; Aubry, J.-M. Olefin Oxidation by the System H2O2MoO2−4: Competition between Epoxidation and Peroxidation. *J. Mol. Catal. Chem.* **1997**, *117* (1–3), 439–447.
(10) Kao, D.; Chaintreau, A.; Lepoittevin, J.-P.; Giménez-Arnau, E. Mechanistic Studies on the Reactivity of Sensitizing Allylic Hydroperoxides: Investigation of the Covalent Modification of Amino Acids by Carbon-Radical Intermediates. *Toxicol. Res.* **2014**, *3* (4), 278–289.
(11) van der Klei, A.; de Jong, R. L. P.; Lugtenburg, J.; Tielens, A. G. M. Synthesis and Spectroscopic Characterization of [1′-14C]Ubiquinone-2, [1′-14C]-5-Demethoxy-5-Hydroxyubiquinone-2, and [1′-14C]-5-Demethoxyubiquinone-2. *Eur. J. Org. Chem.* **2002**, *2002* (17), 3015–3023.
(12) Sharma, V.; Kelly, G. T.; Watanabe, C. M. H. Exploration of the Molecular Origin of the Azinomycin Epoxide: Timing of the Biosynthesis Revealed. *Org. Lett.* **2008**, *10* (21), 4815–4818.
(13) MacPhee, J. A.; Dubois, J.-E. Steric Limits to Ester Alkylation; Synthesis of Highly Hindered Esters via Hexamethylphosphoramide-Favoured Enolization. *J. Chem. Soc. [Perkin 1]* **1977**, No. 6, 694.
(14) Debeuckelaere, C.; Berl, V.; Elbayed, K.; Moussallieh, F.-M.; Namer, I.-J.; Lepoittevin, J.-P. Matrix Effect of Human Reconstructed Epidermis on the Chemoselectivity of a Skin Sensitizing α-Methylene-γ-Butyrolactone: Consequences for the Development of *in Chemico* Alternative Methods. *Chem. Res. Toxicol.* **2015**, *28* (11), 2192–2198.
(15) Nahm, S.; Weinreb, S. M. N-Methoxy-n-Methylamides as Effective Acylating Agents. *Tetrahedron Lett.* **1981**, *22* (39), 3815–3818.
(16) Liu, J.; Ikemoto, N.; Petrillo, D.; Armstrong, J. D. Improved Syntheses of α-BOC-Aminoketones from α-BOC-Amino-Weinreb Amides Using a Pre-Deprotonation Protocol. *Tetrahedron Lett.* **2002**, *43* (46), 8223–8226.

(17) Guanti, G.; Riva, R. Homochiral Isoquinolines by Lipase-Catalysed Resolution and Their Diastereoselective Functionalisation. *Tetrahedron Asymmetry* **2001**, *12* (8), 1185–1200.
(18) Shimizu, T.; Osako, K.; Nakata, T. Efficient Method for Preparation of N-Methoxy-N-Methyl Amides by Reaction of Lactones or Esters with Me2AlCl-MeONHMe·HCl. *Tetrahedron Lett.* **1997**, *38* (15), 2685–2688.
(19) Reetz, M. T.; Drewes, M. W.; Lennick, K.; Schmitz, A.; Holdgrün, X. Non-Racemizing Synthesis and Stereoselective Reduction of Chiral α-Amino Ketones. *Tetrahedron Asymmetry* **1990**, *1* (6), 375–378.
(20) Cao, Y.-Q.; Du, Y.-F.; Li, J.-T. A Practical and Improved Method for the Preparation of Trimethylsilyl Cyanide Catalysed by PEG400 and Zinc Iodide. *J. Chem. Res.* **2003**, *2003* (8), 500–501.
(21) Reetz, M. T.; Chatziiosifidis, I. An Improved Synthesis of Cyanotrimethylsilane. *Synthesis* **1982**, *1982* (04), 330–330.
(22) Rasmussen, J. K.; Heilmann, S. M. A Simple, Safe, and Inexpensive Preparation of Trimethylsilyl Cyanide. *Synthesis* **1979**, *1979* (07), 523–524.
(23) Kündig, E. P.; Enriquez-Garcia, A. Diastereoselective and Enantioselective Reduction of Tetralin-1,4-Dione. *J. Org. Chem.* **2008**, *4*.(37), 1-5.
(24) Evans, D. A.; Carroll, G. L.; Truesdale, L. K. Synthetic Applications of Trimethylsilyl Cyanide. Efficient Synthesis of β-Aminomethyl Alcohols. *J. Org. Chem.* **1974**, *39* (7), 914–917.
(25) Ma, C.; Schiltz, S.; Le Goff, X. F.; Prunet, J. Ring-Closing Metathesis in the Synthesis of BC Ring-Systems of Taxol. *Chem. Eur. J.* **2008**, 14 (24), 7314-7323.
(26) Vinson, W. A.; Prickett, K. S.; Spahic, B.; Ortiz De Montellano, P. R. ChemInform Abstract: Synthesis of carbon and phosphorus esters of α-fluoro alcohols. *Chem. Informationsdienst* **1984**, *15* (21).
(27) Wisse, P.; Gold, H.; Mirzaian, M.; Ferraz, M. J.; Lutteke, G.; van den Berg, R. J. B. H. N.; van den Elst, H.; Lugtenburg, J.; van der Marel, G. A.; Aerts, J. M. F. G.; *et al*. Synthesis of a Panel of Carbon-13-Labelled (Glyco)Sphingolipids: Synthesis of a Panel of Carbon-13-Labelled (Glyco)Sphingolipids. *Eur. J. Org. Chem.* **2015**, *2015* (12), 2661–2677.
(28) Binns, F.; Hayes, R.; Hodgetts, K. J.; Saengchantara, S. T.; Wallace, T. W.; Wallis, C. J. The Preparation and Electrocyclic Ring-Opening of Cyclobutenes: Stereocontrolled Approaches to Substituted Conjugated Dienes and Trienes. *Tetrahedron* **1996**, *52* (10), 3631–3658.
(29) Gardner, H. W.; Weisleder, D.; Kleiman, R. Addition OfN-Acetylcysteine to Linoleic Acid Hydroperoxide. *Lipids* **1976**, *11* (2), 127–134.
(30) Grossi, L. Evidence of an Electron-Transfer Mechanism in the Peroxynitrite-Mediated Oxidation of 4-Alkylphenols and Tyrosine. *J. Org. Chem.* **2003**, *68* (16), 6349–6353.
(31) Lepoittevin, J-P.; Benezra, C. Chimie de l'allergie de contact. *Rev. Fr. Allergol. Immunol. Clin.* **1991**, *31* (4), 235–241.
(32) Suffert, J. Simple Direct Titration of Organolithium Reagents Using N-Pivaloyl-o-Toluidine and/or N-Pivaloyl-o-Benzylaniline. *J. Org. Chem.* **1989**, *54* (2), 509–510.

Chapter 2

Electron paramagnetic resonance (cw-EPR) investigation of free radicals induced by skin sensitizers: from pure in vitro studies to the use of a reconstructed human epidermis model

As discussed in the introduction of the manuscript, this first step in the development of skin sensitization to a chemical and further contact dermatitis is the binding of the allergen to skin proteins after penetration into the epidermis. The antigenic adduct so formed is then recognized by the immune system as foreign to the body. Allergenic hydroperoxides derived from autoxidation of natural terpenes are believed to form antigens through radical-mediated mechanisms. So far, *in vitro* investigations on reactive radical intermediates derived from these compounds have been conducted in solution, yet with experimental conditions being far away from real life sensitization.[1–3]

In the present chapter we propose to probe the radical intermediates issued from ROOHs derived from linalool and *R*-(+)-limonene, considered as skin sensitizers, and cumene hydroperoxide, using continuous wave Electron Paramagnetic Resonance (cw-EPR) spectroscopy combined with the spin-trapping technique. The objective was to transfer this technology to the investigation of these radicals generation *in situ* in a reconstructed human epidermis model. After a brief description of the technique and its principal physical principles, a two steps experimental approach is discussed in the following sections: (1) *in vitro* generation of free radicals and (2) *in situ* generation using a 3D reconstructed human epidermis (later referred as to RHE) as model system.

1 ELECTRON PARAMAGNETIC RESONANCE

1.1 Introduction

EPR spectroscopy can be divided into two different categories: continuous wave (*cw*-EPR) and pulsed spectroscopy (p-EPR).[4] Only the first cited one will be discussed here and will later be referred as to EPR. In comparison with nuclear magnetic resonance (NMR) which focus on the behavior of the proton, EPR relies on an unpaired electron within an external magnetic field and a subsequent electromagnetic absorption. EPR has found applications from solid state physics to biomedical use.[5,6] In particular it has been successfully applied to the understanding of many physiological processes ranging from *in vivo* detection-characterization of reactive nitrogen (RNS) and oxygen species (ROS) and tumors oximetry, to the assessment of redox state in biological tissues.

In 1945 E. Zavoïsky was the first to observe an EPR signal.[7]

Free electrons have an intrinsic angular momentum called spin that is present without external forces. Therefore, every free electron induces a magnetic field due to the moving charge and it acts as a small bar magnet / magnetic dipole having a magnetic moment (Figure 2.1).

In contrast to diamagnetic materials where all electrons are paired and share their orbitals with another electron (*i.e.* net spin = 0), a paramagnetic material possess an unpaired electron and thus exhibits an intrinsic magnetic moment. EPR spectroscopy is adapted for the investigation of materials with unpaired electrons *i.e.* with magnetic moments that can align either parallel or antiparallel to an external magnetic field (Figure 2.1). In EPR studies, paramagnetic systems with an unpaired electron are seen such as: transition metals, radicals and salts.

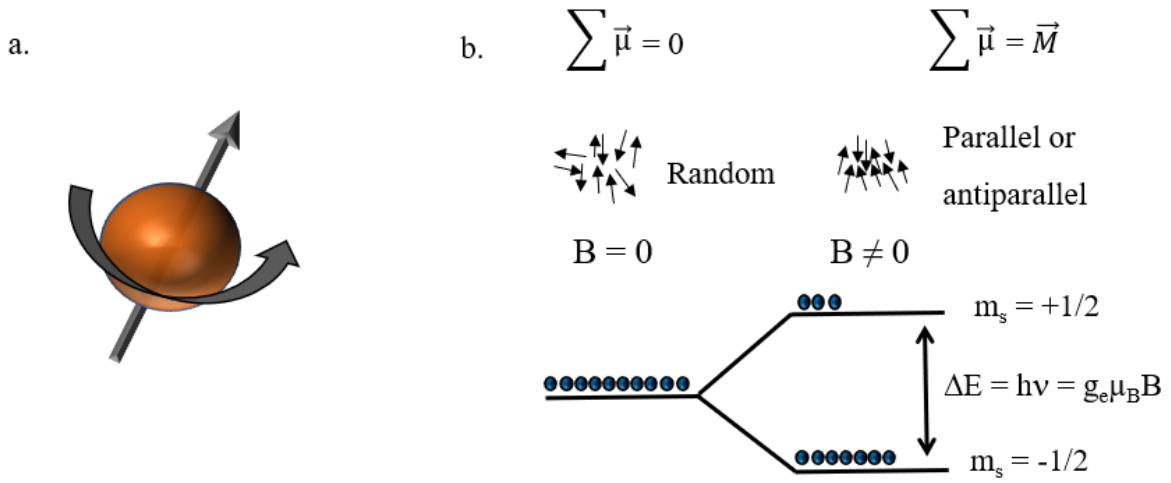

Figure 2.1 Schematic view of (a) an unpaired electron with a spin angular momentum (curved arrow) and magnetic moment (tilted arrow); (b) paramagnetic system in the presence of an external magnetic Field: the classical (up) and quantum approach (bottom)[8]

1.2 Zeeman effect

EPR consists in inducing transitions between two electronic spin states whose degeneracy is lifted when a magnetic field is applied. This is the so-called Zeeman effect, named after the Dutch physicist Pieter Zeeman, who was awarded by the Nobel Prize in Physics in 1902 for this pioneering discovery.[9] If we consider an isotropic system of electronic spin S=½, the resulting spin magnetic moment μ will be given by

$$\vec{\mu} = g\beta_e\vec{S} \qquad \text{(I)}$$

where:

- $\beta_e = \frac{e\hbar}{2m_e}$ being the Bohr's magneton (β_e = 9.27401.10^{-24} A.m^2) with m_e the electron mass, e its charge and $\hbar$ the reduced Planck constant.
- g is a dimensionless factor also called Landé's factor or "g factor" where $g = g_e$ = 2.0023193043617 for a free electron. This value has been predicted by quantum electrodynamics and later verified experimentally.[10] In the isotropic case, g can be assumed as a scalar.
- $\vec{S}$ is the electronic spin operator.

In the absence of a magnetic field, the electronic levels are degenerated, but when placed into an external magnetic field $\overrightarrow{B_0}$ oriented against the z axis, the energy's electron is defined following the equation:

$$E = -\vec{\mu}.\overrightarrow{B_0} \quad \text{(II)}$$

and the degeneracy is lifted as described by the electronic Zeeman Hamiltonian $\overrightarrow{H_{EZ}}$:

$$\overrightarrow{H_{EZ}} = -\vec{\mu}.\overrightarrow{B_0} = \beta_e B_0 S_z \quad \text{(III)}$$

where dimensionless S_z is the projection of the electronic spin operator on the z axis. Such Hamiltonian acts on the electron spin functions |m> and consequently the two degenerated levels of the spin states split with $m_S = +\frac{1}{2}$ (spin parallel to the magnetic field) and $m_S = -\frac{1}{2}$ (spin anti parallel to the magnetic field), as described in Figure 2.2. The resulting eigen energy of the electronic level becomes:

$$E_{\pm} = g\mu B_0 m_S = \pm\frac{1}{2}\, g\mu B_0 \quad \text{(IV)}$$

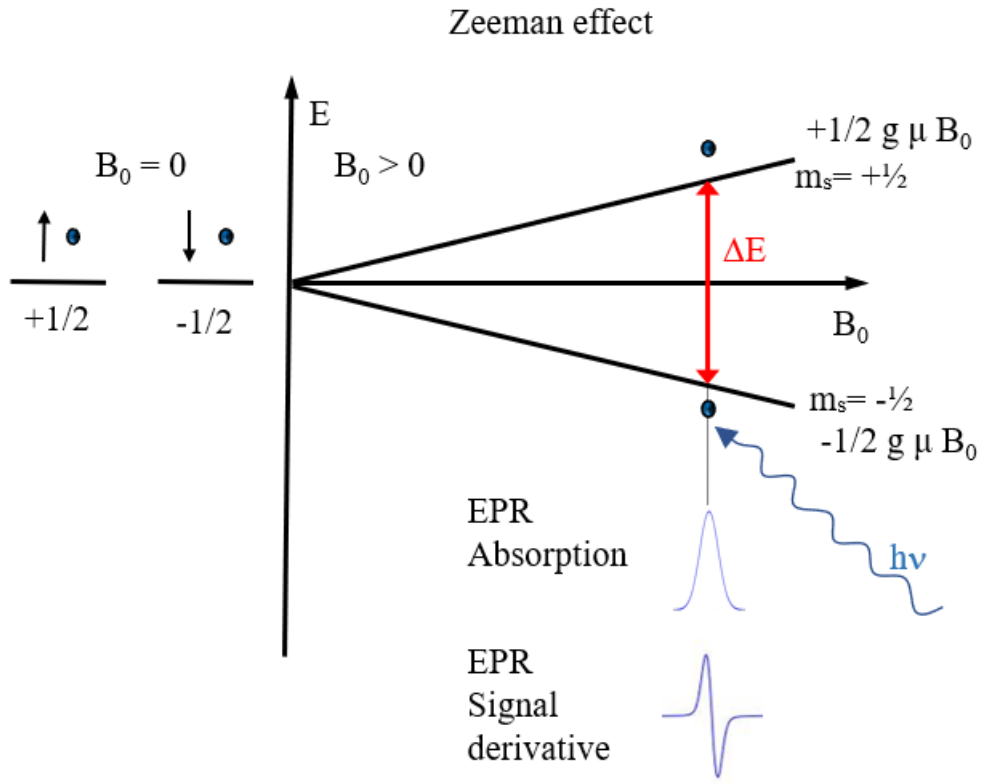

Figure 2.2 Schematic description of the Zeeman effect for an isotropic electronic spin system *S*=½ placed into an external magnetic field B_0 and the resulting microwave absorption and EPR signal when the resonance condition ($\Delta E = h\nu = E_+ - E_- = g\beta_e B_0^{res}$) is verified.

At this stage, the absorption of an electromagnetic radiation with the appropriate frequency ν will induce a resonant electronic transition from the lower energy spin energy level ($m_S = -\frac{1}{2}$) to the upper one ($m_S = +\frac{1}{2}$). Based on these elements, EPR experiment consists in inducing electronic transitions, allowed by the selection rule $\Delta m_S = \pm 1$ between the two energy levels, by applying an electromagnetic radiation $\overrightarrow{B_1}$ oscillating at the frequency ν, and meeting the following conditions:

- $\overrightarrow{B_1} \perp \overrightarrow{B_0}$
- The resonance condition must be fulfilled, i.e.:

$$\Delta E = h\nu = E_+ - E_- = g\beta_e B_0^{res} \qquad \text{(V)}$$

From the practical point of view, EPR is achieved while varying the static magnetic field $\overrightarrow{B_0}$ until reaching the resonance condition (Figure 2.2), where $\overrightarrow{B_1}$ is absorbed. Therefore, EPR is an

absorption spectroscopy and in the present work, the frequency ν of $\overrightarrow{B_1}$ is of ca. 9.5 GHz which belongs to the microwave range and corresponds to so-called X-band. Also, to enhance the sensitivity of the detection in cw-EPR, $\overrightarrow{B_0}$ is modulated in amplitude (lock-in detection system, at usually 100 kHz).[11] Hence, the observed EPR signal corresponds to the first derivative of the absorption signal.

1.3 Hyperfine interaction

In the case of paramagnetic compounds, if the unpaired electron is in the vicinity of nuclei with spin I with non-zero values, the resulting interaction is called hyperfine interaction between the magnetic moments of the electronic (S) and nuclear spins (I). Such interaction is described by the Hamiltonian spin $\overrightarrow{H_{HF}}$ also called Fermi contact:

$$\overrightarrow{H_{HF}} = \vec{S}A_{iso}\vec{I} \qquad \text{(VI)}$$

$\vec{I}$ is the nuclear spin operator and A_{iso} is the isotropic hyperfine coupling constant (hfcc) that represent the energy of interaction between the electronic and the nuclear spin. Such interaction is very much dependent of both the spin density on the nucleus and the gyromagnetic of the nucleus.[12] Stronger are these two parameters stronger is the hyperfine coupling constant. The natural abundance, nuclear spin and gyromagnetic ratio of common nucleus are given in Table 2.1.

Table 2.1: Natural abundance, nuclear spin (*I*) and gyromagnetic ratio of common nucleus

Nucleus	Natural abundance (%)	Nuclear spin (I)	Gyromagnetic ratio (rad.s^{-1}.T^{-1})
^{1}H	99.987	1/2	267.513
^{13}C	1.07	1/2	67.262
^{14}N	99.634	1	19.338
^{17}O	0.038	5/2	-36.279
^{19}F	100	1/2	25.181
^{31}P	100	1/2	108.291

The Hamiltonian $\overrightarrow{H_{SI}}$ describing the electronic (*S*) and nuclear (*I*) spin system is the following:

$$\overrightarrow{H_{SI}} = \overrightarrow{H_{EZ}} + \overrightarrow{H_{HF}} = g\beta_e\vec{B}.\vec{S} + \vec{S}A_{iso}\vec{I} \qquad \text{(VII)}$$

In fine, such interaction leads to the splitting of each electronic spin level into $2I+1$ sub-levels corresponding to each of the m_I values whose the electronic energy is:

$$E(m_S, m_I) = g\beta_e B_0 m_S + m_I A_{iso} m_S \quad \text{(VIII)}$$

A simple example is when an electronic spin system (m_S = ±½) is in interaction with a neighboring nitrogen nucleus ^{14}N (m_I = 0, ±1). The diagram of the magnetic energy levels is described in Figure 2.3. Consequently, $2I+1=3$ transitions can be there observed when applying the selection rules:

- $\Delta m_S = \pm 1$
- $\Delta m_I = 0$,

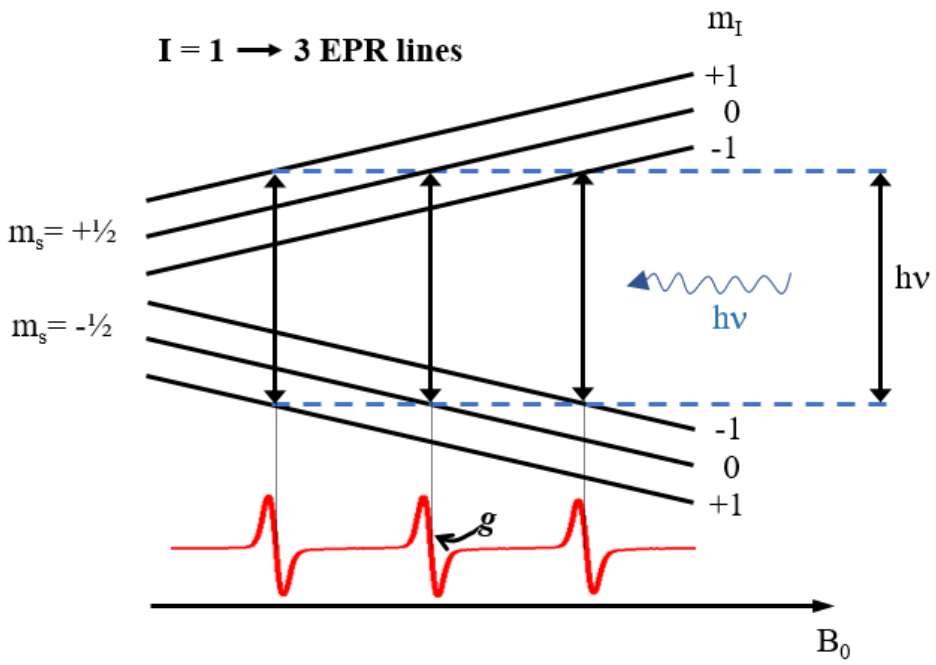

Figure 2.3 Schematic description of the magnetic energy level diagram and the allowed transitions for an unpaired electron in interaction with a nitrogen nucleus (^{14}N, $I=1$), leading to the classical 3 lines EPR spectrum e.g. obtained for a nitroxide derivative compound.

EPR spectra can be easily complexified whether the paramagnetic probe "is seeing" a multiple set of nuclei with non-zero nuclear spins.

Considering a system with a X set of equivalent nuclei interacting with the unpaired electron, as all the involved hyperfine couplings are identical, the EPR spectrum will be composed by $2nI+1$ peaks, equally spaced. The relative intensities of the absorption peaks are given by the

binomial expansion $(1+a)^X$ and the corresponding coefficients by the Pascal's triangle (see Table 2.1 and Figure 2.4).

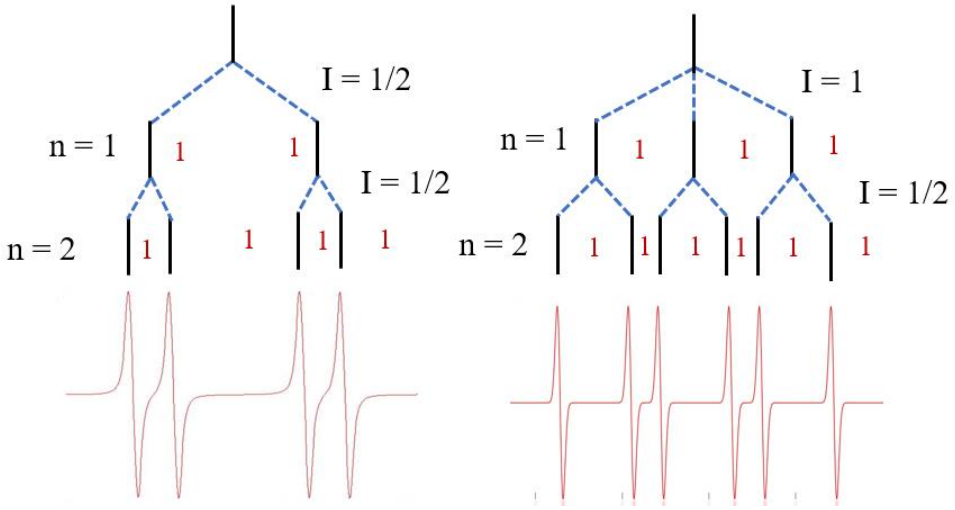

Figure 2.4: Two examples of electron delocalized on 2 equivalents (left side two protons) and 2 nonequivalent (right side a proton and a nitrogen) nucleus, nuclear spin *I* and n number of nucleus (red numbers indicates the relative intensity of the signal)

Considering a system with Y sets of inequivalent nuclei, the corresponding hyperfine couplings, will lead to an EPR spectrum with N peaks with a 1:1 intensity ratio where:

$$N = \prod_{n=1}^{Y}(2XI_n + 1) \qquad \text{(IX)}$$

1.4 Spin-trapping approach: from the reactive species to the EPR fingerprint

EPR is a dedicated spectroscopy for the study of free radicals reactive species. However, in our experimental conditions (aqueous solution at room temperature) most of the reactive species are not detectable *per se*. This is either due to their spin configuration (e.g. $^1\Delta_g$) and/or mostly to their short lifetime (nano- to milliseconds) which go hand in hand with their great reactivity. In these cases, the so-called spin-trapping approach is employed.[13] A schematic description of the technique is given in Figure 2.5.

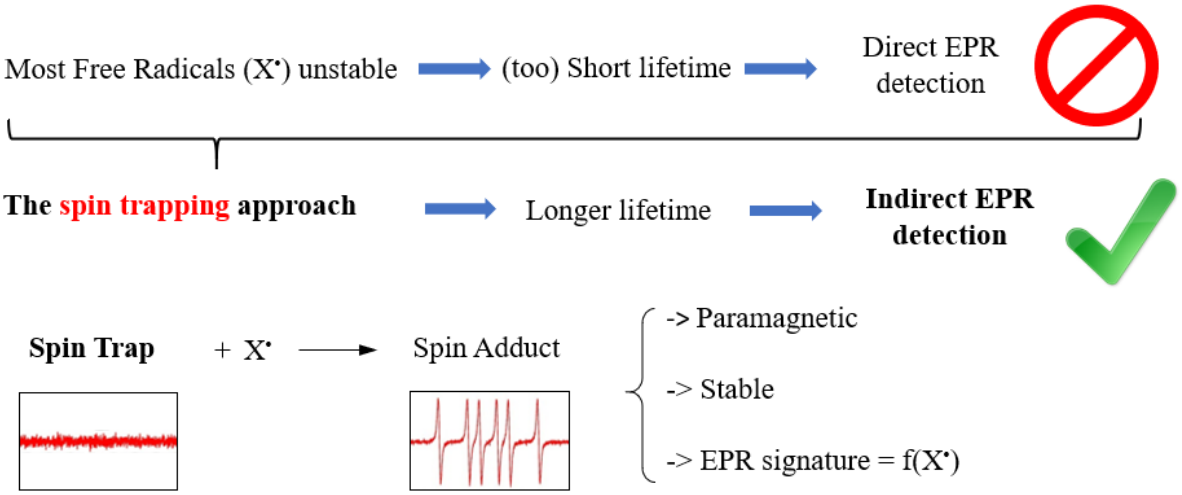

Figure 2.5: Schematic description of the spin-trapping approach: free radicals lifetimes are usually in the micro- to nanosecond time scale. Therefore, direct EPR characterization is not often possible. By reacting with a diamagnetic substrate (the spin-trap), the targeted reactive specie produces a paramagnetic spin-adduct with much longer lifetime (minutes to hours), whose the EPR signature is related to the nature of the trapped specie.

This technique developed in the late 1960's, is based on the use of a diamagnetic molecule known as the spin-trap, that reacts with transient reactive species to form a paramagnetic spin-adduct detectable by EPR.[14] The most commonly used spin-traps are nitroso or nitrone compound that lead to stable nitroxide radical adducts such as: PBN (N-*tert*-butyl-α-phenylnitrone), DMPO (5,5-dimethyl-1-pyrroline-*N*-oxide, 2,2-dimethyl-3,4-dihydro-2*H*-pyrrole 1-oxide) and DEPMPO (5-(diethoxyphosphoryl)-5-methyl-1-pyrroline-*N*-oxide).

Spin-adducts are obtained by addition of transient short-lived reactive species to the α-carbon of the nytronyl group (Figure 2.6), and their lifetime depends on the spin-trap used, ranging from some minutes to several hours.[15,16]

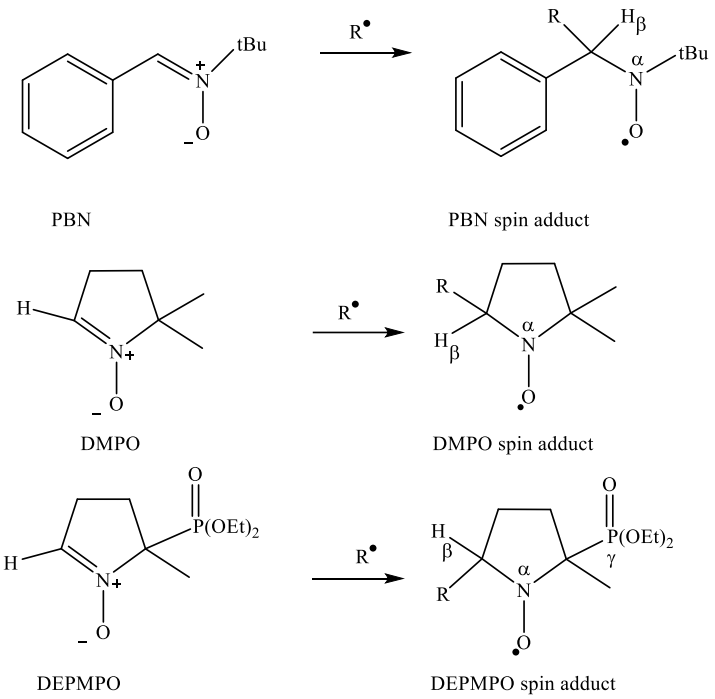

Figure 2.6: Different spin-trapping with their respective spin-adducts representation: α, β and γ indicate the positions of the nuclear spin ($I \neq 0$) interacting with the electron spin.

The resulting spin-adduct gives valuable information concerning the probed reactive species, as its EPR fingerprint is function of the trapped reactive species. Also, the intensity of the observed signal is directly related to the amount of trapped species. Nevertheless, it should be kept in mind that the spin trapping approach is an indirect method: we are observing spin-adducts and not the reactive species itself. Therefore, quantitative analysis is tempered by the spin-adduct lifetime and affinity constant.

A comprehensive analysis of the EPR fingerprint through the characterization of both the *g* factor(s) and hyperfine coupling(s) constant(s) allows to identify the trapped reactive species(s), by matching the obtained values with existing literature and databases.[17,18]

If we take DMPO spin-adduct as an example (Figure 2.7) in aqueous media at room temperature, different scenarios can be envisaged as DMPO is able to trap oxygen- and carbon-centered radicals. If a methyl radical ($^{\bullet}CH_3$) is trapped, the resulting unpaired electron of DMPO-CH_3 spin-adduct interacts with neighboring ^{14}N ($I_N = 1$) and ^{1}H ($I_H = ½$) in the β position (Figure 2.7A). Such system is assumed to give $(2I_N+1)(2I_H+1) = 6$ peaks. Hyperfine coupling constant are here known to be of *ca.* 16 G and 23 G for the a_N and $a_{H\beta}$ respectively.[17] If a

hydroxyl (•OH) radical is trapped, the DMPO-OH spin-adduct has another characteristic EPR fingerprint. In this case, $a_N = a_{H\beta}$ and is of *ca.* 15 G. As a direct consequence, only four lines are visible with a typical 1:2:2:1 intensity ratio (Figure 2.7B).[19] If an superoxide radical is trapped ($O_2^{\bullet -}$), the resulting spin-adduct DMPO-OOH exhibits twelve peaks (see Figure 2.7C). Such fingerprint was first wrongly attributed to the superposition of the two conformers of the corresponding spin-adduct, but Clement *et al.* identified it as a contribution of a third nucleus Hγ (located on the pyrroline group in the equatorial position) leading to a relatively smaller $a_{H\gamma}$ of *ca.* 1 G.[20] Unfortunately, the half-life of this spin-adduct is rather short (< 1 min) and it will rapidly convert into DMPO-OH spin-adduct. Consequently, distinguishing from superoxide anion to hydroxyl radical contribution is hardly reachable when using DMPO. Yet in real life scenarios, very often a mixture of different spin-adducts is observed (Figure 2.7D) and the resulting EPR spectrum needs to be deconvoluted to decipher the relative amount of the involved reactive species, this amount will be given in percentage.[21]

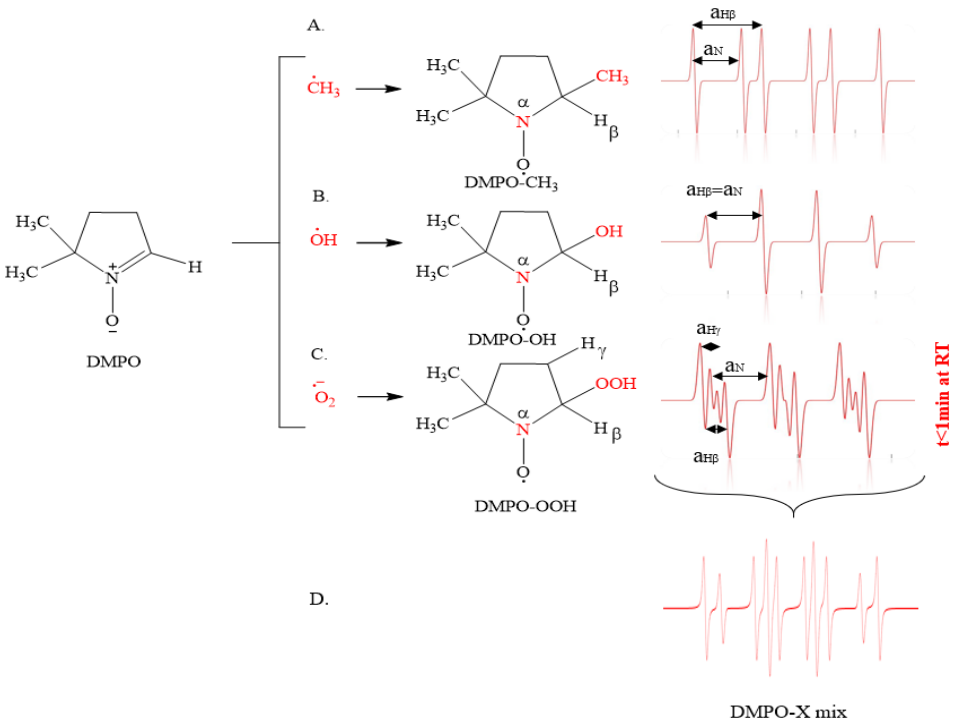

Figure 2.7: Example of DMPO spin-adducts EPR fingerprints: EPR signature (DMPO-X mix) with deconvoluted simulation of two oxygen radical and a carbon radical trapped. (A). methyl radical trapped, (B). hydroxyl radical trapped and (C). peroxyl radical trapped EPR fingerprints.

1.5 Limits of the technique and usual artefacts.

The first limit is the quantification of the radicals trapped, also working on the detection limits of the spectrometer due to the low concentrations used. The spectrum interpretation is more difficult in the case of anisotropy and the coupling between electron and orbital moment. Herein, quantitative assumptions are made here more difficult. It is important to underline the fact that other reaction can form nitroxides such as ene-reaction, Forrester-Hepburn reaction and Inverted Spin Trapping (IST).

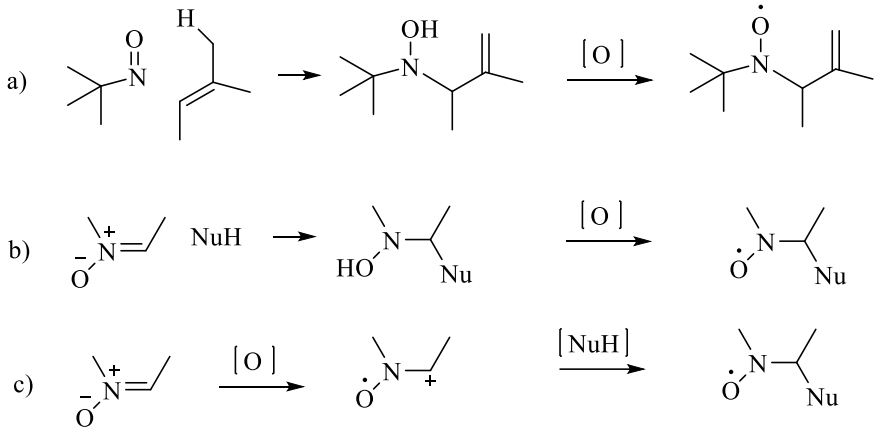

Figure 2.8: Nitroxide formation from nitrone or nitroso compounds without radical trapping. a) ene-reaction: MNP reacting with an olefin; b) Forrester-Hepburn reaction: addition of a nucleophile and oxidation; c) IST oxidation of the nitrone forming a radical cation followed by a nucleophile addition[4]

The ene-reaction occurs when a nitroso function reacts with an olefin (Figure 8.A). A pericyclic reaction produces a hydroxylamine then an oxidation transforms it to a nitroxide function, similar to the spin-adduct of a carbon centered radical.[22]

Forrester-Hepburn reaction produces a hydroxylamine by addition of a nucleophile to the spin-trap then an oxidation occurs using oxygen for example to synthesize nitroxide (Figure 8.B), similar to the spin-adduct of a hydroxyl radical is observed.[23]

IST an oxidation of the spin-trap producing a cation radical using a strong oxidant such as H_2O_2, similar to the spin-adduct of a hydroxyl radical is observed.[24]

Finally, the purity of the spin trap can also lead to parasitic signals and further purification such as distillation, recrystallization or activated charcoal filtration might be necessary.[25] For all of the above, performing all the necessary control experiment appears crucial.

1.6 Data analysis – from ruler and pencil to simulation and fitting

In front of a spin-adduct EPR spectrum, the first step is to determine roughly the *hfccs* (a_P, a_N and $a_{H\beta}$) values as well as the *g* factor by hand with "a ruler and pencil". An example is given in Figure 2.9, for the case of a methyl radical trapped by the DEPMPO spin-trap.

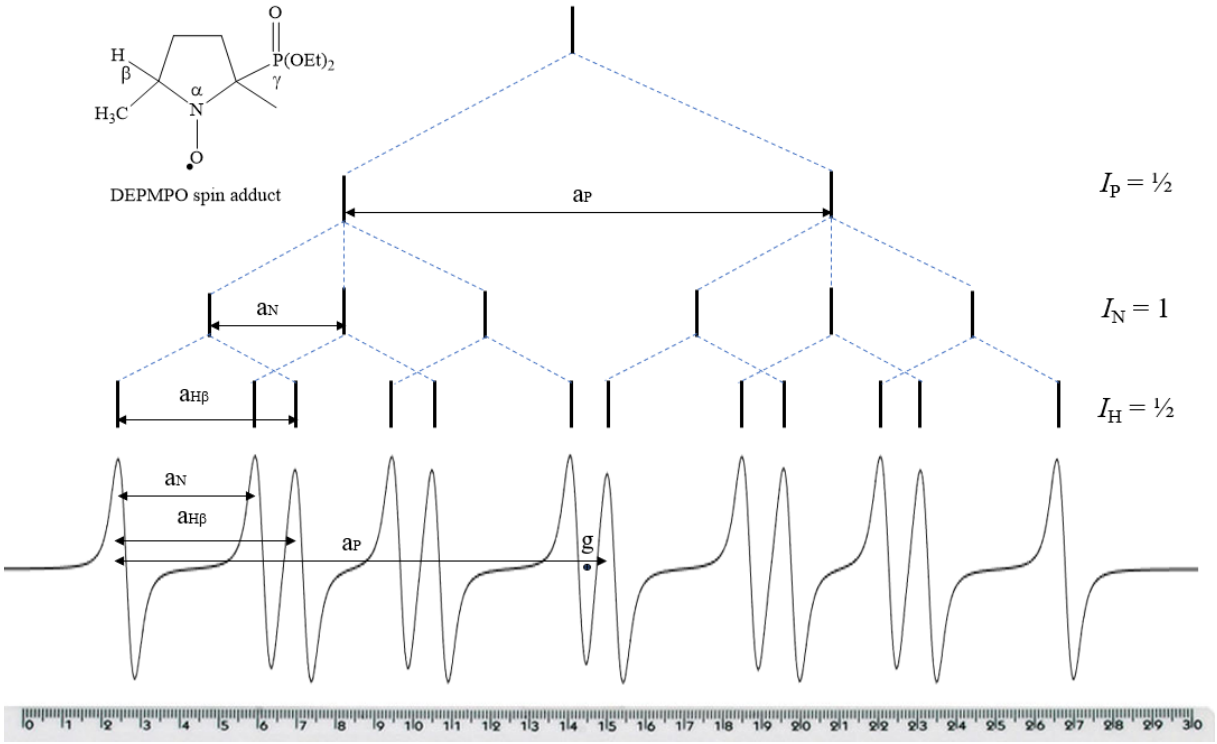

Figure 2.9: Schematic interpretation of a simple EPR spectrum: DEPMPO-CH_3 is the spin-adduct represented here. It deals with a carbon radical trapped characterized by three *hfccs* a_N, $a_{H\beta}$, a_P and *g*-factor in the middle of the spectra

However, very often EPR spectra are a mixture of several spin-adducts resulting from trapping various reactive species. In such scenarios, the above described rough analysis becomes more difficult to achieve, emphasized by the relatively weak signal to noise ratio (S/N) often observed in the *in situ* investigation of biological systems.[26]

For this reason, labmade routine to simulate EPR experimental data were developed, based on Easyspin, a computational EPR toolbox developed by Dr. Stefan Stoll *et al.*, under Matlab environment.[27] After a comprehensive simulation and fitting to the experimental data, the program can deconvolute the EPR mixed signature and determine the ratio of the different spin-adducts composing the reaction mixture. Both the *hfccs* and *g* values for each system are thus obtained and can be compared to the existing literature, spin databases, and/or DFT calculations.[17,18] This approach is especially useful when dealing with weak S/N (Figure 2.10).

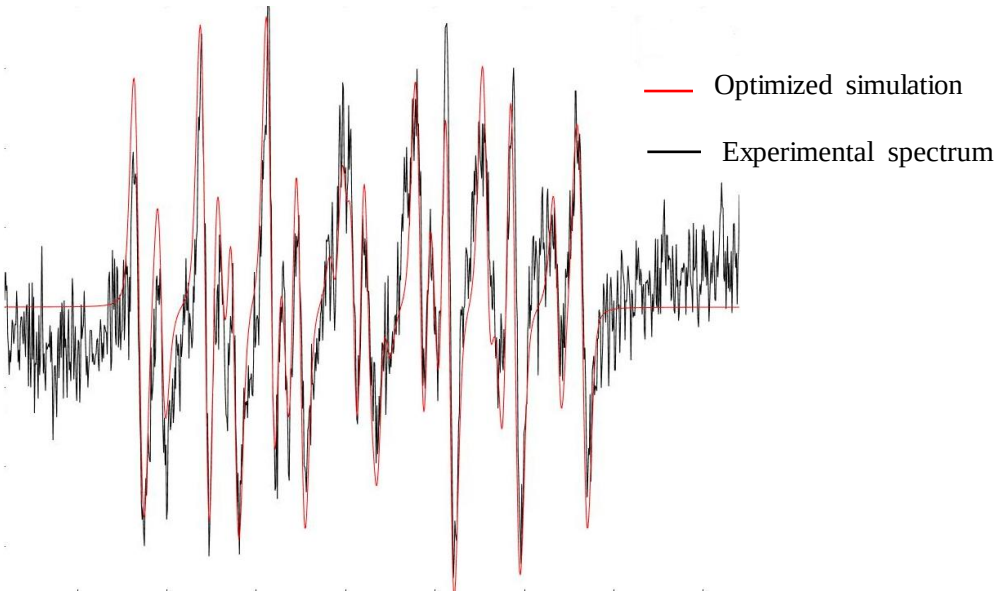

Figure 2.10: Detection limit conditions justifying the utility of the software Easyspin/Matlab used to fit and simulate experimentally obtained spectra.

The above described protocol based on "ruler and pencil" data analysis together with computational approaches paved the way of the analysis working method especially developed in the context of this PhD work.

1.7 EPR instrumentation

A schematic representation of an EPR spectrometer is shown in Figure 2.11. Major components are: an electro-magnet, a microwave bridge, the resonant cavity, the console and the work station.

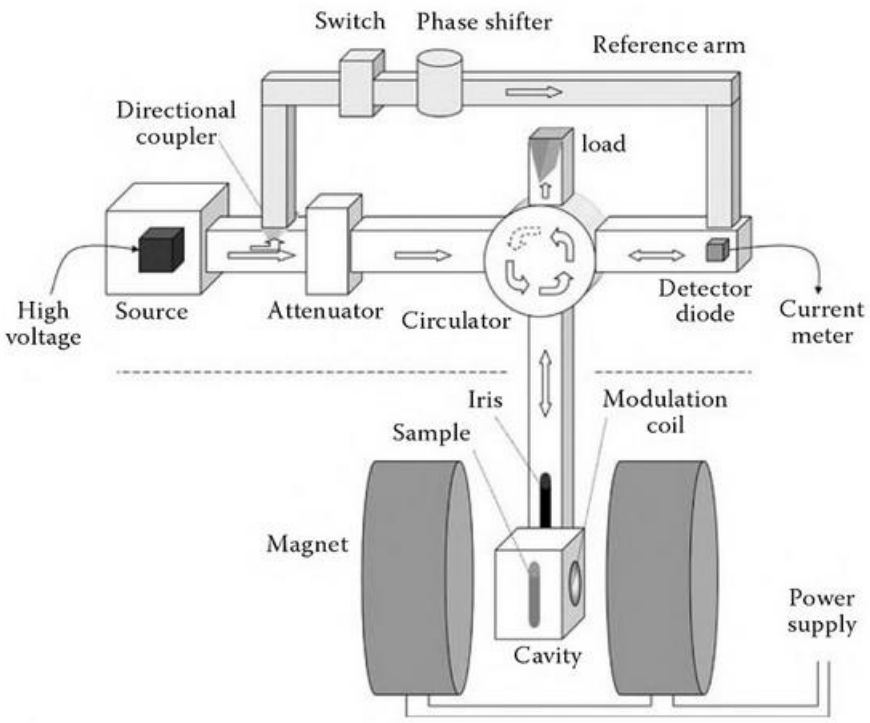

Figure 2.11: Schematic description of an EPR spectrometer composed of a microwave bridge (including the microwave source, the attenuator, the reference arm, the circulator and the detector) and a resonant-cavity between two electro-magnets.[28]

During EPR measurements, the electro-magnets generating a magnetic field (in Gauss) is applied to the cavity and thus the sample, leading to the Zeeman effect. An EPR scan is carried out by varying the $\overrightarrow{B_0}$ field at a constant microwave frequency ν of ca. 9.5 GHz (*i.e.* X-band), until reaching the resonance conditions. The coupling between the microwaves arising from the waveguide and the cavity is achieved through an iris whose aperture is adjusted to tune the microwaves entering and reflected from the cavity.

In resonant cavity, a standing electromagnetic wave is created where the electric and magnetic field components are out of phase. By placing the sample in the maximum magnetic field and therefore in the lowest electric field, an optimal signal can be measured. This is especially critical when dealing with system with high dielectric constant (such as aqueous solution at room temperature), where the major part of electrical component is absorbed by the system (as for a regular microwave oven) and significantly deteriorate the sensitivity of the experiment (Figure 2.12). Consequently, specific geometry of the investigated samples is required: (i) for

in vitro studies submillimeter quartz or glass capillaries vertically positioned into the cavity are mandatory; (ii) for biological tissue studies a flat cell will be preferred.

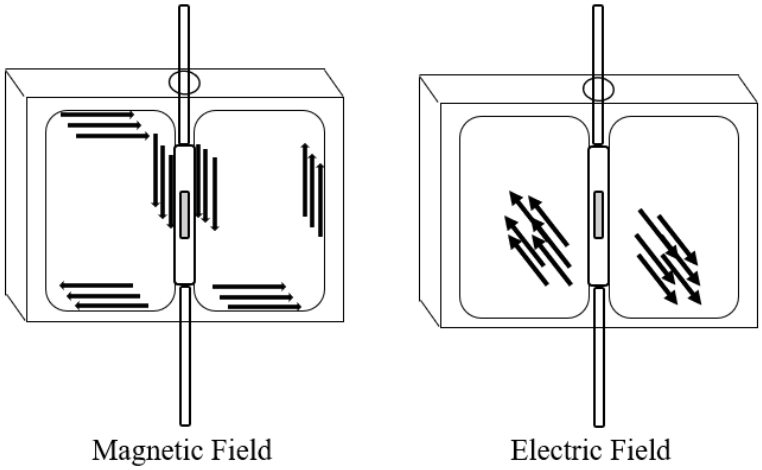

Figure 2.12: Schematic illustration of the Magnetic (left) and electric field (right) in a standard EPR cavity containing a flat cell.

Noteworthy, when considering the microwave intensity (few milliwatts in the present work), heating of the sample is not here questioned.

2 IDENTIFICATION OF RADICALS DERIVED FROM ROOHS: STUDIES IN SOLUTION

Studies in solution were firstly carried out to set up the optimal experimental conditions providing a good S/N while keeping low ROOHs and spin-trap concentrations, thus suitable for physiological conditions. Radical initiation was triggered by Fe^{II}-induced Fenton-like reaction. The final aim was to transfer these experimental conditions to a reconstructed human epidermis (RHE) model.

2.1 Key players

Target compounds

ROOHs that have been chosen for these studies are: cumene hydroperoxide (Cum-OOH), limonene hydroperoxide (Limo-OOH) and a 2:3 mixture of linalool-7-hydroperoxide (Lina-7-OOH) and linalool-6-hydroperoxide (Lina-6-OOH) (Figure 2.13).

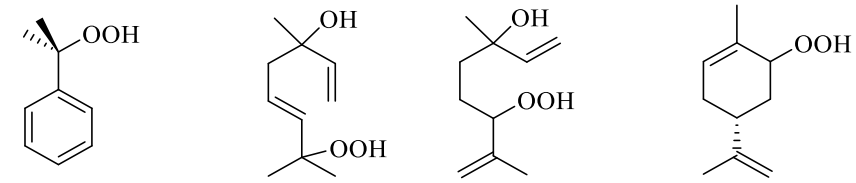

Figure 2.13: Chemical structures of the target hydroperoxides used in the studies in solution.

Radical initiation: Fe(II) sulfate

It is known that Fe(II) initiates the decomposition of hydroperoxides into alkoxyl radicals and hydroxyl ions, by a mechanism similar to that of Fenton reaction.[29-30] Following such radical initiation, unstable alkoxyl radicals can evolve through different pathways. For example, the abstraction of a hydrogen from the hydroperoxide ROO-H function is possible, leading to an alcohol and peroxyl radicals. These can interact together leading to tetroxide (ROOOOR) compounds able to regenerate alkoxyl radicals together with the release of molecular oxygen. Peroxyl radicals can also abstract a hydrogen to produce carbon-centered radicals (Figure 2.14).

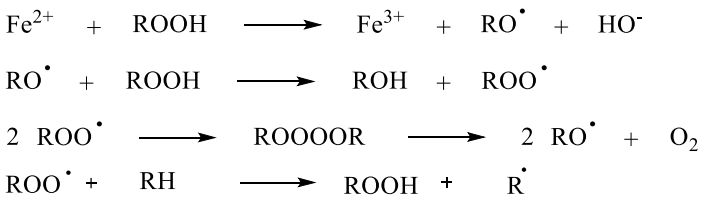

Figure 2.14: Fenton-like reaction and subsequent radical generation in the case of ROOHs

The spin-traps

Spin-traps used were: PBN (N-*tert*-butyl-α-phenylnitrone), DMPO (5,5-dimethyl-1-pyrroline-*N*-oxide, 2,2-dimethyl-3,4-dihydro-2*H*-pyrrole 1-oxide) and DEPMPO (5-(diethoxyphosphoryl)-5-methyl-1-pyrroline-*N*-oxide).

PBN spin-adducts *hfccs* arise from the interaction of the unpaired electron with the ^{14}N (I_N=1) and the surrounding ^{1}H (I_H = ½) (Figure 2.6). In our experimental conditions (*i.e.* aqueous solution, neutral pH and room temperature), the *g* factor does not appear as a discriminatory parameter and will be always of *ca.* 2.006. This is indeed the case for all spin-traps discussed here. The reactivity of PBN is relatively high and allows the detection of low quantities of radicals. Yet, the relatively low specificity of the hyperfine couplings towards the nature of the

trapped species, together with low steric hindrance of the radical within the spin-adduct leading to bio-reduction limit its use in *in vivo* experiments.

DMPO spin-adducts *hfccs* arise from the interaction of the unpaired electron with the ^{14}N (I_N=1) and the ^{1}H (I_H=½) in position β (see Figure 2.6). For this spin-trap, the hyperfine couplings between the electron and the nitrogen and hydrogen nuclei are greatly dependent of the nature of trapped radical. As for PBN, DMPO spin-trap is commonly used in biological media but the low resistance to bio-reductions of its spin-adducts limits the potential use in *in vivo* applications.[31]

DEPMPO spin-adducts *hfccs* arise from the interaction of the unpaired electron with the ^{14}N (I_N=1), ^{1}H (I_H= ½) in position β and ^{31}P(I_P=½) in position γ (see Figure 2.6) and produces spin-adducts with longer lifetime, particularly for the superoxide and alkylperoxyl radicals adducts.[32] Thus it presents a pertinent alternative for the experiments within 3D reconstructed human epidermis.

The spin-adduct lifetime depends on the spin-trap as well as its environment (e.g. presence of reductant compounds) and goes from minutes to hours.[33]

Solvent and concentration of reagents

Spin-traps, in H_2O/CH_3CN (9:1), 10 mM phosphate buffer (PB) or HEPES buffer, were employed in an excess concentration (25 mM) with respect to ROOH (1-10 mM). The spin-trap solution was then mixed with aqueous ferrous sulfate (0-1.7 mM) and the ROOH was lastly added to the mixture which was inserted in a 25 µL glass capillary (Hirschman ringcaps), and investigated by EPR after different reaction times (1 minute to 2 hours).

High concentrations of both the spin-trap (500 mM) and the hydroperoxide (10 mM) were initially used and thereafter gradually decreased (up to 25 and 0.5 mM respectively). We started the studies with Limo-OOH in pure water solution by decreasing the spin-traps and the Limo-OOH concentrations while keeping a decent S/N with a minimum amount of spin-trap and Limo-OOH. The second step was to transpose these conditions into a medium more suitable for biological assays, by using Cum-OOH and phosphate buffer (PB). It was shown that in PB, radical generation was not detected with a catalytic amount of Fe(II) (0.1 mM). Therefore, we decided then to use HEPES buffer in which radical generation occurred with a catalytic amount of Fe(II). Finally, HEPES buffer was chosen to characterize radical generation from Lina-

OOHs. Here HEPES buffer was also combined to the cell culture medium (CM): the nutrients medium of the RHE (potential source of antioxidant), with a ratio 4:1 then 1:1 v/v to probe the influence of CM on radical generation. The main idea was to use as much as possible physiological compatible conditions to investigate radicals in the RHE without starving and/or stressing the cells by the sole experimental conditions.

To be clear and concise, we will present the use of DEPMPO allowing the identification of different oxygen and carbon-centered radicals derived from ROOHs. PBN and DMPO complementary studies, respective EPR spectra, *hfccs* and *g* values are presented in annexes to this chapter. DEPMPO has been successfully used for the *in vivo* detection of oxygen-centered radicals due to the high persistency of its superoxide and alkylperoxyl radicals adducts.[34] DEPMPO is also able to distinguish between oxygen and carbon-centered radicals.[16]

2.2 System Limo-OOH, spin-trap, H_2O and Fe(II)

Here we will use the example of Limo-OOH in water medium and in the presence of DEPMPO as spin-trap to present the methodology used to identify the formed spin-adducts. Firstly, the "ruler and pencil" approach (see section 1.6) was used to identify the probable spin-adducts together with their approximative *hfccs* and *g* values. Then, specific simulation and fitting routines (using Easyspin/Matlab toolbox) were applied to the experimental spectrum (Figure 2.15) in order to refine the *hfccs* and *g* for all present spin-adducts together with their relative concentration (when applicable). Worthy of note, relative quantifications of generated radicals remain possible if the spin-adducts lifetimes and efficiency are assumed comparable. For the treatment and characterization of all spectra obtained during this work the identical procedure was applied. In the example presented here, *i.e.* for Limo-OOH/DEPMPO/H_2O system, two spin-adducts were identified whose the principal characteristics are summarized in Table 2.2. According to existing literature, those two spin-adducts were attributed to hydroxyl (DEPMPO-OH) and carbon-centered (DEPMPO-carbon R) radicals.[34]

Table 2.2: *Hfccs*, *g* and relative quantification for spin-adducts identification in system Limo-OOH/DEPMPO/H_2O.

DEPMPO-OH **1** (*ca.* 80%)	DEPMPO-carbon R **2** (*ca.* 20%)
g=2.0055	g=2.0054
a_N=14.1	a_N=14.9
a_H=13.5	a_H=22.1
a_P=47.6	a_P=46.9

Both the nature and the relative concentration of spin-adducts remain unchanged when decreasing the concentration of Limo-OOH from 10 to 1 mM (Annex 1., Figure A1.1). Moreover, the hydroxy spin-adduct **1** was formed with *ca.* 4-fold concentration when compared to the carbon spin-adduct **2** at 1mM Limo-OOH.

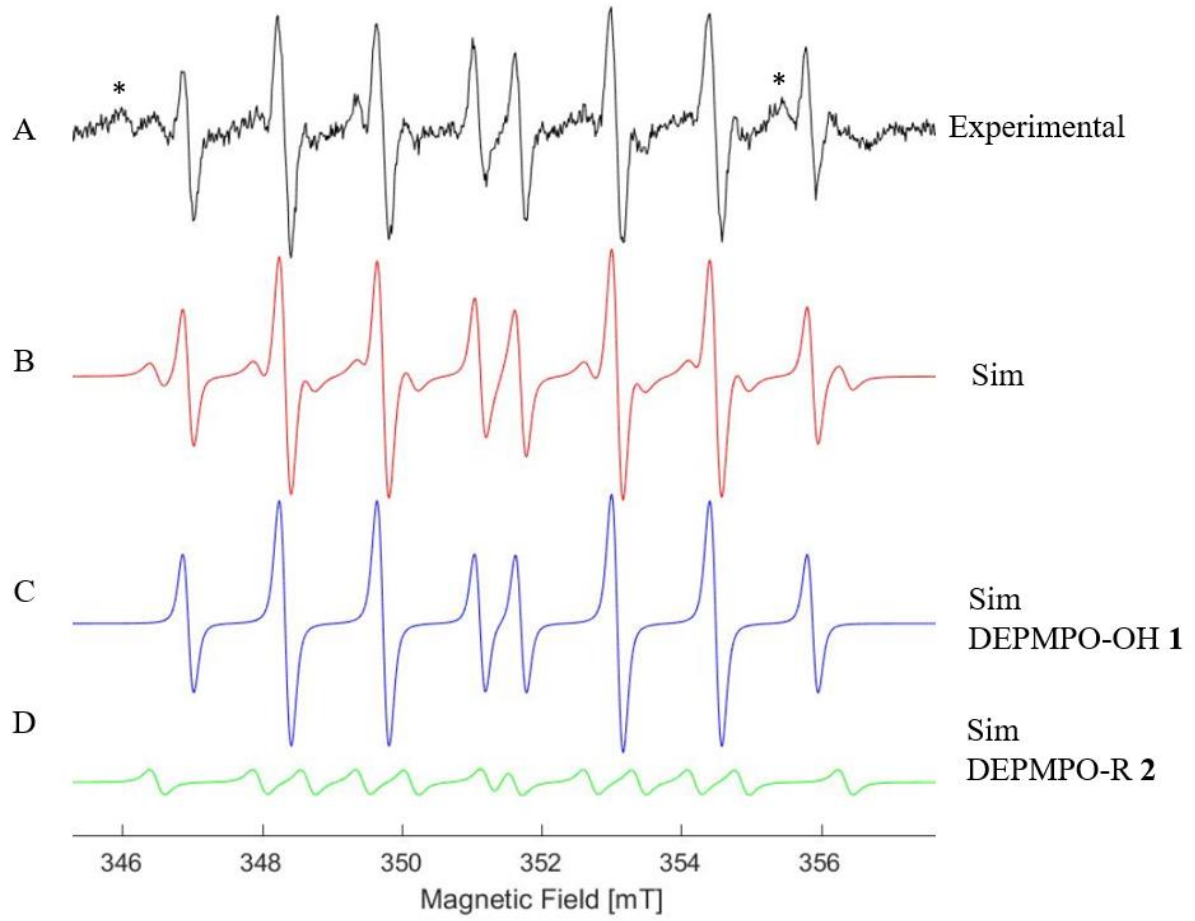

Figure 2.15: (A) EPR spectrum of DEPMPO (25 mM) spin-adducts formed from Limo-OOH (1 mM)/Fe(II) (0.1 mM) in H_2O; (B) computer simulation and (C and D) deconvolution of DEPMPO-OH (*ca.* 80 %) **1** and DEPMPO-R (*ca.* 20 %) **2** (more available data in Annex 1, Figure A1.1), (* cavity contamination).

By decreasing the Limo-OOH concentration (10 mM to 1 mM), both the hydroxyl spin-adduct **1** and carbon spin-adduct **2** were observed. But the relative concentrations remained stable. The decrease of the DEPMPO (from 500 to 25 mM) concentration does not influence the formed radicals (data not shown). By increasing Fe(II) concentrations (0.1 mM to 1.7 mM) in the mixture of Limo-OOH (1 mM) and DEPMPO (25 mM), the carbon spin-adduct ratio increased from *ca.* 20 to 50 % (Annex 2, Figure A2.1).

In the studies using PBN (50 mM) in a mixture of Limo-OOH (1 mM) and Fe(II) (0.1 mM) in H_2O, a spin-adduct (**3**) attributed to a carbon-centered radical was observed (Annex 4, Figure A4.1). The same mixture using acetonitrile as solvent produced a carbon spin-adduct **4** probably due to the decomposition of the acetonitrile in the experimental conditions.[35] Figure 2.16 summarizes the mechanistical hypotheses for the observed spin-adducts.

In parallel investigations with DMPO, only hydroxyl radical spin-adduct (5) was observed. Moreover, the relatively short half-life of the DMPO spin-adduct (*ca.* minutes) leads to its rapid disappearance.

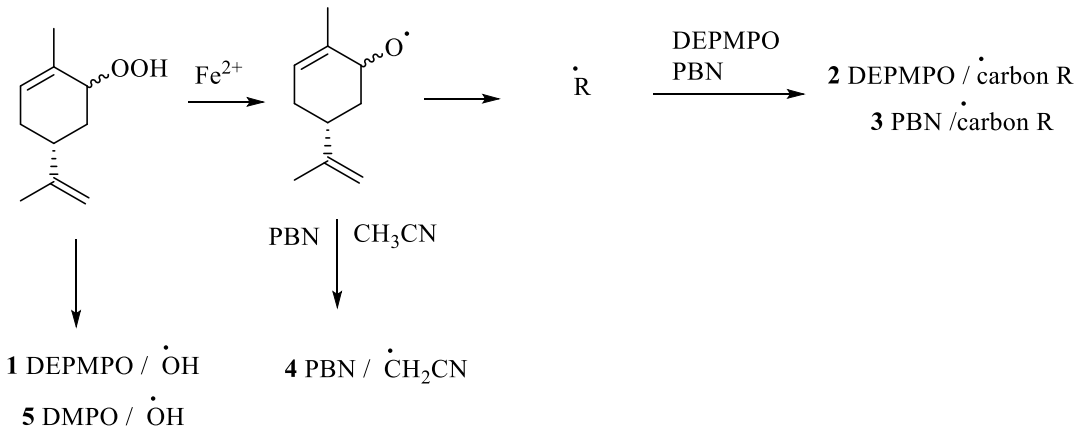

Figure 2.16: Hypothetical spin-adducts obtained using Limo-OOH

The next step was to transpose these experimental conditions into a medium more suitable for biological assays and by using Cum-OOH as a reference compound.[36–38]

2.3 System Cum-OOH, spin-trap, PB or HEPES and Fe(II)

According to Pazos *et al.*, the concentration of Fe(II) is a limiting factor in the generation of radical species in PB, when they used 0.1 mM of Fe(II) and 0.54 mM of Cum-OOH it was sufficient to observe oxidation processes.[30] Yet, in our experiments 0.1 mM of Fe(II) was not enough to start the reaction in 10 mM PB whatever was the spin-trap (at 25 mM). At higher

concentrations of Fe(II) (0.5 mM and above), the radical generation rate significantly increased and spin-adducts were already detected after only 1 min of reaction time (Annexes 6-8, Figures A6.1, A7.1, A8.1). The inhibition of Fe(II)-catalyzed CumOOH oxidation at low concentrations is ascribed to the ability of phosphate to catalyze oxidation of Fe(II), forming Fe(III) that is rather insoluble and hence decreasing Fe(II) content in the reaction mixture.[39] PB was thus replaced by 10 mM HEPES buffer, known for its stability at physiological pH.[40] In these conditions, a catalytic amount of Fe(II) (0.1 mM) was enough to start the reaction. Moreover, keeping all other parameters identical the signal intensity observed in HEPES investigations were of an order of magnitude higher than the one observed with PB.

Experiments were then performed in 10 mM HEPES within 0.1-1.7 mM range of Fe(II) together with 25 mM of DEPMPO, DMPO or PBN (Annexes 6-8, Figures A6.2, A7.2, A8.2). Figure 2.17 shows the results obtained for 0.5 mM of Fe(II) in the presence of 0.54 mM of Cum-OOH and 25 mM of DEPMPO. Three distinct spin-adducts were observed in the experimental spectrum. Once deconvoluted the following spin-adducts were identified: DEPMPO-OH (*ca.* 50 %) **1**, DEPMPO-carbon R (*ca.* 20 %) **6** and DEPMPO-OCH3/OOCum **7** (*ca.* 30 %).

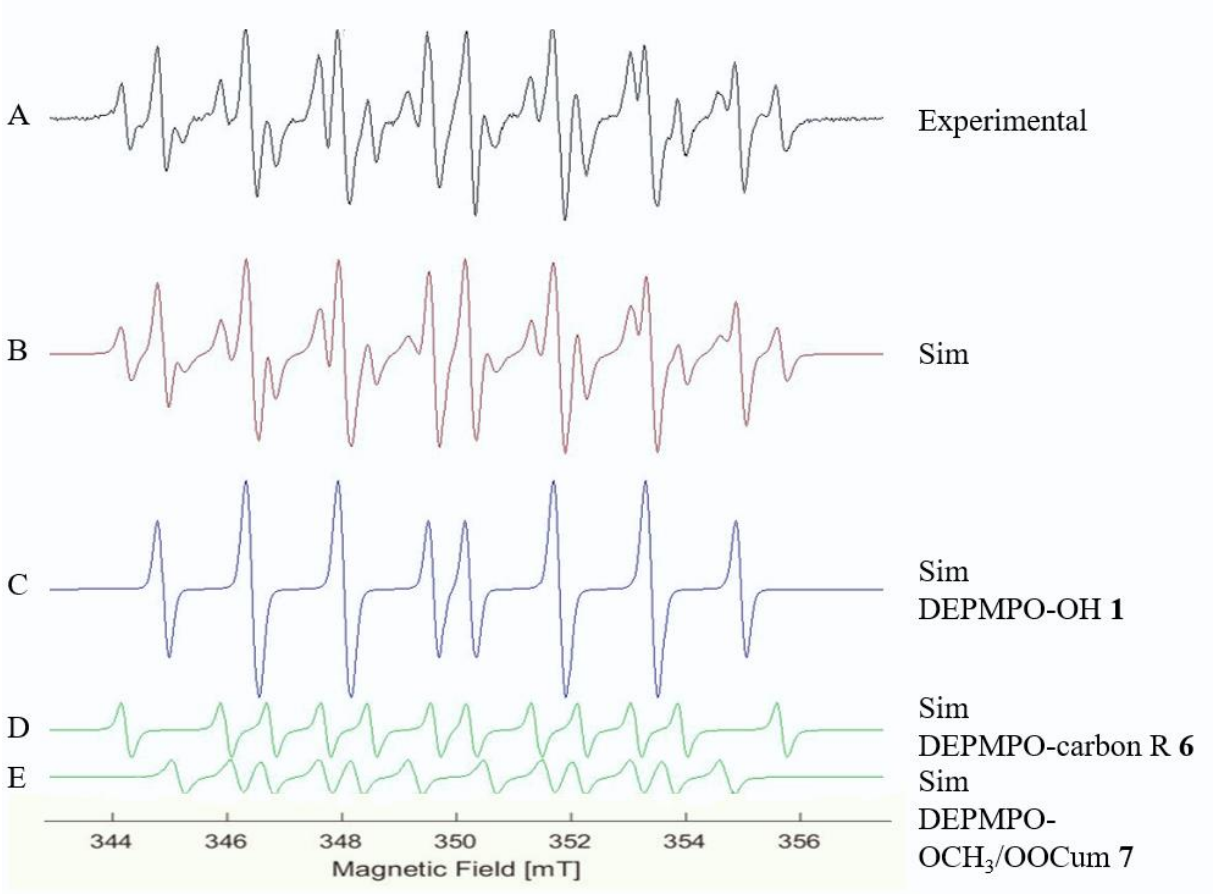

Figure 2.17: (A) EPR spectrum of DEPMPO (25 mM) spin-adducts formed from Cum-OOH (0.54 mM) / Fe(II) (0.5 mM) in HEPES, (B) computer simulation and (C, D and E) deconvolution of DEPMPO-OH (*ca.* 50 %) **1**, DEPMPO-carbon R (*ca.* 20 %) **6** and DEPMPO-OCH_3/OOCum **7** (*ca.* 30 %) (more data available in Annex 6, Figure A6.2).

The DEPMPO-OH **1** (Figure 2.17C) originates from the homolytic scission of Cum-OOH (one electron mechanism).[34] The DEPMPO-carbon R **6** (Figure 2.17D) most probably arises from the $^{\bullet}CH_3$ radical derived from the β-scission, and confirmed using both DMPO (Annex 7, Figure A7.2) and PBN (Annex 8, Figure A8.2).[34] The spin-adduct **7** (Figure 2.17E) is ascribed to either $^{\bullet}OCH_3$ or $^{\bullet}$OOCum radical following the mechanisms schematized in Figure 2.19.[34] On the one hand, following the β-scission the methyl radical can react with molecular oxygen forming peroxymethyl radicals, that can combine into tetraoxodimethyl, and leading to methoxy radical by releasing molecular oxygen. Noteworthy, this methoxy radical issued from the from β-scission was only reported in the presence of either amino acids or ethanol in the reaction mixtures which was not the case in the present work.[30,41,42] On the other hand, hydrogen

abstraction within Cum-OOH forming •OOCum radical can react directly with the spin-trap leading to **7**.

EPR spectra shown in Figure 2.17 and Annex 6 (Figures A6.1 and A6.2) highlighted a mixture of spin-adducts formed by DEPMPO trapping of hydroxyl •OH (**1**), carbon-centered (**6**), $CH_3O^{\bullet}$ and/or possible peroxyl CumOO• radicals (**7**).[34] It was confirmed the direct formation of these radicals at catalytic Fe(II) concentration (0.1 mM) in HEPES buffer (Annex A6, Figure A6.2).

Concerning PBN investigations in HEPES (Annex 8, Figure A8.2), the only spin-adduct observed at low Fe(II) concentration (< 0.5 mM) is testimony of the β-scission. Above 1 mM of Fe(II) the *hfccs* a_N of the spin-adduct significantly increased from *ca.* 15 to 16 G. An explanation could be the trapping of oxaspiro radicals in equilibrium with CumO•, which are suspected intermediates in known *O*-neophyl rearrangement processes (Figure 2.18).[43] Such rearrangement would be favorized as the electron reservoir is higher (i.e. higher concentration of Fe(II)).

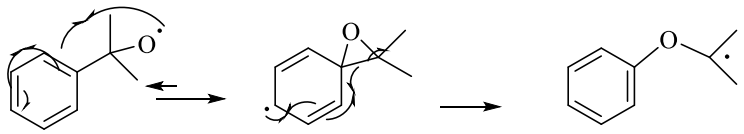

Figure 2.18: *O*-Neophyl rearrangement processes described in the literature.[43]

As regards the DMPO-OCH_3 spin-adduct **8** was yet detected at catalytic Fe(II) levels (0.1 mM), and $CH_3^{\bullet}$ radicals also formed and trapped (**9**) at higher Fe(II) concentrations (Annex A7, Figures A7.1 and A7.2).[44]

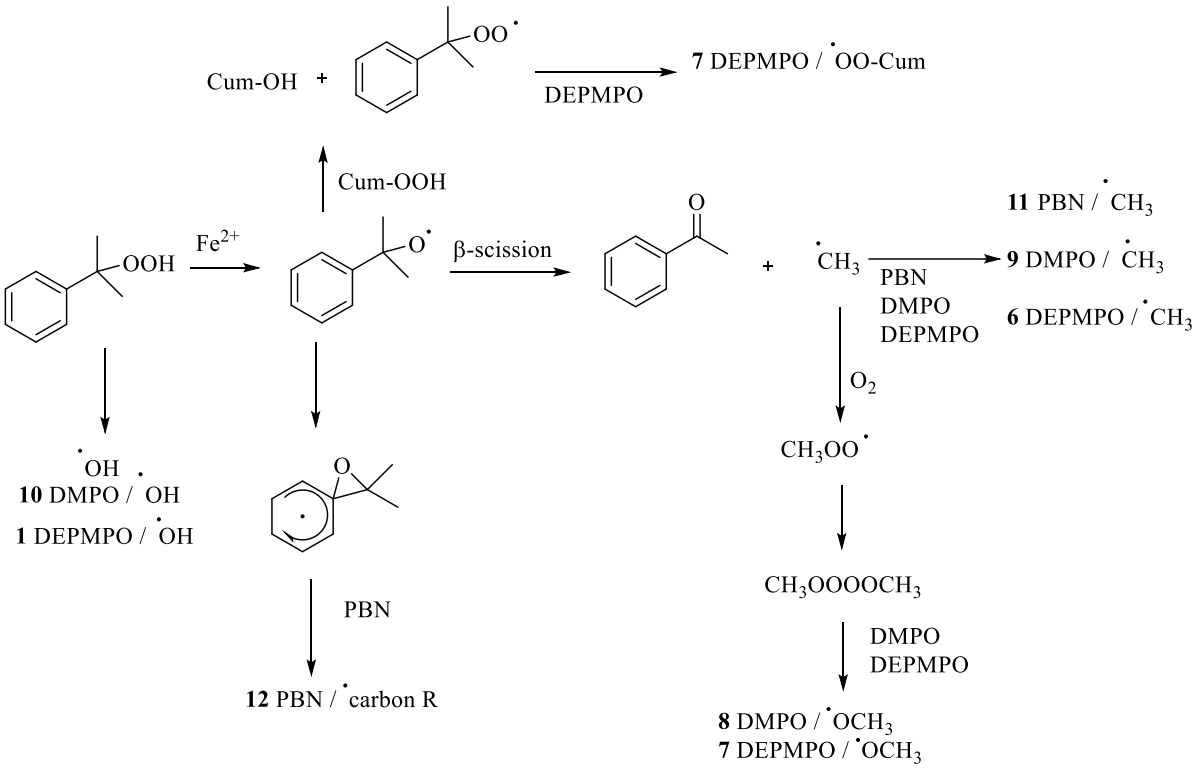

Figure 2.19: Formation of CumOOH/Fe(II) spin-adducts and related mechanisms.

Noteworthy, DEPMPO was in the present work the spin-trap affording the most complete picture on the different radical intermediates derived from Cum-OOH (Figure 2.19).

Regarding the following section dealing with Lina-OOHs, the aim was to get closer to what could happen in the RHE, using DEPMPO, HEPES buffer later combined with cell culture medium (CM).

2.4 System Lina-OOHs, spin-trap, HEPES and Fe(II)

In the case of Lina-7-OOH, one of the isomers deriving from autoxidation of linalool, the literature shows that oxygen-centered radicals can produce carbon-centered radicals by different rearrangement processes. Allyloxyl radicals formed from cleavage of the O-OH bond can follow β-scission and 3-*exo*-trig cyclization for example that can further evolve to form several other oxygen- and carbon-centered radicals (Figure 2.20).[45]

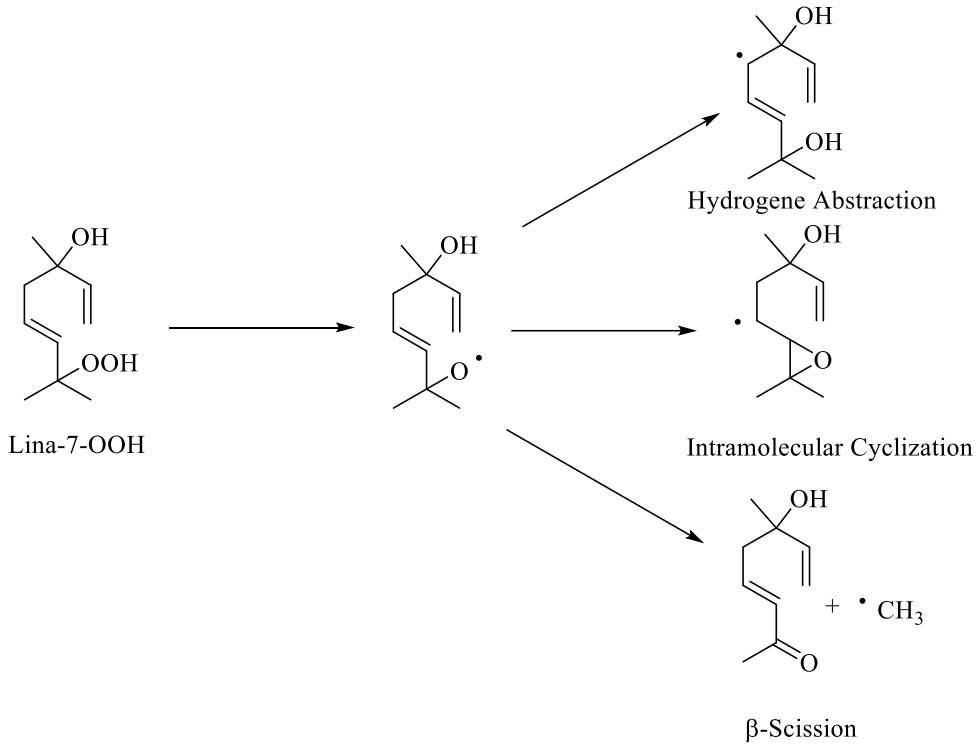

Figure 2.20: Radicals generated from Lina-7-OOH and different involved mechanisms.[45]

Figure 2.21 shows the experimental data and subsequent simulations for the DEPMPO investigations when using Lina-OOHs mixture (Lina-7-OOH and Lina-6-OOH). Three spin-adducts were clearly distinguished. The first one corresponds to DEPMPO-OH 1 (Figure 2.21C), ascribed to hydroxyl radical as previously discussed in the Cum-OOH section. The second one is attributed to DEPMPO-carbon R 13 (Figure 2.21D). It was indeed confirmed by the PBN and DMPO investigations (Annexes 12, 13 and Figures A12.1, A13.1&2 respectively).

The third detected spin-adduct (**14**, Figure 2.21E) is thought to arise either from the $^{\bullet}OCH_3$ radical or $^{\bullet}$OOLina following the same approach described previously in the Cum-OOH section.

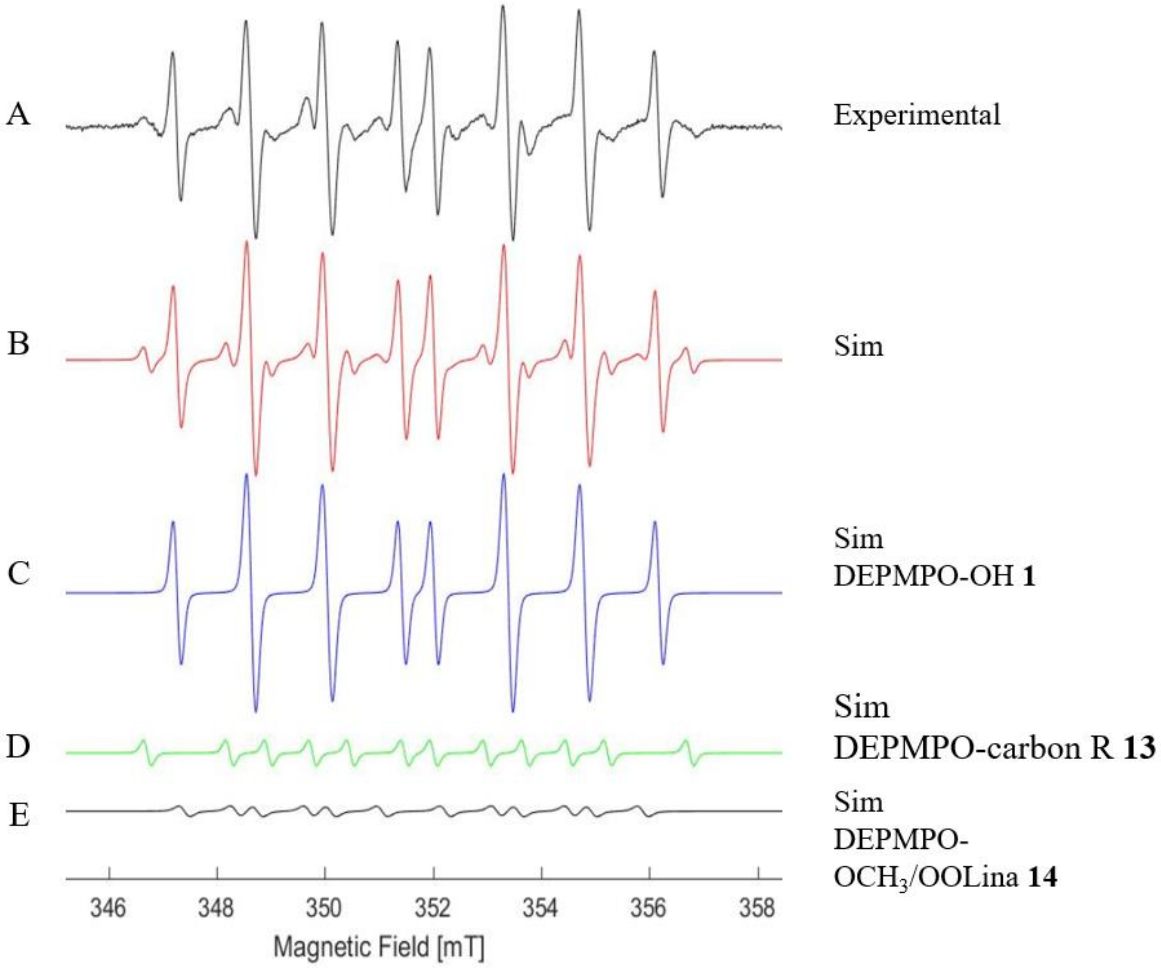

Figure 2.21: (A) EPR spectrum of DEPMPO (25 mM) spin-adducts formed from Lina-OOHs (1 mM) / Fe(II) (0.1 mM) in HEPES, (B) computer simulation and (C, D and E) deconvolution of DEPMPO-OH (*ca.* 70 %) **1**, DEPMPO-carbon R (*ca.* 15 %) **13** and DEPMPO-OCH_3/OOLina **14** (*ca.* 15 %) (more data are available in the Annex 9, Figure A9).

Interestingly, at 0.1 mM of Fe(II), the DEPMPO-OH **1** fraction is predominant when compared to spin-adducts **13** and **14**. However, when increasing the Fe(II) concentration to 1 mM and above the relative concentration ratio of **13**/**1** increases (Annex 9, Figure A9.1) until reaching comparable values.

Some experiments have been also carried out using as solvent the cell culture medium (CM) dedicated for the RHE Episkin™ (HEPES/CM 4:1 then 1:1 v/v). Worthy of note, CM was provided by Episkin to maintain the RHE, lacking any of other information regarding the component of the medium. First, there is a significant difference in the EPR fingerprints intensities when comparing HEPES/CM investigations to pure HEPES ones. Clearly, the

presence of CM (and its antioxidant compounds) competes with the spin-trap action and/or with the lifetime of the spin-adduct itself (by reducing it). Nevertheless, it appears that hydroxyl radicals and carbon radicals were equally trapped when using 1 mM of Fe(II). Increasing Fe(II) concentration to 1.7 mM relative carbon radical formation **13** increased while hydroxyl radical formation seemed to decrease. Importantly, the spin-adduct **14** was not observed when solvent HEPES/CM was used whatever was the HEPES/CM ratio (Annexes 10-11 Figures A10.1, A10.2, A11.1 and A11.2). This points to the antioxidative potential of the CM.

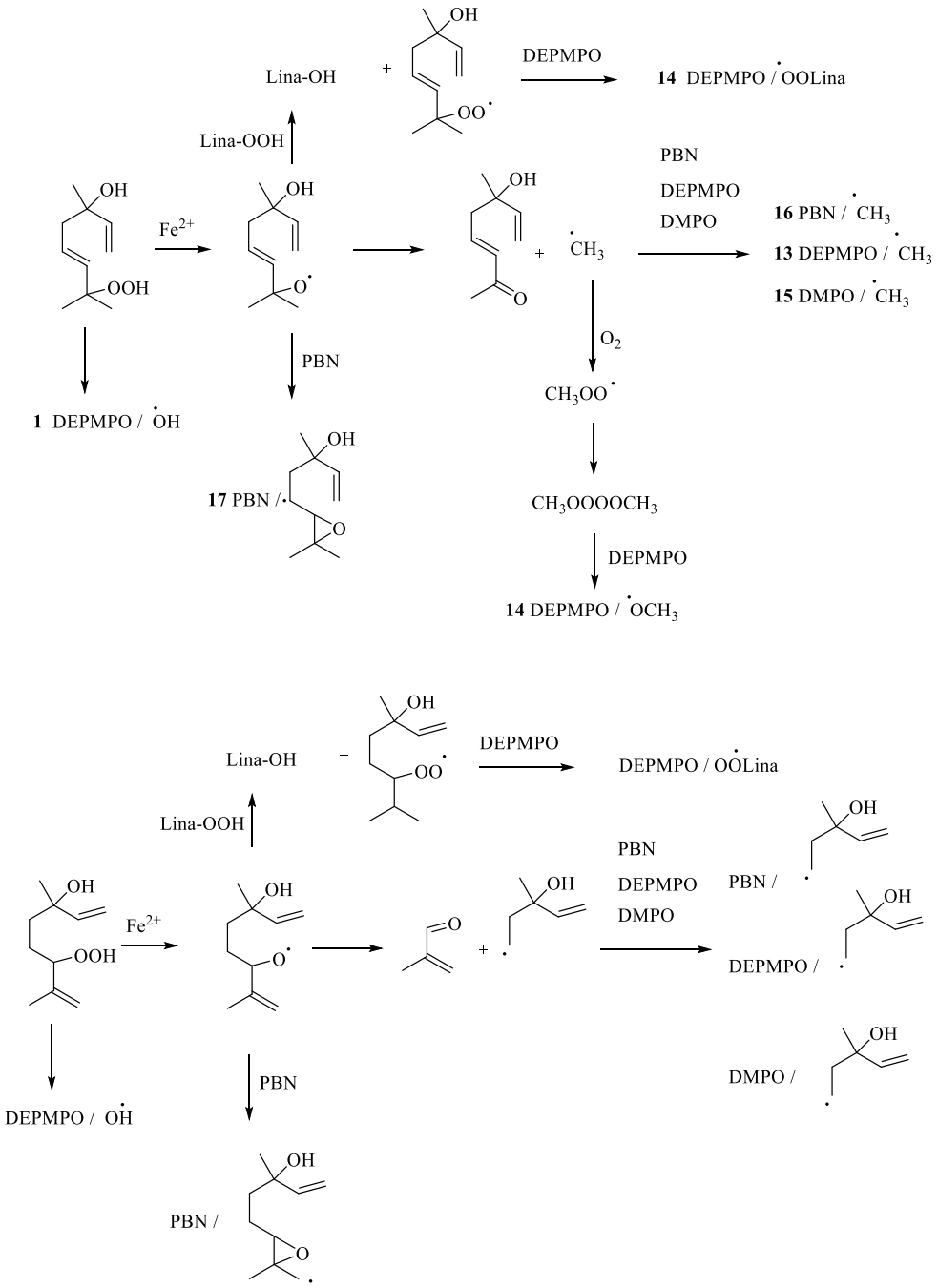

Figure 2.22: Schematic description of the potential mechanisms leading to the formation of the spin-adducts arising from Lina-OOHs/Fe(II).

2.5 Conclusion

The spin-trapping technique using PBN, DMPO, and DEPMPO, combined with EPR spectroscopy, allowed us to characterize radical intermediates issued from Cum-OOH, Limo-OOH, and Lina-OOHs in solution. Using Fe(II) as radical initiator, the formation of alkoxyl,

peroxyl and carbon-centered radicals has been observed. When the solvent was exclusively acetonitrile, the proportion of carbon radicals trapped considerably increased, probably due to the decomposition of the solvent. Moreover, it seems that ROOH undergo initially a homolytic scission. Hydroxyl radical spin-adduct were detected using DEPMPO and DMPO. Peroxy cumyl and peroxy linalyl radicals were also identified by using DEPMPO as well as methoxy radicals that were detected by both DEPMPO and DMPO. Finally, carbon radicals were also identified by using PBN, DMPO, and DEPMPO. Interestingly, it appeared that Cum-OOH and Lina-OOHs exhibit a similar behavior rather different from that observed from Limo-OOH as summarized in Table 2.3

Table 2.3: Table of all radicals trapped in solution studies from target R-OOH

Spin-traps	Limo-OOH	Cum-OOH	Lina-OOHs
DEPMPO	•OH, •carbon R	•OH, •carbon R, CH_3O•, CumOO•	•OH, •carbon R, CH_3O•, LinaOO•
DMPO	•OH	•OH, CH_3•, CH_3O•	•carbon R
PBN	•carbon R, •CH_2CN	•carbon R, CumO•	•carbon R, LinaO•

Such studies revealed that several reactive radical intermediates issued from the ROOHs are possible depending on their chemical structure, suggesting that specific immunogenic protein chemical modifications could lead to sensitization. However, such studies were carried out in solution (aqueous buffer or semi-organic), far from mimicking what may actually happen in real-life scenario, *i.e.* in the skin.

3 IDENTIFICATION OF RADICALS DERIVED FROM ROOHS: *IN SITU* APPROACH IN RHE

The objective of the present work was to develop an EPR spin-trapping methodology with the potential to investigate the formation and behavior of radicals issued from ROOHs in a reconstructed human epidermis 3D model (RHE). RHE Episkin™ (Lyon, France) is an *in vitro* reconstructed human epidermis from normal cultured keratinocytes (13-days stratification) on the collagen matrix at the air-liquid interface.[46] Keratinocytes are the major cell type in the epidermis and play a key role in skin inflammatory reactions.

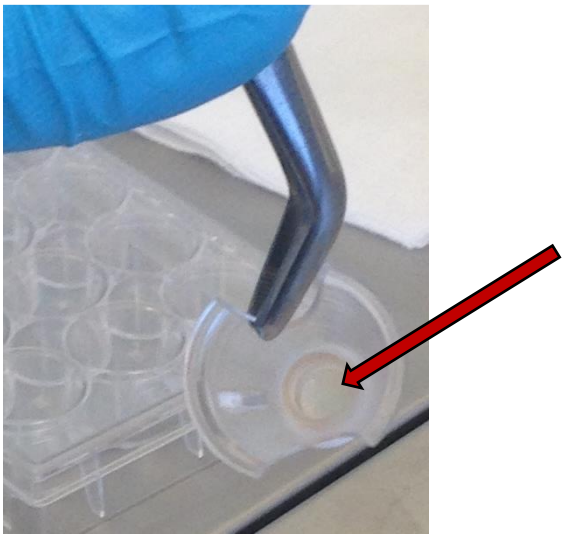

Figure 2.23: Episkin™ model RHE

RHE Episkin™ (0.38 cm^2) were stored at arrival in 2 mL provided maintenance medium at 37°C, 5% CO_2 saturated in humidity atmosphere.

DEPMPO was chosen as spin-trap based on the results of the studies in solution where an extensive view of all sort of radicals were observed all at once with catalytic Fe(II) concentration. EPR technical adjustments needed initially to be established to obtain EPR fingerprints with reasonable signal to noise ratio (S/N). The use of aqueous solution (complicating EPR measurement due to its high dielectric constant), keeping the cell viability of the RHE in the flat cell during experiment and the use of important concentration of both R-OOH and DEPMPO were some of the major challenges to overcome. Several procedures were thus tested to develop the optimum and most efficient EPR spin-trapping methodology. The optimized procedure finally applied for RHE/EPR studies is described Figure 2.24.

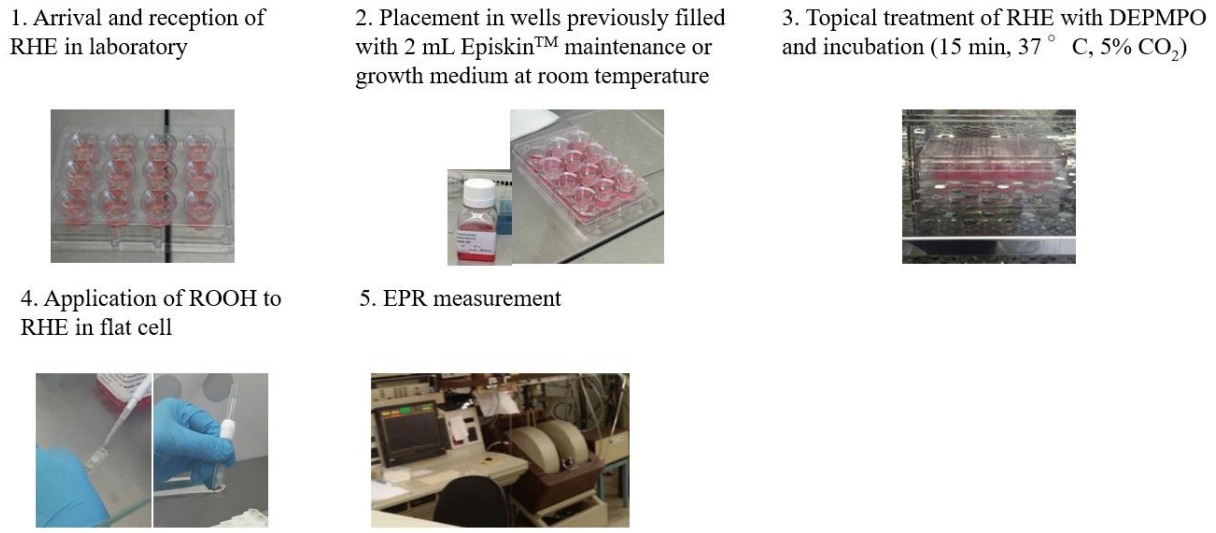

Figure 2.24: Experimental methodology *by topical application* developed for RHE EPR studies

The rational process followed to develop this methodology is described in the following sections.

3.1 Cum-OOH as proof of concept

Cum-OOH was initially used as proof of concept. It is often used in EPR studies as a reference compound.[36–38] Moreover, CumOOH has been reported as a significant sensitizer in guinea-pigs, and positive specific responses have been reported in allergy cross-reactivity studies with allergenic cyclohexene hydroperoxides.[47]

3.1.1 Incubation in the assay medium - application from the bottom

Preliminary attempts were conducted by incubating Cum-OOH (0.54 mM) and DEPMPO (25 mM) in a mixture HEPES/assay medium (AM) (4:1 v/v). AM was provided by Episkin™, dedicated as its name suggested it for the experiment with the RHE. As for CM, no information regarding the component of the medium was given, except that AM is significantly depleted than compared to CM. Evidently, no Fe(II) was used for *in situ* approaches with RHE. The aim was to avoid the epidermis barrier function and check at a first sight using absorption from the bottom of RHE if Cum-OOH-mediated radicals could be formed within the epidermis. Even though Episkin™ RHE barrier function has been described to be less developed than that of normal skin (different lipids composition and organization), it may not be neglected.[48] For control purposes, a sample from assay medium was regularly taken (20 µL) during incubation

(37°C, 5% CO_2, 1 min to 2 h), inserted into a capillary, sealed and measured by EPR at room temperature. No EPR signal was observed at any time of incubation. After 2 h incubation, the RHE was placed in a EPR tissue cell (Wilmad) equipped with a silica window and EPR spectra were recorded. Although being noisy, a signal was then observed increasing with time (Figure 2.25 C-E). Major peaks assigned to a carbon-centered radical DEPMPO adduct (spin-adduct **6**) based on the set of *hfcc*s a_N=15.4 G, a_H=22.5 G, a_P=48.3 G (Figure 2.25 F), the minor peaks assigned to oxygen centered radicals whose the *hfcc*s were hardly definable in a precise manner (Figure 2.25 F) and comparable with our data in solution (Annex A6).

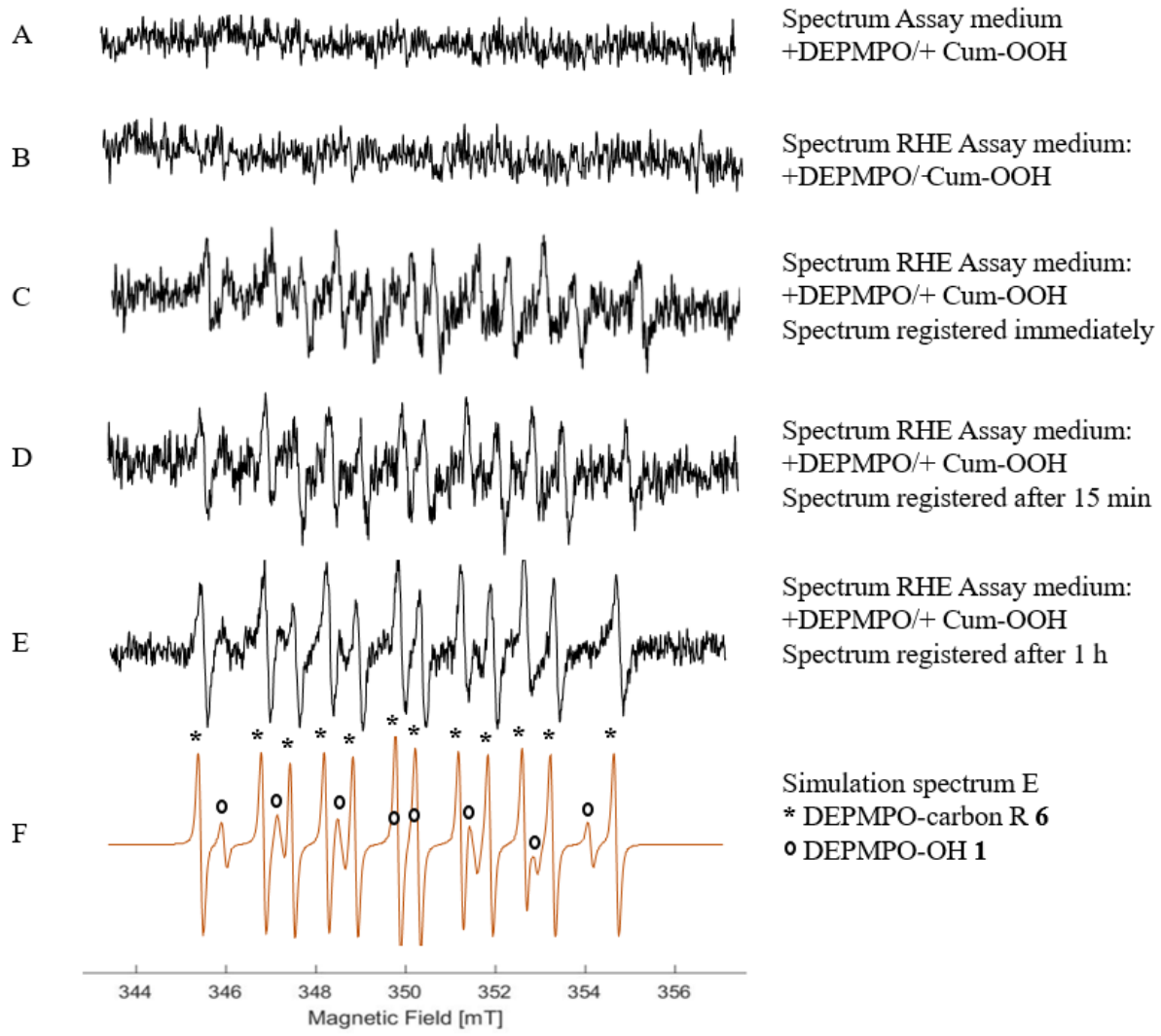

Figure 2.25: Preliminary trials incubating CumOOH (0.54 mM) and DEPMPO (25mM in HEPES) in the assay medium: (A) sample from the assay medium after 2 h incubation with DEPMPO and CumOOH; (B) spectrum of RHE when the assay medium is incubated 2 h with

single DEPMPO; (C) spectrum of RHE when the assay medium is incubated with DEPMPO and CumOOH, registered immediately; (D) registered after 15 min; (E) registered after 1 h; (F) computer simulation of spectrum with labels identifying each radical formed (**6**-like DEPMPO-carbon R and **1** DEPMPO-OH).

After penetrating the RHE, CumOOH radical initiation was certainly induced by RHE itself as no Fe(II) was included this time. This certainly better mimics real-life skin allergy situation. One can hypothesize that reaction of organic peroxides in the skin in the presence of one-electron donor agents (*i.e.* amino and thiol groups containing amino acids, metals, enzymes) may start electron transfer processes and thus skin proteins haptenation.[49,50]

Control experiments without CumOOH were performed (Figure 2.25 A and B), *i.e.* after only DEPMPO incubation in the RHE and showed no EPR signal, corroborating that most probably this spin-adduct arose from trapping a carbon-centred radical issued from the hydroperoxide.

In the recent OECD guideline on *in vitro* skin irritation assessment by using this RHE system it is specified that test chemicals must be applied topically to the RHE model.[51] In consequence, with the acquired knowledge that CumOOH radicals can be formed in RHE as described above, and in order to get closer to real life situation, further experiments were based on a topical application procedure.

3.1.2 Incubation by topical application to the RHE.

At the beginning, RHE were treated with Cum-OOH in acetone (1 mM, 20 µL) topically and incubated for different time periods (37°C, 5% CO_2, 1 minute to 24 hours). RHE negative controls were treated only with acetone (20 µL). After the incubation time, the RHE were placed in the EPR tissue cell, DEPMPO (50 mM in 10 mM HEPES, 20 µL) was applied to the epidermis taking care to ensure that the spin-trap was only applied to the epidermis top. EPR spectra were recorded immediately afterwards. After 5 min of incubation, the fingerprint of a carbon-centered radical DEPMPO adduct was detected as previously observed during incubation protocol (spin-adduct **6**), with hfccs a_N=15.4 G, a_H=22.7 G, a_P=48.1 G, and yet with a better signal-to-noise ratio (Figure 2. 26 B; Table 2.4).

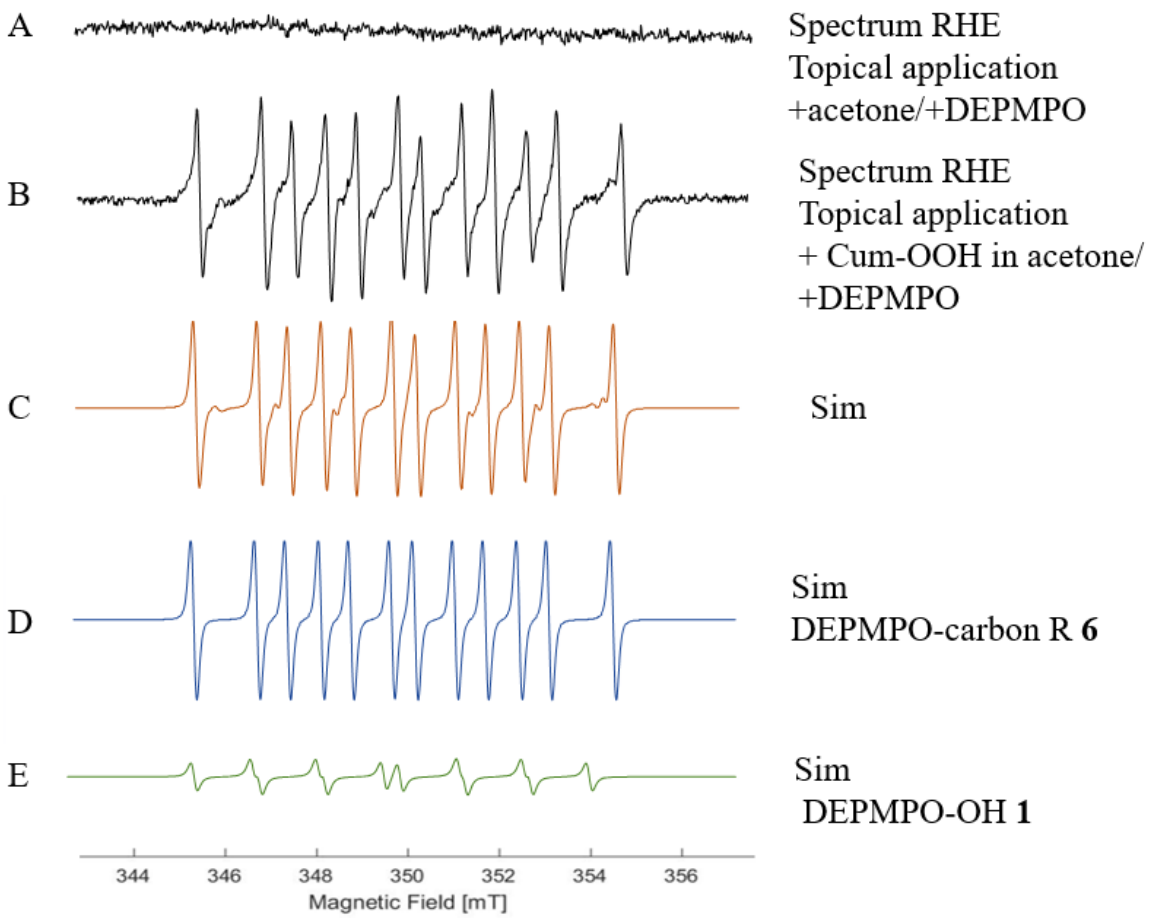

Figure 2.26: EPR spectra obtained in RHE topical application experiments by using Cum-OOH (1 mM in acetone) and DEPMPO (50mM in HEPES): (A) RHE control experiment with single DEPMPO and vehicle; (B) RHE spectra after CumOOH application and incubation (5 min, 37 °C, 5% CO_2) followed by DEPMPO addition; (C) computer simulation of spectrum (B); (D–E) deconvolution of **6** and **1**.

Negative controls (incubation of the sole acetone, followed by DEPMPO addition) gave no signal, indicating that the carbon radical arose from CumOOH and not by induction of radical formation on a RHE biomolecule (Figure 2.26 A). Best computer simulation obtained from Figure 2.26 B is shown in Figure 2.26 C where spin-adduct **6** seemed to be predominant. Higher incubation times resulted in a weaker signal-to-noise ratio pointing to carbon radicals formed in the epidermis shortly after hydroperoxide topical application. Characterized spin-adducts are resumed in Table 2.4, it appeared clearly that a carbon centered radical was obtained in majority in both approaches and most probably a methyl radical.

Table 2.4 Spin-adducts formed from CumOOH/DEPMPO system in RHE.[26,34,52]

Incubation in assay medium assignment, *g*, *hfccs* (Gauss)		Topical application assignment, *g*, *hfccs* (Gauss)	
DEPMPO-OH **1**	DEPMPO-carbon R **6**	DEPMPO-OH **1**	DEPMPO-carbon R **6**
g=2.0055 a_N=14.6 a_H=13.2 a_P=46.2	g=2.0050 a_N=15.4 a_H=22.6 a_P=48.1	g=2.0050 a_N=15.0 a_H=13.4 a_P=44.8	g=2.0052 a_N=15.4 a_H=22.7 a_P=48.0

However, despite these very encouraging results, all the numerous attempts using the above described approach with Limo-OOH and Lina-OOHs were vain. Therefore, we decided to invert the order of application of the spin-trap and hydroperoxyde and increase their respective concentrations. Spin trap was topically applied and pre-incubated for a period of time then hydroperoxide was topically added.

3.2 LinaOOHs experiments

CM of the RHE was replaced by 10 mM HEPES. The RHE were firstly treated with 20µL of 250 mM DEPMPO in 10 mM HEPES, applied topically and incubated for different time periods (37°C, 5% CO_2, during 7.5, 15 and 30 minutes).[53] After incubation, RHE were placed in the EPR tissue cell, Lina-OOHs in acetone (10 mM, 20 µL) was then topically applied ensuring that the solution was only applied to the epidermis top. EPR spectra were then recorded. If a noisy but detectable spectrum was observed after 7.5 minutes, the best S/N was achieved after 15 minutes of DEPMPO incubation. At 30 minutes a significative decay of the spin-adduct was observed. The observed EPR spectrum correspond to the spin-adduct ascribed to a carbon-centered radical (spin-adduct **14**) and hydroxyl radical (spin-adduct **1**), with the very similar *hfccs* than in solution investigations (Figure 2.27).

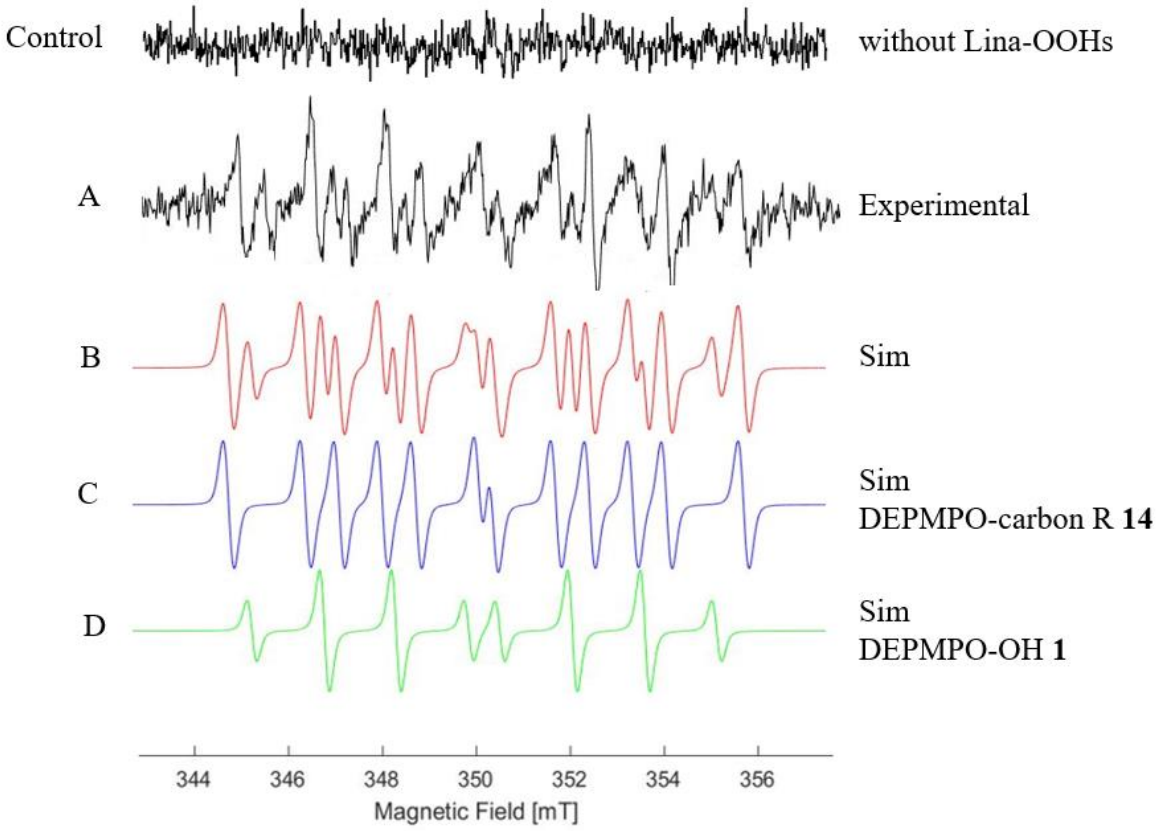

Figure 2.27: EPR spectra obtained in RHE topical application experiments by using Lina-OOH (10 mM in acetone) and DEPMPO (250mM in HEPES): (A) EPR spectrum spin-adducts formed, (B) computer simulation and (C and D) deconvolution of DEPMPO-OH **1** and DEPMPO-carbon R **14**

Negative controls (sole incubation of DEPMPO) remain free of EPR signals, indicating that carbon radicals were most probably formed from Lina-OOHs and not by induction of radical formation on a RHE biomolecule. Best computer simulation obtained from Figure 2.27 A is shown in Figure 2.27 B, where spin-adduct **14** seems to be predominant with *hfccs* a_N = 14.5 G, a_H = 22.9 G and a_P = 47.5 G. Characterized spin-adducts are resumed in Table 2.5. It appeared that a carbon centered radical was predominantly obtained.

Table 2.5. Spin-adducts formed from Lina-OOHs/DEPMPO system in RHE.[26,34,52]

Spin-adducts topical application assignment, *g*, *hfccs* (Gauss)	
DEPMPO-OH **1**	DEPMPO-carbon R **14**
g=2.0052	g=2.0050
a_N=13.9	a_N=14.9
a_H=14.0	a_H=21.5
a_P=47.5	a_P=48.2

3.3 Limo-OOH investigations

An identical protocol as the one used for Lina-OOHs was applied to Limo-OOH. The best results were obtained after 30 minutes of DEPMPO incubation (Figure 2.28). However, the EPR spectrum corresponding to a carbon-centered spin-adduct **2** was observed, with *hfccs* of a_N = 14.6, a_H = 22.2 G and a_P = 47.2 G. i.e. very much comparable with solution studies.

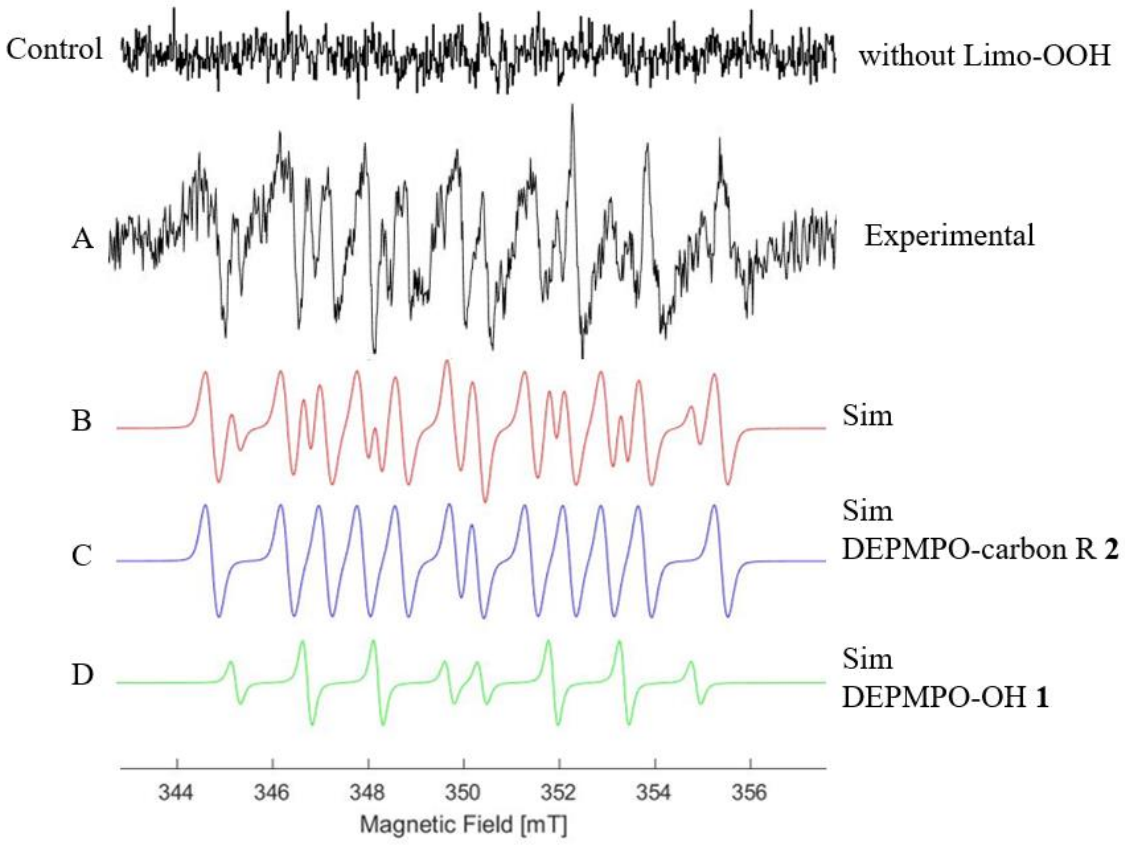

Figure 2.28: EPR spectra obtained in RHE topical application experiments by using Limo-OOH (10 mM in acetone) and DEPMPO (250mM in HEPES): (A) EPR spectrum spin-adducts

formed, (B) computer simulation and (C and D) deconvolution of DEPMPO-OH **1**, DEPMPO-carbon R **2**

Negative controls (sole incubation of DEPMPO) remained free of EPR signals, indicating that carbon radicals were the most probably formed from Limo-OOH and not by induction of radical formation on a RHE biomolecule (Figure 2.28). Best computer simulation obtained from Figure 2.28 A is shown in Figure 2.28 B, where spin-adduct **2** seemed to be predominant. Spin-adducts characterized are resumed in Table 2.6.

Table 2.6. Spin-adducts formed from Limo-OOH/DEPMPO system in RHE.[26,34,52]

Spin-adducts topical application assignment, *g*, *hfccs* (Gauss)	
DEPMPO-OH **1**	DEPMPO-carbon R **2**
g=2.0055	g=2.0053
a_N=13.8	a_N=14.7
a_H=14.4	a_H=22.1
a_P=44.6	a_P=47.2

3.4 Conclusion

EPR spin-trapping allowed us for the first time to study the formation of carbon radicals issued from organic hydroperoxides in a 3D epidermis model. This will open perspectives and new insights for the molecular understanding of skin sensitization processes to autoxidized natural fragrance terpenes.

Cum-OOH produced a better signal to noise ratio when compared to Limo-OOH and Lina-OOHs, having they probably different reactivities in the RHE environment. It was necessary to increase the concentration of those hydroperoxides and of the spin-trap to see a well resolved signal to noise ratio.

Concerning the initiation of the radical generation the question of who gave the first electron is still open. It could be residual iron of the RHE or amino acids themselves. For this purpose, a system Lina-OOHs/*N*-acetyl-L-cysteine methyl ester/DEPMPO, was tested in solution. This system produced spin-adducts as defined in Figure 2.29. Therefore, it seems that this amino acid can induced radical generation.

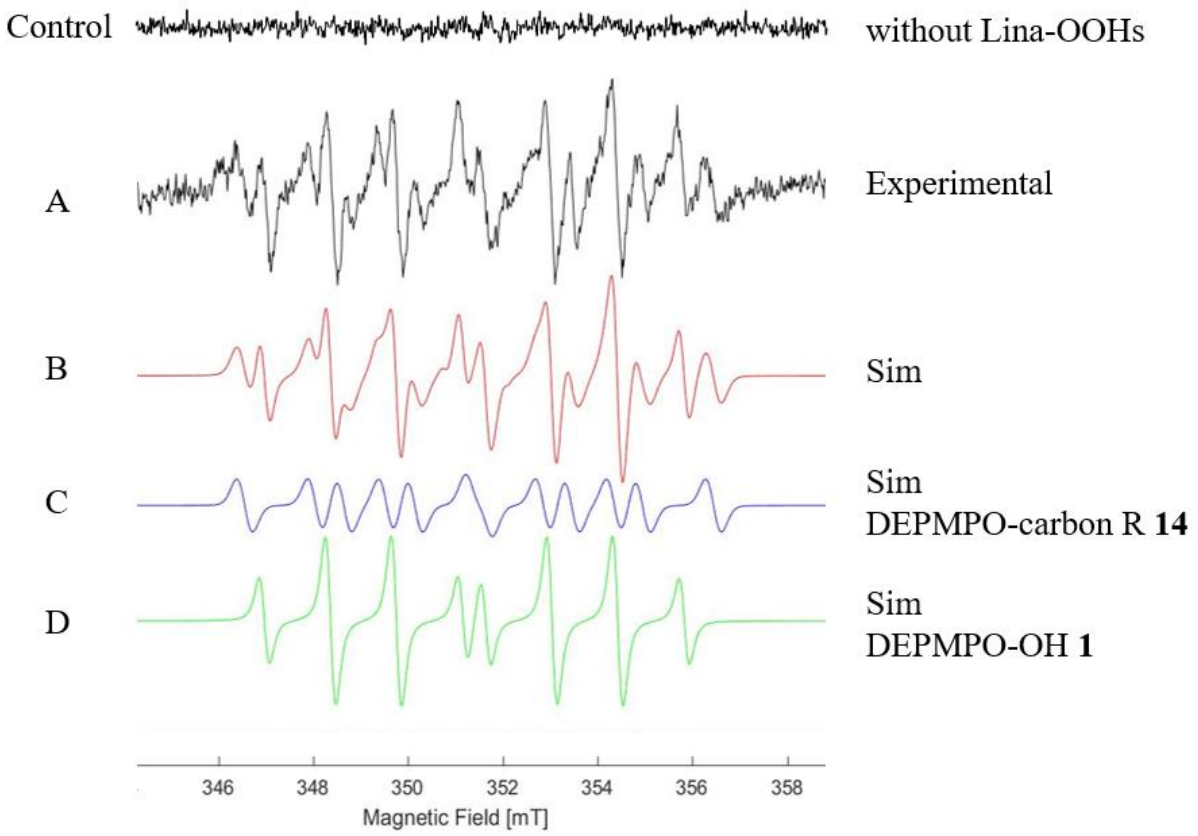

Figure 2.29: EPR spectra obtained in solution experiments: (A) EPR spectrum of DEPMPO (50 mM) spin-adducts formed from Lina-OOHs (1 mM)/*N*-acetyl-L-cysteine methyl ester (10 mM) in HEPES, (B) computer simulation and (C and D) deconvolution of DEPMPO-OH **1**, DEPMPO-carbon R **14**

In all cases, oxygen-centered spin-adducts were detected and attributed to hydroxyl radical generation. Even if it could be hypothesized, due to the control experiments, that radicals were directly issued from the ROOHs, it is necessary still to prove if the ROOHs themselves could indirectly generate radical oxygen species (ROS) in the cellular matrices that could eventually also be trapped.

4 MATERIALS AND METHODS

4.1 Studies in solution

4.1.1 Chemicals and reagents

Cumene hydroperoxide (Cum-OOH) and spin-traps α-phenyl-*N*-*tert*-butyl nitrone (PBN) (98%) and 5,5-dimethyl-1-pyrroline *N*-oxide (DMPO) were purchased from Sigma-Aldrich (Saint-Quentin Fallavier, France) and used as received. 5-Diethoxy-phosphoryl-5-methyl-1-pyrroline *N*-oxide (DEPMPO) was synthesized as reported in the literature.[54] HEPES (≥ 99.5 %), ferrous sulfate heptahydrate $FeSO_4.7H_2O$ and acetonitrile CH_3CN (99.8%) were acquired from Sigma-Aldrich (Saint-Quentin Fallavier, France), and sodium phosphates monobasic NaH_2PO_4 and dibasic Na_2HPO_4 from Merck KGaA (Darmstadt, Germany). Aqueous solutions were prepared with deionized water.

4.1.2 Buffer Solutions

Phosphate buffer solution PB (10 mM, pH 7.4) was prepared by adding 202.5 mL Na_2HPO_4 (20 mM) and 19 mL NaH_2PO_4 (20 mM) then complete were deionized water up to 500 mL.

To prepare HEPES buffer solution (10 mM, pH 6.8), 1.19 g HEPES was dissolved in 400 mL deionized water, 4 g NaCl and 0.1 g KCl were added. To attain pH 6.8, NaOH pellets were added. If the pH went too high, it was lowered back by carefully adding HCl until the pH remained stable to 6.8. Finally, deionized water was added to a final volume of 500 mL.

4.1.3 EPR equipment

EPR spectra were recorded on an EPR X-band spectrometer (EMXplus, Bruker Biospin GmbH, Germany), equipped with a high sensitivity resonator (hsw0821, Bruker Biospin GmbH, Germany). The *g* calibration standard was a strong pitch of known *g* factor 2.0028. The spectrometer was operated at 9.87 GHz and spectrometer settings were 100 kHz modulation frequency, microwave power 7 mW, sweep width 70-120 G, sweep time 120.04 s, modulation amplitude 0.5 G and time constant 81.92 s. Spectra were recorded at room temperature (295K±1K) as soon as possible after mixing the reagents and introducing the reaction mixture into an EPR quartz capillary tube (25 µL) with an internal diameter of 0.75 mm (Wimmad, Buena, NJ, USA). An EPR spectrum of the reaction mixture was registered directly by placing the quartz capillary tube in the spectrometer cavity. EPR spectra were treated and hyperfine splitting assignments obtained by means of computer simulation using the Easyspin launched

in Matlab software (version 2015b) (http://www.easyspin.org). Hyperfine coupling constants were in agreement with those reported in the literature.

4.1.4 General procedure in solution

Stock solutions were prepared for CumOOH (5.4 mM, PBS or HEPES/CH_3CN 9/1), the spin-traps (100 mM in PBS or HEPES) and $FeSO_4.7H_2O$ (10 mM in deionized water). 12.5 µL of spin-trap solution were mixed with $FeSO_4.7H_2O$ (*i.e.* 0.5 µL for a final concentration in the reaction mixture of 0.1 mM), 5 µL CumOOH solution added and final volume completed to 50 µL. This way, final concentrations in the reaction mixture were 25 mM spin-trap and 0.54 mM CumOOH. The reaction mixture was subjected to stirring, further introduced into the EPR quartz capillary tube, sealed on both ends, and EPR spectra registered.

4.2 Reconstructed human epidermis studies

4.2.1 Chemicals and reagents

Episkin™ (Lyon, France) is an *in vitro* reconstructed human epidermis (RHE) from normal human keratinocytes cultured for 13 days on a collagen matrix at the air-liquid interface. It is a 3D epidermis model histologically similar to human epidermis. The small 0.38 cm^2 format was chosen for the studies. Immediately after arrival in the laboratory, the 3D reconstructed epidermis was removed from the agarose-nutrient solution in the shipping multiwell plate under a sterile airflow. Then, they were immediately placed on a plate in which each well was previously filled with 2 mL Episkin™ maintenance or growth medium at room temperature. It was necessary to act quickly as the tissue cultures dry out rapidly when not in contact with the medium. Samples were placed in the incubator at 37 °C, 5% CO_2 and saturated humidity at least 24 hours before incubation. Episkin ™ (Lyon, France) furnished the assay medium used for the incubations.

4.2.2 EPR equipment

EPR spectra were recorded on an EPR X-band spectrometer (ESP300E, Bruker Biospin GmbH, Germany), equipped with a high sensitivity resonator (8950opt300, Bruker Biospin GmbH, Germany). The *g* calibration standard was a strong pitch of known *g* factor 2.0028. The spectrometer was operated at 9.8 GHz and spectrometer settings were 100 kHz modulation frequency, microwave power 5.1 mW, sweep width 160 G, sweep time 327.7 s, modulation amplitude 1 G and time constant 163.8 s. Spectra were recorded at room temperature (295°K ±

1°K) as soon as possible after incubating the reagents. Treated RHE were placed in an EPR tissue cell equipped with a silica window (Bruker Biospin GmbH #ER162TC-Q) and EPR spectra recorded. EPR spectra were treated and hyperfine splitting assignments obtained by means of computer simulation using Easyspin launched in Matlab software (version 2015b) (http://www.easyspin.org).

4.2.3 General procedure in RHE

Incubation in the assay medium

CumOOH (200 µL of 5.4 mM HEPES/CH_3CN 9/1 stock solution) and DEPMPO (100 µL of 500 mM stock solution in HEPES) were introduced in a mixture of 300 µL assay medium and 1400 µL of HEPES buffer. The RHE model was then placed in a well containing this mixture. After 2 hours incubation, RHE was placed in the EPR tissue cell and EPR spectra recorded.

Incubation by topical application to the RHE

RHE were topically treated with DEPMPO in HEPES (250 mM, 20 µL) and post-incubated (37 °C, 5% CO_2) different time periods (7 to 30 minutes). After the incubation time, the RHE were placed in the EPR tissue cell and ROOH (1 to 10 mM in HEPES buffer, 20 µL) was applied to the epidermis taking care to ensure that the solution was only applied to it. EPR spectra were then recorded.

4.3 Synthesis

4.3.1 Synthesis DEPMPO[52]

Diethyl-(2-methyl-2-pyrrolidinyl)phosphonate synthesis

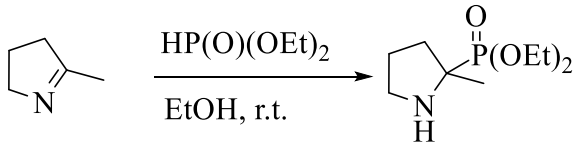

In a round bottom flask under argon, diethyl phosphite (98%; 32.4 mL; 246 mmol; 1.2 equiv.) was slowly added to a solution of 2-methylpyrroline (95%; 20.0 mL; 201 mmol) in ethanol (60 mL). The mixture was stirred for 7 days at room temperature. Then the solvent was evaporated under reduced pressure to obtain a brown oil. A solution of hydrochloric acid (10 %; 200 mL)

was then added. The solution was washed with dichloromethane (3 × 80 mL). The aqueous phase was basified with a saturated solution of sodium carbonate up to pH 9. Then the product was extracted with chloroform (3 × 100 mL). Organic phases were dried over magnesium sulfate, filtered and concentrated under reduced pressure to obtain diethyl-(2-methyl-2-pyrrolidinyl)phosphonate as a brown oil (30,2 g ; 136 mmoles ; 67 %).

Formula: $C_9H_{20}NO_3P$

Molar mass: 221.23 $g.mol^{-1}$

CAS: 157230-68-7

CCM: Rf = 0.60 (dichloromethane/ethanol 9/1): PMA

NMR ^{1}H ($CDCl_3$, δ, ppm): 1,10 (td, 6H, 2 × $OCH_2C\mathbf{H_3}$, $^3J_{HH}$ = 7.1 Hz, $^3J_{PH}$ = 2.4 Hz); 1,29 (d, 3H, $CC\mathbf{H_3}$, $^3J_{PH}$ = 15.2 Hz); 1,34-1,76 (m, 4H, $CC\mathbf{H_2}C\mathbf{H_2}$); 2.21-2.39 (m, 1H, N**H**); 2,71-2,79 (m, 1H, $NHC\mathbf{H_2}$); 2,86-2,95 (m, 1H, $NHC\mathbf{H_2}$); 3,98-4,16 (m, 4H, 2 × $OC\mathbf{H_2}CH_3$)

NMR ^{13}C ($CDCl_3$, δ, ppm):16,9 (d, 2 × $OCH_2\mathbf{C}H_3$, $^3J_{PC}$ = 5.6 Hz); 24,4 (d, $C\mathbf{C}H_3$, $^2J_{PC}$ = 6.2 Hz); 26,3 (d, $CCH_2\mathbf{C}H_2$, $^3J_{PC}$ = 4,3 Hz); 35,3 (d, $C\mathbf{C}H_2CH_2$, $^2J_{PC}$ = 2.5 Hz); 47,5 (d, $NH\mathbf{C}H_2$, $^3J_{PC}$ = 7.4 Hz); 59,9 (d, $\mathbf{C}CH_3$, $^1J_{PC}$ = 166.5 Hz); 62,0 (d, $O\mathbf{C}H_2CH_3$, $^2J_{PC}$ = 4.4 Hz); 62,3 (d, $O\mathbf{C}H_2CH_3$, $^2J_{PC}$ = 4,3 Hz)

5-Diethoxyphosphoryl-5-methyl-1-pyrroline-*N*-oxide DEPMPO

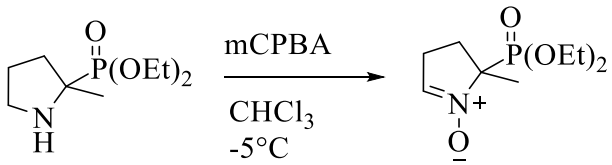

In a round bottom flask under argon, diethyl-(2-methyl-2-pyrrolidinyl)phosphonate (15.0 g; 67.8 moles) was dissolved in chloroform (150 mL). The temperature of the solution was maintained under -5°C. A suspension of 3-chloroperbenzoic acid (77%; 31.0 g; 135 moles; 2 equiv.), in chloroform (250 mL) was slowly added. The color passed from green to white. A saturated solution of sodium carbonate (130 mL) was added and the solution was vigorously

stirred for 15 minutes, then a clear green color appeared. Organic phases were washed with a sodium chloride saturated solution (150 mL), dried over magnesium sulfate, filtered and the solvent removed under reduced pressure. The crude product was purified by silica gel chromatography (dichloromethane/ethanol 9/1) and DEPMPO was obtained as a yellow oil (4.8 g; 20.4 moles; 29 %).

Formula: $C_9H_{18}NO_4P$

Molar mass: 235.22 $g.mol^{-1}$

CAS: 157230-67-6

CCM: Rf = 0.30 (dichloromethane/ethanol 9/1) : PMA

NMR ^{1}H ($CDCl_3$, δ, ppm): 1,02 (t, 3H, $OCH_2C\mathbf{H_3}$, $^3J_{HH}$ = 7.0 Hz); 1,14 (t, 3H, $OCH_2C\mathbf{H_3}$, $^3J_{HH}$ = 7.0 Hz); 1,33-1,52 (m, 1H, $CC\mathbf{H_2}CH_2$); 1,59 (d, 3H, $CC\mathbf{H_3}$, $^3J_{PH}$ = 14.6 Hz); 1,59-1,68 (m, 1H, $CC\mathbf{H_2}CH_2$); 2,21-2,37 (m, 1H, $CCH_2C\mathbf{H_2}$); 2,49-2,63 (m, 1H, $CCH_2C\mathbf{H_2}$); 3,83-4,02 (m, 2H, $OC\mathbf{H_2}CH_3$); 4,24-4,38 (m, 1H, $OC\mathbf{H_2}CH_3$); 4,41-4,55 (m, 1H, $OC\mathbf{H_2}CH_3$); 6,34 (q, 1H, NOC**H**, $^3J_{HH}$ = 2.9 Hz, $^4J_{PH}$ = 2.9 Hz)

NMR ^{13}C ($CDCl_3$, δ, ppm): 16,3 (d, $OCH_2\mathbf{C}H_3$, $^3J_{PC}$ = 6.2 Hz); 16,4 (d, $OCH_2\mathbf{C}H_3$, $^3J_{PC}$ = 6.2 Hz); 21,1 (s, $C\mathbf{C}H_3$); 25,4 (s, $CCH_2\mathbf{C}H_2$); 31,1 (s, $C\mathbf{C}H_2CH_2$); 61,7 (d, $O\mathbf{C}H_2CH_3$, $^2J_{PC}$ = 7.5 Hz); 64,2 (d, $O\mathbf{C}H_2CH_3$, $^2J_{PC}$ = 5.6 Hz); 75,2 (d, $\mathbf{C}CH_3$, $^1J_{PC}$ = 154.1 Hz); 132,1 (s, NO**C**H)

4.3.2 Synthesis of Limonene-2-hydroperoxide Limo-OOH

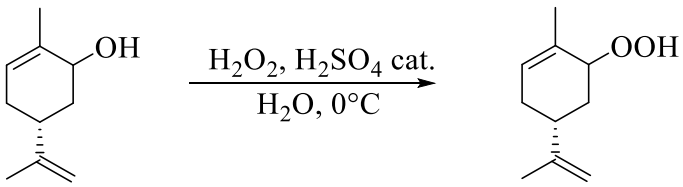

To an aqueous solution of hydrogen peroxide (50%; 85 mL) were added at 0°C some drops of sulfuric acid and (-)-carveol (97%; 6.0 g; 38.2 mmol). The mixture at 0°C was stirred for 2 days then extracted with pentane (5 × 200 mL). Organic phases assembled were dried over magnesium sulfate, filtered, and evaporated under reduced pressure. Limo-OOH was obtained

using neutralized silica gel chromatography (pentane/diethyl ether 8/2) as a clear oil (2.7 g; 16.0 mmol; 42 %).

Formula: $C_{10}H_{16}O_2$

Molar mass: 168.23 $g.mol^{-1}$

CAS: 1045725-54-9

CCM: Rf = 0.21 (petroleum ether/ethyl acetate 95:5): Anisaldehyde.

NMR ^{1}H (500 MHz; $CDCl_3$):

Compound (mixture of two diastereoisomers) : 1,42-1,51 (m, 2 × 1H, 2 × C**H**$_2$(CH)OOH); 1,75 and 1,76 (s, 2 × 3H, 2 × C**H**$_3$C(CH_2)); 1,76 and 1,81 (s, 2 × 3H, 2 × C**H**$_3$(C)CH(OOH)); 2,14-2,40 (m, 2 × 4H, 2 × (C**H**$_2$(CH)C(CH_2), C**H**C(CH_2) and C**H**$_2$(CH)OOH)); 4.37 (s, 1H, C**H**(OOH)); 4,55 (m, 1H, C**H**(OOH)); 4,76 (s, 2 × 2H, 2 × C**H**$_2$C(CH_3)); 5,76 (d, 1H, C**H**(C)CH(OOH), $^{3}J_{HH}$ = 5.0 Hz); 5,65 (m, 1H, C**H**(C)CH(OOH)); 7,99 and 7,65 (s, 2 × 1H, 2 × OO**H**)

NMR ^{13}C (75 MHz; $CDCl_3$):

Compound (mixture of two diastereoisomers) : 19,4 and 21,5 (2 × **C**H$_3$(C)CH(OOH)); 20,6 and 21,1 (2 × **C**H$_3$C(CH_2)); 31,1 and 31,4 (2 × **C**H$_2$(CH)C(CH_2) or 2 × **C**H$_2$(CH)OOH); 32,8 (2 × **C**H$_2$(CH)C(CH_2) or 2 × **C**H$_2$(CH)OOH); 35,4 and 40,8 (2 × **C**HC(CH_2)); 82,8 and 84,5 (2 × **C**H(OOH)); 109,3 and 109,4 (2 × **C**H$_2$C(CH_3)); 127,3 and 129,9 (2 x **C**H(C)CH(OOH); 129,6 and 132,8 (2 × **C**(CH)OOH); 148,8 and 149,3 (2 × **C**(CH_2))

4.3.3 Synthesis of (5E)-7-Hydroperoxy-3,7-dimethylocta-1,5-dien-3-ol and 5-(^{13}C)-6-hydroperoxy-3,7-dimethylocta-1,7-dien-3-ol (Lina-OOHs)

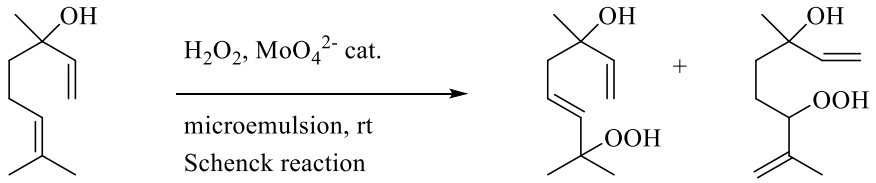

A microemulsion was prepared by slowly adding a sodium molybdate solution (3.38 g in 18 mL distilled water) to a suspension of sodium dodecyl sulfate (27.9 g) in butanol (34 mL) and dichloromethane (166 mL). At the end of the addition, the microemulsion became clear after 5 minutes stirring.

Linalool (2.83 g; 17.8 mmol; 1 eq.) was introduced in the microemulsion at room temperature. Hydrogen peroxide (aqueous solution 35%; 1 mL one fraction) was then added. The solution was instantly red colored. After 20 minutes stirring the solution became yellow. Fourteen other fractions of hydrogen peroxide (aqueous solution 35%; 1 mL each) were added successively by an interval of 10 minutes each. The resulting yellow solution was stirred overnight at room temperature. When the reaction was thoroughly translucent, linalool was completely oxidized. The solvent was removed under reduced pressure at 40 °C. The semi-solid white product obtained was suspended in dichloromethane (900 mL) and vigorously stirred for 48 hours. The suspension was filtered to recover sodium molybdate and sodium dodecyl sulfate. The filtrate, partially evaporated under reduced pressure, was washed using distilled water (3 × 100 mL) and the aqueous phase was extracted with dichloromethane (100 mL). Combined organic phases were dried over magnesium sulfate, filtered and concentrated under reduced pressure to give a crude yellow oil. A mixture of hydroperoxides Lina-OOHs (ratio 2/3) was obtained using silica gel column chromatography (petroleum ether/AcOEt 4/1, then 3/2) as a yellow oil (2.97 g; 15.97 mmol; 90%).

Formula: $C_{10}H_{18}O_3$

Molar mass: 186.25 $g.mol^{-1}$

CAS: Isomer Lina-7-OOH: 51276-32-5 – Isomer Lina-6-OOH: 51276-31-4

TLC = 0.24 (petroleum ether/AcOEt 7/3): APM/Ce

NMR ^{1}H ($CDCl_3$, δ, ppm)

Isomer Lina-7-OOH (mixture of two enantiomers): 1.28 (s, 3H, C**H**$_3$C(OH)), 1.32 (s, 6H, (C**H**$_3$)$_2$C(OOH)), 2.29 (m, 2H, C**H**$_2$C(OH)), 5.06 (dd, 1H, C**H**$_2$(CH)C(OH), $^3J_{HH}$ = 1.1 Hz, $^2J_{HH}$ = 10.8 Hz), 5.22 (dd, 1H, C**H**$_2$(CH)C(OH), $^3J_{HH}$ = 1.1 Hz, $^2J_{HH}$ = 17.4 Hz), 5.50-5.65 (m, 2H, C**H**C**H**), 5.93 (dd, 1H, $^3J_{HH}$ = 10.7 Hz, $^2J_{HH}$ = 17.3 Hz, C**H**C(OH)).

Isomer Lina-6-OOH (mixture of four diastereoisomers) : 1.29 (s, 6H, 2 × C**H**$_3$C(OH)), 1.51-1.67 (m, 4H, 2 × C**H**$_2$CH$_2$), 1.74 (s, 6H, 2 × C**H**$_3$(C)CH(OOH)), 4.29 (m, 2H, 2 × C**H**(OOH)), 5.01 (m, 4H, 2 × C**H**$_2$(C)CH(OOH)), 5.08 (dd, 2H, 2 × C**H**$_2$(CH)C(OH), $^3J_{HH}$ = 1.1 Hz, $^2J_{HH}$ =

10.8 Hz), 5.18 (dd, 1H, C**H**$_2$(CH)C(OH), $^3J_{HH}$ = 1.1 Hz, $^2J_{HH}$ = 17.4 Hz), 5.21 (dd, 1H, C**H**$_2$(CH)C(OH), $^3J_{HH}$ =1.6 Hz, $^3J_{HH}$ = 17.4 Hz), 5.87 (dd, 1H, C**H**C(OH), $^3J_{HH}$ = 10.8 Hz, $^2J_{HH}$ = 17.4 Hz), 5.88 (dd, 1H, C**H**C(OH), $^3J_{HH}$ =10.8 Hz, $^2J_{HH}$ = 17.4 Hz).

NMR ^{13}C (CDCl$_3$, *δ*, ppm):

Isomer Lina-7-OOH (mixture of two enantiomers): 24.5 (2 × (**C**H$_3$)$_2$C(OOH)), 27.9 (**C**H$_3$C(OH)), 45.2 (**C**H$_2$C(OH), 72.9 (**C**(OH)), 82.2 (**C**(OOH)), 112.3 (**C**H$_2$(CH)C(OH)), 126.7 (CH$_2$(^{13}**C**H)CH), 138.0 (**C**HC(OOH)), 144.8 (**C**HC(OH))

Isomer Lina-6-OOH (mixture of four diastereoisomers) : 17.2 (2 × **C**H$_3$(C)CH(OOH)), 25.2 (2 × **C**H$_2$(CH)OOH), 28.2 and 28.4 (2 × **C**H$_3$C(OH)), 37.7 and 37.8 (2 × **C**H$_2$C(OH), 73.1 (2 × **C**(OH)), 89.2 and 89.7 (2 × **C**H(OOH), 112.3 (2 × **C**H$_2$(CH)C(OH)), 114.2 and 114.3 (2 × **C**H$_2$(C)CH(OOH)), 143.6 (2 × **C**(CH)OOH), 144.7 and 144.8 (2 × **C**HC(OH)).

ANNEXES

Annexes 1-12 resume all the experimental data in PB and in HEPES for all spin-traps and all spin-adducts, including *g* (*g* = +/- 0.0005) values, *hfccs* and ratios of spin-adducts formed in the mixtures.

Annex 1. Fe(II) (0.1 mM) / DEPMPO (25 mM) system in H_2O with Limo-OOH varying concentrations

Limo-OOH	Spin-adducts in H_2O assignment, *g*, *hfccs* (Gauss)	
1 mM	**1** (80%) DEPMPO-OH *g*=2.0055 a_N=14.0 a_H=13.6 a_P=47.7	**2** (20%) DEPMPO-R *g*=2.0056 a_N=14.1 a_H=22.3 a_P=47.1
2 mM	**1** (80%) DEPMPO-OH *g*=2.0055 a_N=14.0 a_H=13.6 a_P=47.6	**2** (20%) DEPMPO-R *g*=2.0057 a_N=14.7 a_H=22.2 a_P=46.9
5 mM	**1** (80%) DEPMPO-OH *g*=2.0055 a_N=14.0 a_H=13.6 a_P=47.6	**2** (20%) DEPMPO-R *g*=2.0058 a_N=14.6 a_H=24.6 a_P=46.8
10 mM	**1** (80%) DEPMPO-OH *g*=2.0055 a_N=14.2 a_H=13.3 a_P=47.8	**2** (20%) DEPMPO-R *g*=2.0058 a_N=15.1 a_H=24.4 a_P=45.7

Figure A1.1: Spin-adducts **1** and **2** formed in H_2O with different Limo-OOH concentrations

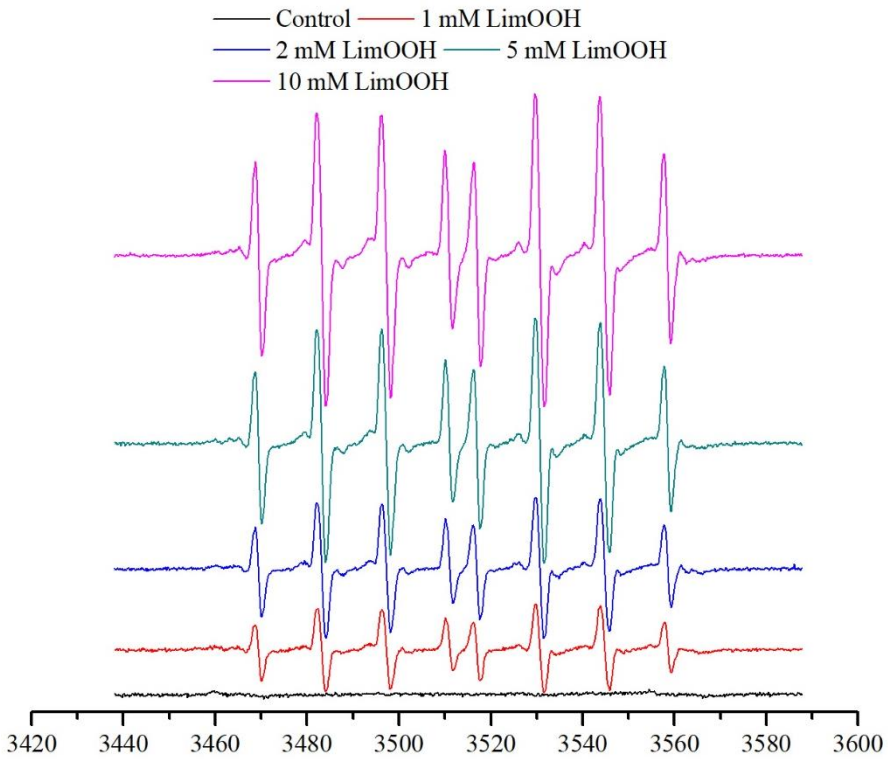

By decreasing the Limo-OOH concentration, both hydroxyl radicals and carbon radicals were trapped. However, the relative concentration of one to the other stayed the same. In general, hydroxy radical was formed in a five-fold factor compared to the carbon radical.

Annex 2. Limo-OOH (1 mM) / DEPMPO (25 mM) system in HEPES and H_2O with Fe(II) varying concentrations

Fe(II)	Spin-adducts in HEPES assignment, *g*, *hfccs* (Gauss)	Spin-adducts in H_2O assignment, *g*, *hfccs* (Gauss)	
0.1 mM	**1** DEPMPO-OH g=2.0057 a_N=14.0 a_H=14.0 a_P=47.5	**1** (80%) DEPMPO-OH g=2.0055 a_N=14.1 a_H=13.6 a_P=47.6	**2** (20%) DEPMPO-R g=2.0054 a_N=14.7 a_H=21.7 a_P=46.8
0.5 mM	**1** DEPMPO-OH g=2.0057 a_N=14.2 a_H=13.5 a_P=47.8	**1** (70%) DEPMPO-OH g=2.0056 a_N=14.1 a_H=13.5 a_P=47.7	**2** (30%) DEPMPO-R g=2.0056 a_N=14.6 a_H=21.7 a_P=46.9
1.0 mM	**1** DEPMPO-OH g=2.0057 a_N=14.2 a_H=13.5 a_P=47.7	**1** (60%) DEPMPO-OH g=2.0056 a_N=14.1 a_H=13.6 a_P=47.7	**2** (40%) DEPMPO-R g=2.0056 a_N=14.6 a_H=21.8 a_P=46.9
1.7 mM	-	**1** (50%) DEPMPO-OH g=2.0056 a_N=14.1 a_H=13.6 a_P=47.6	**2** (50%) DEPMPO-R g=2.0057 a_N=14.5 a_H=21.6 a_P=46.7

In HEPES only a low generation of hydroxy radical was seen. In H_2O radical hydroxyl was generated but also carbon radicals. By increasing the iron concentration in the mixture, the carbon radical generated ratio increased.

Figure A2.1: Spin-adducts in HEPES, Limo-OOH (1 mM) / DEPMPO (25 mM), Fe II concentration varying

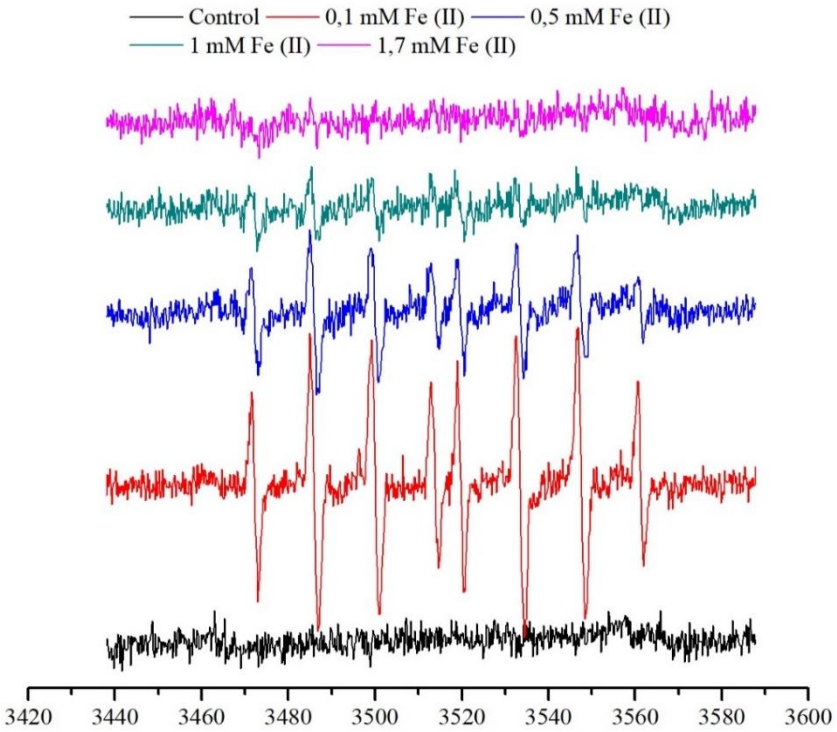

Figure A2.2: Spin-adducts in H_2O, Limo-OOH (1 mM) / DEPMPO (25 mM), Fe II concentration varying

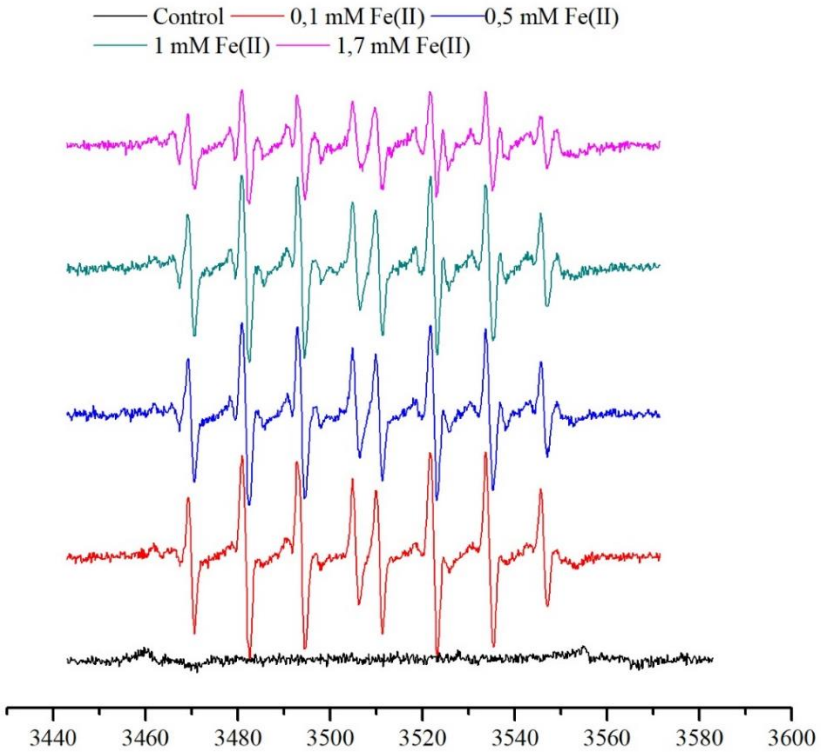

Annex 3. Spin-adducts formed from Limo-OOH (1 mM) / DMPO (25 mM) system in HEPES with Fe(II) varying concentrations

Fe(II)	Spin-adducts in HEPES assignment, *g*, *hfccs* (Gauss)
0.1 mM	**5** DMPO-OH *g*=2.0056 a_N=15.0 a_H=15.2
0.5 mM	**5** DMPO-OH *g*=2.0056 a_N=15.1 a_H=15.0
1.0 mM	--
1.7 mM	--

Limo-OOH generates low concentration of radical in HEPES. At t=30min no signal was observed due to the short half-life of the DMPO spin-adduct (data not shown).

Figure A3.1: Spin-adducts in HEPES / Limo-OOH (1 mM) / DMPO (25 mM), Fe(II) concentration varying

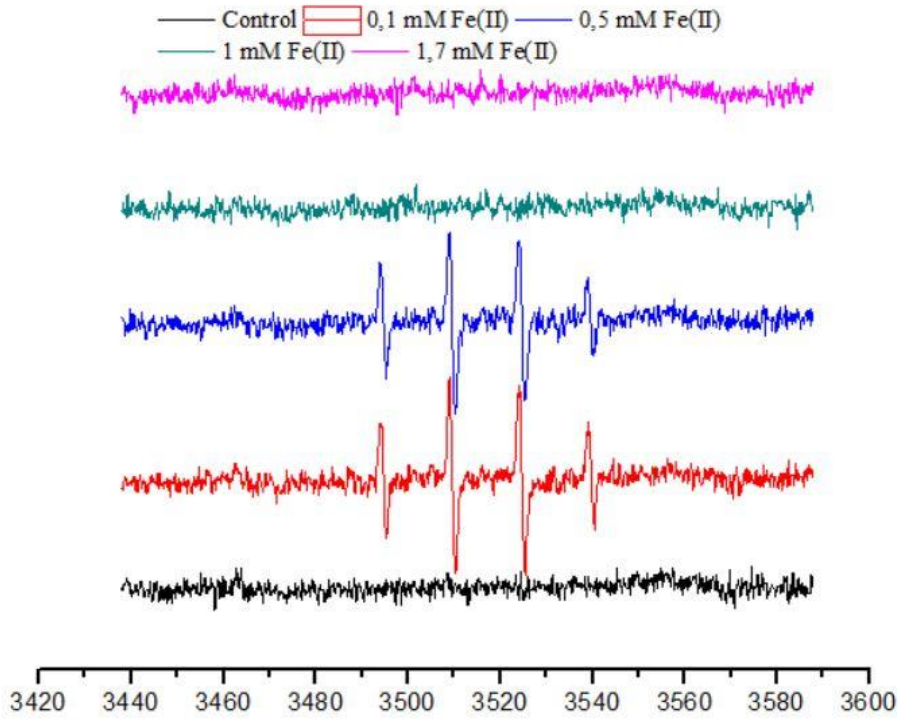

Annex 4. Limo-OOH (1 mM) / PBN (50 mM) system in H_2O with Fe(II) varying concentrations[17]

Fe(II)	Spin-adducts in H_2O assignment, *g*, *hfccs* (Gauss)
0.1 mM	**3** PBN-R g=2.0056 a_N=15.4 a_H=3.4
0.5 mM	**3** PBN-R g=2.0056 a_N=15.4 a_H=3.4
1.0 mM	**3** PBN- R g=2.0056 a_N=15.4 a_H=3.4
1.7 mM	--

Here we can see using literature and databases that it deals with a carbon radical adduct.

Figure A4.1: Spin-adducts in H_2O spectra Limo-OOH (1 mM) / PBN (50 mM) with Fe(II) varying concentrations

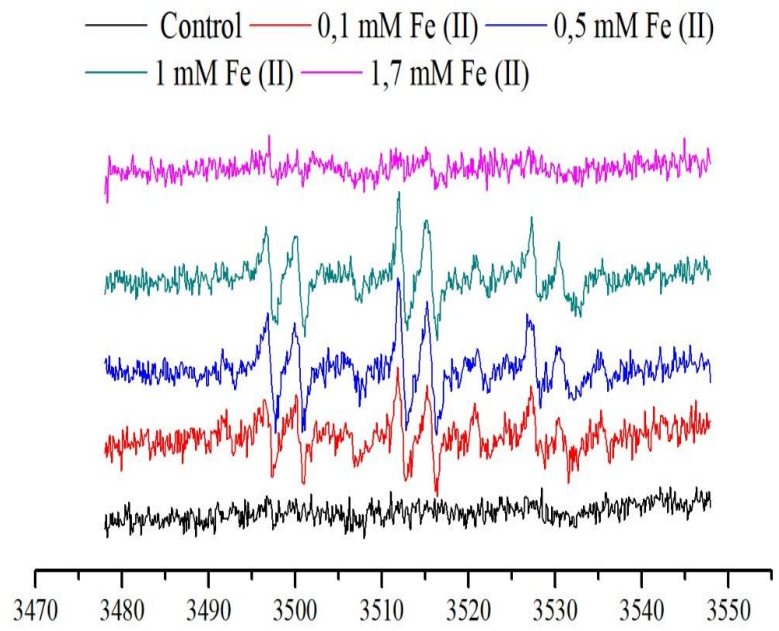

In those conditions in HEPES or PB, we don't observe any spin-adduct using PBN as a spin-trap (data not shown).

Annex 5. Spin-adducts formed from Fe(II) (0.1 mM) / PBN (50 mM) system in H_2O and CH_3CN with Limo-OOH varying concentrations

Limo-OOH	Spin-adducts in H_2O assignment, *g*, hfccs (Gauss)	Spin-adducts in CH_3CN assignment, *g*, hfccs (Gauss)
1 mM	**3** PBN-R *g*=2.0051 a_N=15.4 a_H=3.3	**4** PBN-CH_2CN *g*=2.0057 a_N=14.2 a_H=2.2
2 mM	**3** PBN-R *g*=2.0051 a_N=15.3 a_H=3.2	**4** PBN-CH_2CN *g*=2.0057 a_N=14.2 a_H=2.1
5 mM	**3** PBN-R *g*=2.0052 a_N=15.3 a_H=3.1	**4** PBN-CH_2CN *g*=2.0057 a_N=14.2 a_H=2.1
10 mM	**3** PBN-R *g*=2.0053 a_N=15.2 a_H=3.1	**4** PBN- CH_2CN *g*=2.0057 a_N=14.1 a_H=2.1

Figure A5.1: Fe(II) (0.1 mM) / PBN (50 mM) system in H_2O with Limo-OOH varying concentrations

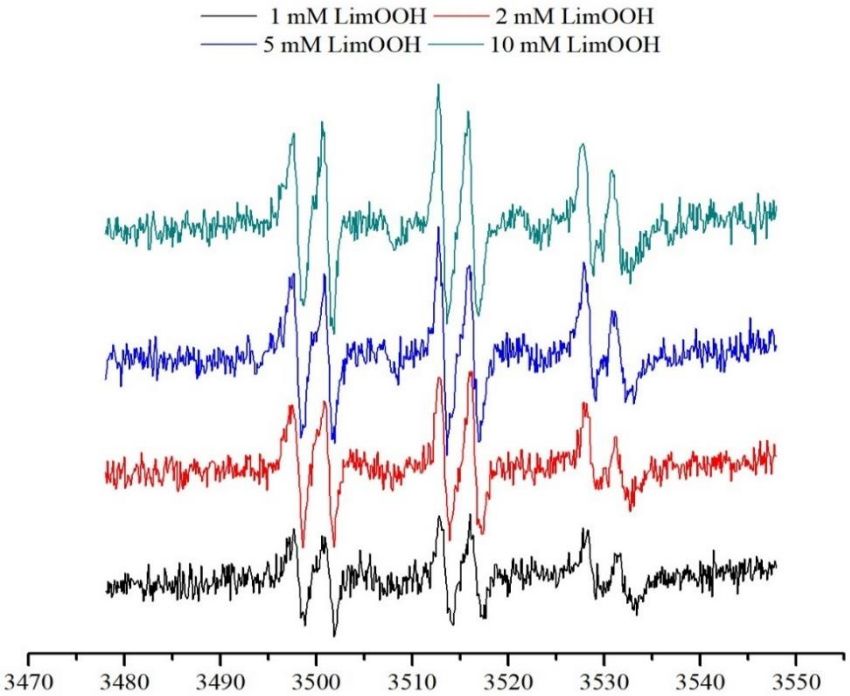

Figure A5.2: Fe(II) (0.1 mM) / PBN (50 mM) system in CH_3CN with Limo-OOH varying concentrations

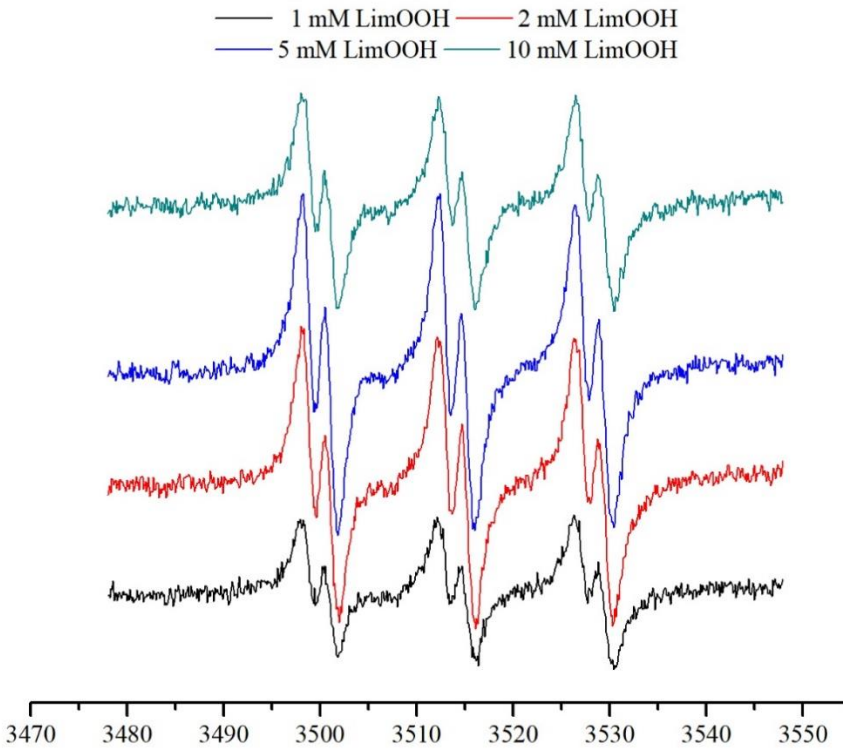

Comparing those spectra, a weak ratio signal/noise increasing by hydroperoxide concentration in H_2O or in CH_3CN was observed, using PBN spin-trap.

Annex 6. Spin-adducts formed from Cum-OOH (0.54 mM) /DEPMPO (25 mM) system in PB and HEPES with Fe(II) varying concentrations

Fe(II)	Spin-adducts in PB assignment, *g*, *hfccs* (Gauss)			Spin-adducts in HEPES assignment, *g*, *hfccs* (Gauss)		
0.1 mM	-	-	-	**1** (60%) DEPMPO-OH *g*=2.0059 a_N=14.1 a_H=13.3 a_P=47.5	**6** (20%) DEPMPO-carbon R *g*=2.0058 a_N=15.2 a_H=22.4 a_P=48.0	**7** (20%) DEPMPO-OCH_3/OOCum *g*=2.0059 a_N=13.6 a_H=9.4 a_P=48.2
0.5 mM	**1** (40%) DEPMPO-OH *g*=2.0058 a_N=14.2 a_H=13.5 a_P=47.5	**6** (30%) DEPMPO-carbon R *g*=2.0056 a_N=15.3 a_H=22.6 a_P=47.8	**7** (30%) DEPMPO-OCH_3/OOCum *g*=2.0058 a_N=13.8 a_H=8.9 a_P=48.1	**1** (60%) DEPMPO-OH *g*=2.0059 a_N=14.1 a_H=13.3 a_P=47.5	**6** (20%) DEPMPO-carbon R *g*=2.0057 a_N=15.3 a_H=22.5 a_P=47.9	**7** (20%) DEPMPO-OCH_3/OOCum *g*=2.0059 a_N=13.5 a_H=9.3 a_P=48.2
1.0 mM	**1** (40%) DEPMPO-OH *g*=2.0058 a_N=14.3 a_H=13.4 a_P=47.5	**6** (60%) DEPMPO-carbon R *g*=2.0055 a_N=15.4 a_H=22.6 a_P=47.9		**1** (50%) DEPMPO-OH *g*=2.0059 a_N=14.2 a_H=13.5 a_P=47.4	**6** (30%) DEPMPO-carbon R *g*=2.0057 a_N=15.3 a_H=22.8 a_P=48.0	**7** (20%) DEPMPO-OCH_3/OOCum *g*=2.0053 a_N=13.4 a_H=9.1 a_P=48.2
1.7 mM	**1** (20%) DEPMPO-OH *g*=2.0058 a_N=14.2 a_H=13.3 a_P=47.5	**6** (80%) DEPMPO-carbon R *g*=2.0055 a_N=15.3 a_H=22.7 a_P=48.0		**1** (70%) DEPMPO-OH *g*=2.0059 a_N=14.2 a_H=13.4 a_P=47.6	**6** (30%) DEPMPO-carbon R *g*=2.0057 a_N=15.3 a_H=22.6 a_P=47.9	

Some radical identifications were pretty difficult because they had similar hyperfine coupling constants. We were not able to differentiate for example DEPMPO-OCH_3 and DEPMPO-OOCum.

Figure A6.1: Spin-adducts in PB, Cum-OOH (0.54 mM) /DEPMPO (25 mM), with Fe(II) varying concentrations

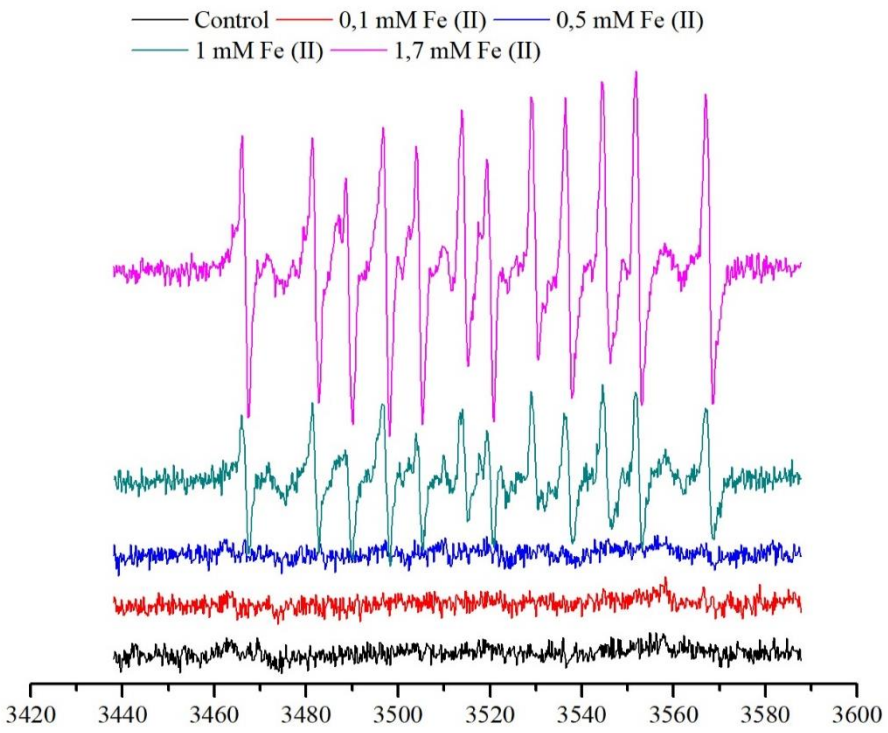

Figure A6.2: Spin-adducts in HEPES, Cum-OOH (0.54 mM) /DEPMPO (25 mM), with Fe(II) varying concentrations

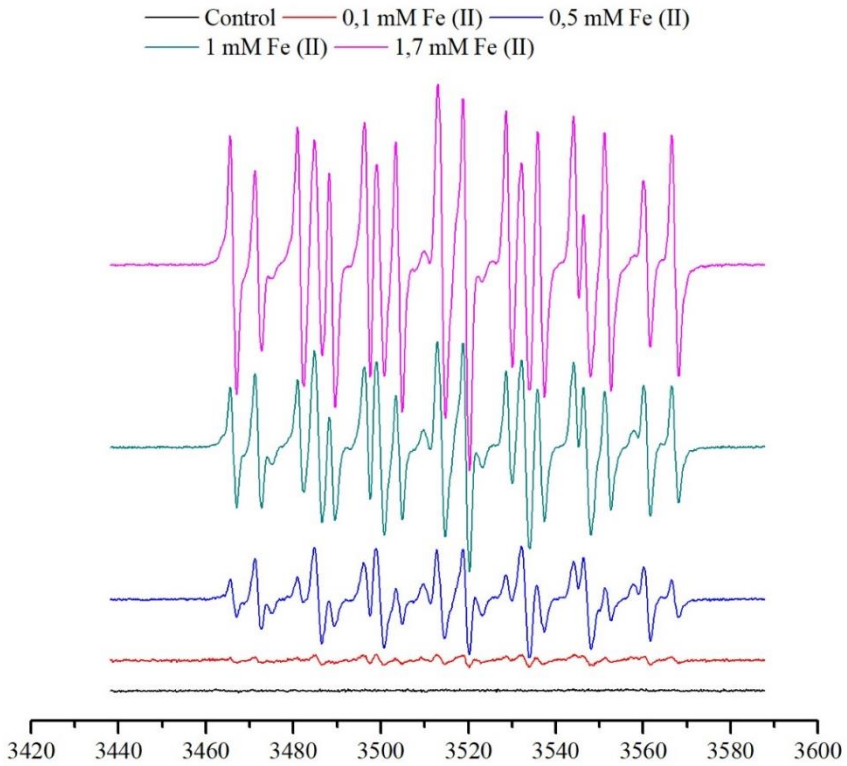

In Figure A6.1, no spin-adducts are observed at 0.1 and 0.5Mm. It is possible that PB chelates Fe II which therefore prevents radical generation at low concentration.

Annex 7. Spin-adducts formed from Cum-OOH (0.54 mM) / DMPO (25 mM) system in PB and HEPES with Fe(II) varying concentrations

Fe(II)	Spin-adducts in PB assignment, *g*, *hfccs* (Gauss)			Spin-adducts in HEPES assignment, *g*, *hfccs* (Gauss)		
0.1 mM	-	-	-	-	-	
0.5 mM	-	-	-	**8** (60%) DMPO-OCH_3 g=2.0055 a_N=14.65 a_H=10.77 (1.27)	**9** (20%) DMPO-carbon R g=2.0053 a_N=16.40 a_H=23.87	**10** (20%) DMPO-OH g=2.0057 a_N=15.30 a_H=15.02
1.0 mM	**8** (50%) DMPO-OCH_3 g=2.0056 a_N=14.55 a_H=10.80 (1.32)	**9** (40%) DMPO-carbon R g=2.0054 a_N=16.61 a_H=23.70	**10** (10%) DMPO-OH g=2.0056 a_N=15.13 a_H=15.01	**8** (70%) DMPO-OCH_3 g=2.0055 a_N=14.61 a_H=10.97 (1.44)	**9** (15%) DMPO-carbon R g=2.0055 a_N=16.65 a_H=24.00	**10** (15%) DMPO-OH g=2.0057 a_N=15.30 a_H=15.02
1.7 mM	**8** (49%) DMPO-OCH_3 g=2.0056 a_N=14.63 a_H=10.81 (1.34)	**9** (40%) DMPO-carbon R g=2.0054 a_N=16.56 a_H=23.65	**10** (11%) DMPO-OH g=2.0057 a_N=15.30 a_H=15.02	**8** (80%) DMPO-OCH_3 g=2.0055 a_N=14.61 a_H=10.97 (1.44)	**9** (10%) DMPO-carbon R g=2.0053 a_N=16.45 a_H=23.64	**10** (10%) DMPO-OH g=2.0057 a_N=15.30 a_H=15.02

Figure A7.1: Spin-adducts in PB, Cum-OOH (0.54 mM) / DMPO (25 mM), Fe(II) varying concentrations

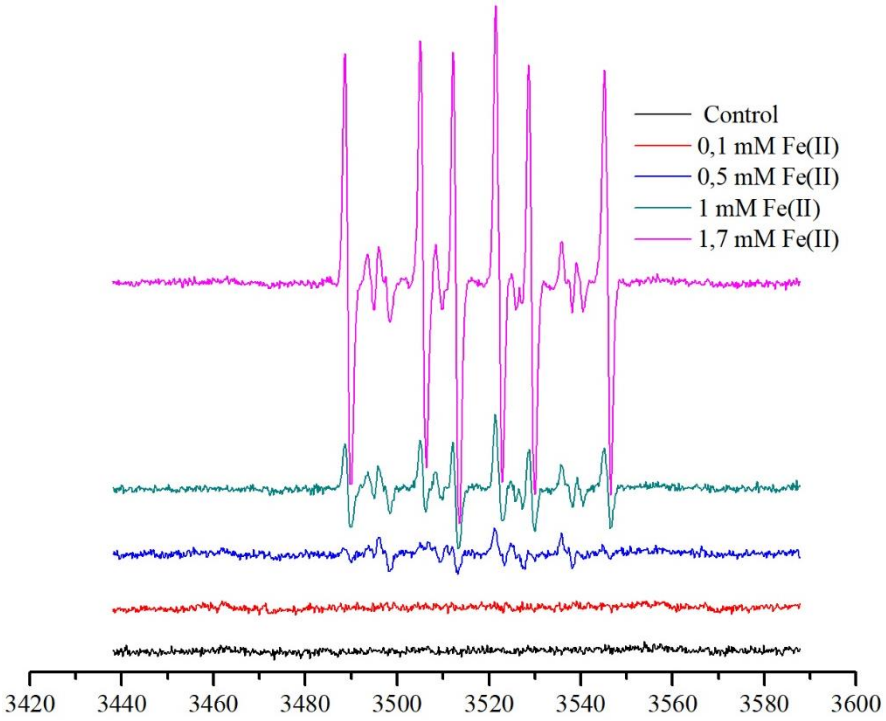

Figure A7.2: Spin-adducts and HEPES, Cum-OOH (0.54 mM) / DMPO (25 mM), Fe(II) varying concentrations

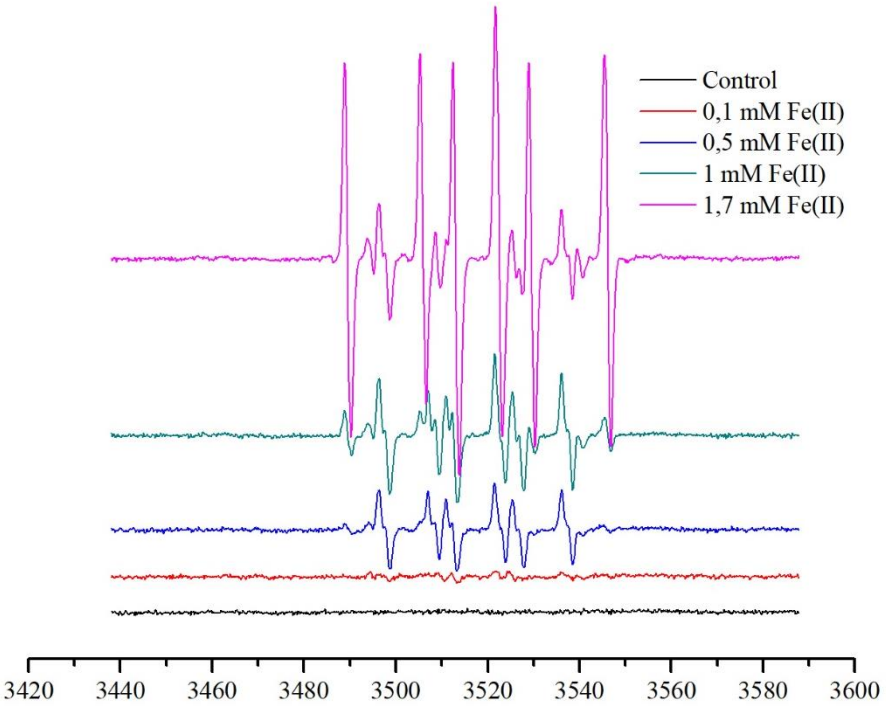

In Figure A7.1 and 2 shows that the same kind of radicals were generated. In HEPES buffer radical generation stared at catalytic amount compared to PB, that is the reason why we will use HEPES buffer for the further tests and also in RHE.

Annex 8. Spin-adducts formed from Cum-OOH (0.54 mM) / PBN (25 mM) system in PB and HEPES with Fe(II) varying concentrations[17,30,41,43]

Fe(II)	Spin-adducts in PB assignment, *g*, *hfccs* (Gauss)		Spin-adducts in HEPES assignment, *g*, *hfccs* (Gauss)	
0.1 mM	**11** PBN-carbon R *g*=2.0060 a_N=15.2 a_H=3.5		**11** PBN-carbon R *g*=2.0061 a_N=15.3 a_H=3.5	
0.5 mM	**11** PBN-carbon R *g*=2.0060 a_N=15.3 a_H=3.4		**11** (55%) PBN-carbon R *g*=2.0060 a_N=15.3 a_H=3.5	**12** (45%) PBN-carbon R *g*=2.0059 a_N=16.6 a_H=3.6
1.0 mM	**11** PBN-carbon R *g*=2.0060 a_N=15.3 a_H=3.5		**11** (55%) PBN-carbon R *g*=2.0060 a_N=15.3 a_H=3.5	**12** (45%) PBN-carbon R *g*=2.0059 a_N=16.6 a_H=3.6
1.7 mM	**11** (60%) PBN-carbon R *g*=2.0060 a_N=15.3 a_H=3.6	**12** (40%) PBN-carbon R *g*=2.0059 a_N=16.5 a_H=3.5	**11** (30%) PBN-carbon R *g*=2.0061 a_N=15.3 a_H=3.5	**12** (70%) PBN-carbon R *g*=2.0059 a_N=16.6 a_H=3.6

Figure A8.1: Cum-OOH (0.54 mM) / PBN (25 mM) system in PB with Fe(II) varying concentrations

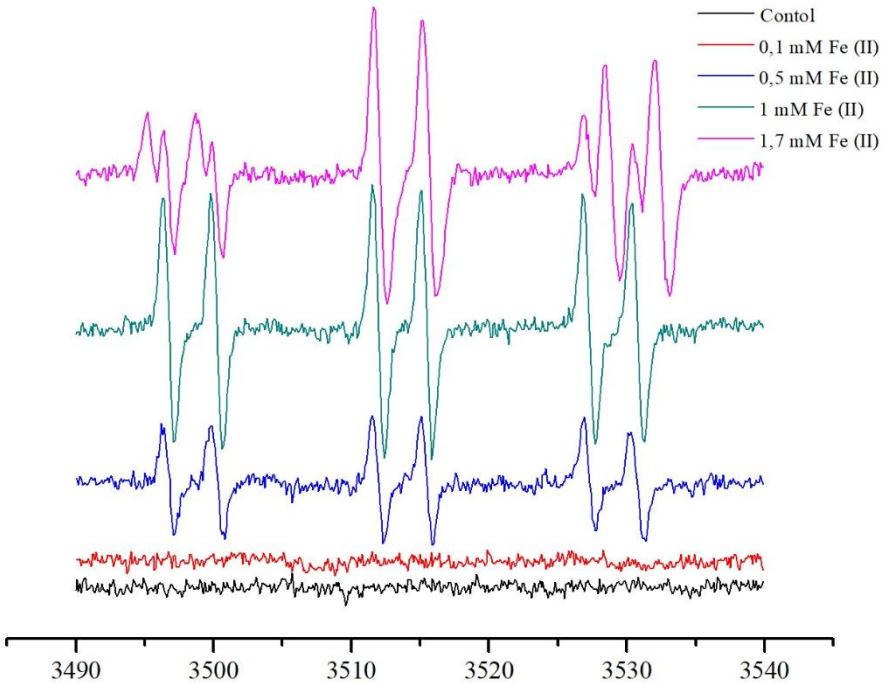

In Figure A8.1 we can see radical generation starting at one equivalent iron to CumOOH in PB. And also, the transition 15 to 16 Gauss is also seen at high Fe(II) concentration.

Figure A8.2: Cum-OOH (0.54 mM) / PBN (25 mM) system in PB and HEPES with Fe(II) varying concentrations spectra at t = 0 minutes (above) and 30 minutes (bellow) respectively

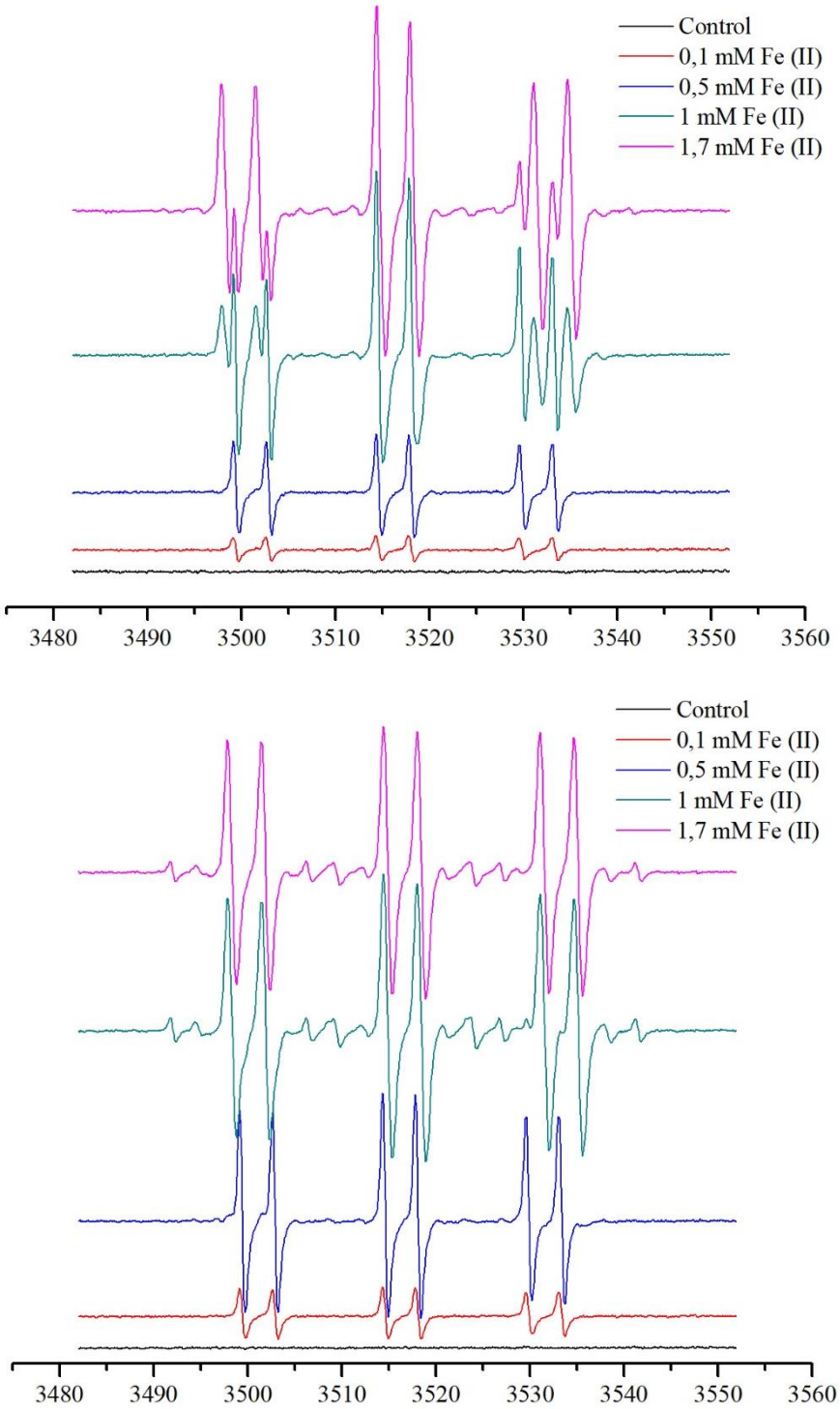

In Figure A8.2, radical generation starting at weak Fe(II) concentration in PB compared to HEPES. Also, the transition 15 to 16 Gauss was also seen at lower Fe(II) concentration than in PB. In here it becomes clear at 1mM of Fe(II) concentration at t = 0 min conversion starts but at and t = 30 min it's complete.

Annex 9. Spin-adducts formed from Lina-OOHs (1 mM) /DEPMPO (25 mM) system in HEPES with Fe(II) varying concentrations

Fe(II)	Spin-adducts in HEPES assignment, *g*, *hfccs* (Gauss) t = 0 min			Spin-adducts in HEPES assignment, *g*, *hfccs* (Gauss) t = 30 min		
0.1 mM	**1** (70%) DEPMPO-OH	**13** (15%) DEPMPO-carbon R	**14** (15%) DEPMPO-OCH_3/OOLina	**1** (70%) DEPMPO-OH	**13** (15%) DEPMPO-carbon R	**14** (15%) DEPMPO-OCH_3/OOLina
	g=2.0055 a_N=14.0 a_H=13.6 a_P=47.6	*g*=2.0054 a_N=15.2 a_H=22.4 a_P=47.7	*g*=2.0059 a_N=13.5 a_H=9.6 a_P=48.2	*g*=2.0055 a_N=14.1 a_H=13.3 a_P=47.7	*g*=2.0054 a_N=15.3 a_H=22.5 a_P=47.7	*g*=2.0059 a_N=13.5 a_H=9.6 a_P=48.2
0.5 mM	**1** (60%) DEPMPO-OH	**13** (20%) DEPMPO-carbon R	**14** (10%) DEPMPO-OCH_3/OOLina	**1** (40%) DEPMPO-OH	**13** (50%) DEPMPO-carbon R	**14** (10%) DEPMPO-OCH_3/OOLina
	g=2.0055 a_N=14.0 a_H=13.6 a_P=47.6	*g*=2.0054 a_N=15.1 a_H=22.4 a_P=47.6	*g*=2.0059 a_N=13.5 a_H=9.3 a_P=48.2	*g*=2.0055 a_N=14.1 a_H=13.3 a_P=47.6	*g*=2.0053 a_N=15.1 a_H=22.3 a_P=47.8	*g*=2.0059 a_N=13.5 a_H=9.3 a_P=48.2
1.0 mM	**1** (35%) DEPMPO-OH	**13** (50%) DEPMPO-carbon R	**14** (15%) DEPMPO-OCH_3/OOLina	**1** (40%) DEPMPO-OH	**13** (40%) DEPMPO-carbon R	**14** (20%) DEPMPO-OCH_3/OOLina
	g=2.0055 a_N=14.1 a_H=13.5 a_P=47.7	*g*=2.0053 a_N=15.2 a_H=22.4 a_P=48.2	*g*=2.0053 a_N=13.6 a_H=9.2 a_P=48.2	*g*=2.0053 a_N=14.1 a_H=13.3 a_P=47.6	*g*=2.0053 a_N=15.2 a_H=22.8 a_P=48.0	*g*=2.0053 a_N=13.6 a_H=9.1 a_P=48.2
1.7 mM	**1** (30%) DEPMPO-OH	**13** (50%) DEPMPO-carbon R	**14** (20%) DEPMPO-OCH_3/OOLina	**1** (35%) DEPMPO-OH	**13** (50%) DEPMPO-carbon R	**14** (15%) DEPMPO-OCH_3/OOLina
	g=2.0055 a_N=14.1 a_H=13.4 a_P=47.6	*g*=2.0053 a_N=15.2 a_H=22.6 a_P=48.0	*g*=2.0059 a_N=13.6 a_H=9.4 a_P=48.2	*g*=2.0055 a_N=14.1 a_H=13.7 a_P=47.6	*g*=2.0053 a_N=15.1 a_H=22.3 a_P=47.6	*g*=2.0059 a_N=13.6 a_H=9.4 a_P=48.2

In Annex 9, by increase iron concentration two radicals were trapped. There are two times more hydroxy radical then carbon radical at 0.1 mM Iron II. After 1 mM of iron II there is two times more carbon radical then hydroxy radical. The same facts are observed at t 30 min.

At t = 24 h 40% DEPMPO-R et 60 % DEPMPO-OH (Data not shown)

Figure A9.1: Spin-adducts formed in HEPES / Lina-OOHs (1 mM) / DEPMPO (25 mM) system, Fe(II) varying concentrations at 0 min

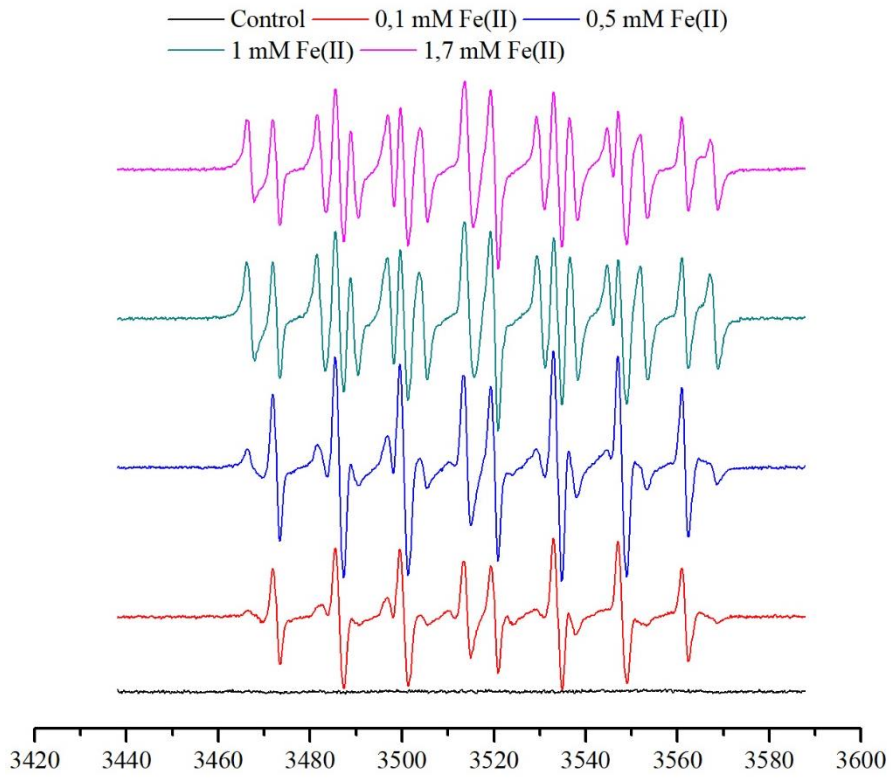

Figure A9.1: Spin-adducts formed in HEPES / Lina-OOHs (1 mM) /DEPMPO (25 mM), Fe(II) varying concentrations at 30 min

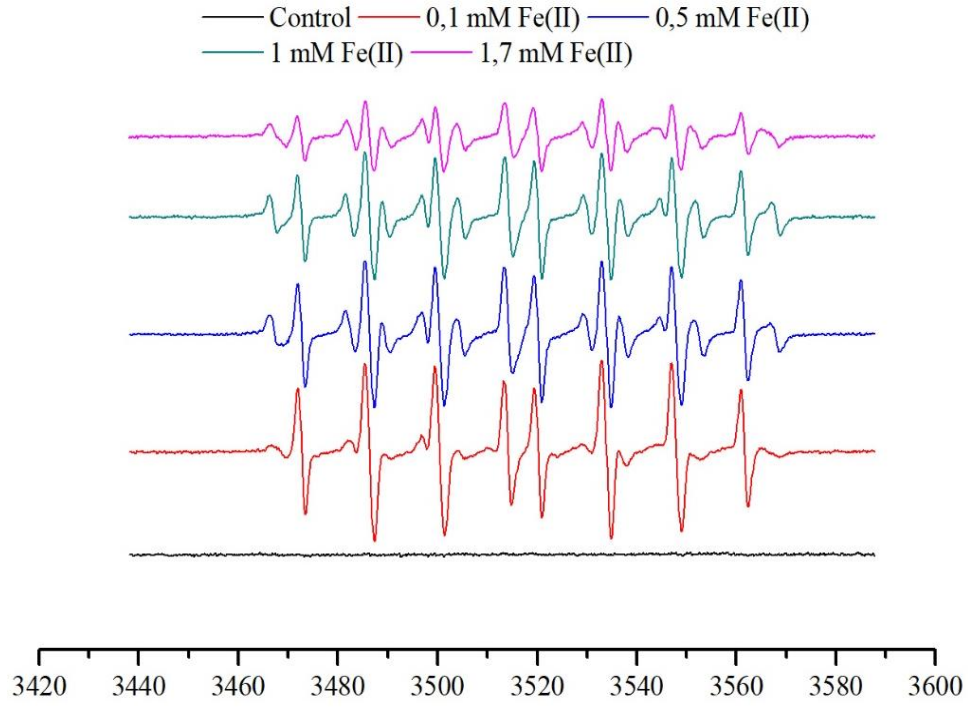

After 30 min reaction started, carbon radical trapped decrease.

Annex 10. Spin-adducts formed from Lina-OOHs (1 mM) /DEPMPO (25 mM) system in HEPES-CM (4-1/v-v) with Fe(II) varying concentrations (Culture Medium)

Fe(II)	Spin-adducts in HEPES assignment, *g*, *hfccs* (Gauss) t = 0 min		Spin-adducts in HEPES assignment, *g*, *hfccs* (Gauss) t = 30 min	
0.1 mM	**1** (50%) DEPMPO-OH *g*=2.0055 a_N=14.1 a_H=13.5 a_P=47.5	**13** (50%) DEPMPO-carbon R *g*=2.0053 a_N=15.3 a_H=22.1 a_P=47.8	**1** (60%) DEPMPO-OH *g*=2.0055 a_N=14.1 a_H=13.5 a_P=47.7	**13** (40%) DEPMPO-carbon R *g*=2.0054 a_N=15.3 a_H=22.3 a_P=47.7
0.5 mM	**1** (40%) DEPMPO-OH *g*=2.0055 a_N=14.1 a_H=13.4 a_P=47.5	**13** (60%) DEPMPO-carbon R *g*=2.0054 a_N=15.3 a_H=22.3 a_P=47.6	**1** (50%) DEPMPO-OH *g*=2.0055 a_N=14.1 a_H=13.5 a_P=47.6	**13** (50%) DEPMPO-carbon R *g*=2.0054 a_N=15.3 a_H=22.4 a_P=47.4
1.0 mM Fe(II)	**1** (25%) DEPMPO-OH *g*=2.0055 a_N=14.1 a_H=13.7 a_P=47.3	**13** (75%) DEPMPO-carbon R *g*=2.0053 a_N=15.2 a_H=22.1 a_P=47.7	**1** (25%) DEPMPO-OH *g*=2.0055 a_N=14.1 a_H=13.7 a_P=47.5	**13** (75%) DEPMPO-carbon R *g*=2.0053 a_N=15.0 a_H=22.0 a_P=47.4
1.7 mM Fe(II)	-	**13** DEPMPO-carbon R *g*=2.0053 a_N=15.2 a_H=22.3 a_P=47.9	-	-

Here, radical hydroxy and carbon radical were trapped. A catalytic amount of Iron II an equal proportion of them is observed but at t = 30 min carbon radical decreased and hydroxy radical increased. By increasing Iron II concentration carbon radical formation was increased and hydroxyl radical formation was decreased up to disappear at 1.7 mM Iron II. At t = 30 min same behavior is observed. At 1.7 mM Iron II and t = 0 min only carbon radical was observed. CM seemed to have a role in to the formation of carbon radical because here the ration oxygen/carbon radical was increased compared to this ratio without using CM.

Figure A10.1: Spin-adducts HEPES-CM (4-1/v-v), Lina-OOHs (1 mM) /DEPMPO (25 mM), Fe(II) varying concentrations at 0 min

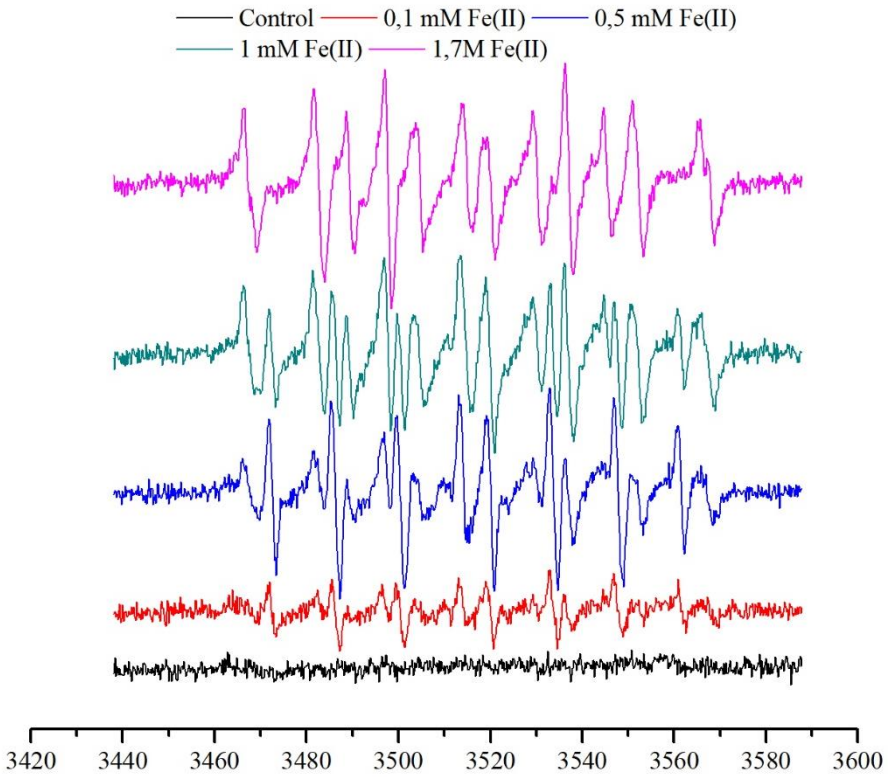

Figure A10.2: Spin-adducts HEPES-CM (4-1/v-v), Lina-OOHs (1 mM) /DEPMPO (25 mM), Fe(II) varying concentrations at 30 min

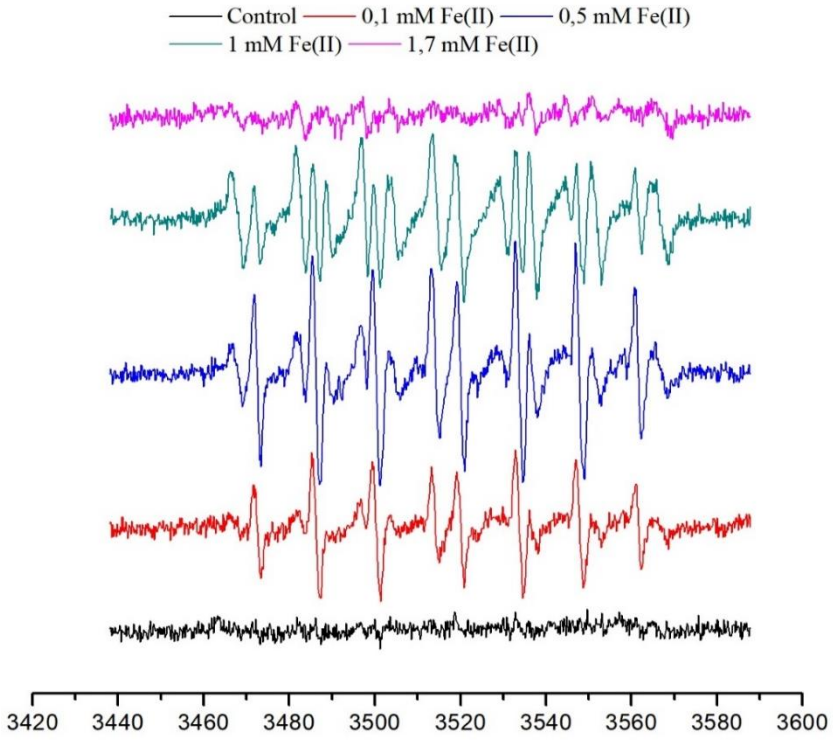

Annex 11. Spin-adducts formed from Lina-OOHs (1 mM) /DEPMPO (25 mM) system in HEPES-CM (1-1/v-v) with Fe(II) varying concentrations

Fe(II)	Spin-adducts in HEPES assignment, *g*, *hfccs* (Gauss) t = 0 min		Spin-adducts in HEPES assignment, *g*, *hfccs* (Gauss) t = 30 min	
0.1 mM	-	-	**1** (70%) DEPMPO-OH g=2.0055 a_N=14.05 a_H=13.77 a_P=47.65	**13** (30%) DEPMPO-carbon R g=2.0054 a_N=15.14 a_H=22.28 a_P=47.81
0.5 mM	**1** (40%) DEPMPO-OH g=2.0055 a_N=14.08 a_H=13.40 a_P=47.61	**13** (60%) DEPMPO-carbon R g=2.0054 a_N=15.07 a_H=21.85 a_P=47.74	**1** (50%) DEPMPO-OH g=2.0055 a_N=14.10 a_H=13.54 a_P=47.54	**13** (50%) DEPMPO-carbon R g=2.0054 a_N=15.01 a_H=22.03 a_P=47.45
1.0 mM	**1** (25%) DEPMPO-OH g=2.0055 a_N=14.12 a_H=13.69 a_P=47.31	**13** (75%) DEPMPO-carbon R g=2.0054 a_N=15.17 a_H=22.14 a_P=47.54	**1** (30%) DEPMPO-OH g=2.0055 a_N=14.07 a_H=13.70 a_P=47.53	**13** (70%) DEPMPO-carbon R g=2.0054 a_N=15.20 a_H=22.16 a_P=47.67
1.7 mM	**1** (10%) DEPMPO-OH g=2.0055 a_N=14.45 a_H=13.73 a_P=46.55	**13** (90%) DEPMPO-carbon R g=2.0055 a_N=15.18 a_H=22.26 a_P=47.62	-	-

Radical generation at low concentration of Iron II was not observed at t = 0 min whereas it was at t = 30 min. The same radicals were obtained in HEPES, HEPES-CM 8/2 and HEPES-CM 5/5 but the carbon radical generated seemed to increase by adding CM. We studied those proportion in order to mimic what could happen on RHE.

The idea is to see if radical nature changes when in contact with residual CM contained in RHE. The experiment showed that CM influenced the ratio oxygen/carbon radical generation and but not their nature.

Figure A11.1: Spin-adducts HEPES-CM (1-1/v-v), Lina-OOHs (1 mM) /DEPMPO (25 mM), Fe(II) varying concentrations at 0 min

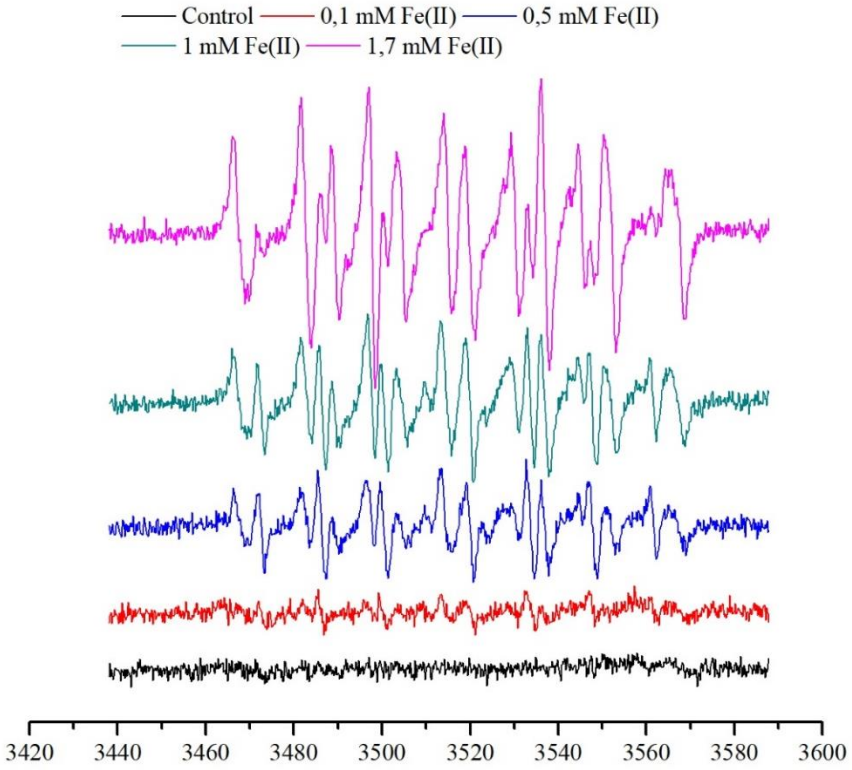

Figure A11.2: Spin-adducts HEPES-CM (1-1/v-v), Lina-OOHs (1 mM) /DEPMPO (25 mM), Fe(II) varying concentrations at 30min

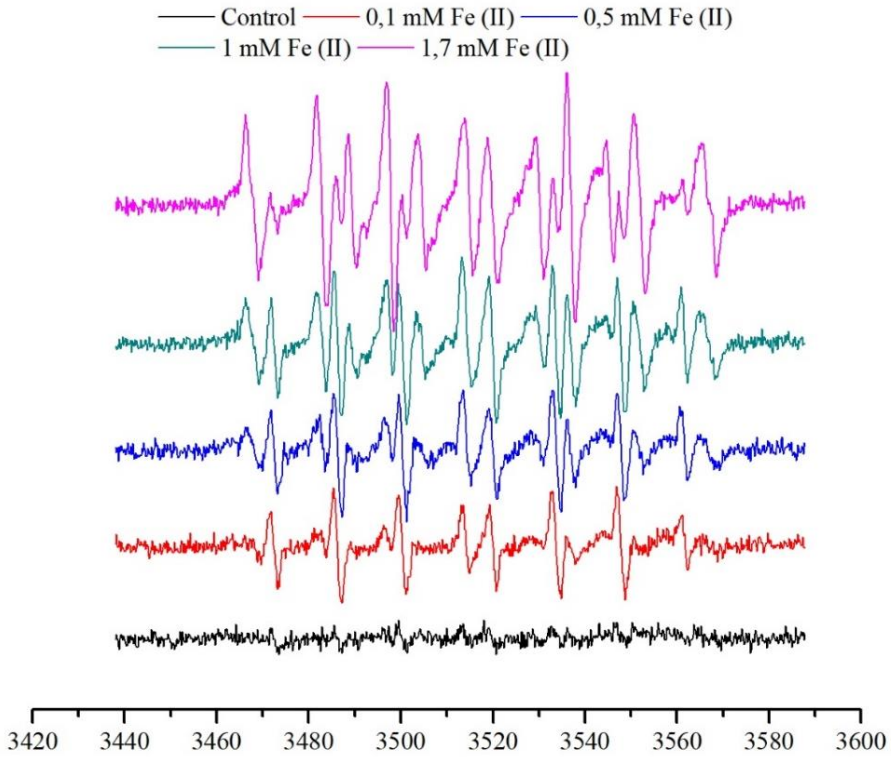

Annex 12. Spin-adducts formed from Cum-OOH/DMPO system in HEPES with Fe(II) varying concentrations

Fe(II)	Spin-adducts in HEPES assignment, *g*, *hfccs* (Gauss)
0.1 mM	-
0.5 mM	-
1.0 mM	**15** DMPO-carbon R g=2.0052 a_N=16.4 a_H=23.6
1.7 mM	**15** DMPO-carbon R g=2.0052 a_N=16.4 a_H=23.6

Figure A12.1: Spin-adducts HEPES, Lina-OOHs, DMPO, Fe(II) varying concentrations

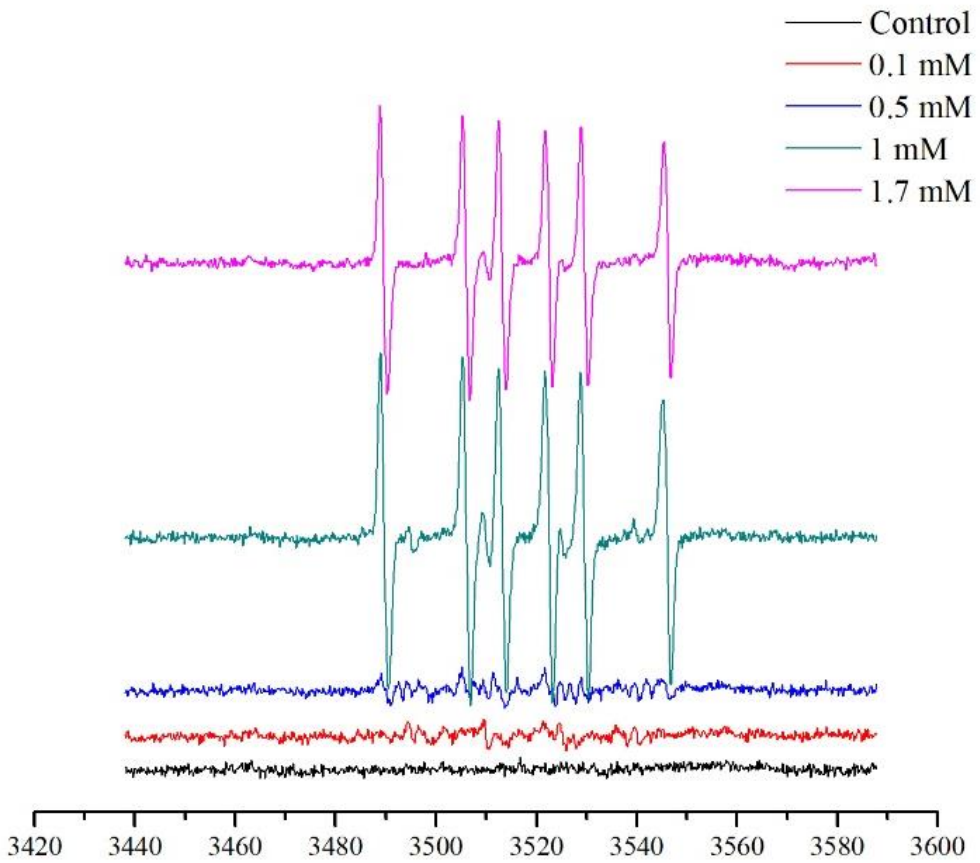

Annex 13. Spin-adducts formed from Lina-OOHs (1 mM) / PBN (50 mM) system in HEPES with Fe(II) varying concentrations

Fe(II)	Spin-adducts in HEPES assignment, *g*, *hfccs* (Gauss) t = 0 min		Spin-adducts in HEPES assignment, *g*, *hfccs* (Gauss) t = 30 min	
0.1 mM	**16** PBN-R *g*=2.0056 a_N=15.3 a_H=3.5	-	**16** PBN-R *g*=2.0056 a_N=15.3 a_H=3.5	-
0.5 mM	-	**17** PBN-carbon R *g*=2.0054 a_N=16.4 a_H=3.5	-	**17** PBN-carbon R *g*=2.0054 a_N=16.5 a_H=3.5
1.0 mM	-	**17** PBN-carbon R *g*=2.0054 a_N=16.5 a_H=3.5	-	**17** PBN-carbon R *g*=2.0060 a_N=16.5 a_H=3.5
1.7 mM	**16** (60%) PBN-R *g*=2.0056 a_N=15.3 a_H=3.4	**17** (40%) PBN-carbon R *g*=2.0059 a_N=16.5 a_H=3.4	**16** (70%) PBN-R *g*=2.0056 a_N=15.3 a_H=3.4	**17** (30%) PBN- carbon R *g*=2.0059 a_N=16.6 a_H=3.6

The radical generation started at weak iron concentration compared to Cum-OOH in HEPES. Also, the opposite transition 15 to 16 Gauss was seen at high Iron II concentration. In here it becomes clear at 1mM of Iron concentration at t = 30 min conversion is complete.

Figure A13.1: Spin-adducts in HEPES spectra at t = 0 min

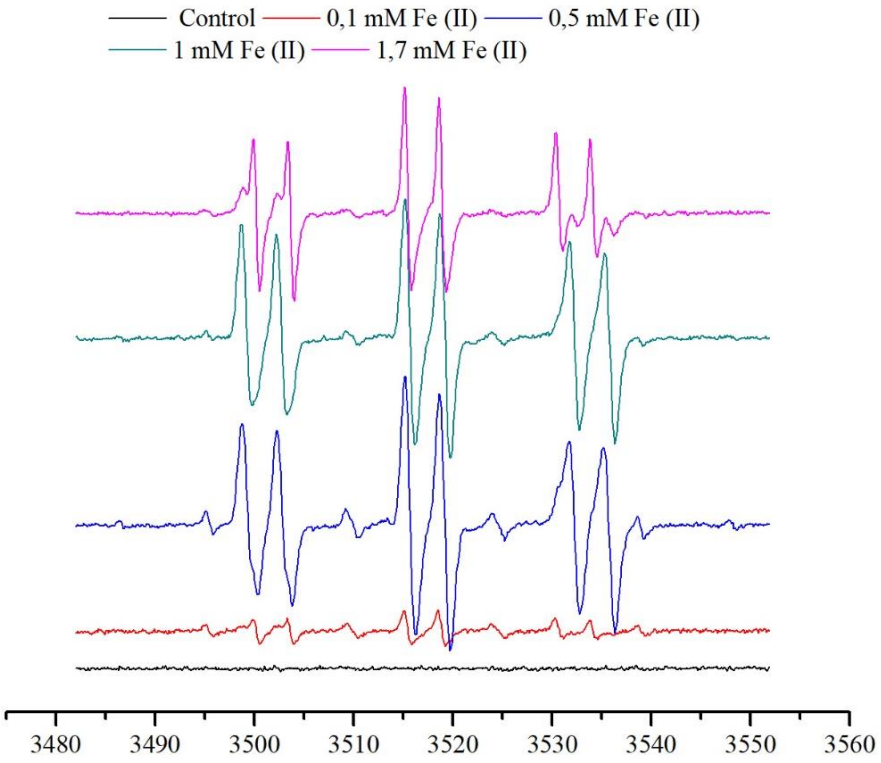

Figure A13.2: Spin-adducts in HEPES spectra at t = 30 min

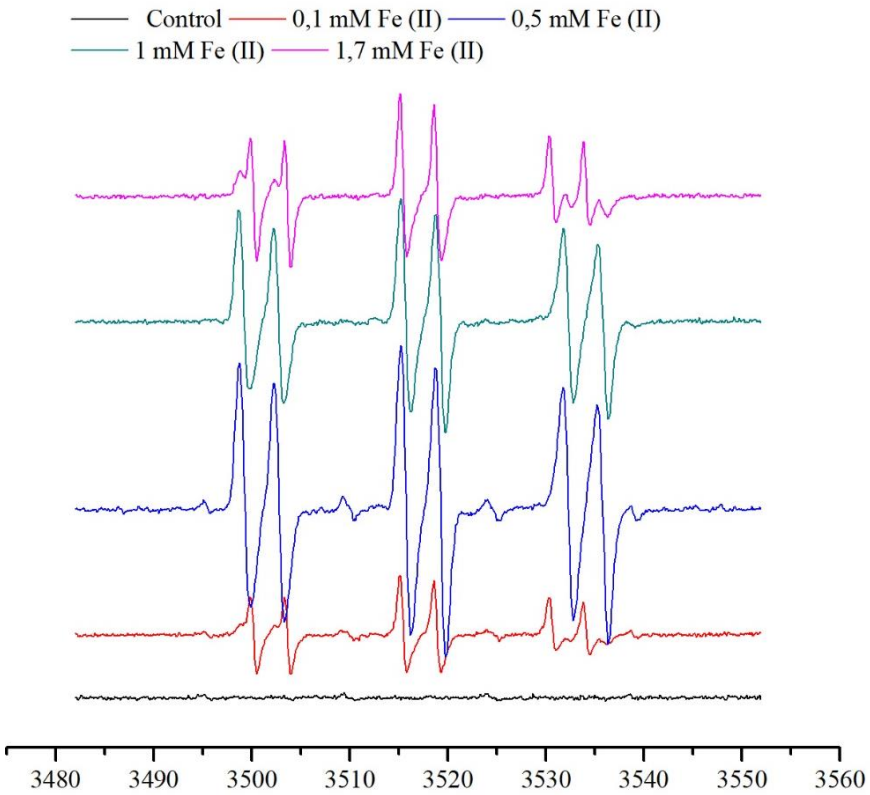

Literature:

(1) Giménez-Arnau, E.; Haberkorn, L.; Grossi, L.; Lepoittevin, J.-P. Identification of Radical Species Derived from Allergenic 15-Hydroperoxyabietic Acid and Insights into the Behaviour of Cyclic Tertiary Allylic Hydroperoxides in Fe(II)/Fe(III) Systems. *Tetrahedron* **2008**, *64* (24), 5680–5691.
(2) Johansson, S.; Giménez-Arnau, E.; Grøtli, M.; Karlberg, A.-T.; Börje, A. Carbon- and Oxygen-Centered Radicals Are Equally Important Haptens of Allylic Hydroperoxides in Allergic Contact Dermatitis. *Chem. Res. Toxicol.* **2008**, *21* (8), 1536–1547.
(3) Kao, D.; Chaintreau, A.; Lepoittevin, J.-P.; Giménez-Arnau, E. Synthesis of Allylic Hydroperoxides and EPR Spin-Trapping Studies on the Formation of Radicals in Iron Systems as Potential Initiators of the Sensitizing Pathway. *J. Org. Chem.* **2011**, *76* (15), 6188–6200.
(4) Bertrand, P. *La spectroscopie de résonance paramagnétique électronique: [fondements*; EDP Sciences: Les Ulis, **2010**.
(5) Loubser, J. H. N.; Wyk, J. A. van. Electron Spin Resonance in the Study of Diamond. *Rep. Prog. Phys.* **1978**, *41* (8), 1201–1248.
(6) Kuppusamy, P. EPR Spectroscopy in Biology and Medicine. *Antioxid. Redox Signal.* **2004**, *6* (3), 583–585.
(7) Zavoïsky, E. K. Paramagnetic Relaxation of Liquid Solutions for Perpendicular Fields. Journal of Physics. July 28, **1945**, p pp.170–173.
(8) Abou Fadel, M. Chemometric Contributions to Electron Paramagnetic Resonance Spectroscopy: New Perspectives for Processing of Spectral Data with Spatial Dimension (Imaging) and / or Time Evolution. Thèse de Doctorat: Optique, Lasers, Physico-Chimie et Atmosphère Université Lille 1 – Sciences et Technologies.
(9) Https://Www.Nobelprize.Org/Nobel_prizes/Physics/Laureates/1902/Zeeman-Facts.Html.
(10) Odom, B.; Hanneke, D.; D'Urso, B.; Gabrielse, G. New Measurement of the Electron Magnetic Moment Using a One-Electron Quantum Cyclotron. *Phys. Rev. Lett.* **2006**, *97* (3).
(11) Jiang, J.; Weber, R. T. EPR Spectrometer Users Manual Basic Operations. EPR Division Bruker BioSpin Corporation Billerica, MA USA.
(12) Getz, E. B.; Xiao, M.; Chakrabarty, T.; Cooke, R.; Selvin, P. R. A Comparison between the Sulfhydryl Reductants Tris(2-Carboxyethyl)Phosphine and Dithiothreitol for Use in Protein Biochemistry. *Anal. Biochem.* **1999**, *273* (1), 73–80.
(13) Eaton, G. R.; Eaton, S. S.; Salikhov, K. M. *Foundations of Modern EPR*; World scientific, **1998**.
(14) Janzen, E. G. Spin Trapping. *Acc. Chem. Res.* **1971**, *4* (1), 31–40.
(15) Yamazaki, I.; Piette, L. H.; Grover, T. A. Kinetic Studies on Spin Trapping of Superoxide and Hydroxyl Radicals Generated in NADPH-Cytochrome P-450 Reductase-Paraquat Systems. Effect of Iron Chelates. *J. Biol. Chem.* **1990**, *265* (2), 652–659.
(16) Stolze, K.; Udilova, N.; Nohl, H. Spin Trapping of Lipid Radicals with DEPMPO-Derived Spin Traps: Detection of Superoxide, Alkyl and Alkoxyl Radicals in Aqueous and Lipid Phase. *Free Radic. Biol. Med.* **2000**, *29* (10), 1005–1014.
(17) Buettner, G. R. Spin Trapping: ESR Parameters of Spin Adducts 1474 1528V. *Free Radic. Biol. Med.* **1987**, *3* (4), 259–303.
(18) Https://Tools.Niehs.Nih.Gov/Stdb/Index.Cfm.
(19) Makino, K.; Hagiwara, T.; Hagi, A.; Nishi, M.; Murakami, A. Cautionary Note for DMPO Spin Trapping in the Presence of Iron Ion. *Biochem. Biophys. Res. Commun.* **1990**, *172* (3), 1073–1080.

(20) Clement, J.-L.; Gilbert, B. C.; Ho, W. F.; Jackson, N. D.; Newton, M. S.; Silvester, S.; Timmins, G. S.; Tordo, P.; Whitwood, A. C. ChemInform Abstract: Use of a Phosphorylated Spin Trap to Discriminate Between the Hydroxyl Radical and Other Oxidizing Species. *ChemInform* **1998**, *29* (49), 1715–1717.
(21) Tuccio, B.; Lauricella, R.; Fréjaville, C.; Bouteiller, J.-C.; Tordo, P. Decay of the Hydroperoxyl Spin Adduct of 5-Diethoxyphosphoryl-5-Methyl-1-Pyrroline N-Oxide: An EPR Kinetic Study. *J Chem Soc Perkin Trans 2* **1995**, No. 2, 295–298.
(22) Triquigneaux, M.; Charles, L.; André-Barrès, C.; Tuccio, B. Ene-Reaction between a Dienolic Compound and 2-Methyl-2-Nitrosopropane: An EPR-MS Study. *Tetrahedron Lett.* **2010**, *51* (48), 6220–6223.
(23) Forrester, A. R.; Hepburn, S. P. Spin Traps. A Cautionary Note. *J. Chem. Soc. C Org.* **1971**, 701.
(24) Eberson, L. 'Inverted Spin Trapping'. Reactions between the Radical Cation of α-Phenyl-N-Tert-Butylnitrone and Ionic and Neutral Nucleophiles. *J Chem Soc Perkin Trans 2* **1992**, No. 10, 1807–1813.
(25) Scott, M. J.; Billiar, T. R.; Stoyanovsky, D. A. N-Tert-Butylmethanimine N-Oxide Is an Efficient Spin-Trapping Probe for EPR Analysis of Glutathione Thiyl Radical. *Sci. Rep.* **2016**, *6* (1).
(26) Kuresepi, S.; Vileno, B.; Turek, P.; Lepoittevin, J.-P.; Giménez-Arnau, E. Potential of EPR Spin-Trapping to Investigate *in Situ* Free Radicals Generation from Skin Allergens in Reconstructed Human Epidermis: Cumene Hydroperoxide as Proof of Concept. *Free Radic. Res.* **2018**, 1–9.
(27) Stoll, S.; Schweiger, A. EasySpin, a Comprehensive Software Package for Spectral Simulation and Analysis in EPR. *J. Magn. Reson.* **2006**, *178* (1), 42–55.
(28) Hagen, W. R. *Biomolecular EPR Spectroscopy*; CRC Press: Boca Raton, 2009.
(29) Winterbourn, C. C. Toxicity of Iron and Hydrogen Peroxide: The Fenton Reaction. *Toxicol. Lett.* **1995**, *82–83*, 969–974.
(30) Pazos, M.; Andersen, M. L.; Skibsted, L. H. Amino Acid and Protein Scavenging of Radicals Generated by Iron/Hydroperoxide System: An Electron Spin Resonance Spin Trapping Study. *J. Agric. Food Chem.* **2006**, *54* (26), 10215–10221.
(31) Edmonds, P. D.; Sancier, K. M. Evidence for Free Radical Production by Ultrasonic Cavitation in Biological Media. *Ultrasound Med. Biol.* **1983**, *9* (6), 635–639.
(32) Liu, K. J.; Miyake, M.; Panz, T.; Swartz, H. Evaluation of DEPMPO as a Spin Trapping Agent in Biological Systems. *Free Radic. Biol. Med.* **1999**, *26* (5–6), 714–721.
(33) Janzen, E. G.; Kotake, Y.; Hinton, R. D. Stabilities of Hydroxyl Radical Spin Adducts of PBN-Type Spin Traps. *Free Radic. Biol. Med.* **1992**, *12* (2), 169–173.
(34) Karoui, H.; Chalier, F.; Finet, J.-P.; Tordo, P. DEPMPO: An Efficient Tool for the Coupled ESR-Spin Trapping of Alkylperoxyl Radicals in Water. *Org. Biomol. Chem.* **2011**, *9* (7), 2473–2480.
(35) Rehorek, D.; Janzen, E. G. Spin-Trapping von Radikalen bei der Zersetzung aromatischer Diazoniumsalze mittels Ultraschall. *J. Fr Prakt. Chem.* **1984**, *326* (6), 935–940.
(36) Davies, M. J.; Slater, T. F. Studies on the Photolytic Breakdown of Hydroperoxides and Peroxidized Fatty Acids by Using Electron Spin Resonance Spectroscopy. Spin Trapping of Alkoxyl and Peroxyl Radicals in Organic Solvents. *Biochem. J.* **1986**, *240* (3), 789–795.
(37) Ueda, J.; Saito, N.; Ozawa, T. ESR Spin Trapping Studies on the Reactions of Hydroperoxides with Cu (II) Complex. *J. Inorg. Biochem.* **1996**, *64* (3), 197–206.

(38) Taffe, B. G.; Takahashi, N.; Kensler, T. W.; Mason, R. P. Generation of Free Radicals from Organic Hydroperoxide Tumor Promoters in Isolated Mouse Keratinocytes. Formation of Alkyl and Alkoxyl Radicals from Tert-Butyl Hydroperoxide and Cumene Hydroperoxide. *J. Biol. Chem.* **1987**, *262* (25), 12143–12149.
(39) Bar-On, P.; Mohsen, M.; Zhang, R.; Feigin, E.; Chevion, M.; Samuni, A. Kinetics of Nitroxide Reaction with Iron(II). *J. Am. Chem. Soc.* **1999**, *121* (35), 8070–8073.
(40) Baicu, S. C.; Taylor, M. J. Acid–base Buffering in Organ Preservation Solutions as a Function of Temperature: New Parameters for Comparing Buffer Capacity and Efficiency. *Cryobiology* **2002**, *45* (1), 33–48.
(41) Davies, M. J.; Fu, S.; Dean, R. T. Protein Hydroperoxides Can Give Rise to Reactive Free Radicals. *Biochem. J.* **1995**, *305* (2), 643–649.
(42) Augusto, O.; Ortiz de Montellano, P. R.; Quintanilha, A. Spin-Trapping of Free Radicals Formed during Microsomal Metabolism of Ethylhydrazine and Acetylhydrazine. *Biochem. Biophys. Res. Commun.* **1981**, *101* (4), 1324–1330.
(43) Salamone, M.; Bietti, M.; Calcagni, A.; Gente, G. Phenyl Bridging in Ring-Substituted Cumyloxyl Radicals. A Product and Time-Resolved Kinetic Study †. *Org. Lett.* **2009**, *11* (11), 2453–2456.
(44) Guo, Q.; Qian, S. Y.; Mason, R. P. Separation and Identification of DMPO Adducts of Oxygen-Centered Radicals Formed from Organic Hydroperoxides by HPLC-ESR, ESI-MS and MS/MS. *J. Am. Soc. Mass Spectrom.* **2003**, *14* (8), 862–871.
(45) Kao, D.; Chaintreau, A.; Lepoittevin, J.-P.; Giménez-Arnau, E. Mechanistic Studies on the Reactivity of Sensitizing Allylic Hydroperoxides: Investigation of the Covalent Modification of Amino Acids by Carbon-Radical Intermediates. *Toxicol. Res.* **2014**, *3* (4), 278–289.
(46) Tinois, E.; Tiollier, J.; Gaucherand, M.; Dumas, H.; Tardy, M.; Thivolet, J. In Vitro and Post-Transplantation Differentiation of Human Keratinocytes Grown on the Human Type IV Collagen Film of a Bilayered Dermal Substitute. *Exp. Cell Res.* **1991**, *193* (2), 310–319.
(47) Bråred Christensson, J.; Matura, M.; Bäcktorp, C.; Börje, A.; Nilsson, J. L. G.; Karlberg, A.-T. Hydroperoxides Form Specific Antigens in Contact Allergy. *Contact Dermatitis* **2006**, *55* (4), 230–237.
(48) Ponec, M.; Boelsma, E.; Gibbs, S.; Mommaas, M. Characterization of Reconstructed Skin Models. *Skin Pharmacol. Physiol.* **2002**, *15* (1), 4–17.
(49) Moriarty-Craige, S. E.; Jones, D. P. Extracellular thiols and thiol/disulfide redox in metabolism. *Annu. Rev. Nutr.* **2004**, *24* (1), 481–509.
(50) Grossi, L. The Mechanism of Oxidation of Aniline by Peroxy-Compounds: Can E.P.R. Spectroscopy Help to Discriminate between One-Electron Transfer and a Nucleophilic Substitution Process? *Res. Chem. Intermed.* **1993**, *19* (8), 697–705.
(51) OECD. *Test No. 439: In Vitro Skin Irritation: Reconstructed Human Epidermis Test Method*; OECD Guidelines for the Testing of Chemicals, Section 4; OECD Publishing, **2015**.
(52) Frejaville, C.; Karoui, H.; Tuccio, B.; Moigne, F. L.; Culcasi, M.; Pietri, S.; Lauricella, R.; Tordo, P. 5-(Diethoxyphosphoryl)-5-Methyl-1-Pyrroline N-Oxide: A New Efficient Phosphorylated Nitrone for the in Vitro and in Vivo Spin Trapping of Oxygen-Centered Radicals. *J. Med. Chem.* **1995**, *38* (2), 258–265.
(53) Timmins, G. S.; Davies, M. J. Free Radical Formation in Murine Skin Treated with Tumour Promoting Organic Peroxides. *Carcinogenesis* **1993**, *14* (8), 1499–1503.

(54) Barbati S, Clément JL, Olive G, Roubaud V, Tuccio B, Tordo P. In Minisci F. Free Radicals in Biology and Environment.

Chapter 3

In-cellulo studies with dendritic cells

The Keap1-Nrf2 activation pathway

Sensitizers derived from oxidation processes are often potent oxidants that could be able to interfere with the cell redox balance. There is a belief that oxidative stress induced by these compounds on epithelial cells may produce a new danger signal, synergistic with reactivity and thus would help to explain the strong allergenic activity.

The aim here was to evaluate how the inherent oxidative properties of allylic hydroperoxides, together with their reactivity, behave as danger signal and translate into a biological response using the activation of the Keap1-Nrf2 cellular sensor pathway in dendritic cells, involved in detoxification and antioxidant effects.

These studies have been conducted in collaboration with Pr Saadia Kerdine-Römer, Allergy, Immunotoxicology and Immunopathology Unit, Université Paris Sud, INSERM UMR 996.

Previous studies conducted with this team showed that allergens, depending on their chemical structure, may activate the Nrf2 pathway in dendritic cells.[1]

Compounds used for the studies were linalool (Lina), limonene (Limo), cumene (Cum), 1-*tert*-butyl-1-cyclohexene (Mod) and their respective allylic hydroperoxides, the cyclic model hydroperoxide (Mod-OOH) that has been used as model for 15-hydroperoxy abietic acid studies, cumene hydroperoxide (Cum-OOH), limonene hydroperoxide (Limo-OOH) and linalool hydroperoxides (Lina-OOHs) (Figure 3.1).[2]

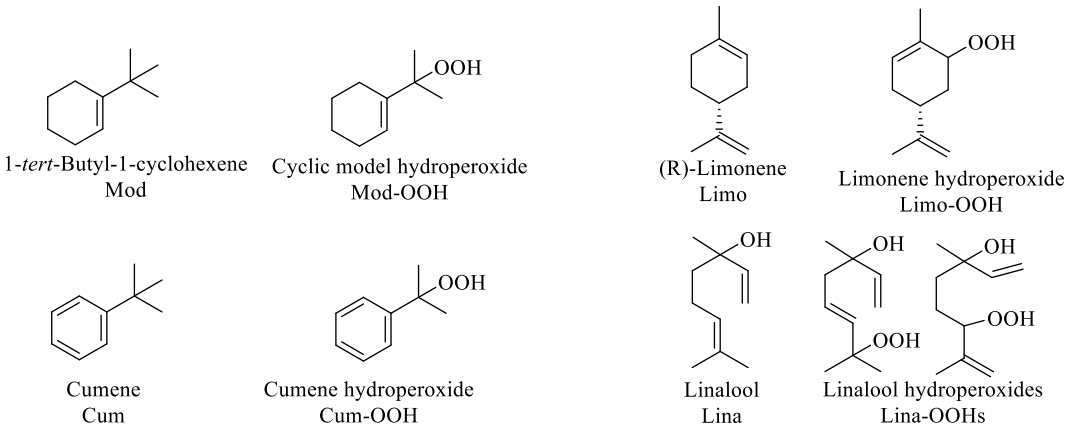

Figure 3.1: Allylic hydroperoxides used for Keap1-Nrf2 cellular sensor pathway activation studies

1. THE KEAP1-NRF2 PATHWAY

Figure 3.2 shows the general mechanism of the Keap1-Nrf2 pathway, which is the major regulator of cytoprotective responses to oxidative and electrophilic stress.

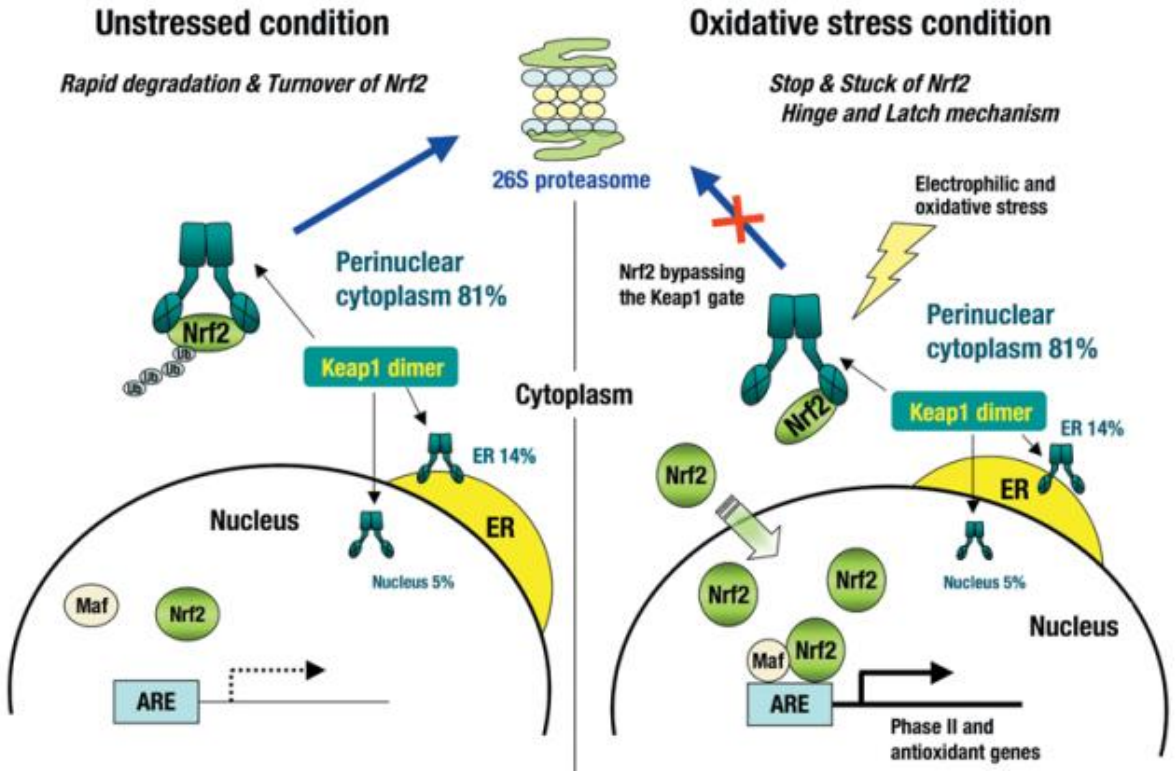

Figure 3.2: Keap1-Nrf2 signaling pathway under unstressed and oxidative stress conditions[1]

Shortly, without oxidative stress, Nrf2 (Nuclear Factor Erythroid 2-Related Factor 2) is linked to Keap1 (Kelch-like ECH-associated protein 1) by thiol groups from amino acids present in Keap1.[3] These thiol groups are very sensitive to oxidative stress and can recognize it leading to the release of Nrf2. The free Nrf2 is then able to migrate to the nucleus, bind to a Maf (musculoaponeurotic fibrosarcoma) protein and then the heterodimer access the antioxidant response element (ARE).[4]

The THP-1 cell line, used as surrogate of dendritic cells, also uses the Keap1-Nrf2 system in order to keep cell homeostasis. Keap1 is the cytosolic repressor of Nrf2. In unstressed conditions Nrf2 is sequestered by the Kelch-like EC-associated protein 1 (Keap1) homodimer in the cytoplasm. Its expression is maintained to be low and ubiquitinated proteasomal degradation occurs. Under oxidative or electrophilic stress, cysteine residues of Keap1 are oxidized changing the homodimer 3D-configuration. Nrf2 degradation is then interrupted and a rapid cytoplasmic accumulation occurs.[5] Nrf2 translocates into the nucleus and combines with

small Maf proteins. The new heterodimer activates the antioxidant response element (ARE)-dependent gene expression, leading to the transcription of genes involved in detoxification, such as heme oxygenase-1 (*ho-1*) or NADPH-quinone oxidoreductase 1 (*nqo1*) and pro-inflammatory cytokines (*il-8*).[6] It has been shown that Nrf2 can be activated by different haptens.[1,7]

We used the THP-1 cell line as a model of dendritic cells in order to study the activation of the Keap1-Nrf2 pathway by our target compounds. The idea was to follow the genotype and phenotype of these cells exposed to the hydroperoxides and to evaluate the oxidative stress produced by allergenic allylic hydroperoxides on the THP-1 cell line.

2. TARGET COMPOUNDS SYNTHESES

Target compounds are shown in Figure 3.1. Their oxygenated and carbon radical intermediates could trigger the Keap1-Nrf2 antioxidant response in THP-1 cells.

Cum, Cum-OOH, Limo, Lina and Mod were purchased from Sigma-Aldrich (Saint Quentin Fallavier, France). Mod-OOH was synthesized as described by Lepoittevin and Karlberg.[8] The synthesis started from 1-acetyl-1-cyclohexene which was transformed to the tertiary alcohol Mod-OH by addition of methyllithium. Then, a solution of H_2O_2 (35 % in water) in acidic conditions gave the hydroperoxide Mod-OOH (Figure 3.3).

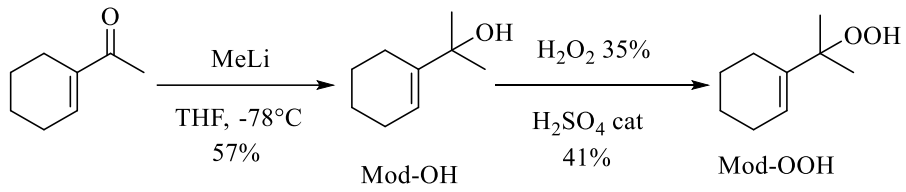

Figure 3.3: Mod-OOH synthesis as described by Lepoittevin and Karlberg[8]

Limo-OOH and Lina-OOHs were synthesized as described by Kao *et al*.[9] Only one step was needed to obtain Limo-OOH (Figure 3.4). (-)-Carveol was treated with an aqueous solution of hydrogen peroxide (35 %) in presence of a catalytic amount of concentrated sulfuric acid. The obtained Limo-OOH derived from R-(+)-limonene (Limo), was purified by column chromatography on neutralized silica.

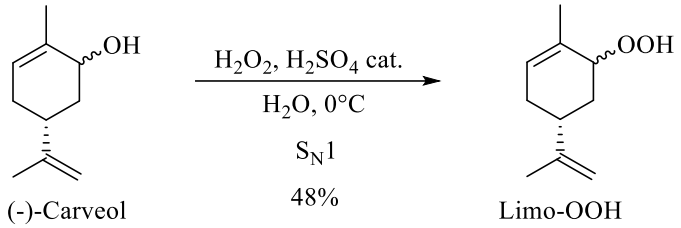

Figure 3.4: Synthesis of Limo-OOH derived from autoxidation of R-(+)-limonene (Limo)

Synthesis of the mixture of Lina-OOHs is shown in Figure 3.5. The ene-Schenck reaction on linalool afforded the mixture Lina-7-OOH/Lina-6-OOH with a yield of 92 % (ratio 2:3).

In order to isolate these two position isomers, a method was developed in the laboratory by Kao *et al*.[9] It consisted on a selective chemical derivatization of the allylic hydroperoxide Lina-7-OOH by meaning of introducing a protective group.

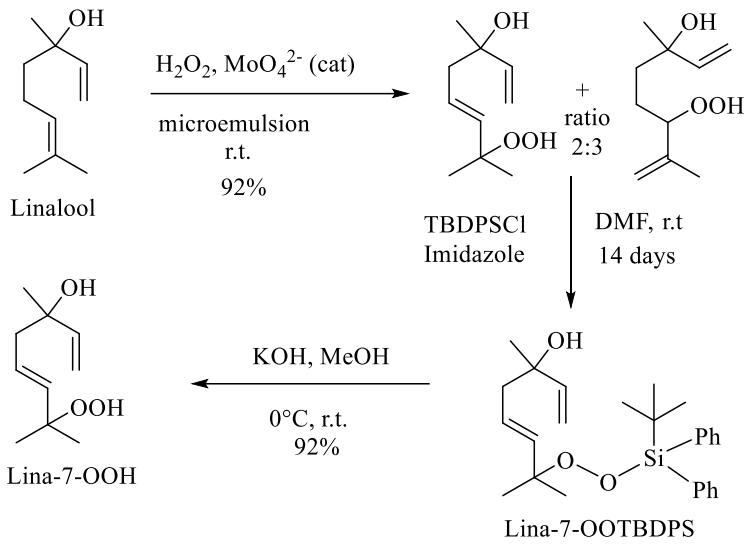

Figure 3.5: Chemical derivatization allowing to obtain single isomer Lina-7-OOH[9]

The chemical derivatization was carried out with *tert*-butyl(chloro)diphenylsilane and only Lina-7-OOH was protected.

Deprotection of the peroxy silane Lina-7-OOTBDPS was carried out in the presence of a methanolic solution of potassium hydroxide making it possible to obtain Lina-7-OOH in a yield of 92% over the two last steps. The methodology was reproducible. However, even if the global yield of the desired hydroperoxide Lina-7-OOH was good enough, a drawback was that it was not possible to obtain Lina-6-OOH inexplicably lost in the reaction.

In order to obtain enough amounts of both hydroperoxides for the *in cellulo* assays, we established a collaboration with Dr. Aurélie Urbain form the Laboratoire d'Innovation Thérapeutique (Faculté de Pharmacie, Université de Strasbourg CNRS UMR 7200) to try to isolate the compounds from the mixture by high performance liquid chromatography (HPLC).

An HPLC analytical method published by Calandra *et al*. was applied to the mixture of linalool hydroperoxides and detected Lina-7-OOH and Lina-6-OOH. An HPLC chemiluminescence detection method was employed with a C_{18} Luna column and a gradient combining methanol and acetonitrile (Figure 3.6).

time (min)	CH_3CN	MeOH	H_2O
0	10	40	50
8	10	40	50
10	45	5	50
30	45	5	50
45	45	50	5
60	45	50	5

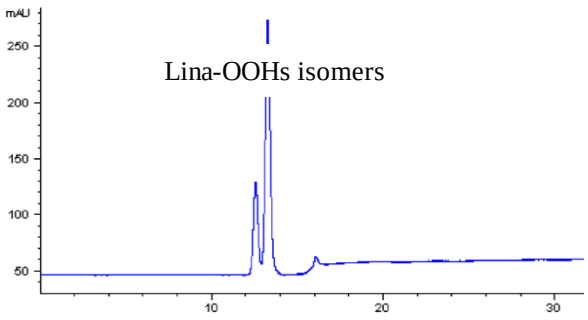

Figure 3.6: Calandra *et al*. HPLC analytical methodology gradient[10]

By applying this methodology to a Kinetex C_{18} column (Kinetex C_{18}, 100Å, 100 × 3 mm, 2.6 µm) we were not able to see both compounds separated (Figure 3.7).

time (min)	CH_3CN	MeOH	H_2O
0	10	40	50
0.4	10	40	50
4.3	45	5	50

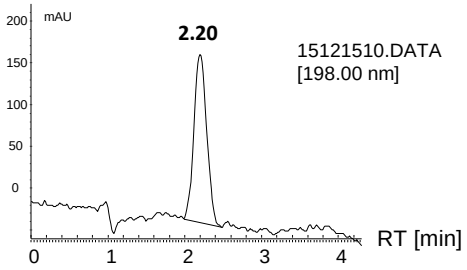

Figure 3.7: Use of the C_{18} Kinetex column

The combination of three solvents, acetonitrile/methanol/water, didn't allowed to obtain the isomer isolation from the mixture neither. After several assays using acetonitrile/water as the mobile phase it was possible to see the separation of the two isomers with a resolution factor of 1.46 and in less than 5 minutes (Figure 3.8).

Time (min)	CH_3CN	H_2O
0	15	85
3	25	75
5	38	62
6	38	62

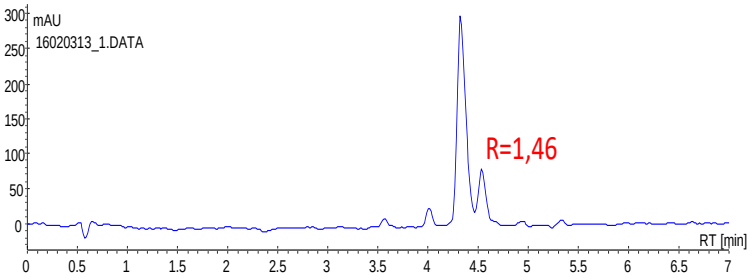

Figure 3.8: Three successive injections of the isomers mixture

Based on these results, the purification was carried out on an Axia Phenomenex column (100 × 21.2 mm; 5 µm) on a freshly synthesized sample of Lina-OOHs (Figure 3.9).

The first tests indicated that no more than 10 µL of the sample should be injected. Otherwise there was saturation of the column, and therefore of the signal. The chosen method was:

time (min)	CH_3CN	H_2O
0	12	88
3	25	75
5	37	63
5,5	37	63

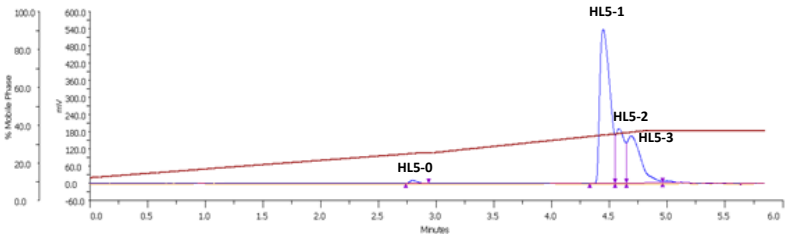

Figure 3.9: Three successive injections of the isomers mixture on C_{18} preparative column

The experience was done at 22°C and with a 25 mL/min debit. The presence or absence of formic acid in the solvent did not change the resolution of the separation. Four peaks were detected in relation to the two observed using the Kinetex analytical column.

The four peaks were collected and stored at -80 ° C (2 times separately). They were extracted with petroleum ether (3 × 20 mL), the organic phase was dried over anhydrous Na_2SO_4 for 20 minutes, then filtered and evaporated under reduced pressure. The product obtained was submitted to NMR analysis. Fractions HL5-0, HL5-1 and HL5-3 were taken up in deuterated chloroform, the HL5-2 fraction in deuterated methanol and analyzed by NMR. We never observed the spectra of Lina-6-OOH or Lina-7-OOH. It looked like the compounds were degraded. Thus, it was finally decided to use the mixture of Lina-7-OOH and Lina-6-OOH for the biological studies.

3. RESULTS AND DISCUSSION

The accumulation of protein Nrf2 and the expression of antioxidant genes (*ho-1, il8,* and *nqo1*) were measured by Western Blot and polymerase chain reaction (PCR) respectively.

During the two and a half weeks I spent in the laboratory Allergy, Immunotoxicology and Immunopathology (INSERM, UMR 996) in Paris, we worked on the development of the experimental conditions of the model and the cytotoxicity of the hydroperoxides (Limo-OOH and Lina-OOHs) on the THP-1 cell-line.

Table 3.1: Cytotoxicity for the terpene chemicals based on trypan blue assays

	Cytotoxicity > 30 % (mM)	**Tested concentrations (mM)**
Lina	2 mM	0.25, 0.5, 1
Lina-OOH (6+7)	1 mM	0.25, 0.5, 1
Limo	3 mM	0.5, 1, 1.5
Limo-OOH	1.5 mM	0.5, 1, 1.5

In the next sections results on the activation of the Keap1-Nrf2 pathway are described.

3.1 *Nrf2 cytoplasmic accumulation studies: Four molecules and their respective hydroperoxides*

The ARE is the promotor region of antioxidant genes. Nrf2 is a transcription factor that will bind to this ARE promoter sequence and induce cytoplasm protective genes expression such as (*ho-1*) and phase II detoxification genes (*nqo-1*) as well as pro-inflammatory cytokines (*il-8*).

After exposure of the THP-1 cell line to the mixture Lina-6-OOH and Lina-7-OOH (1 mM in acetonitrile/water 25/75), an increase of Nrf2 was observed during the first 6 hours, then a decrease at 8 hours (data not shown). In contrast to the parent compound linalool, the hydroperoxides mixture seemed to induce the accumulation of Nrf2 in THP-1 cells (Figure 3.10). A strong protein accumulation of Nrf2 was observed after 6 hours exposure with Lina-6-OOH and Lina-7-OOH (1 mM mixture in acetonitrile/water, ratio 2:3) while we didn't observe this accumulation with Lina in comparison with the vehicle assay (acetonitrile/water).

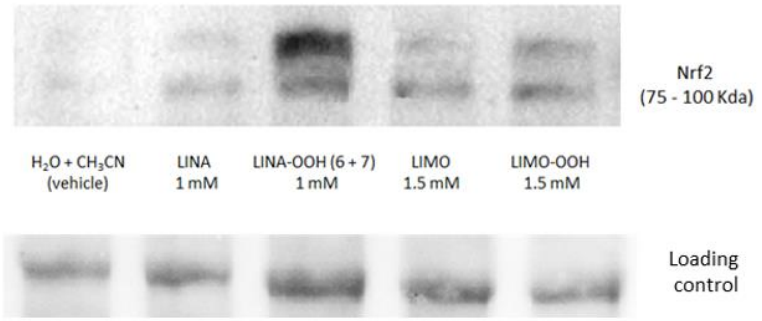

Figure 3.10: Nrf2 cytoplasmic accumulation following exposure of Lina, Limo, Lina-OOHs and Limo-OOH in comparison to vehicle (acetonitrile/water) as negative control and the loading control

These results have been published by Raffalli *et al*. that also tested Limo and Limo-OOH at 1.5 mM concentration and showing a not so strong Nrf2 accumulation compared to Lina-OOHs.[11] Also, after exposure to Limo-OOH (1 mM in acetonitrile/water 25/75), no increase of Nrf2 was observed during the exposure from 2 to 8 hours. Compared to the parent compound limonene, the hydroperoxide of limonene didn't seemed to induce the accumulation of Nrf2 in THP-1 cells (Figure 3.11).

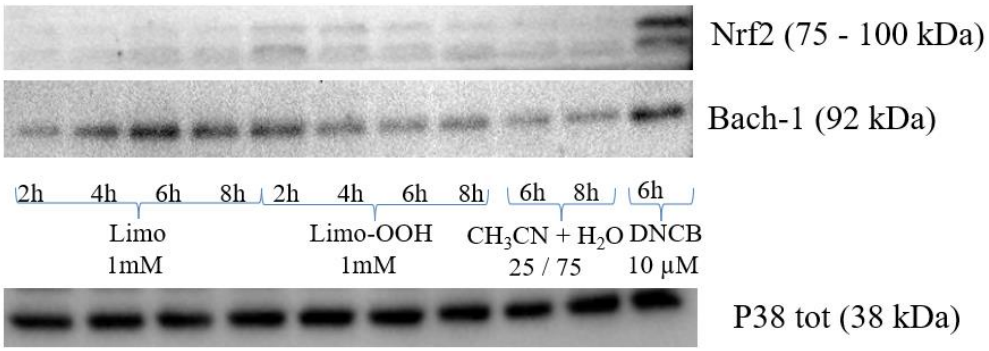

Figure 3.11: Nrf2 cytoplasmic accumulation following exposure of Limo and Limo-OOH, in comparison to Bach-1 (Nrf2 repressor), 2,4-dinitrochlorobenzene (DNCB) as positive control, vehicle (acetonitrile/water) as negative control and the loading control p38 tot

There was presence of Bach-1 in cells stimulated with Limo (1 mM) with a decrease after 6 hours exposure. Bach-1 was less present in cells stimulated with the Limo-OOH (1 mM), which was in line with the results observed for the accumulation of Nrf2.

A strong protein accumulation of Nrf2 was observed after 6 hours exposure with DNCB while we didn't observe this accumulation with Limo (1 mM) in comparison with the vehicle assay (acetonitrile/water).

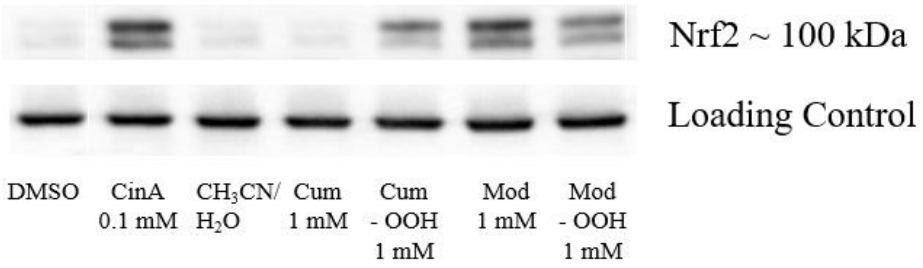

Figure 3.12: Nrf2 cytoplasmic accumulation following exposure of Cum and Mod and their respective hydroperoxides Cum-OOH and Mod-OOH, in comparison cinnamaldehyde (CinA) as positive control in DMSO (vehicle), vehicle (acetonitrile/water) as negative control and the loading control

After exposure of the THP-1 cell line for 6 hours to the hydroperoxide Cum-OOH and Mod-OOH (1 mM in acetonitrile/water), an increase of Nrf2 was observed for both hydroperoxides. In contrast to the parent compound cumene, the hydroperoxides of cumene seemed to induce the accumulation of Nrf2 in THP-1 cells (Figure 3.12). Surprisingly a strong protein accumulation of Nrf2 was observed after exposure with Mod and Mod-OOH while we didn't observe this accumulation for negative controls. DMSO and CH_3CN/H_2O were used as negative controls, as they were used to dissolve the target compounds.

Nrf2 DNA binding is an experience showing the activation of the transcription of the ARE genes. A three-fold factor Nrf2 binding ARE was observed after 6 hours exposure with Lina-6-OOH/Lina-7-OOH (1 mM mixture in acetonitrile/water, ratio 2:3), Cum-OOH (1 mM), Mod (1 mM) and Mod-OOH (1 mM) compared to Lina (1 mM) and Cum (1 mM) exposure. Those compounds induced accumulation and DNA binding of Nrf2, whereas Limo (1.5 mM), Limo-OOH (1.5 mM) and Cum didn't. A significant difference in accumulation wasn't observed with the Limo (1.5 mM) and Limo-OOH (1.5 mM) compared to the vehicle (Figure 3.13).

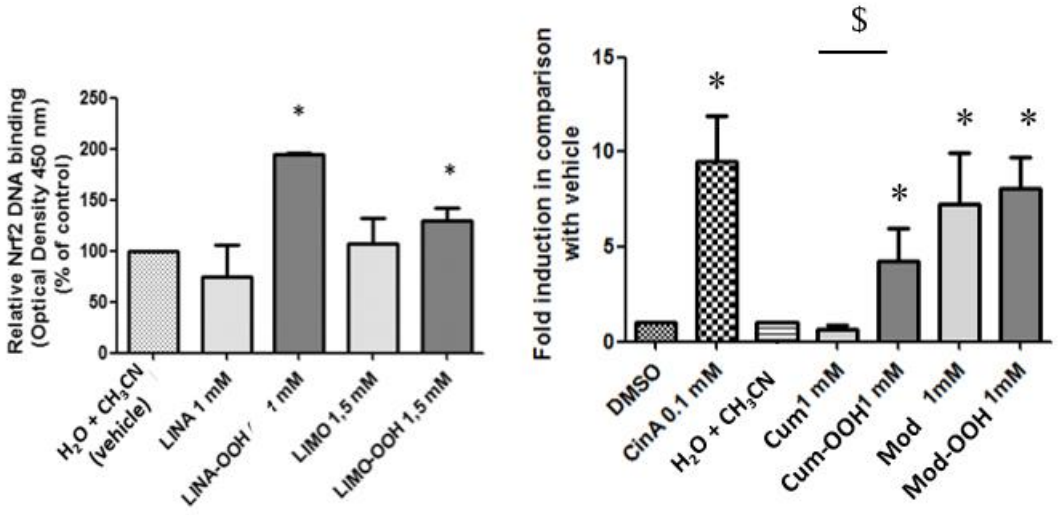

Figure 3.13: Nrf2 protein binding ARE, in comparison with cinnamaldehyde (CinA) as positive control, vehicle (acetonitrile) as negative control and the loading control DMSO

No difference in protein accumulation of Nrf2 was observed after exposure with Mod-OOH (1 mM) and Mod (1 mM), but the activation of the Mod (1 mM) could use a different way than the one used by the hydroperoxides.

3.2 Anti-oxidant gene expression modulation

Induction of the transcription of Nrf2 target genes *ho-1, nqo1* and *il-8* by ROOHs was studied.

As described in the section above, the ROOHs led to the cytoplasm accumulation of Nrf2. Nrf2 plays the role of the transcription factor for over-expression of genes such as *ho-1*, *nqo1* and *il-8*. Lina-6-OOH and Lina-7-OOH (1 mM mixture in acetonitrile/water, ratio 2:3) significantly induced the expression of *ho-1* and *nqo-1* whereas this induction was not observed for Lina (1 mM). *Il-8* was not induced by any molecule in all assays.

Limo-OOH (1.5 mM) didn't induce the expression of *ho-1, nqo1* and *il-8* genes compared to Limo. Furthermore, the same basal gene expression was observed as in the example on Lina exposure. DNCB and *t*BHP (*tert*-butylhydroperoxide) as positive controls underlined the genes overexpression in the case of Lina-OOHs.

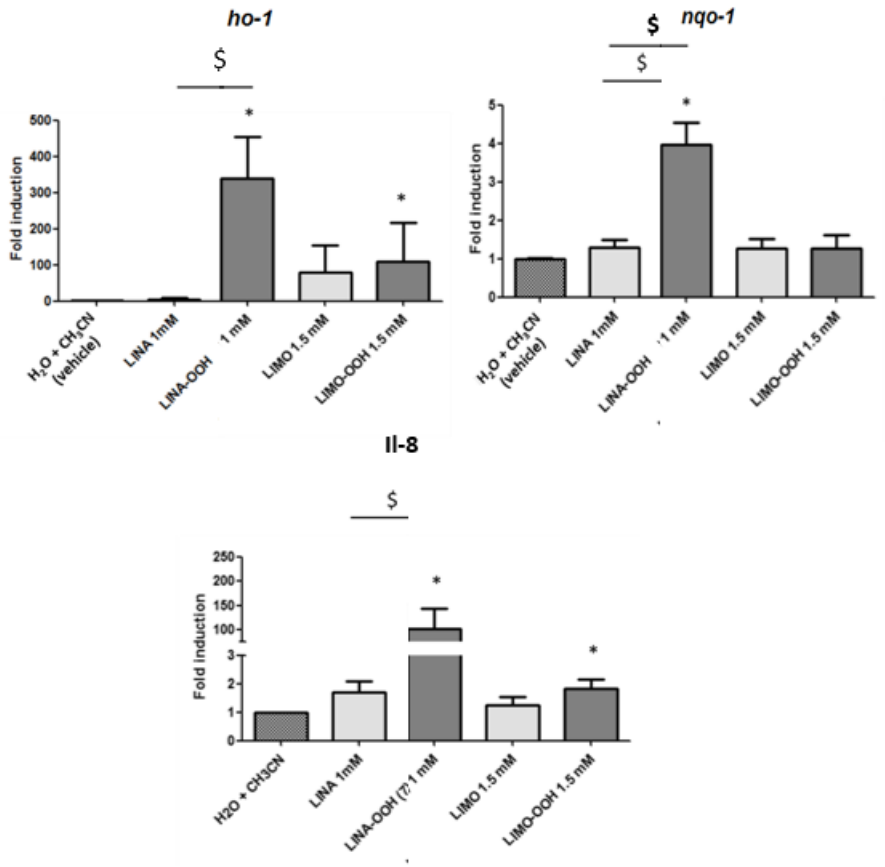

Figure 3.14: Lina, Limo and their respective hydroperoxides Lina-OOHs and Limo-OOH inducing *ho-1*, *nqo-1* and *il-8* genes overexpression

Even if higher concentration of Limo-OOH (1.5 mM) compared to Lina-OOHs (1 mM) was used, no evidence of Nrf2 cytoplasm accumulation, DNA binding or ARE gene over expression was seen. A hypothetical explanation for the different behavior between the biological answers of Lina-OOHs (1 mM) and Limo-OOH (1.5 mM) could lie in the fact that Lina-OOHs (1 mM) can produce more different radical intermediates than Limo-OOH (1.5 mM). It is due to its chemical structure where the possibility of radical rearrangements is less limited than for Limo-OOH (1.5 mM).

Cum-OOH (1 mM) significantly induced the expression of *ho-1*, *nqo-1* and *il-8* while this induction was not observed for Cum in comparison with vehicle (acetonitrile/water).

Finally, Mod-OOH (1 mM) and Mod (1 mM) significantly induced the expression of *ho-1*, *nqo-1* and *il-8*. Surprisingly, Mod was reactive even if no hydroperoxide function is present in its

chemical structure. This suggested that Mod (1 mM) activated the Keap1-Nrf2 pathway by another mechanism to that of the hydroperoxides (Figure 3.15).

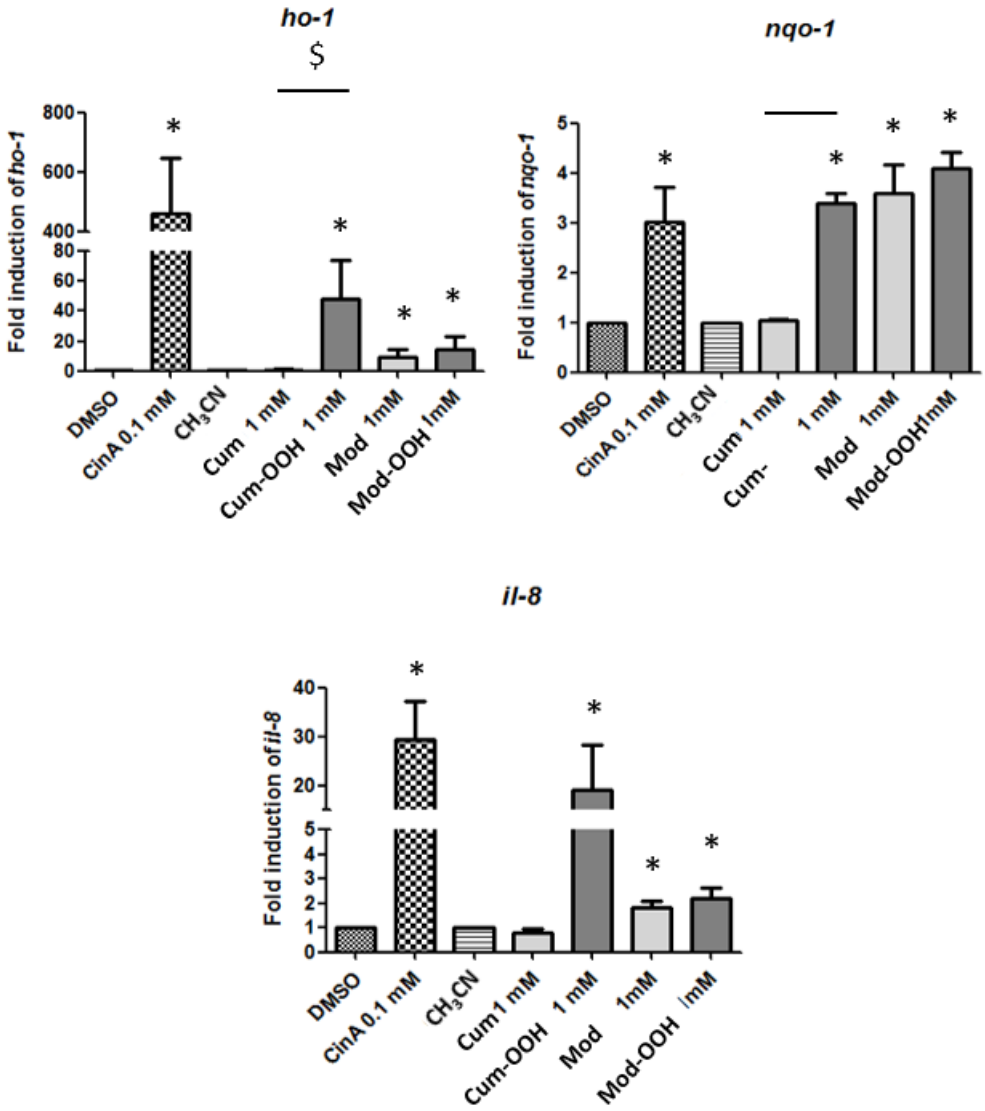

Figure 3.15: Cum, Mod and their respective hydroperoxides Cum-OOH and Mod-OOH inducing *ho-1*, *nqo-1* and *il-8* genes overexpression

4. CONCLUSION

This study underlined that the tested allylic hydroperoxides seemed not to be equal for DC activation in regard to Nrf2 cytoplasmic accumulation. Results showed that Lina and Limo need to be oxidized to activate THP-1 cells. Lina-OOHs (1 mM) seemed to be stronger activators of THP-1 cells than Limo-OOH (1.5 mM). Only the hydroperoxides were able to activate the Nrf2 pathway and to induce the transcription of target genes *ho-1*, *nqo1* and *il-8*, except Mod (1 mM)

that was also activating the Nrf2 pathway surprisingly. According to the results, Lina-OOHs (1 mM), Cum-OOH (1 mM) and Mod-OOH (1 mM) behaved as stronger activators of THP-1 cells than Limo-OOH (1.5 mM). No significant differences between Mod (1 mM) and Mod-OOH (1 mM) were measured. A hypothesis could be that more radical rearrangements could lead to a stronger activation of THP-1 cells and could explain for example why cells are more activated after treatment with Lina-OOHs (1 mM).

Experimental Chapter 3

5. MATERIALS AND METHODS:

Different molecules were tested: linalool (Lina), limonene (Limo), cumene (Cum), 1-*tert*-butyl-1-cyclohexene (Mod) and their respective allylic hydroperoxides, the cyclic model hydroperoxide (Mod-OOH), cumene hydroperoxide (Cum-OOH), limonene hydroperoxide (Limo-OOH) and linalool hydroperoxides (Lina-OOHs)

Chemicals

Tert-butyl hydroperoxide (tBHP), dithiothreitol (DTT), acetonitrile (CH_3CN), (R)-(+)-limonene (LIMO) and linalool (LINA) were all purchased from Sigma-Aldrich (St Quentin-Fallavier, France).

Synthesis of Mod-OH

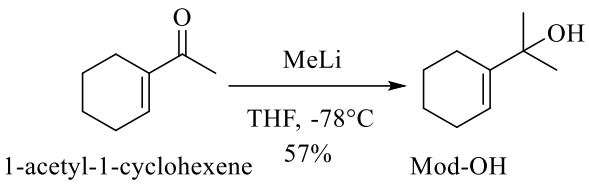

To 1-acetyl-1-cyclohexene (15.5 g, 125 mmol) in tetrahydrofuran (150 mL) was added, at -78 °C, methyllithium (87.5 mL, 140 mmol, 1.6 M in Et_2O). After 2 h stirring at -78 °C, the reaction mixture was allowed to warm up to room temperature. Aqueous NH_4Cl (50 mL) was carefully added and the mixture extracted with ether (3 × 50 mL). Then combined organic layers were dried over magnesium sulfate, filtered, and concentrated under reduced pressure to lead to the crude alcohol, which was purified by column chromatography on silica (petroleum ether/ hexane 9/1) to yield 16.68 g (94 % yield) of pure alcohol (Mod-OH) as a colorless oil.

Formula: $C_9H_{16}O$

Molar mass: 140.23 $g.mol^{-1}$

Cas N°: 25910-97-8

TLC: Rf = 0.26 (petroleum ether/ethyl acetate 9/1): UV, APM/Ce

NMR ^{1}H ($CDCl_3$, δ, ppm):

1.28 (s, 3H, CH_3), 1.31 (s, 3H, CH_3), 1.50-1.67 (m, 5H, CH_2 + OH), 2.02-2.06 (m, 4H, 2 × $=CCH_2$), 5.73 (dd, l H, $^{3}J_{HH}$ = 2.0 Hz, $^{3}J_{HH}$ = 3.6 Hz, =CH).

NMR ^{13}C ($CDCl_3$, δ, ppm):

22.5 (s, $=CHCH_2\mathbf{C}H_2$); 23.5 (s, $=CCH_2\mathbf{C}H_2$); 24.6 (s, 2 × $\mathbf{C}H_3$); 25,5 (s, $=CH\mathbf{C}H_2$); 29.3 (s, $=C\mathbf{C}H_2$); 78.3 (s, $\mathbf{C}(CH_3)_2OH$); 119.1 (s, =**C**H); 144.1 (s, **C**=CH);

Synthesis of Mod-OOH

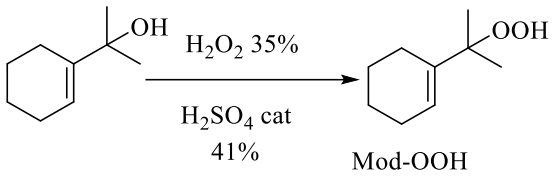

To a solution of hydrogen peroxide (250 mL, 35% in water) was added, at 0 °C, one drop of sulfuric acid (98 %) and Mod-OH (10 g; 71.4 mmol). The reaction mixture was vigorously stirred for 3 hours at °C then extracted with pentane (3 × 200 mL). Combined organic layers were dried over magnesium sulfate, filtered, and evaporated under reduced pressure to give the crude hydroperoxide, which was purified by column chromatography on silica gel (petroleum ether/ hexane 9/1) to give 4.48 g (42 % yield) of the pure hydroperoxide Mod-OOH as a colorless oil.

Formula: $C_9H_{16}O_2$

Molar mass: 156.23 g.mol^{-1}

Cas N°: Not exist

TLC: Rf = 0.3 (petroleum ether/ethyl acetate 9/1): UV, APM/Ce

NMR ^{1}H ($CDCl_3$, δ, ppm):

1.31 (s, 6H, 2 × C**H**$_3$); 1.56-1.68 (m, 4H, $=CHCH_2C\mathbf{H}_2$ + $=CCH_2C\mathbf{H}_2$); 2.00-2.09 (m, 4H, $=CC\mathbf{H}_2$ + $=CHC\mathbf{H}_2$); 5.75 (m, lH, =C**H**); 7.25 (s, lH, OO**H**)

NMR ^{13}C ($CDCl_3$, δ, ppm):

22.2 (s, $=CHCH_2\mathbf{C}H_2$); 23.0 (s, $=CCH_2\mathbf{C}H_2$); 23.8 (s, 2 × $\mathbf{C}H_3$); 24,0 (s, $=CH\mathbf{C}H_2$); 25.2 (s, $=C\mathbf{C}H_2$); 84.6 (s, =**C**H); 123.1 (s, **C**=CH); 139.8 (s, $\mathbf{C}(CH_3)_2OOH$)

Synthesis of Limo-OOH

See Chapter 2. Section 4.3.2

Synthesis of LinaOOHs

See Chapter 2. Section 4.3.3

Chemical treatment

THP-1 cells were cultured for at least 12 hours at 8×10^5 cells/ml in complete medium without 2-mercaptoethanol. On the next day, the cells were seeded in complete medium at 1×10^6 cells/ml and treated with chemicals. CinA was diluted in DMSO and tBHP, terpenes and allylic hydroperoxides in CH_3CN as they were water-insoluble. Final concentrations of solvent in culture media did not exceed 0.1%.

Measurement of cell viability

THP-1 cells were seeded in 24-well plates (1×10^6 cells/ml, 1 ml/well) with various concentrations of each chemical ranging from 0.25 to 1.5 mM for 24 hours (Table 3.1). Cells were washed twice with PBS and harvested cells were incubated with annexin-V-PE and 7-aminoactinomycin D (7-AAD) according to the manufacturer's protocol (BD Biosciences). Cell viability was measured using the FL-3 wavelength on a FACScalibur flow cytometer (Becton Dickinson, Le Pont de Claix, France). Data acquisition was performed using the CellQuest software (BD Biosciences). At least four independent experiments were performed for each chemical.

Immunoblotting

Western blot was performed as previously described.[1] THP-1 cells (10^6 cells/ml, 2 ml/well) were exposed to the test compounds at a subtoxic concentration. Cells were washed twice in cold PBS before lysis in 40 µL of lysis buffer (20 mM Tris pH 7.4, 137 mM NaCl, 2mM EDTA pH 7.4, 2mM sodium pyrophosphate, 1% Triton, 10% glycerol, 1mM PMSF, 1mM Va_3VO_4, 25 mM β-glycerophosphate, 10 µg/ml aprotinin, 10 µg/ml leupeptin and 10 µg/ml pepstatin) and left in ice for 20 min. Then, they were centrifuged at 17600 × g for 20 min at 4°C, before the supernatants were collected. Total protein concentration was evaluated using bicinchoninic acid assay, and equal amounts of denatured proteins (30 µg) were loaded on 12% polyacrylamide gels (TGX Stain-Free FastCast; Bio-Rad Laboratories, Hercules, CA) for approximately 30 min at 300V in running buffer. Stain-free gels were activated by exposure to

UV for 1 min. Proteins were transferred to PVDF membrane (Bio-Rad Laboratories, Hercules, CA) using the Bio-Rad Trans-Blot Turbo Transfer System for 7 min. Total proteins on membranes were detected using the Stain-free method.[12] For the Nrf2/Keap1 analysis pathway, membranes were incubated with antibodies raised against Nrf2 (H-300; Santa Cruz Biotechnology, Heidelberg, Germany). Immunoreactive bands were detected by chemiluminescence (ECL solution, Amersham Biosciences).

Total RNA isolation

THP-1 cells (10^6 cells/ml, 2 ml/well) were exposed to test compounds at a subtoxic concentration for 6 hours. This time point was determined in preliminary experiments and was found to be optimal to study the expression of Nrf2 target genes (data not shown). For the RNA extraction, the Macherey Nagel kit was used according to the manufacturer protocol. Treated cells were washed twice with cold PBS. 350 µL of Lysis Buffer was added to the cell pellet and the tubes were vortexed vigorously. The viscosity was reduced and the lysate was cleared by filtration through a filter, the mixture was added to the filter and the tubes were centrifuged for 1 min at 11000 × g. The filter was discarded and 350 µL of ethanol (70%) was added and mixed by pipetting up and down in order to adjust the RNA binding conditions. The lysate was loaded onto a new column which binds to the RNA and the tubes were centrifuged 30 seconds at 11000 × g. The column was placed in a new tube and 350 µL of Membrane Desalting Buffer was added. The tubes were centrifuged 1 minutes at 11000 × g to dry the membrane. Then the silica membrane was washed three times with different buffers and the RNA eluted in 40 µL of RNAse-free water. Total RNA yield was quantified by spectrophotometry using two dilutions (total RNA diluted at 1:100 and 1:200, two independent measurements).

Reverse transcription

RNA concentrations were adjusted (80 ng/µl for THP-1 cells in 11 µl final volume) and combined with 2 µl of deoxynucleotide triphosphate mixture and 2 µl of 50 µM oligo(dT) primers. Mixes were denatured at 70°C for 10 min and then quickly cooled at 4°C in a Biometra thermocycler (Goettingen, Germany). Reverse transcription was carried out in AMV Reverse Transcriptase Reaction Buffer (Promega, Charbonnières-les-Bains, France) with final concentrations of 2 U/µl of RNase inhibitor (RNasine, Promega) and 0.2 U/µl of AMV Reverse Transcriptase (Promega), and RNase-free water to make up a final volume of 10 µl. The reaction was then performed for 1 h 30 min at 42°C in the thermocycler. A control without reverse

transcriptase was performed to confirm that no DNA contamination had occurred. The final product was stored at −20°C and used in the PCR step.

Analysis of gene expression using real-time PCR

Real-time PCR analysis was performed using the SYBR Green technology on a Biorad CFX96 system. Each reaction consisted of cDNA (1:50 diluted for THP-1 cells in 4 µl final volume of nuclease-free water), 0.5 µM each of the forward and reverse primers (*ho-1* [5′-GGCCTGGCCTTCTTCACCTT-3′ and 5′-GAGGGGCTCTGGTCCTTGGT-3′], *nqo1* [5′-GGGCAAGTCCATCCCAACTG-3′ and 5′-GCAAGTCAGGGAAGCCTGGA-3′], *il*-8 [5′-TCTCTTGGCAGCCTTCCTGA-3′ and 5′-TGGGGTGGAAAGGTTTGG AG-3′], *gapdh* [5′-GGGCAAGTCCATCCCAACTG-3′ and 5′-GCAAGTCAG- GGAAGCCTG GA-3′], or *β-actin* [5′-GGCATCCTCACCCTGAAGTA-3′ and 5′-GCACACGCAGCTCATTGTAG′]), and Sso Fast EvaGreen Supermix (Bio-rad, Marnes la Coquette, France) in a total reaction volume of 10 µl. After 30 seconds at 95°C for Sso7d-fusion polymerase activation, amplification was allowed to proceed up to 44 cycles, each consisting of denaturation at 95°C for 5 seconds and annealing/extension at 62°C for 5 seconds. Six-fold serial dilutions of mixed cDNA (from different samples) were analyzed for each target gene and allowed us to construct linear standard curves, from which the efficiency (*E*) of each PCR reaction was evaluated and taken into account. The SYBR green fluorescence was detected at the end of each elongation cycle, after which a melting curve was assessed to confirm the specificity of the PCR products. The quantification was performed with the Biorad CFX Manager software, and data were analyzed using the delta-delta Ct method (ΔΔCt). The ratio was calculated as the geometrical mean of $(1 + E)^{-\Delta\Delta Ct}$ values, where *E* is the efficiency and ΔΔCt is the target gene expression of treated cells compared with normal levels in untreated cells and corrected using the expression of the reference genes *gapdh* and *β-actin*. Results were expressed as fold induction (i.e., ratio of $(1 + E)^{-\Delta\Delta Ct}$ of treated cells/$(1 + E)^{-\Delta\Delta Ct}$ of vehicle-treated cells).

Measurement of Nrf2 DNA binding

DNA binding was analyzed using specific ELISA-based TransAM kits from Active Motif as described by [13]. After being treated THP-1 cells were lysed in a hypertonic buffer constituted of Non-diet P40 (NP40), 20% glycerol, 20 mM HEPES-KOH pH 7.9, 420 mM NaCl, 1 mM DTT, 1mM sodium orthovanadate, 1 mM pyrophosphate sodium, 125 mM okadaic acid, 62.5 mM EDTA, 40 mM EGTA, 0.5 mM PMSF, 1 g/ml aprotinin, 1 g/ml pepstatin and 1 g/ml

leupeptin. After being left in ice for 20 min, THP-1 cells were centrifuged 20 min at 4°C at 17600 × g. Total protein concentration was evaluated using bicinchoninic acid assay and 20 µg of protein were used for the assay. Total protein cell extracts (20 mg) were incubated for 1 hour in a 96-well plate to which oligonucleotides, containing consensus binding sites for Nrf2, had been immobilized. After washing, the plate was incubated for 1 hour with the appropriate primary Ab, which specifically detected an epitope accessible only when Nrf2 is activated and bound to its cognate oligonucleotide. The plate was then washed and incubated with horseradish peroxidase-conjugated secondary Ab (1:1000) for 1 hour at room temperature. Colorimetric readout was quantified by spectrophotometry at 450 nm. Independent experiments were repeated at least three times.

Literature

(1) Migdal, C.; Botton, J.; El Ali, Z.; Azoury, M.-E.; Guldemann, J.; Giménez-Arnau, E.; Lepoittevin, J.-P.; Kerdine-Römer, S.; Pallardy, M. Reactivity of Chemical Sensitizers Toward Amino Acids In Cellulo Plays a Role in the Activation of the Nrf2-ARE Pathway in Human Monocyte Dendritic Cells and the THP-1 Cell Line. *Toxicol. Sci.* **2013**, *133* (2), 259–274.

(2) Giménez-Arnau, E.; Haberkorn, L.; Grossi, L.; Lepoittevin, J.-P. Identification of Radical Species Derived from Allergenic 15-Hydroperoxyabietic Acid and Insights into the Behaviour of Cyclic Tertiary Allylic Hydroperoxides in Fe(II)/Fe(III) Systems. *Tetrahedron* **2008**, *64* (24), 5680–5691.

(3) Zhang, D. D.; Hannink, M. Distinct Cysteine Residues in Keap1 Are Required for Keap1-Dependent Ubiquitination of Nrf2 and for Stabilization of Nrf2 by Chemopreventive Agents and Oxidative Stress. *Mol. Cell. Biol.* **2003**, *23* (22), 8137–8151.

(4) Kobayashi, A.; Kang, M.-I.; Watai, Y.; Tong, K. I.; Shibata, T.; Uchida, K.; Yamamoto, M. Oxidative and Electrophilic Stresses Activate Nrf2 through Inhibition of Ubiquitination Activity of Keap1. *Mol. Cell. Biol.* **2006**, *26* (1), 221–229.

(5) Itoh, K.; Wakabayashi, N.; Katoh, Y.; Ishii, T.; Igarashi, K.; Engel, J. D.; Yamamoto, M. Keap1 Represses Nuclear Activation of Antioxidant Responsive Elements by Nrf2 through Binding to the Amino-Terminal Neh2 Domain. *Genes Dev.* **1999**, *13* (1), 76–86.

(6) Moi, P.; Chan, K.; Asunis, I.; Cao, A.; Kan, Y. W. Isolation of NF-E2-Related Factor 2 (Nrf2), a NF-E2-like Basic Leucine Zipper Transcriptional Activator That Binds to the Tandem NF-E2/AP1 Repeat of the Beta-Globin Locus Control Region. *Proc. Natl. Acad. Sci. U. S. A.* **1994**, *91* (21), 9926–9930.

(7) Natsch, A.; Emter, R. Nrf2 Activation as a Key Event Triggered by Skin Sensitisers: The Development of the Stable KeratinoSens Reporter Gene Assay. *ATLA* **2016**, *44* (5), 443–451.

(8) Lepoittevin, J. P.; Karlberg, A. T. Interactions of Allergenic Hydroperoxides with Proteins: A Radical Mechanism? *Chem. Res. Toxicol.* **1994**, *7* (2), 130–133.

(9) Kao, D.; Chaintreau, A.; Lepoittevin, J.-P.; Giménez-Arnau, E. Synthesis of Allylic Hydroperoxides and EPR Spin-Trapping Studies on the Formation of Radicals in Iron Systems as Potential Initiators of the Sensitizing Pathway. *J. Org. Chem.* **2011**, *76* (15), 6188–6200.

(10) Calandra, M. J.; Impellizzeri, J.; Wang, Y. An HPLC Method for Hydroperoxides Derived from Limonene and Linalool in Citrus Oils, Using Post-Column Luminol-Mediated Chemiluminescence Detection: An HPLC Method for Limonene and Linalool Hydroperoxides. *Flavour Fragr. J.* **2015**, *30* (2), 121–130.

(11) Raffalli, C.; Clouet, E.; Kuresepi, S.; Damiens, M.-H.; Lepoittevin, J.-P.; Pallardy, M.; Ferret, P.-J.; Giménez-Arnau, E.; Kerdine-Römer, S. Editor's Highlight: Fragrance Allergens Linalool and Limonene Allylic Hydroperoxides in Skin Allergy: Mechanisms of Action Focusing on Transcription Factor Nrf2. *Toxicol. Sci.* **2018**, *161* (1), 139–148.

(12) Gilda, J. E.; Gomes, A. V. Stain-Free Total Protein Staining Is a Superior Loading Control to b-Actin for Western Blots. *Anal. Biochem.* **2013**, *440* (2), 186–188.

(13) Macoch, M.; Morzadec, C.; Génard, R.; Pallardy, M.; Kerdine-Römer, S.; Fardel, O.; Vernhet, L. Nrf2-Dependent Repression of Interleukin-12 Expression in Human Dendritic Cells Exposed to Inorganic Arsenic. *Free Radic. Biol. Med.* **2015**, *88* (Part B), 381–390.

Overview and perspectives

ACD is a disease widespread in the population, induced by repeated contact with a chemical compound that is able, after penetration into the epidermis, to chemically modify skin proteins.[1] Chemically modified proteins are treated by DCs, playing the role of antigen presenting cells in the epidermis. DCs, expressing the MHC II, will present the modified peptides to T lymphocytes in the local lymph nodes. This will generate selective activation of T lymphocytes having the specific receptor of the presented peptide modification on their surface. After a second contact with the same allergen specific T lymphocytes are reactivated and will generate an immune reaction that will produce clinical symptoms such as edema eczema and erythema in the zone where allergen was in contact with the epidermis.[2]

Allergen or haptens are xenobiotics with low molecular weight (less than 1000 Da), capable of penetrating the first layer of the epidermis. In the epidermis these molecules can react with side chains amino acids through the formation of stable covalent bond. The mechanism commonly accepted for this step, forming the hapten-protein complex, is a two electrons mechanism. In general, allergenic compounds contain electrophilic chemical functions that react with nucleophilic side chains of amino acids. However, in the case of allergenic allylic hydroperoxides no electrophilic function is present and one electron radical mechanisms are suspected.[3] This Ph.D. work focused on the comprehension of skin sensitization mechanisms to allylic hydroperoxides derived from autoxidation of terpenes. More precisely to Lina-OOHs and Limo-OOH identified as potent skin sensitizers derived from autoxidation of linalool and limonene, respectively, widely used for their odorant properties.[4,5] The main goal was to evaluate the influence of radical mechanisms in the interaction between these allylic hydroperoxides and proteins.

The first part of this work was to synthesize 5-(^{13}C)-Lina-OOHs and 4-(^{13}C)-Lina-OOHs to study their behavior in presence of some amino acids prompt to react by radical mechanisms. The synthetic pathways developed in order to synthesize 5-(^{13}C)-Lina-OOHs and 4-(^{13}C)-Lina-OOHs are exposed in the first chapter. The mixture of 5-(^{13}C)-Lina-OOHs was synthesized in a nine-steps synthesis with a global yield of 3.8 %. The mixture of 4-(^{13}C)-Lina-OOHs synthesized in six-steps synthesis with a global yield of 9.5 %. Reactivity studies with several amino acids were then followed up by mono-dimensional ^{13}C-NMR and heteronuclear bi-dimensional ^{1}H-^{13}C-NMR (HSQC and HMBC). Only reaction with the side chain of *N*-acetyl-L-cysteine methyl ester was observed, and a variety of hypothetical compounds was obtained. Some hypothesis of the exact structures of these compounds have been proposed.

The second part of this work, was focused on the evaluation and characterization of free radicals (oxygen and carbon-centered) generation from target compounds. EPR spectroscopy combined with the spin-trapping technique was used. Spin-traps used were PBN, DMPO and DEPMPO. First trials were done in solution by using Fe (II) as radical initiator as it is suspected to play a role in the *in vivo* hydroperoxides degradation.[6] In second part of the study, we developed the model to study the *in situ* generation of these radicals on a 3D-reconstructed human epidermis (RHE) model (Episkin^{TM}). No Fe (II) radical initiator was used here to be closer to a real-life scenario exposure of the skin. Carbon-centered radicals, peroxyl and allyloxyl radicals, derived from allylic hydroperoxides (Lina-OOHs, Limo-OOH and Cum-OOH) were identified in solution and in the RHE environment. In solution, a more extensive generation of radicals was seen compared to RHE. However in both systems oxygen-centered, and carbon-centered radicals were observed, proving the crucial role of radical mechanisms.[7] Control experiments in RHE suggest that radicals observed are derived from the ROOHs themselves and not from biomolecules radical degradation in RHE. However, further investigations are necessary to confirm this. These RHE results could be in agreement with reported animal and clinical experimentations that have ruled out the existence of cross-reactivity between different allergenic hydroperoxides.[8] These studies confirmed that immune responses to the antigenic hapten-protein complex are necessarily specific. Carbon-centered, allyloxyl and organic peroxyl radicals observed in the RHE could form specific complexes which is not the case of the hydroxyl radical.

The third part of this work was focused on the activation of the Nrf2-Keap1 cellular pathway in DCs by allylic hydroperoxides. Lina-OOHs, Limo-OOH, Mod-OOH and Cum-OOH seemed to activate this pathway. However, it also appeared that they were not equal for DCs activation regarding Nrf2 cytoplasmic accumulation because Limo-OOH seemed not to be activating it. They also induced the transcription of target genes *ho-1, nqo1* and *il-8*, except Mod that was also activating the Nrf2 pathway.[9]

The futures perspectives of the present work are as various as promising to decipher how molecular phenomena occur in ACD caused by allylic hydroperoxides. Firstly, reactivity studies between 5-(^{13}C)-Lina-OOHs and 4-(^{13}C)-Lina-OOHs and amino acids were performed in CH_3CN/H_2O (1/1, v/v) solvent using NMR (1 and 2D), which is very much different of the RHE environment. Studies in HEPES or PB at 37 °C should allow to obtain adducts prone to better mimic the behavior closer to the human skin.

Secondly, the EPR original methodology that we successfully developed in this work made possible to investigate *in situ* situations closer to a real-life skin allergy situation.[7] The principal aim of this manuscript was to set up the technology transfer from studies in solutions to the model *in situ* using RHE. Now the challenge will be to apply the novel approach to important skin allergens reacting through radical mechanisms and check all different secondary reactions that could occur because of the radical initiation, the potential oxidation of biomolecules in RHE skin cells, and/or induced by the buffer. A substantial question that remains is where the radical initiation occurs. Our assumption based on the investigations presented in chapter 2, is that the spin-adducts issued from Cum-OOH would be formed on cell surfaces whereas for Lina-OOH and Limo-OOHs the reaction would occur within the cells. As a matter of fact, the cell cytoplasm is known to constitute an efficient reductive environment, and this could explain both the lower S/N ratio and the weaker lifetime observed for Lina-OOH and Limo-OOH spin-adducts when compared to Cum-OOH experiments. For this purpose, CD-DEPMPO spin-trap described by Abbas *et al*. would lead to a better localization of the hydroperoxide-mediated radical generation.[10] Indeed, such spin-trap is assumed not to penetrate within the cells whereas DEPMPO probably does. On the other hand, Hardy *et al*. described mitochondrial target spin-trap (Mito-DEPMPO) which could be tested to probe potential hydroperoxide radical generation within the cells.[11]

Furthermore, the ^{13}C substitution on e.g. of Cum-OOH's methyl would allow to distinguish whether the methyl radical observed stem for the hydroperoxide or not. Finally, a variety of molecules susceptible to undergo a radical intermediate during the reactivity process can be tested such as antioxidants, colour dye, peptides etc.

Literature

(1) Lepoittevin, J.-P.; Frosch, P. J.; Menne, T. *Contact Dermatitis*; Springer-Verlag Berlin Heidelberg: New York, **2006**.
(2) Frosch, P. J.; Lepoittevin, J.-P.; Menne, T. *Contact Dermatitis*; Springer-Verlag Berlin Heidelberg: New York, **2006**.
(3) Karlberg, A.-T.; Bergström, M. A.; Börje, A.; Luthman, K.; Nilsson, J. L. G. Allergic Contact Dermatitis—Formation, Structural Requirements, and Reactivity of Skin Sensitizers. *Chem. Res. Toxicol.* **2008**, *21* (1), 53–69.
(4) Sköld, M.; Börje, A.; Harambasic, E.; Karlberg, A.-T. Contact Allergens Formed on Air Exposure of Linalool. Identification and Quantification of Primary and Secondary Oxidation Products and the Effect on Skin Sensitization. *Chem. Res. Toxicol.* **2004**, *17* (12), 1697–1705.
(5) Matura, M.; Goossens, A.; Bordalo, O.; Garcia-Bravo, B.; Magnusson, K.; Wrangsjö, K.; Karlberg, A.-T. Patch Testing with Oxidized R-(+)-Limonene and Its Hydroperoxide Fraction. *Contact Dermatitis* **2003**, *49* (1), 15–21.
(6) Bezard, M.; Giménez-Arnau, E.; Meurer, B.; Grossi, L.; Lepoittevin, J.-P. Identification of Carbon-Centred Radicals Derived from Linalyl Hydroperoxide, a Strong Skin Sensitizer: A Possible Route for Protein Modifications. *Bioorg. Med. Chem.* **2005**, *13* (12), 3977–3986.
(7) Kuresepi, S.; Vileno, B.; Turek, P.; Lepoittevin, J.-P.; Giménez-Arnau, E. Potential of EPR Spin-Trapping to Investigate *in Situ* Free Radicals Generation from Skin Allergens in Reconstructed Human Epidermis: Cumene Hydroperoxide as Proof of Concept. *Free Radic. Res.* **2018**, 1–9.
(8) Bråred Christensson, J.; Matura, M.; Bäcktorp, C.; Börje, A.; Nilsson, J. L. G.; Karlberg, A.-T. Hydroperoxides Form Specific Antigens in Contact Allergy. *Contact Dermatitis* **2006**, *55* (4), 230–237.
(9) Raffalli, C.; Clouet, E.; Kuresepi, S.; Damiens, M.-H.; Lepoittevin, J.-P.; Pallardy, M.; Ferret, P.-J.; Giménez-Arnau, E.; Kerdine-Römer, S. Editor's Highlight: Fragrance Allergens Linalool and Limonene Allylic Hydroperoxides in Skin Allergy: Mechanisms of Action Focusing on Transcription Factor Nrf2. *Toxicol. Sci.* **2018**, *161* (1), 139–148.
(10) Abbas, K.; Babić, N.; Peyrot, F. Use of Spin Traps to Detect Superoxide Production in Living Cells by Electron Paramagnetic Resonance (EPR) Spectroscopy. *Methods* **2016**, *109*, 31–43.
(11) Hardy, M.; Poulhés, F.; Rizzato, E.; Rockenbauer, A.; Banaszak, K.; Karoui, H.; Lopez, M.; Zielonka, J.; Vasquez-Vivar, J.; Sethumadhavan, S.; et al. Mitochondria-Targeted Spin Traps: Synthesis, Superoxide Spin Trapping, and Mitochondrial Uptake. *Chem. Res. Toxicol.* **2014**, *27* (7), 1155–1165.